Studies of polymeric membranes modified for amperometric H_2O_2 and pO_2 sensing with needle-type electrodes

Monika M. Schönleber

Thesis submitted for the degree of Doctor of Philosophy

Interdisciplinary Research Centre in Biomedical Materials (IRC)
Queen Mary, University of London,
Mile End Road, London, E1 4NS, UK

Abstract

Materials used for medical devices are far from ideal for the body, so polymers are applied at the outermost region to counteract the body's natural defences. Component-based failures such as delamination and biocompatibility-based failures such as membrane fouling and degradation still remain a significant challenge. This study focuses on the surface properties and modification of polyurethane and silicone rubber as coating material for amperometric sensing devices.

Effective synthesis of polyurethane, as well as surface modification techniques performed on polymers already attached to sensing devices, are proposed. Phase inversion resulted in increased soft segment content on the surface (confirmed by FTIR with a decreased C=O/C=C ratio). It is proposed that such an optimised polymer surface enhances the yield of further surface modification, such as hydroxylation (using potassium peroxodisulphate) and sulphonation (employing sodium hydride, triisobutylaluminium and 1,3 propane sultone). A novel method to generate an SO_3-derivatised PU surface was proposed. Additionally, successful synthesis of silicone rubber for induced permeability of H_2O_2 was demonstrated. The physical and chemical properties of these modified polymers were examined and evaluated via FTIR, SEM, TGA and contact angle measurements. The biocompatibility of modified polymers was confirmed with retarded protein adsorption; cytotoxicity testing showed that polymers were non-toxic to cells.

Steady state amperometry on polymer modified needle-type electrodes showed enhanced performance with surface modified polymers to oxygen and H_2O_2, both of which are potential biological assay targets. Synthesised Prussian Blue (redox mediator) on platinum surfaces showed that the electrochemical response to H_2O_2 was increased threefold; and in combination with sulphonated polyurethane, interfering current responses could be successfully eliminated.

"Ihre Arbeit ist gekrönt worden mit dem Nobelpreis für Otto Hahn."

Renate Feyl über
Lise Meitner (1878-1968)

Contents

List of Figures

List of Tables

Statement Of Originality

I hereby certify that the work embodied in this thesis is the result of original research and is entirely my own work. It has not previously been submitted for a degree in any University, and to the best of my knowledge contains no material previously published or written by another person except where due acknowledgement in accordance with standard referencing practices is made in the thesis itself.

During the course of this degree, parts of the research have been presented in poster or oral forms at various scientific meetings and conferences. Written articles have also been contributed for publication. These are listed in the Appendices.

Abbreviations

a	activity
Å	Angstroem
A	surface area
AA	ascorbic acid
AFM	atomic force microscopy
Ag/AgCl	silver/silver chloride
ATR-FTIR	attenuated total reflection Fourier transform infrared spectroscopy
Au	gold
BD	1,4 butadiene
BSA	bovine serum albumin
C_o	surface concentration gradient
CA	contact angle
CE	counter electrode
CED	cohesive energy density
CV	cyclic voltammetry
D, D_o	diffusion coefficient
DC	direct current
DCM	dichloromethane
ΔG_m	Gibbs free energy change
ΔH	energy of vaporisation
ΔH_m	change in enthalpy
ΔS_m	change of entropy
DMEM	Dubelcco's Modified Eagle's Medium
DMMHS	dimethyl,methyl hydrogensiloxane
DMSO	dimethyl sulphoxide
E	potential
e^-	electron
E_o	standard potential
E_pa	peak oxidation potential
E_pc	peak reduction potential
η	overpotential
F	Faraday constant
FSA	foetal serum albumin
GA	glutaraledhyde
H_{12}MDI	4,4'-dicylohexylmethane diisocyanate
H_2O_2	hydrogen peroxide
HBI	hydrogen bonding index

HCl	hydrochloric acid
HEMA	2-hydroxyethyl methacrylate
HS-ratio	hard- and soft segment ratio
I,i	current
i_pa	peak anodic current
IEPS	isoelectric point of a surface
IPA	isopropanol
i_pc	peak cathodic current
IPDI	isophorone diisocyanate
i_r	recovery time
J_o	flux
KCl	potassium chloride
LOD	limit of detection
LSS	limitting solution strength
M_n	total molecular weight of polymer
M_O	molecular weight of repeat unit
MDI	4,4'-diphenylmethane diisocyanate
MSDS	material safety data sheet
n	number of electrons transferred
N_2O	nitrous oxide
NaH	sodium hydride
NC	negative toxicity control
NHE	normal hydrogen electrode
O	oxidised species
PA-FTIR	photoacoustic Fourier transform infrared spectroscopy
PB	Prussian Blue
PBS	phosphate buffer solution
PC	positive toxicity control
PCL	polycaprolactone diol
PCU	polycarbonate urethane
PCU-OH	hydroxylated polycarbonate urethane
PCU-SO_3	sulphonated polycarbonate urethane
PDMS	polydimethyl siloxane
PEO	polyethylene glycol
PEU	polyether urethane
PEU-OH	hydroxylated polyether urethane
PEU-SO_3	sulphonated polyether urethane

PHEC	poly(1,6-hexyl 1,2-ethyl carbonate)
pI	isoelectric point
pK_a	acid dissociation constant
pO_2	partial pressure of oxygen
PPDS	potassium peroxodisulphate
PS	1,3 propane sultone
Pt	platinum
PTMEG	poly(tetramethylene ether) glycol
PTMO	polytetramethylene oxide
PU	polyurethane
PVC	polyvinyl chloride
PW	Prussian White
R	gas constant
R	reduced species
R^2	coefficient of determination
RE	reference electrode
ROS	reactive oxidative species
RT	room temperature (25°C)
S	slope, gradient
SDS	sodium dodecyl sulphate
SEM	scanning electron microscope
SR	silicone rubber
T	absolute temperature
t	time
T_a	time of analyte injection
TDI	2,6-toluene diisodyanate
T_g	glass transition temperature
TGA	thermogravimetric analysis
THF	tetrahydrofuran
TIBA	triisobutylaluminium
T_o	time before analyte injection
T_r	response time
UA	uric acid
V_m	molar volume
WE	working electrode
X, x	distance
X_n	degree of polymerisation

Acknowledgements

Firstly, I would like to thank Professor Pankaj Vadgama for the constant support and advice which encouraged me to work independently, develop mentally, and provided insightful views to the world of academia. I would also like to greatfully acknowledge the financial support. For administrative support, many thanks to Mrs. Catherine Jones.

Secondly, Dr. Mike Grahn, my co-advisor, and many others in the ICMS building. My thanks go to all of the helpful and knowledgeable people over there; specifically Dr. Thomas C. H. Going, Mrs. Julia Spring (Blood Gas Analyser), Sahira Khalaf (cell culture), Mr. Keith Pell (cell fixation), Jaina, Diti, Bo Su and Felix.

I also want to thank Dr. John Mitchell, for his knowledge and experience and Mr. John Cowley, the in-house glassblower - great skills, fantastic work and the SEM-Team, you are all just too good. Dr. Jon Popplewell and Dr. Eugenia Leitao for sharing their knowledge in electrochemistry, very nice and helpful people. Dr. Alison Willows, she worked only briefly in our department, but her knowledge in electrochemistry was invaluable and her cheerful attitude was like a fresh breeze.

Further, I also would like to thank Dr. Steffi Krause, as her comments and advice from the transfer viva had a strong impact on subsequent reporting. To Dr. Fanya Ismail, I thank her for her help and support during the "Healthy Aims" project. I wish her all the best with her new career and the future. I would like to thank Dr. Loo-Teck for collaborative work with plasticised polymers for controlled drug release, Prof. R. A. Brown for getting me involved in cell seeded cross-linked hydrogel membranes for use in bioreactor (TIBS), Prof. D. Mandler for getting me involved in Langmuir-Blodgett films of cellulose acetate (BBMO) and Dr. Ivan Hoh for collaborative work in cancer research in biological system. I learned a lot. I would also like to thank Mr. George Nevill for his

thorough and swift work when cutting my electrodes - great job!

I would like to thank Dr. Rasa Pauliukaite; she taught me lots of valuable practical electrochemistry skills. Prof. Christopher Brett, her supervisor, was also a useful source of information and advice. Prof. Mike Braden needs to be mentioned, it was an honour to have met him and a pleasure to have discussed science with. To Prof. A. Karyakin and E. Karyakina and Dr. Mikhail Yu. Vagin from the University of Moscow, thank you all so much for all of the help and advice.

Dr. Joseph Gargiuli was a constant source of cheer and encouragement and very knowledgeable in organic chemistry; he also provided valuable contacts within the University. For all of this, I am very grateful. There were many others who have helped me during my study that I would like to thank, far too many to mention. To name but a few: Dr. Joshua Eniwumide, for the secret of how to survive; Dr. Monisha Phillips, you are an angel heaven sent; Dr. George Kyriacou, you were right all along; Dr. Zimei Rong, you are a great mathematician; Sarah Rashid, I wish you all the best; Dr. Wei Li, thanks for allowing me to use your lab when needed; Mr. Jim Kirkland for the swift response for oxygen and nitrogen gas supply; Dr. Katie Smith, thanks for allowing me to use the contact angle machine; Dr. Ihtesham Rehman for the tuition in FTIR and Dr. Nima Roohpour for further help; Dr. Stephen Mellon; Dr. Richard Twycross-Lewis, Dr. Monica Pino, Dr. Davidson Ateh, Dr. Natalie Vaughan, Dr. Oto-ola Akanji, Dr. Simon Bloxham for their cheerful attitude.

The biggest thank you goes the most important person in my life (and PhD), Dr. Colin Lewis. He helped me so much, spending endless hours reading my work, supplying valuable suggestions, writing code for assistance in data processing, and making it possible for me to spend time solely on writing up. I am also greatly indebted to him for listening to me and being able to redirect some of my negative energy into positive energy. His unwavering faith helped me to believe this gargantuan task was possible.

And last but not least, I would like to infinitely thank my family and friends for all of their love and support. These fruitful and invaluable phone calls with Silvia offered a great deal of encouragement and joy - thank you!!

Chapter 1

Introduction

In most cases, materials for medical devices are far from ideal for the body and cannot be readily replaced with fully biocompatible components. As a solution to this impediment, thin membranes are frequently applied at the outermost regions of the device to serve as biocompatible interfaces and protective barriers. Since most medical devices are mass produced, the choice of material for the encapsulate has been defined more in terms of manufacturability than functionality. As a result, these devices may not be optimal for a specific use. However, these encapsulates can be modified by various mechanisms and approaches according to desired needs. There is a caveat to this proposed approach in that the chemicals used might have a detrimental biological effect or adversely affect the device and/or on the encapsulate layer itself.

1.1 Membrane Technology for Electrochemical Sensing Devices

The way in which different membrane properties affect sensor behaviour at the transducer/analyte interface varies by sensor type and by application. The most common sensor types are electrochemical devices using chronoamperometric principles, potentiometric devices and optical devices, respectively. In this study, electrochemical devices in the form of needle-type electrodes were used for amperometric determination of hydrogen peroxide (H_2O_2) and partial pressure of oxygen (pO_2) as potential assay targets for biomedical study. The role for the polymer here is not only to protect the device physically; it can also be involved in the generation of an appropriate signal, restricting the transfer of electroactive interference compounds to the electrode surface, preventing elec-

trode passivation, reducing membrane biofouling thus increasing biocompatibility, whilst allowing the transport of target analyte across to the sensor surface.

1.2 Prussian Blue for Electrochemical H_2O_2 Sensing

Amperometric H_2O_2 oxidation requires a high overpotential at which not only H_2O_2, but other substances which are present in biological samples (ascorbic acid, uric acid and acetaminophen) give additional interfering current responses. To overcome this obstacle and to improve the analyte selectivity and sensitivity, artificial electron transfering agents (mediators) are utilised which operate at lower redox potentials than the other electrochemically active interfering species [Karyakin *et al.* (2004)].

Most commonly used mediators are: ferrocene and derivatives, tetrathiafulvalene, tetracyanoquinodimethane, conducting salts, quinones and ferric/ferrocyanide [Chaubey *et al.* (2002)]. Prussian Blue (PB) is one of the most widely used inorganic mediator which is synthesised by mixing ferric and hexacyanoferrate ions with different oxidation state of iron atoms, where $Fe(CN)_6^{3-}$ is reduced to $Fe(CN)_6^{4-}$.

The ideal mediator should not participate in side reactions during electron transfer, should be able to react rapidly, should exhibit reversible heterogeneous kinetics and should operate at low electrode potential, the reduced form should not react with oxygen, should be pH independent and should have stable oxidised and reduced forms. Some redox mediators can only work in an deoxygenated environment because the reduced form of the mediator competes with molecular oxygen, diverting the flow of electrons to the electrode surface [Itaya *et al.* (1984)]. PB is known to be a selective electrocatalyst of H_2O_2 reduction/oxidation; electrons are shuttled to the surface of the indicator electrode during which the mediator is cycled between its oxidised and reduced forms. A schematic of mediated electron transfer using PB for H_2O_2 is illustrated in Figure 1.1.

There are concerns reported by various researcher regarding poor pH stability and solubility of PB [Curulli *et al.* (2004), de Mattos *et al.* (2000a,b), Garjonyte *et al.* (1999)]. However, Karyakin *et al.* (1999) reported that an increase in acidity of the initial solution before depositing PB on electrodes would result in a more regular growth of PB crystals, hence improved stability. The reason for poor pH stability was thought to lie in strong interactions between ferric and OH ions whereby Fe-(CN)-Fe bonds are disrupted resulting in the formation of $Fe(OH)_3$ [Ricci *et al.* (2005)]. Nevertheless, a Pt surface is still a challenge for PB stability.

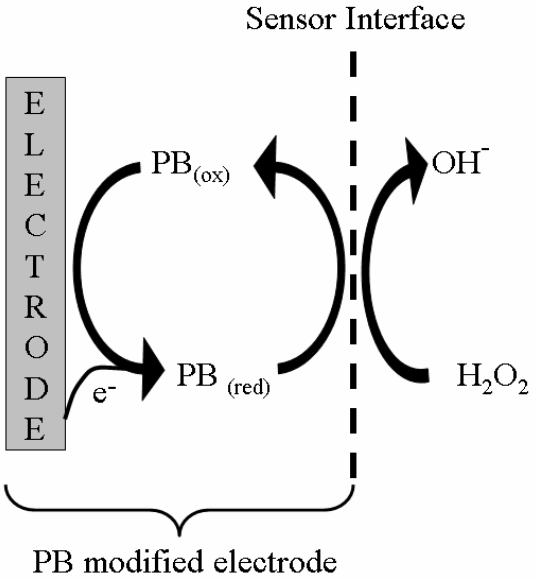

Figure 1.1: Schematic of PB-mediated electron transfer for H_2O_2 [adapted from Ricci *et al.* (2005)]

1.3 Biocompatibility

A major limitation for polymer use in medical applications is the adverse interaction and incompatibility with bodyfluids and tissues. A foreign body reaction, setting off with protein adsorption followed by cell adhesion, and the formation of an avascular collagenous capsule will inevitably occur in tissue [Castner *et al.* (2002), Sun *et al.* (2003), Wisniewski *et al.* (2000)]. The surface interaction is called *biofouling* and is scarcely avoidable in applications since all materials (hydrophobic and hydrophilic) are recognised by the human body as non-self. A non-specific protein adsorption cascade is illustrated in Figure 1.2.

Basmadjian *et al.* (1997) summarised in his review the results of mathematical modelling studies regarding blood coagulation on biomaterials. The theoretical understanding of events from the time of first contact of the biomaterial with flowing blood to the final production of thrombin is examined in detail. After assessing the unequivocal physical and biochemical processes, Basmadjian supported the notion that the ideal non-thrombogenic material may be impossible to find. Essentially, every material provokes some degree of biological response.

The quest is to produce a material that can provide an appropriate performance with minimal adverse effects without inducing activation of cellular or plasma protein cascades. The past four decades have witnessed an explosion of publications regarding

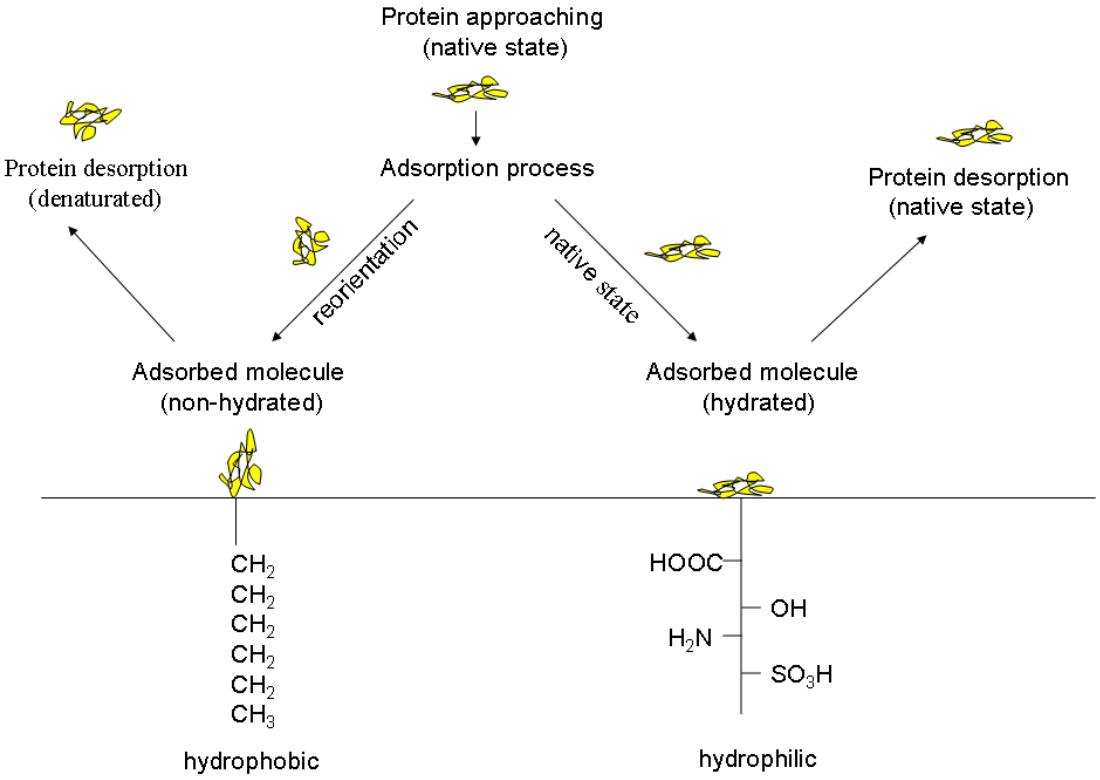

Figure 1.2: Non-specific protein adsorption on hydrophobic and hydrophilic surfaces

different types of polymers with various chemical, morphological and structural features delineating possible applications in respect to their properties.

1.4 Surface Modifications

In extension to the lack of biocompatibility of medical sensing devices, polymeric materials applied as the outer most layer may not show ideal performance in specific applications and environments either. Hence, surface modification offers the possibility of tailoring the chemical surface compostition of the polymer to specific needs.

Chemical reactions occur mostly at surfaces and interfaces not only because they provide high accessibility for reactive agents, but also because they offer a low energy barrier to facilitate complex reactions. Effective bulk modification is one way to achieve desired surface properties with polymeric materials. A combination of different polymers and different casting solutions can dramatically change the conformation, size and symmetry of a polymer network in dry polymers [Kiremitçi *et al.* (1990), Kruczek *et al.* (2003), Lamba *et al.* (1998)]. Two of the most commonly used polymers for coating medical devices are silicone rubber and polyurethane [Sun *et al.* (2003), Wisniewski *et al.* (2000)]; representative chemical structures are shown in Figure 1.3.

Direct surface modification is an effective way to improve biocompatibility without changing the bulk properties of a polymer. Various attempts to modify polymer surfaces have been outlined in literature, such as grafting, high-energy treatment, self-assembled monolayers, surface patterning and the immobilisation of functional groups and molecules. More generally, negatively charged polymer surfaces are of advantage when used as coating material for biomedical sensing devices as they act as a barrier for the negatively charged compounds present in biological fluids.

Most surface modification techniques require aggressive or toxic chemicals and are not ideal for a polymer already attached to a delicate sensing device. Bamford *et al.* (1994) proposed a method for surface functionalisation (hydroxylation) using mild chemicals in aqueous media. Such functionalised polymers can then undergo further grafting reactions, such as sulphonation.

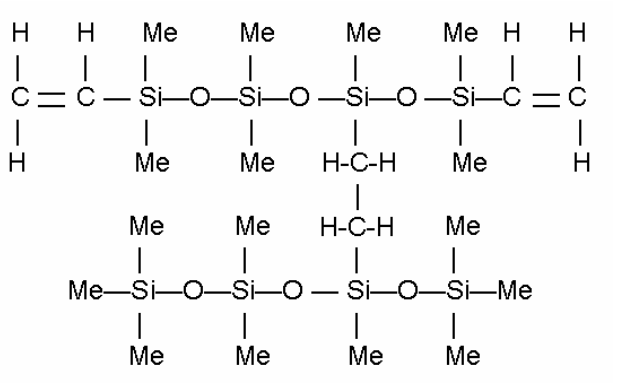

(a)

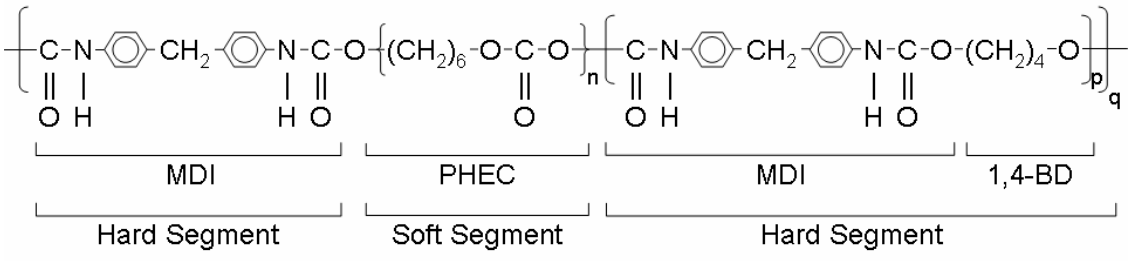

(b)

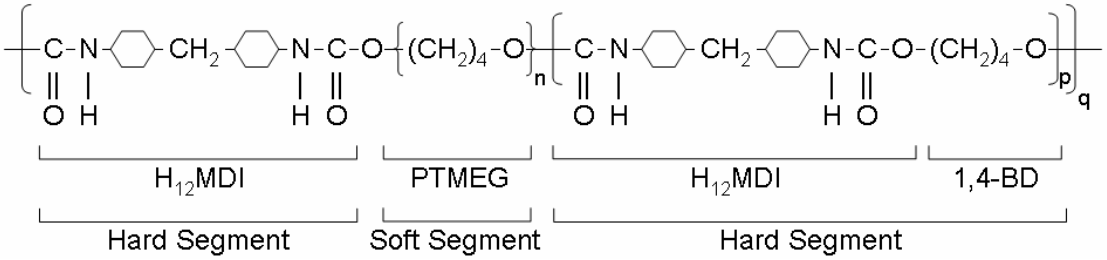

(c)

Figure 1.3: Chemical structures of (a) crosslinked SR; (b) repeat unit of PCU; (c) repeat unit of PEU

1.5 Project Aims

The aim of this project was to develop polymeric materials with desired surface properties specific for hydrogen peroxide and oxygen measurements using amperometric sensing devices. For this purpose, polyurethane and silicone rubber were used and further modified. Interfacial reactions were the area of focus. Initially chemical structures, characteristics, morphology and modification strategies were considered along with potential rearrangement of surface functional groups when used for analyte detection purposes. For polyurethane, a suitable modifying and grafting agent was identified and a method for functionalisation and sulphonation of the polymer surface was developed. After successful hydroxylation of the outer surface of polymer coated sensing devices, grafting of sulphonated groups onto the functionalised polymer surface was investigated. For silicone rubber different physical and chemical properties as well as surface changes were obtained by changing the composition and type of casting solutions including preparation conditions. The modified polymers were characterised via photoacoustic Fourier transform infrared spectroscopy (PA-FTIR), thermogravimetric analysis (TGA), contact angle measurements (CA), scanning electron micropscopy (SEM), light microscopy, protein adsorption and cytotoxicity. A method for surface modification of already coated sensors and a method for bulk modification suitable as coating material of delicate sensing devices were proposed. Needle-type electrodes were used as a platform for this study. These electrodes were also further chemically modified with Prussian Blue and characterised regarding their analytical performance. Attention had to be taken to not compromise on the functionality of the mediator.

Chapter 2

Literature Review

2.1 Silicone Elastomer

2.1.1 Introduction and Chemistry

Silicone rubber, also known as polysiloxane, is a hydrophobic, highly elastic and chemically inert material. It has an extremely low glass transition temperature of about $-125°C$; the siloxane chain is highly flexible due to large bond angles and bond lengths and it has high molecular weight chains, which are in a liquid state even at room temperature. It has high gas permeability and is essentially of non-toxic nature [Loetters *et al.* (1997)]. It is used in many medical applications such as a coating material for sensing devices [Aussedat *et al.* (2000), Gifford *et al.* (2006), Peteu *et al.* (1996)], indwelling catheters and implants [Schuettler *et al.* (2001)], prostheses [Bellamy *et al.* (2003)] and membrane separation units [El-Kalay *et al.* (1987)].

Fabrication and Processing

Silicone elastomers for medical applications are commercially available and are supplied in uncured form as either one package containing all of the formulation components or as two packages which are to be mixed in specific proportions before fabrication. Two of the most common curing systems are the peroxide cure and the addition cure [Morton (1987)].

Peroxide Cure

Elastomers using the peroxide cure system are more commonly provided as one-part material though two-part materials are also available. This cure system involves the generation of free radicals of an organic peroxide. These radicals initiate deprotonation

of the alkyl group (CH_3) attached to the silicon atoms along the polymer chain, forming organic radicals. As this reaction is repeated, these organic radicals then form a crosslink network. A certain amount of working time has to be allowed before the crosslink network builds to acceptable levels.

Peroxides are classified as either non-vinyl specific or vinyl-specific, depending upon the type of radical reaction they promote. Non-vinyl specific peroxides promote the combination of two radicals on adjacent chains, resulting in an ethylene linkage ($_2HC = CH_2$) between the polymer chains. Vinyl-specific peroxides promote the addition of the radical to a vinyl group ($-HC = CH_2$) attached to silicone on a polymer chain, resulting in a propylene linkage (C_3H_6) between the polymer chains. If this type of elastomer is used in medical applications, the decomposition products (for example polychlorinated biphenyl) from organic peroxide break down must be removed as they are highly toxic and a potent carcinogen.

Addition Cure

Elastomers using the addition cure system are two-part elastomers, involving platinum catalysed addition of a silylhydride to an unsaturated side, which is usually a vinyl group. With this cure system, the amount of silylhydride will theoretically determine the crosslink density.

As illustrated in Figure 2.1, one part of the formulation contains the Pt catalyst, an inhibitor and polysiloxane with vinyl functionality on the silicone backbone. The other part of the formulation contains the crosslinker polysiloxane with one or more silylhydrides within the molecule. These two parts are mixed at room temperature and heat is then required to activate the platinum to allow the build up of a crosslink network. This is followed by a prolonged post-cure process, which will set the SR. The amount of working time and the rate of cure are determined by the ratio of these two components, the catalyst and inhibitors used in the formulation. Mixing these two components of the formulation at other than the ratio prescribed by the manufacturer results in altered surface characteristics as well as physical and chemical properties. The addition cure is the most commonly used form of cure as toxic by-products are not formed and it gives a better control over the crosslink density compared to the peroxide cure system.

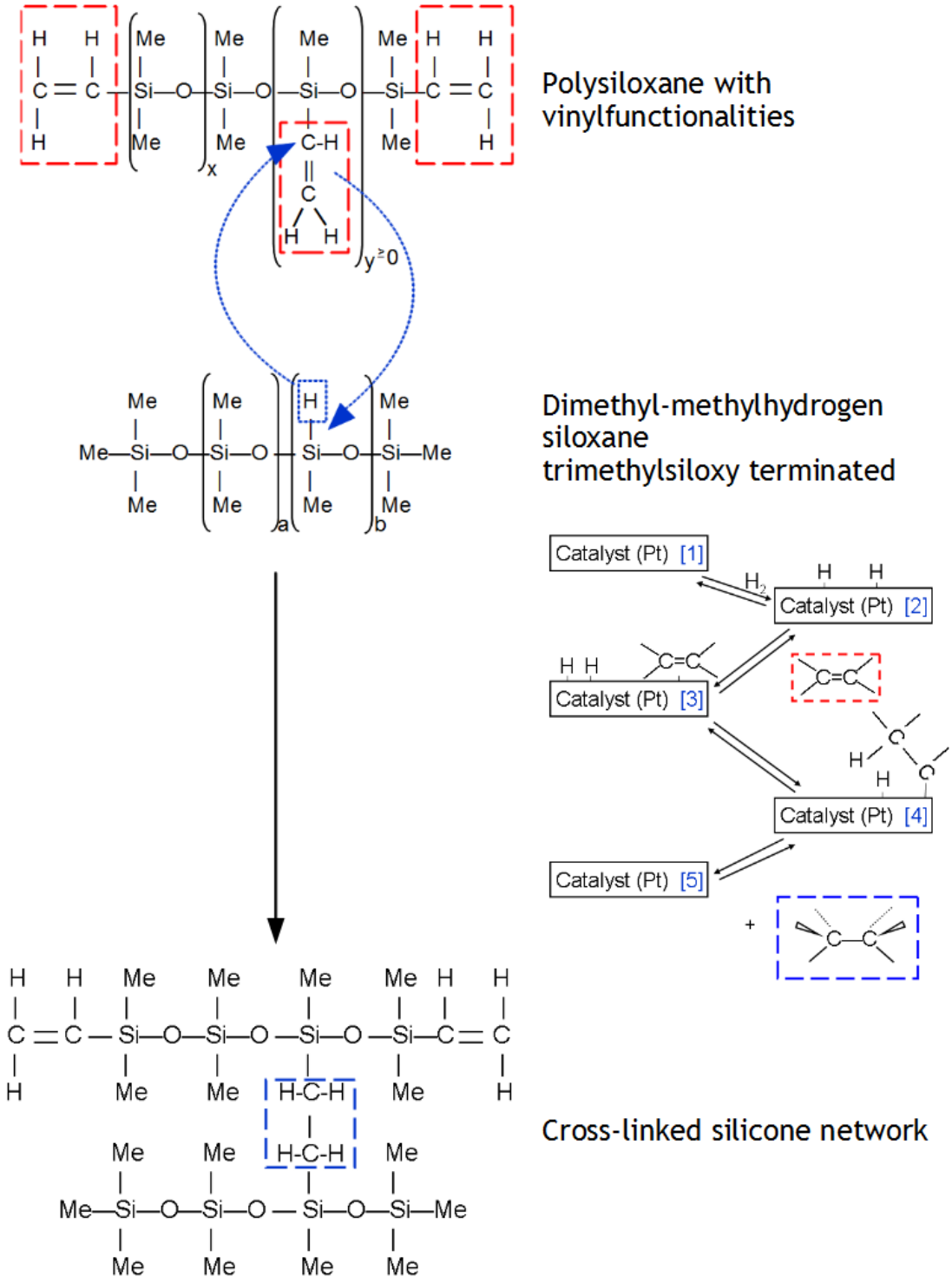

Figure 2.1: Scheme of SR synthesis by hydrosilylation reactions of polysiloxane bearing vinyl functionalities and trimethyl siloxy terminated dimethyl-methylhydrogen siloxane as cross-linker in the presence of platinum-based catalyst (platinum-divinyltetramethyldisiloxane complex) to obtain cross-linked silicone network [modified from Williams-Wynn (2006)]. *The proposed Pt catalysed alkene hydrogenation mechanism is illustrated as such: [1] catalyst, [2] hydrogen adsorption on catalyst surface, [3] formation of a complex of alkene to catalyst, [4] insertion of hydrogen into carbon-carbon double bond, [5] regenerated catalyst and alkane product*

2.1.2 Performance as Coating Material - Impact and Strategies

As encapsulating material for many implants needs to be a moisture barrier *per se*, SR does not qualify as a candidate material as it is very permeable to water vapour. However, it is suggested that if there are no voids such as local failures of adhesion, there is nowhere for the water vapour to condense to so no damage results; only water in the liquid phase is stated to be damaging for electronics [Donaldson (1991)]. Although SR is highly permeable to water vapour, it is relatively impermeable to salts. Donaldson (1991) assessed silicone encapsulated microelectronics regarding to the rate of osmotic water transfer in saline solutions of different strength. It was found that when SR encapsulated parts are surrounded by saline solution, an osmotic gradient drives water out of the implant into the environment, protecting the implant from further damage.

Most commercial polymeric materials, such as silicone elastomer contain various additives. Zhang *et al.* (1996b) reported on hydrophobic processing aid and silicone oil, present on the surface of SR. In comparison with conventional PU, less cell adhesion and cell-material interaction was observed. However, it was found that these contaminants have no biological systemic effects. Donaldson (1991) investigated the impact of these additives to the functioning of microelectronic implants when encapsulated with SR in the case of defective encapsulation.

In case an implant with a void formation would be exposed to extracellular fluid of 0.34 Osm kg^{-1}, water leachable additives from the SR itself would fill up the void with these contaminants including pure water. If the limiting solution strength (LSS) of the aqueous contaminant in the void is < 0.34 Osm kg^{-1}, the osmotic gradient is still favourable for keeping the implant dry. If the LSS is > 0.34 Osm kg^{-1} the osmotic gradient will reverse. In this case water will be drawn into the void, thereby diluting the leachable solution to a concentration below the LSS. Provided there is a back-feed of the contaminant into the void, the LSS will rise again and water will continue to be drawn in. This process would presumably continue until there is no more contaminant left, by which time the void would have grown larger and the implant then waterlogged. This could cause the silicone elastomer to lose adhesion to the underlying substrate and if the contaminant is ionised electrical short-circuits might occur. Donaldson (1991) concluded that if this model is valid, the implant should continue to operate correctly despite the void, providing that water extracts of SR have a limiting solution strength below 0.34 Osm kg^{-1}.

Degradation

Batich *et al.* (1996) reported on changes in the surface chemistry of silicone elastomers when samples were exposed to saline at elevated temperatures. Silanol surface concentration estimates were based on receding contact angle measurements. A decrease in contact angle reflecting an increase in surface coverage of hydroxyls was found; it was considered that these changes were caused by surface hydrolysis. Kennan *et al.* (1997) conducted further investigations to assess whether cure residues affect the hydrolytic stability of medical grade silicone elastomers during exposure to saline with increasing temperatures. Silica-reinforced polydimethylsiloxane silicone rubbers, either peroxide- or hydrosilylation cured, were subjected to saline and assessed for hydrolysis by means of tensile testing and contact angle measurements. However, no evidence of surface or bulk siloxane hydrolysis was found. Whether receding contact angles are a useful tool to estimate the concentration of surface species on polymers is under debate since surface heterogeneity may lead to contact angle hysteresis.

Adhesive Bonding

Adhesion between the implant device and silicone encapsulant is one of the most important factors determining implant lifetime. The durability of joints between silicone elastomers and binary oxides was investigated by Donaldson *et al.* (1995) to find a predictor that would indicate whether a given adhered material can make long-lived bonds. It was found that the isoelectric point of a surface (IEPS) is a promising parameter as the most stable adhesive joints seem to occur when the charge density on the adherent surface has a negative charge. No conclusion could be drawn whether two-part silicone elastomers show a similar correlation as these elastomers utilise different bonding mechanisms [Donaldson (1997)]. Strong metal-polymer adhesion can also be achieved with O_2-plasma modification of a polymer surface. This treatment is said to provide the necessary surface functionalities, such as carbonyl, carboxyl, hydroxyl and ether groups in order to create metal-oxygen-carbon type covalent linkages [Liston *et al.* 1994]. However, such a surface modified polymer will also show increased hydrophilicity.

Hydrophobicity

Silicone elastomers are widely used in biomedical applications not only for their flexibility, compliance and relatively good biocompatibility, but also for their hydrophobic and

semi-permeable character. However, such hydrophobic materials are known to adsorb high quantities of protein [DeFife *et al.* (1999), Gifford *et al.* (2006)] and for some applications, in particular in biomedical sensing applications, protein adsorption is detrimental to their performance. Thus, for reduced protein adsorption, it is desirable to alter the hydrophilicity. To achieve this, various attempts have been undertaken, such as the addition of organic functionalities on silicone surfaces including plasma polymerisation [Williams *et al.* (2004), Olander *et al.* (2004)], ultraviolet polymer grafting using a mercury lamp for radical generation [Hu *et al.* (2002)] and oxygen based plasma for protein patterning [Papra *et al.* (2001)]. Hron (2003) reviewed possibilities to obtain enhanced hydrophilicity with special attention to silicone rubber-hydrogel composite materials based on acrylic and methacrylic acid derivatives.

DeFife *et al.* (1999) utilised photochemical treatment to covalently coupled hydrophilic polymers including hyaluronan and a polypeptide. These modified surfaces were thought to inhibit adhesive protein adsorption and prevent both fibrin deposition and fibrosis. Though it was found that protein adhesion was considerably reduced. Chen *et al.* (2005) functionalised the surface of PDMS elastomers by creating high-density surface Si-H groups to subsequently graft PEO onto these end groups. The choice of solvent was considered to be critical. It was found that solvents that swell the silicone (chloroform, ether, tetrahydrofuran, acetone), would cause the hydrosiloxane groups to be incorporated within the polymer matrix. Methanol, however, was found to induce the incorporation of Si-H groups only to the polymer surface. The presence of Si-H during this process and the presence of PEO was confirmed by ATR-FTIR. The modified surface showed reduced protein adsorption.

Crosslink Density

Mirzadeh *et al.* (2003) studied the effect of crosslink density in SR on cell behaviour. Varied amounts of curing agent were used for altered crosslink degrees to obtain different surface molecular chain motions. The results showed that varied crosslink density, hence varied chain mobility had an impact on the quantity of cell attachment and proliferation. However, surface characteristics including morphology, critical surface tension, rigidity and chemistry have to be considered in combination to crosslink density.

The properties of the casting solvent was shown to affect polymer conformation and the size and symmetry of polymer coils within the polymer matrix. In dilute polymer

solutions the extent of deformation of polymer chains depends on the relative strengths of polymer-polymer and polymer-solvent interactions. In a strong solvent the polymer is unfolded, as the polymer-solvent interactions are more favourable than the polymer-polymer interactions. In a weak solvent the polymer molecules remain folded because of more favourable polymer-polymer interactions. Solvent effects on polymer properties have been reported by a number of researchers. Mohr *et al.* (1991) studied the permeation rate of several gasses on poly(4-methyl-1-pentene) films prepared with varied casting solvents. The permeability coefficients showed significant differences due to casting solvent induced changes in crystalline formation concomitant with varied spatial arrangements of the crystallites within the polymer matrix. By analogy with SR, Okuno *et al.* (1993) found that the density and crystallinity of PVC membranes increased with the increasing relative viscosity of the casting solutions. With increased crystallinity, the permeability and diffusivity of water vapour decrased, while solute separation increased. Furthermore, morphology was significantly affected by the choice of solvent.

Analogy work with sulphonated poly(2,6-dimethyl-1,4-phenylene oxide) films, Kruczek *et al.* (2003) showed that polymer-solvent interactions expressed by the relative viscosity of casting solutions determined surface morphology. An increase in surface roughness was observed with an increase in relative viscosity of the casting solution. However, the gas transport properties appeared to be governed by solvent volatility rather than polymer-solvent interactions.

2.2 Polyurethane

2.2.1 Introduction and Chemistry

Polyurethane was discovered in 1937 by Otto Bayer, an employee of I.G. Farbenindustrie in Germany. The introduction of these materials into the market for medical application is reported to have come from three independent paths. The earliest was in the late 1950s when Pangman disclosed in his patent polyester urethane foam for a breast prosthesis. In the mid 1960s Cordis Corporation marketed PU for a diagnostic catheter [Pinchuk (1994)]. The first *in vivo* experiments utilising polyurethane-urea polymers were reported by Boretos *et al.* (1967), (1968) and Lyman *et al.* (1971) and claimed good haemocompatibility. These elastomeric materials now come in a wide range of chemical compositions and are used for biomedical applications from the cardiovascular through

to artificial organs, tissue replacement and augmentation, controlled drug delivery, contraceptives and as coating material for sensing devices.

Regarding the nomenclature, PU would denote a polymer in which the components, the hard and soft segments, are bound together by a urethane function. However, the term "polyurethane" is actually a misrepresentation as the most predominant repeating units within this polymer are not the urethane linkages but linkages inherent in the macroglycol, including ester, ether and carbonate linkages [Pinchuk (1994)]. Nevertheless, the nomenclature has been used for decades and is now established.

PU is composed of hard and soft segments arranged either randomly, in an alternating manner, or as a combination of segments or block copolymers. The hard segment has a high glass transition temperature, imparts mechanical strength and consists of aromatic or aliphatic diisocyanates linked to a chain extender of low molecular weight. The most common isocyanates are illustrated in Figure 2.2.

2,4- 2,6-Toluene diisocyanate (TDI)

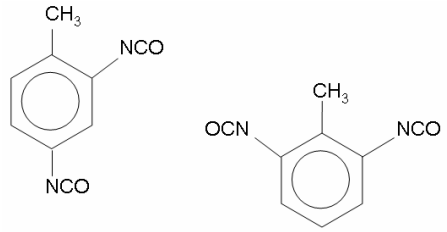

4,4'-Methylene diphenyl diisocyanate (MDI)

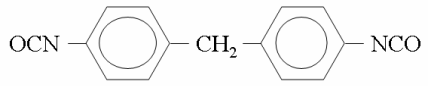

Isophorone diisocyanate (IPDI)

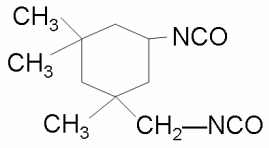

4,4'-Methylene dicyclohexyl diisocyanate (H_{12}MDI)

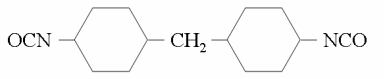

1,6-Hexamethylene diisocyanate (HDI)

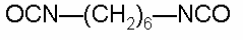

Figure 2.2: Common diisocyanate building blocks for PU

The most important chain extenders are aliphatic diols or diamines such as 1,2-ethane, 1,3-propane, 1,4-butane and 1,6-hexane; cyclic and aromatic diamines and diols are also

used (Figure 2.3). Chain extenders are of low molecular weight and play an important role in PU. However, PU can be formed by directly reacting isocyanate and macrodiol without the chain extender. These polymers would then not exhibit microphase separation and would show poor physical properties because chain extenders increase the hard segment length, permitting hard-segment segregation leading to micorphase separation. Phase separation gives the polymer its unique characteristics, such as increased modulus and glass transition temperature [Bae *et al.* (1999)].

1,4 Butanediol	$HO-(CH_2)_4-OH$
1,6 Hexanediol	$HO-(CH_2)_6-OH$
Ethylene diamine	$H_2N-(CH_2)_2-NH_2$
3,3'-Dichloro-4,4'-diaminodiphenylmethane	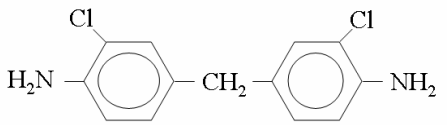

Figure 2.3: Common chain extenders for PU

The soft segment has a low glass transition temperature, imparts elasticity and flexibility to the elastomer and also contributes to the hydrophilicity, lubricity and biostability. Soft segments are also often referred to as polyols, however this nomenclature is ambiguous as it has other meanings such as for a substance containing more than two hydroxyl groups. Therefore, the term diol is used as it refers to an oligomer terminated by two hydroxyl groups. Diols include hydroxy-terminated polyesters, polyethers, hydrocarbons and polydimethylsiloxanes (PDMS) (see Figure 2.4).

Polyurethane Synthesis

The synthesis of PU in its simplest form is a one-step process in which diisocyanate is mixed with a diol and allowed to react. To ensure a certain speed of polymerisation reaction and to achieve a high molecular weight compound, a catalyst is usually used. This method is said to give less reproducible results since the actual chemical reaction is exothermic and can exceed well over 200°C at which thermal degradation may also occur [Mothe *et al.* (2000), Pielichowski *et al.* (1996)]. The two-step process is more commonly used since it typically results in a polymer with a higher yield and a better

Poly(tetramethylene ether) glycol (PTMEG)

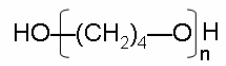

Poly(1,6-hexyl 1,2-ethyl carbonate) (PHEC)

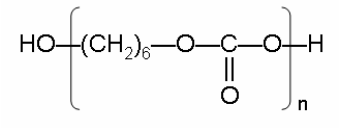

Polydimethylsiloxane (PDMS)

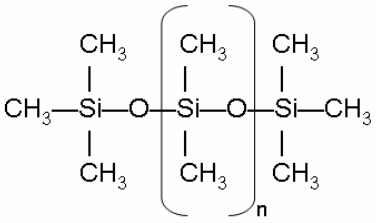

Polycaprolactone diol (PCL)

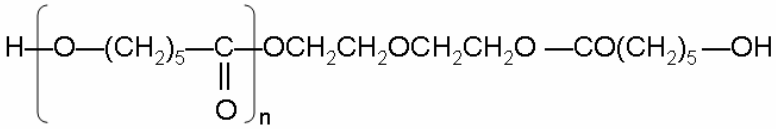

Figure 2.4: Common soft segments for PU

controlled, more regular chemical structure. There are various methods, but all generally involve in the first step a diisocyanate and a diol, which are reacted to form an isocyanate terminated prepolymer. In the second step, a low molecular weight diol as chain extender is added to complete the polymerisation. The reaction of the diisocyanate with the chain extender forms the hard segment (urethane linkage) of the PU chain.

However, there are hundreds of different combinations and permutations of these basic monomers which yield PU of vastly different chemical and physical properties. These PU can be synthesised or acquired commercially according to specific needs (for example biostable for implant material or degradable for controlled drug delivery applications) e.g. Bionate®, CarboSil^{TM}, ChronoFlex®, Elasthane^{TM}, Estane®, Pellethane®, PurSil^{TM}, Tecoflex®, Tecophilic®, Trixene^{TM}.

Phase Separation

Polyurethane is of inhomogeneous structure as the hard- and soft segments are chemically dissimilar and so not completely miscible. Therefore, a two-phase polymer is produced which shows microphase separation or clustering in which the hard segments form discrete domains which are dispersed in a soft segment matrix. The inherent inhomogenity allows the PU to have rigidity whilst maintaining flexibility which imparts physical and mechan-

ical attributes, including elastomeric behaviour, high modulus and enhanced biocompatibility, all of which make this elastomer superior as a biomaterial [Elbert *et al.* (1996)]. Phase separation was first described by Cooper *et al.* (1966) during their study of styrene-butadiene-styrene triblock copolymers via transmission electron microscopy. They postulated that the images, which showed two contrasting regions, reflected clustering or microphase separation. Koberstein *et al.* (1986) found two distinct endotherms in PU block copolymers indicating microphase separation transition from an ordered to disordered phase depending on the annealing temperatures. A generic representation of the phase separation of PU is shown in Figure 2.5.

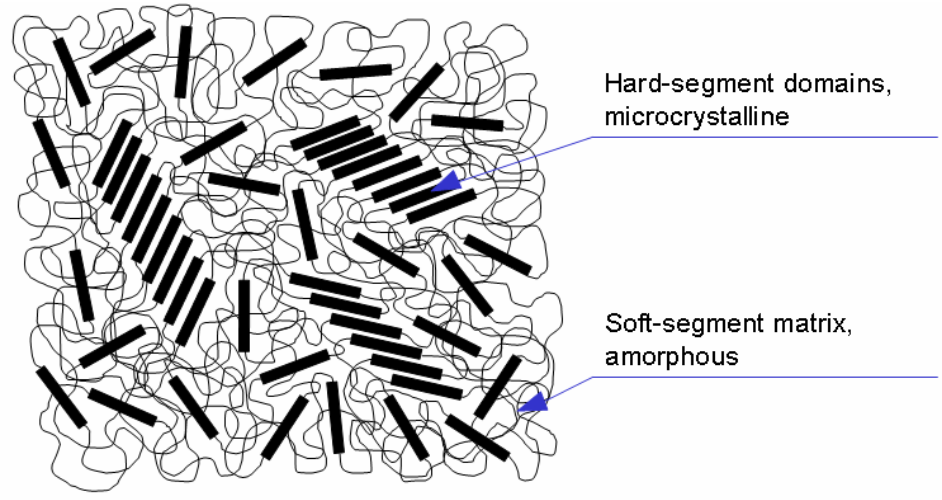

Figure 2.5: Generic representation of phase separation of hard and soft segments in PU [modified from Koberstein *et al.* (1986)]

Several factors have to be considered in microphase separation of PU: the solubility parameter, the degree of polymerisation, conformation, steric effects and the weight fraction of the hard and soft segments [Lamba *et al.* (1998), Pinchuk (1994)].

The Hildebrand solubility parameter is calculated from the square root of the cohesive energy density (CED) and expressed by δ. The CED is the amount of energy needed to completely remove unit volume of molecules from their neighbours to infinite separation, which is equal to the energy of vaporisation (ΔH) divided by the molar volume (V_m). Therefore, CED can be thought of as the sum of all intermolecular interactions between molecules [Burke (1984)], which is given by:

$$\delta = \sqrt{\frac{\Delta H - RT}{V_m}}$$

in which R is the gas constant and T is the absolute temperature. From this value

the degree of interaction between materials, particularly for polymer-solvent interactions, can be estimated. In hard segments of PU these are Van der Waals forces, dipole-dipole interactions and hydrogen bonds. The soft segments show mainly weak dipole-dipole interactions and to a lower extend Van der Waals forces and hydrogen bonding. As hydrogen bonding is the strongest non-covalent interaction, the CED and therefore the solubility parameter of these polymeric pairs may differ substantially.

The degree of relative repulsion or attraction between polymeric pairs is embodied in the free energy of mixing. Flory and Huggins introduced a mathematical model of the thermodynamics of polymer solutions, adapting entropy of mixing which results in an equation for the Gibbs free energy change (ΔG_m) for mixing a polymer with a solvent [Fried (2003)]. The equation for Gibbs free energy change is given by:

$$\Delta G_m = \Delta H_m - T\Delta S_m$$

in which ΔH_m is denoted as the change in enthalpy in the process of mixing, ΔS_m is the change in entropy and T is the absolute temperature. ΔS_m of a polymer mix with two dissimilar components is according to the Flory-Huggins solution theory low and does not therefore contribute much to the total ΔG_m. Differing solubility parameters will result in a positive energy of mixing, hence ΔH_m will be positive. Therefore, ΔG_m will be positive, indicating that the mixing of dissimilar compounds, such as hard and soft segments in PU is thermodynamically unfavourable, resulting in phase separation or segregation [Lamba *et al.* (1998)].

The degree of polymerisation (X_n) is the number of repeat units in an average polymer chain at time t in a polymerisation reaction and is given by:

$$X_n = \frac{M_n}{M_0}$$

in which M_n stands for the total molecular weight of the polymer and M_0 is the molecular weight of the repeat unit. It is defined as the number of monomeric units in a macro- or oligomer molecule, block or chain [McNaught *et al.* (1997)]. Miller *et al.* (1985) studied the effect of varied hard segment length in PU based on PTMO soft segments and a MDI/BD hard segments. It was thought that with increased hard segment length a greater number of hard segments reside within the soft segment matrix, increasing phase separation. This was evidenced by a higher ratio of inter-urethane hydrogen bonding to

non-bonded urethane carbonyls. Additionally, longer hard segments resulted in a higher modulus and a higher stress at failure. This again is attributed to a better hard segment interconnectivity allowing lateral accumulation of the hard segments thus promoting crystallinity.

Velankar *et al.* (1998) found that the degree of microphase separation increased with increasing soft segment block length and was almost single-phased the shorter the block lengths. PU used in their study was based on PCL soft segments and IPDI/BD hard segments. Due to the relatively high polarity of PCL, the miscibility with the hard segments was found to be increased with short soft segment block length whereas long soft segment length was found to show enhanced mobility thus promoting phase segregation.

The degree of phase segregation was studied by Huang *et al.* (1997) in terms of incompatibility of hard and soft segments, conformational effects and steric hindrance of urethane groups and the extend of hydrogen bonding. The least phase mixing was observed with MDI and H_{12}MDI in comparison with IPDI. This was thought to be due to the chemical structures of MDI and H_{12}MDI, which are both linear and would allow more tight packing between the hard segments, leading to increased phase separation. IPDI has steric structure and hence the intermolecular interaction between these hard segments would be lower resulting in phase mixing. In addition, synergistic effect of the polarity and chemical structure of IPDI with respect to the soft segment may have had an adverse effect to the formation of nanocrystalline domains compared to MDI and H_{12}MDI. However, H_{12}MDI is an aliphatic molecule and has multiple conformations. These differing conformations may sterically hinder the process of hydrogen bonding between the hard segments, suggesting less phase separation than MDI based PU.

Hydrogen Bonding

Hydrogen bonding is formed between proton donor groups (N-H) and proton acceptor groups (C=O, C-O-C) and has an estimated strength of about 20-50 kJ/mol, depending on the type of proton acceptors present [Szycher (1999)]. Hydrogen bonds are said to predominantly form between hard segments and can be detected by infrared spectroscopy and atomic force microscopy [Christenson *et al.* (2004a), (2004b)]. However, soft segments may also form hydrogen bonds with the hard segments [Guignot *et al.*(2001)]. An illustration of these bonding is given in Figure 2.6.

The effect of hydrogen bonding and its role in phase separation may explain the

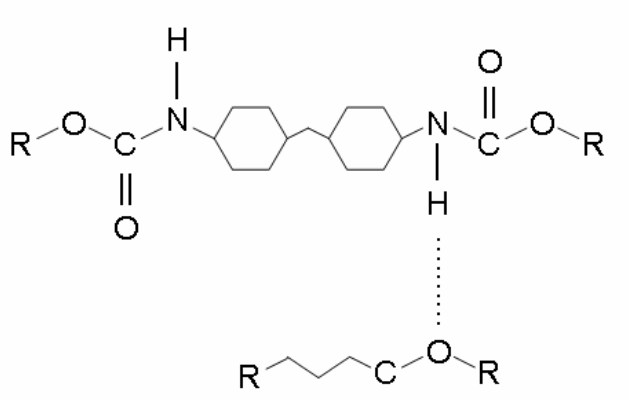

(a)

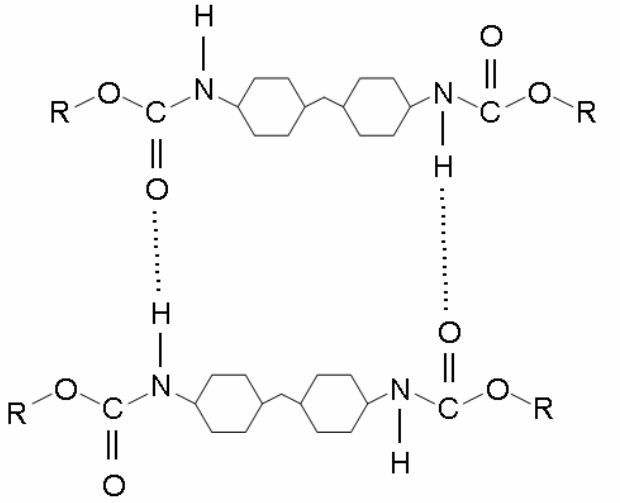

(b)

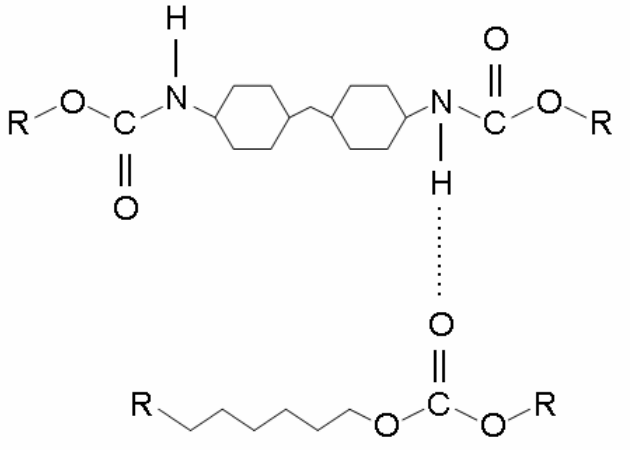

(c)

Figure 2.6: Hydrogen bonding in PU: (a) Urethane Ether, (b) Inter Urethane, (c) Urethane Carbonate

specific mechanical properties of PU. However, some studies have concluded that phase separation does not necessarily enhance the mechanical properties. The extent of hydrogen bonding, or the hydrogen bonding index (HBI), can also be affected by chemical structure and composition of the PU. Christenson *et al.* (2004a) found that PEU exhibits fewer hydrogen bonding than PCU of the same hard segment content. This was thought to be indicative of better phase separation, which was corroborated by the higher modulus data obtainded for PCU. However, AFM images showed clear two-phase morphology of both PUs with no differences in phase mixing. Nevertheless, the effect of hydrogen bonding on the mechanical properties is affected by the number of hydrogen bonds in a segment and the number of interphase bonds. Though it is difficult to isolate these effects from that of the chemical and physical properties of all of the participating molecules.

Plasticisation

Instead of using different types of hard and soft segments, a common method to alter phase separation is to incorporate a plasticiser into the bulk mixture. There are a number of different plasticisers around, which vary in their chemistry (ionic or non-ionic, hydrophobic or hydrophilic), size and shape. Plasticisation of PU may also increase permeability, durability and adhesiveness of a polymer when used in medical sensing applications. All plasticisers increase the elasticity, flexibility and ductility of the polymer with the concomitant reduction of strength, stiffness and toughness. However, low levels of plasticiser may have the effect of decreasing the free volume thus reducing the glass transition temperature. This is known as the anti-plasticisation effect [Vrentas *et al.* (1988)]. With this in mind, an improved mechanical function can be achieved with low levels of plasticiser. This could be especially useful when mechanically weaker components, such as phospholipids or water-rich hydrogels are to be incorporated into a polymer matrix. The role of the polymer as coating material in sensor applications is not only to control the analyte diffusion, to physically protect the device and to improve biocompatibility; it may also act as a fixation matrix for chemical and biological agents. In the later case, the incorporated agent must show resistance to leaching or dissolution by aqueous systems [Davies *et al.* (1992)]. One of the biggest challenge with plasticised polymers is that these plasticising agents migrate and leach. This causes stiffening of the polymer backbone, which may lead to a subsequent decrease in the polymer's lifetime. The interaction of these leachables *in vivo* may also enhance inflammation [Lindner *et al.* (1994)]. In anal-

ogous studies with plasticised PVC, it was found that leachables show to some extend cytotoxicity and may even present a health risk for patients [Hill *et al.* (2003), Tickner *et al.* (2001)].

Plasticisers act by breaking the primary bonds which hold polymer chains together; they then embed themselves between these chains, spacing them apart and thus increasing the free volume which significantly lowers the glass transition temperature. In so doing, the mobility of the polymer chains or chain segments is significantly enhanced. Since these polymer-plasticiser interactions are weak, continuous association and segregation takes place. This enables the plasticiser to diffuse through the polymer and under some circumstances it is able to migrate to the surface. Here it may volatilise if that surface is in contact with air or fluids. Leaching will therefore be a function of the strength of the polymer-plasticiser interaction and the miscibility of the plasticiser respective with the solvent. The most common used plasticisers are phthalates, trimellitates, adipates, phosphates and epoxides [Krauskopf *et al.* (2005)] including ionic and non-ionic surfactants and lipids. While it is understood that polymers used in medical devices need to be chemically inert, leaching of additives and plasticisers is well documented. Numerous studies to identify and quantify leaching components in various polymers have been undertaken [Capek (2005), Hill *et al.* (2003), Jenke (2006), Loff *et al.* (2004), National Toxicology Program (1997), Rahman *et al.* (2006)]; plasticiser for example showed a variable tendency for leaching. In work with PVC, Reddy *et al.* (1997) suggested that plasticiser leaching from the surface of a polymer could provide a surface cleaning action resulting in a protein-free interface therefore improving biocompatibility.

2.2.2 Performance as a Coating Material - Impacts and Strategies

Medical devices, either for long- or short-term use, are an essential part in treating various medical conditions. These devices are made out of synthetic materials, and as they are in intimate contact with living tissue, this could provoke an adverse or delayed adverse effect on the body, e.g. through releasing potential toxins or by triggering an immune response, which would lead to local inflammation and rejection of the device [Wisniewski *et al.* (2000)]. A generic approach to adapting medical devices to the complex biological environment is to apply a polymeric coating to the device, functioning as a protective layer. Characteristics, such as adhesiveness, permeability, mechanical properties, biostability, biocompatibility, surface structure and hydrophilicity are more or less important,

depending on the purpose these polymers, e.g. artificial substitutes for body parts, devices for wireless transmisson, sensors for analyte detection, controlled drug release, encapsulating microspheres or devices collecting energy from the body in order to operate implants.

Adhesive Bonding

The effect of the composition of different segmented PUs with varied crystallinity on adhesion to, for example PVC as an underlying material was investigated by Sanchez-Adsuar (2000). It was found that an increased phase separation and hence higher T_g, resulted in improved adhesion properties. This confirmed the results of Xie *et al.* (1997) in which the adhesive properties of interpenetrating PU on iron as underlying material was tested. Here increased adhesive properties were found the higher the hard segment content. However, adhesiveness of components depends on the chemistry of both, the adherent and the underlying substrate.

Protein Adsorption

Protein adsorption is the first event following the contact of any synthetic material with living tissue [Castner *et al.* (2002)]. Non-specific protein adsorption may occur due to one or more of the following: solvent-protein interactions (supplying the energy to drive proteins from the solution); solvent-surface interactions (adhesion of water to adsorbent surfaces); protein-surface interactions (such as Van der Waals forces, hydrogen bonding, electrostatic and hydrophobic interactions) [Xu *et al.* (2007)]. Analogously to hydration of polymers, Hoffmann (2002) described the character of water in a hydrophilic polymer as follows:

> The first water molecules entering the matrix will hydrate the most polar, hydrophilic groups leading to "primary bound water". As the polar groups are hydrated, the network swells, and exposes hydrophobic groups, which also interact with water molecules, leading to ... "secondary bound water". ... the network will imbibe additional water, due to the osmotic driving force of the network chains towards infinite dilution. This additional swelling is opposed by the covalent or physical crosslinks, leading to an elastic network retraction force.

Hydrophilicity

Surface wettability affects protein adsorption, although scientific reports have not always been consistent. Generally, hydrophobic surfaces are considered to be more protein adsorbent than hydrophilic surfaces. This is due to water molecules being not only attracted to hydrophilic surfaces, but also to hydrophobic surfaces. Van der Waals forces are the main driving force for this hydrophobic hydration [Xu *et al.* (2007)]. When a protein is adsorbed on a hydrophobic surface, its bound water molecules are released at the point of contact and this brings the hydrophobic parts of the protein and the polymer surface into direct contact. This hydrophobic interaction is then followed by a conformational change in the protein as such as hydrophobic amino acids from the core of the protein move to the protein/surface interface. An illustration of a non-specific protein adsorption cascade is illustrated in Figure 1.2.

Ishihara *et al.* (1998) found that for a protein adsorbed on a polymer surface holding a free water fraction similar to an aqueous solution would not need to release bound water molecules during the adsorption process. This protein would then show similar conformation to its native state. It can therefore contact the polymer surface reversibly, avoiding the non-specific build-up of proteins which the body would recognise as foreign. Polarity of a polymer is also crucial since it determines the partitioning and diffusion of solute through a polymer matrix.

The effect of surface hydrophilicity in respect to biofouling has been examined extensively, but with rather controversial outcomes. Very hydrophobic surfaces such as of silicones and fluoropolymers and the hydrophilic and hydrophobic microdomains of PU are also proven to exhibit good biocompatibility.

Surface Texture

Kiremitçi *et al.* (1990) found that polymers with varied physical and chemical properties were obtained with different casting solutions and alteration of preparation conditions. Thus THF and DMF as solvents were leading to nonporous structures, while dioxane produced homogenous porous structures. This was explained by the relative solvency behaviour of a solvent towards a polymer according to Hildebrand values. The nearest these values for solvent and polymer are, the higher the molecular interactions. As a result, the type of solvent has an affect on the precipitation rate; the lower the precipitation rate, the higher the pore density of the polymer.

Studies on the effect of porosity and hydrophilicity regarding to biocompatibility of PU have been conducted by Lin *et al.* (2001). Biocompatibility was examined using myoblasts and monocytes/macrophages. Myoblasts showed the greatest inhibition on smooth, hydrophobic surfaces whereas monocyte/macrophage activation was stimulated at more dense surfaces; hydrophilicity had no influence on activation. In previous studies, Young *et al.* (2000) showed that non-porous polymers inhibited monocyte adhesion. Thus varied surface textures but similar chemistry elicited altered cell proliferation.

Hard- and Soft Segments

Li *et al.* (1996) synthesised PU based on cholesterol and phosphatidyl-choline analogous moieties with varied hard and soft segments. There was a great difference observed for polymer surfaces exposed to air or glass during casting with regard to platelet adhesion. For all of the cast polymers, the air exposed side showed fewer platelets adherent compared to that of the side in direct contact with the glass surface, which was thought to be mainly caused by differences in surface morphology. Lyman *et al.* (1975) and Picha *et al.* (1978) showed that chemical structure, molecular weight and surface morphology were related to protein adsorption and blood coagulation. Sa da Costa *et al.* (1983) reported on platelet retention experiments on PU of varied hard and soft segment ratios showing that there was a clear relationship between these ratios and platelet retention. This was confirmed by further studies, where the concentration of hard segment in PU correlated with thrombogenetic potential. It was suggested that surface mobility, crystallinity and hydrogen bonding play a significant role in platelet adhesion.

Huang *et al.* (1999) investigated the effect of varied hard segment ratio including different preparation techniques. It was found that an increased C=O/C=C ratio, hence increased hard segment content at the surface correlated with increased protein fouling. Bélanger *et al.* (2000) evaluated a range of commercial PU *in vitro* and *in vivo* for their biocompatibility and haemocompatibility. High levels of monocyte viability and reduced cell viability was observed for all of these polymers. However, only PU with carbonate moieties in their soft segments showed haemolytic properties.

Okano *et al.* (1981) studied the effect of hydrophilic and hydrophobic microdomains of a copolymer regarding interaction with blood platelets. Block copolymer composed of hydrophilic (HEMA) and hydrophobic (styrene) monomers were synthesised creating microphase separated structures and altered morphological patterns. A suppressed

platelet adhesion and deformation was observed on the surface of the block copolymers that contained hydrophilic-hydrophobic lamellae or isolated hydrophilic islands. Homopolymers and random copolymers showed a higher degree of platelet adhesion and aggregation. Takahara *et al.* (1991) synthesised various PU containing either hydrophobic or hydrophilic soft segments. Segmented PU based on hydrophobic soft segments showed distinct microphase separation and also the least platelet adhesion, especially the siloxane-based PU. Interestingly, PEO-based PU showed increased platelet deposition over time.

These findings were in contrast to that of Yoo *et al.* (2004) who found multiblock PU containing various amounts of PEO to show less platelet adhesion when more hydrophilic. By analogy with PEO, Jeon *et al.* (1991) found that a large free water fraction (hydrophilicity) is not the sole reason for anti-fouling properties - longer, more flexibile polymer chains as outer polymer coating were suggested to play a vital role in suppressing adsorption. Okkema *et al.* (1989) evaluated the blood-contacting properties of a series of PEU with varied weight percentage of PEO soft segments. The results indicated that the higher the PEO content, the more thrombogenic. It appeared that a threshold concentration of PEO was required to affect the haemocompatibility.

Morimoto *et al.* (2004) reported on reduced platelet adhesion and activation at semi-interpenetrating polymer composed of PU and cross-linked phospholipid polymer chains on the surface. These findings were confirmed by Yoo *et al.* (2005) who reported decreased platelet adhesion with increased amount of phospholipid, hence hydrophilicity. Nair *et al.* (1992) found that highly hydrophilic PU elicit inert responses *in vivo* in contrast to highly hydrophobic PU. They also found that interfacial energy did not correlate with tissue responses whereas previously it was proposed that interfacial energy near zero is a requirement for good biocompatibility. Mathur *et al.* (1997) implanted PEU, PCU and PDMS end capped PEU subcutaneously into rats and found a much reduced total cell coverage with PDMS end-capped PU. PDMS was found to accumulate at the polymer surface increasing hydrophobicity, lowering the surface energy which then has the effect of lowering adsorption of adhesion-mediating proteins, thus lowering macrophage adherence. In addition, the high mobility of the end groups may result in retarded protein deposition. These contradictory findings however suggest that hydrophilicity concomittant with surface free energy plays a role regarding biofouling.

Degradation

The chemical stability of an implant material is important and degradation can lead to significant changes in mechanical properties, surface chemistry and structure. Polymer modifications, for example hydroxylation may be accompanied by significant degradation and care has to be taken regarding the method to choose. Bamford *et al.* (1994) studied polypropylene microporous hollow fibres for degradation as by reason of their construction these fibres are said to be especially sensitive to degradation and can be used as a negative control to evaluate the performance of other polymers e.g. PU. The results showed that whilst degradation occured, it is less severe with PPDS for hydroxylation than other hydroxylation methods, such as the commonly ozonisation. The major cause of degradation at PU is hydrolysis and oxidation [Christenson *et al.* (2004a,b); McCarthy *et al.* (1997); Tanzi *et al.* (1997)].

Polymer degradation in plasma or tissue usually starts off with adsorption of aqueous medium onto the surface and solute diffusion into the bulk. This is then followed by chemical reactions with unstable bonds and leaching of degradation products out of the polymer matrix. If the PU is hydrophobic, degradation is mainly occuring at the surface. However, if the polymer is hydrophilic, water will also be present in the bulk and degradation may occur throughout the material.

During hydrolysis, molecules are split into smaller molecules by reaction with water. This is one of the dominant mechanisms for polymer breakdown in the aqueous environment of the body. *In vivo*, cells might migrate onto or into the polymer matrix releasing acids, oxidants and enzymes which might catalyse hydrolysis. Hydrolytically unstable bonds in PU include ester and amide linkages. When the ester linkage hydrolyses, acid groups are produced, further increasing the acidity surrounding the degrading PU which may autocatalyse its destruction.

Hydrolysis appears to be facilitated by polar groups in the side chain of a polymer backbone. Under physiological conditions, hydrolytic cleavage reactions are essentially irreversible. Mechanisms of oxidation include auto-oxidation, oxidation by peroxides, free radicals, enzymes, environmental stress cracking and metal ion oxidation [Schubert *et al.* (1997a,b); Ward *et al.* (2007)].

During oxidative cleavage of PEU, free oxygen radicals degrade the α-carbon of the ether soft segment to form an ester. This ester linkage may be further degraded via acid-catalysed hydrolysis by cleaving the urethane linkage [Schubert *et al.* (1995)]. Christenson

et al. (2004a) proposed a route of soft segment degradation in PEU as illustrated in Figure 2.7 and that of PCU is illustrated in Figure 2.8; a possible route of hard segment degradation of a generic polyurthane was also proposed and is illustrated in Figure 2.9.

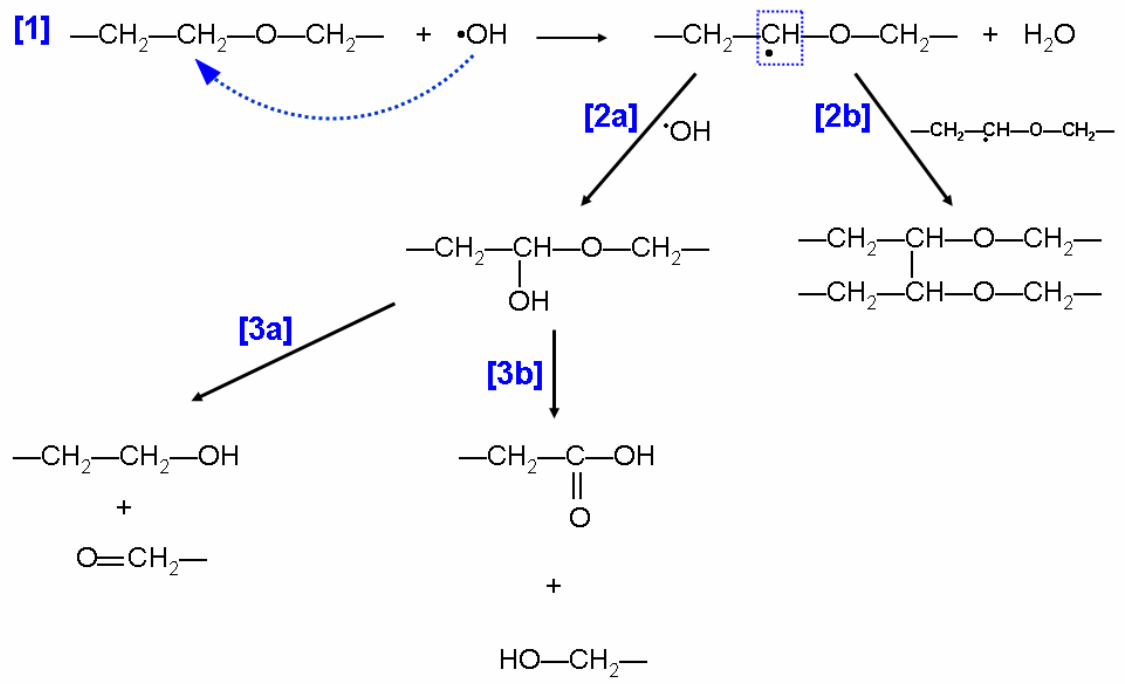

Figure 2.7: Possible route of soft segment oxidation in PEU [modified from Christenson *et al.* (2004a)].
The proposed oxidative degradation starts with [1] radical initiation: a hydroxyl radical abstracts an α-methylene hydrogen atom of the ether soft segment forming a carbon radical; this is followed by [2a] an addition reaction between hydroxyl radical and carbon radical. This hydroxylated soft segment undergos further chain scission forming [3a] an aldehyde or [3b] an alcohol and carboxylic acid. The carbon radical from radical initiation reaction [1] could also crosslink with another carbon radical as shown in [2b].

Takahara *et al.* (1991) found that siloxane soft segments on PU remain unchanged under both hydrolytic and oxidative environments. Polycarbonate soft segments were found to be more stable to biodegradation, environmental stress cracking and metal ion oxidation than polyether soft segments [Stokes *et al.* (1990)], although acid catalysed hydrolysis has been hypothesised to cause biodegradation of the carbonate bond leading to carbon dioxide and alcohols [Mathur *et al.* (1997)].

McCarthy *et al.* (1997) evaluated three different commercial PEU, namely Pellethane, Tecoflex and Biomer, for physical and chemical degradation *in vivo*. Physical degradation in the form of general roughening and cracking was observed in all samples. Uniform pitting and superficial fissuring was observed in Biomer, whereas Pellethane and Tecoflex showed severe localised embrittlement with fissures infiltrating into the bulk.

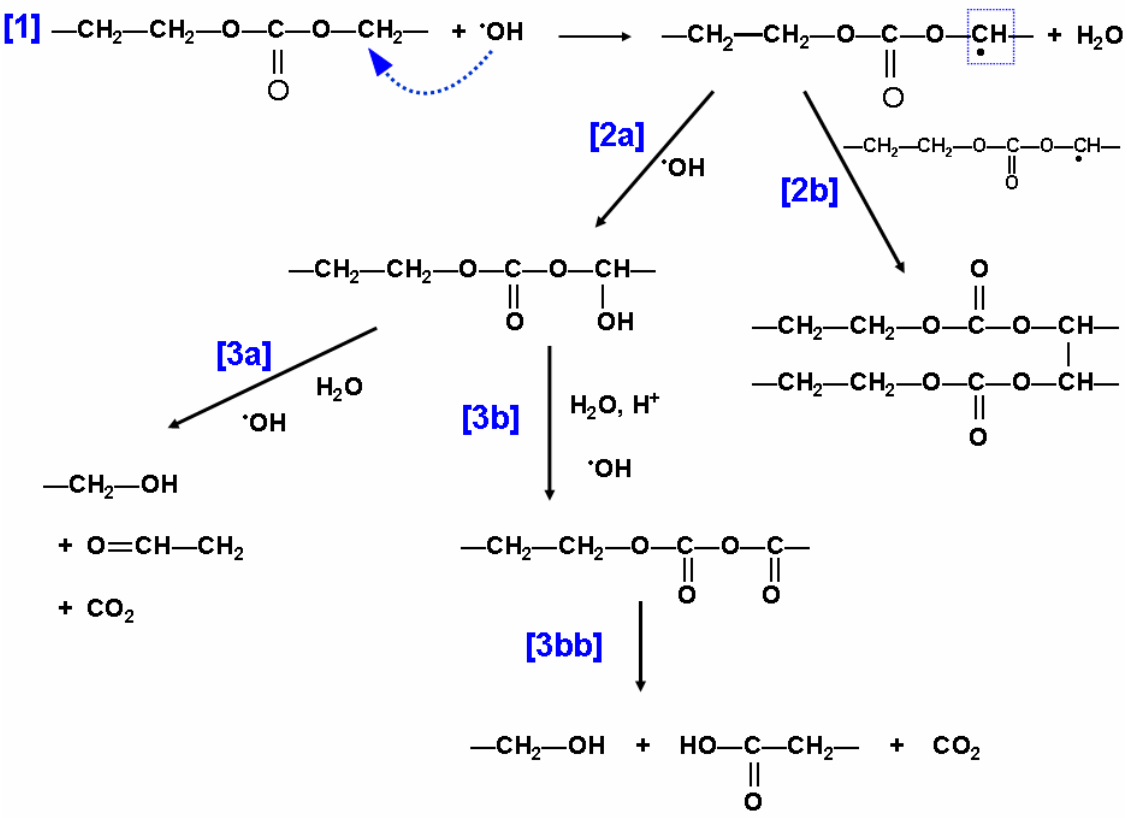

Figure 2.8: Possible route of soft segment oxidation in PCU [modified from Christenson *et al.* (2004a)].
The proposed oxidative degradation starts with [1] radical initiation: a hydroxyl radical abstracts an α-methylene hydrogen atom of the carbonate soft segment forming a carbon radical and water; this is followed by [2a] an addition reaction between hydroxyl radical and carbon radical to form a hemiacetal which then undergoes further oxidation via chain scission with the formation of [3a] aldehyde, alcohol and carbon dioxide or [3b] an intermediate ester followed by scission to [3bb] carboxylic acid, alcohol and carbon dioxide. The carbon radical from radical initiation reaction [1] could also crosslink with another carbon radical as shown in [2b].

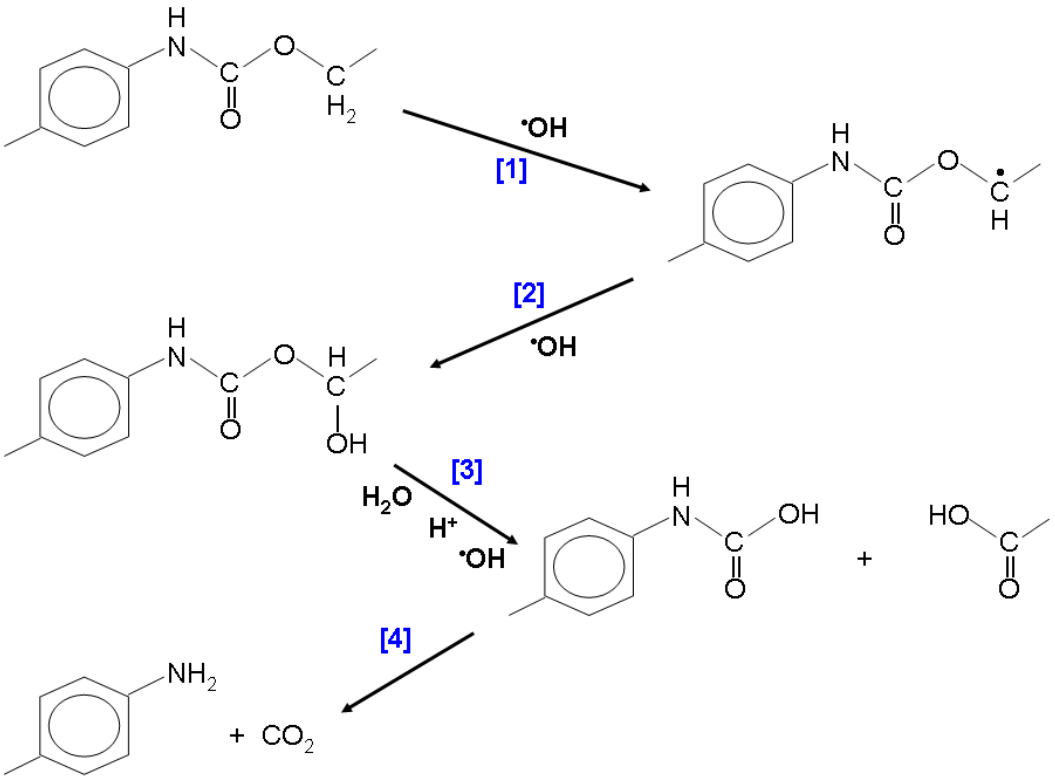

Figure 2.9: Possible route of hard segment oxidation in generic PU [modified from Christenson *et al.* (2004a)].
The proposed oxidative degradation starts with [1] a hydroxyl radical abstracts an α-methylene hydrogen atom of the chain extender at the urethane, this is then followed by [2] intermediate addition reaction between hydroxyl radical and the chain radical to form a carbonyl-hemiacetal; [3] oxidative hydrolysis of the carbonyl-hemiacetal resulting in chain scission to form carbamic acid and carboxylic acid end groups; [4] chain scission of the carbamic acid resulting in the formation of a free amine and carbon dioxide.

The chemical changes associated with biodegradation were observed as severe oxidation of the aliphatic polyether soft segment and hydrolysis of the urethane bonds joining hard to soft segment in all of these samples. Tecoflex was also found to be susceptible to localised hydrolysis of the urethane bond within the aliphatic hard segment. Biomer showed evidence of a significant non-specific hydrolytic degradation, producing uniform changes throughout the bulk. Exposure to light might also have a detrimental effect to the stability of PU, which would depend on what kind of isocyanate is used.

Christenson *et al.* (2004a) published on the oxidative mechanisms of polycarbonate and polyether urethane biodegradation *in vitro* under accelerated conditions using an oxidative solution that simulated the microenvironment at the adherent cell-material interface. Soft segment chain scission and crosslinking was observed at both PU; however, it was more pronounced on PEU. Scanning electron microscope images showed pitting on both PU surfaces though the pit size was smaller on PCU. These results were confirmed with *in vivo* studies conducted by the same group [Christenson *et al.* (2004b)].

2.2.3 Surface Functionalisation - Hydroxylation

Several methods for surface functionalisation are available including ozonisation or nitration, some of which use aggressvie methods or chemicals. As pre-fabricated biomedical devices often include polymers, they could suffer damage under severe treatments. Bamford *et al.* (1994) outlined a procedure requiring mild conditions and aqueous media using potassium peroxodisulphate for surface hydroxylation. Such functionalised surfaces may then be submitted to further treatment such as grafting of phospholipids [Korematsu *et al.* (2002)], sulfo-ammonium zwitterions [Zhang *et al.* (2003)], acrylamides or heparin [Bamford *et al.* (1996)].

The thermal decomposition of peroxodisulphate in aqueous media is likely to occur according to the reactions shown in Figure 2.10:

$$
\begin{aligned}
{}^{-}O_3SO - OSO_3^{-} &\rightarrow 2SO_4^{\bullet -} \\
SO_4^{\bullet -} + H_2O &\rightarrow HSO_4^{-} + {}^{\bullet}OH \\
2{}^{\bullet}OH &\rightarrow H_2O + \tfrac{1}{2}O_2
\end{aligned}
$$

Figure 2.10: Thermal decomposition of peroxodisulphate in aqueous solution [adapted from Bamford *et al.* (1994)]

The formation of a hydroxylated polymer may proceed by a number of routes, since interaction between hydroxyl radicals ($^{\bullet}OH$), sulphate radicals ($SO_4^{\bullet -}$) and peroxodisulphate anions ($^{-}O_3SO - OSO_3^{-}$) or macroradicals are possible [Bamford *et al.* (1996)]. Figure 2.11 shows one possible reaction in which hydrogen abstraction from the polymer by a hydroxyl radical (in this example a simple vinyl polymer) would occur and further, that the resulting macroradical would combine with a second hydroxyl radical yielding a hydroxylated polymer. Other processes which do involve sulphate radicals may also bring about hydroxylation (Figure 2.12).

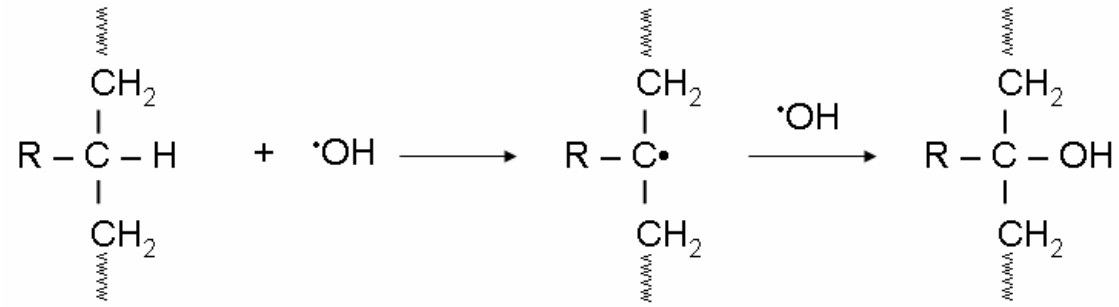

Figure 2.11: Hydroxylation process involving hydroxyl radicals [adapted from Bamford *et al.* (1996)]

Sperling *et al.* (2007) published on *in vitro* blood reactivity of hydroxylated and non-hydroxylated polymer surfaces to investigate on the influence of surface polarity and chemistry towards protein adsorption, utilising an aminosilane layer over a maleic anhydride copolymer. After incubation with human blood, the hydroxylated samples showed the lowest levels for fibrin and fibrinogen adsorption in comparison with the non-hydroxylated samples. These findings confirmed previous studies in which self-assembled monolayers of alkanethiols with various terminating groups such as -OH, $-CH_3$ and -COOH were compared towards haemocompatibility [Sperling *et al.* (2005)].

2.2.4 Surface Grafting - Sulphonation

Another route to combat biofouling is to introduce negative charges to polymer surfaces, acting as a barrier for the negatively charged biological compounds present in biological fluids. The benefit in medical amperometric sensing applications is that electroactive interferents, which are mainly negatively charged, would also be rejected. Lelah *et al.* (1985) chemically modified PEU into zwitterionomer-, anionomer- and cationomer-type polymers and investigated the effect of ionic domains on platelet and fibrinogen deposition in

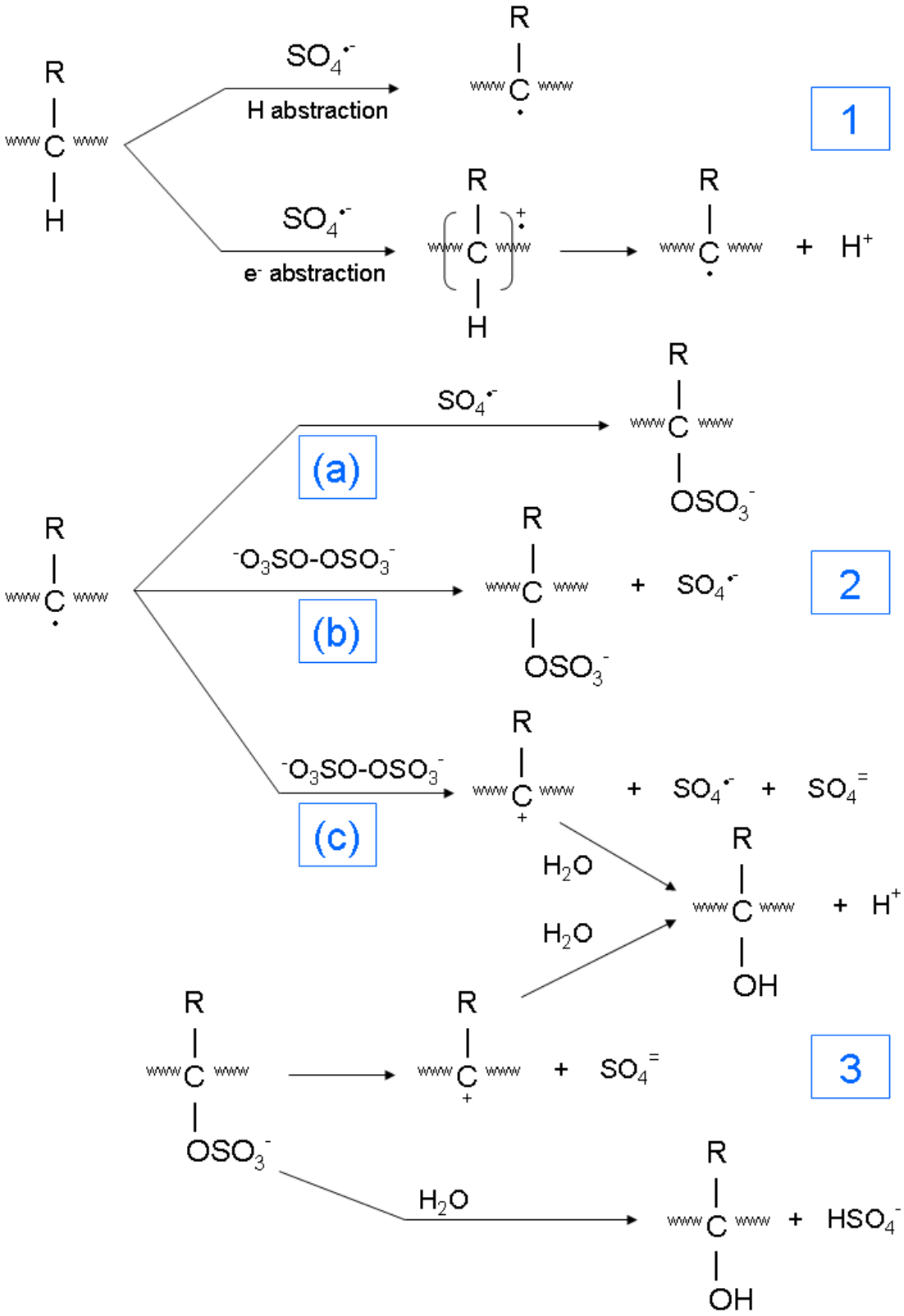

Figure 2.12: Hydroxylation process involving sulphate radicals [adapted from Bamford *et al.* (1996)] *Proposed hydroxylation mechanisms: (1) Formation of intermediate macro radicals either through abstraction of hydrogen or* e^-*. (2) These radicals undergo further reactions (a) with sulphate anion-radical or (b) decomposition of peroxidic initiator (peroxodisulphate anion) and subsequent reaction with sulphate radical or (c)* e^- *abstraction with subsequent formation of a carbo-cation. (3) Formation of an intermediacte carbo-cation with subsequent hydration or direct hydration.*

an *ex-vivo* experiment using canine blood. Cationised surfaces showed increased thrombogenicity and anionised surfaces showed reduced levels of platelet and protein adhesion, however zwitterionic surfaces showed the least fouling. It was suggested that the synergistic effect of both charges created a favourable surface for improved anti-fouling properties. The effect of the isoelectric point (pI) of a protein and the pH of the environment which determines the net charge of a protein as well as the zeta potential of a polymer surface are not inconsequential to biofouling [Gong *et al.* (2004)].

Incorproation of sulphonate groups in biomaterials have been attempted by many investigators and became strong contenders not only due to their negative charge, but also because their key functional groups are similar than thouse present in bioactive molecules, such as the anticoagulant heparin. Heparin is highly sulphated and is said to have the highest negative charge density of any known biological molecule and its sulphonate and aminosulphate groups are believed to be of great importance in its anticoagulant activity. Heparin has also been used directly to give anticoagulant properties at a polymer, e.g. by dispersion, ionic bonding and covalent immobilisation. However, the resulting materials had limitations; heparin lost bioactivity by the covalent binding and was subjected to *in vivo* degradation [Labarre (1990)]. Nevertheless, heparin-like materials bearing functional sulphonate groups has received much attention. Numerous studies on heparinoid polymers have been carried out, typical materials include polyvinylsulphonic acid, sulphonated polydienes, sulphated chitosan, sulphonated polystyrenes, polysaccharides, polysulphohexyl methacrylate and sulphonated PU.

Hunt *et al.* (1996) conducted *in vivo* experiments with PEU in which sulphonate ionic groups were incorporated into the polymer backbone of varied concentrations, resulting in a range of negative charges. Initially, macrophages and neutrophils were observed at all samples, but neutrophils were absent after 12 weeks, with macrophage infiltration elevated initially and reduced in later time points. So while net surface negative charge had an influence on biofouling, results were not conclusive in all cases.

Keogh *et al.* (1996) developed a surface derivatisation technique based on the generation of surface free radicals by Ce^{IV} ion and the subsequent graft copolymerisation of 2-acrylamido-2-methylpropanesulphonic acid monomers directly onto PU surfaces. It was anticipated that the increase of hydrophilicity would prevent non-specific adsorption and denaturation of proteins while the sulphonation might mimic heparinoid activity, displaying anticoagulant properties. *In vitro* experiments conducted in human blood showed

reduced clot formation and platelet activation along with reduced neutrophil adherence, but when materials were implanted in dogs, increased macrophage and thrombus formation was observed. It was suggested that this apparent contradiction was a function of species differences in view of marked heterogeneities among clotting factors of different mammalian species [Dewanjee *et al.* (1992), Shibuya *et al.* (1994)].

Skarja *et al.* (1997) published on platelet interactions of a series of PU with sulphonated chain extenders of different structures. It was thought that the distribution and conformational mobility of sulphonate groups in combination with differences between surface and bulk composition and changes in the degree of phase mixing would affect platelet adhesion and protein adsorption. However, these were found to be high on all materials. This was not expected as it was shown by various investigators that albumin exerts an inhibitory effect on platelet adhesion [Absolom *et al.* (1984), Jenkins *et al.* (1973), Packham *et al.* (1969), Salzman *et al.* (1969)]. It was suggested that this is due to platelets exhibiting binding sites specific for sulphonate groups, which confirmed the findings published by Suda *et al.* (1993) in which it was reported that platelets bind to sulphate groups of heparin via direct ionic interactions due to the positively charged amino acids of the platelet membrane.

Kim *et al.* (2003) investigated the "negative cilia effect" of sulphonated PEO grafted on PEU via bulk modification regarding calcification, protein adsorption and platelet adhesion. Free isocyanate on PU was utilised for coupling with PEO derivatives, these derivatives were converted into sulphonate groups by the reaction with propane sultone. It was hypothesised that grafted $PEO - SO_3$ may exhibit a heparin-like anticoagulant activity and that this may be synergistic with the dynamic mobility of PEO chains and the negatively charged sulphonate groups. The perpendicular orientations of these flexible PEO chains were thought to be increased by electric repulsion between sulphonate end groups. The negatively charged sulphonate groups would also expel negatively charged proteins and platelets. Indeed, platelet adhesion and total protein adsorption was decreased, though albumin adhesion was enhanced. Despite the electrostatic attraction between sulphonate groups and positively charged calcium ions, a decrease in calcification was observed. This suggested that calcification was associated with cell interactions of various phagocytic cells instead of ion interactions.

Evaluation

A wide range of materials are now available and in order to ensure an adequate performance for a given application, the material has to be chosen according to desired chemical and mechanical properties. These properties may include mechanical strength, porosity, mass transport properties, degree of swelling and permselectivity and can be controlled by variations in the polymer composition, the crosslink density and the preparation conditions. Several strategies to design non-fouling biocompatible polymer surfaces have been outlined which employed novel techniques such as incorporation of surface active additives or charged compounds including amphiphiles, blending of siloxane, fluorinated compounds or alkyl chains into the polymer matrix. Biofouling with a concomitant foreign body reaction is a complex process which becomes apparent regardless of the outlined approaches.

Surface wettability plays a major role in protecting against protein fouling and it was found by many investigators that the more hydrophilic the polymer, the less non-specific protein adhesion. However, hydrophobic candidates have also proven to exhibit good biocompatible characteristics. Nevertheless, poor mechanical properties associated with high water content are of detriment when highly hydrophilic materials are used. This could be a problem especially when materials are subjected to mechanical forces, e.g. membrane rupturing has been repeatedly reported [Lewis (2000), Li *et al.* (1997)].

A clear relationship between the hard and soft segment ratios in PU and the platelet retention index has been outlined. Elbert *et al.* (1996) suggested that minimal phase separation was desirable, however, the favourable blood contact properties of PU may in fact come from the presence of microdomains within the polymer matrix, which has an influence on how proteins adsorb to the surface. The charge on the surface is also of importance; net surface negative charge has been found to play a role in biofouling as well as zwitterionic surfaces. Work has also demonstrated that it is not merely the chemical identity of a water-soluble polymer that determines its biocompatibility, but also its molecular weight and the details of its incorporation and display at the material surface. A polymer that is elastomeric, contains a large percentage of water-soluble compounds with resistance to degradation and biofouling has not yet been achieved.

In this study, polymers are developed to be utilised on needle-type electrodes and applied via by dip-coating. Hence it would be more practical to apply a bulk-modified polymer directly onto the electrode surface instead of surface modifying applied poly-

mer coating. This method would appear to be much more gentle to delicate devices as they do not have to undergo possible device damaging procedures such as exposure to strong chemicals, high temperatures, potentially corrosive additives etc. However, every bulk modification will inevitably elicit changes in physical and chemical characteristics concomitant with an altered performance of the polymer.

For PU, there is a range of well characterised materials with acceptable mechanical properties already available and by modifying the surface, the bulk properties will be retained. Some surface modifications include grafting, high-energy treatments, self assembled monolayers, surface patterning, immobilisation of functional groups and molecules. Most of these methods cannot be performed on membranes which surround delicate medical devices without compromising the analytical performance of these devices.

The approach taken in this study for an improved biocompatibility was to alter the polarity of the polymer surface by hydroxilation. However, hydroxylation may affect hydrogen bonding within the polymer matrix, which subsequently would affect the degree of phase separation. Wide research into how hydroxylation affects the surface properties and the electroanalytical performance of PU has not, however, been undertaken. How hydroxylation affects the surface properties and the performance in electrochemical analtye detection was therefore investigated in this study. A new method of surface sulphonation of functionalised PU was pursued and assessed together with hydroxylated and unmodified PU.

For SR, the influence of different solvents towards the properties of solution-cast polymers concomitant with different casting and curing methods was studied. The general aim was to manipulate hydrophilicity, permeability to H_2O_2 and biocompatibility.

2.3 Electrochemical Analyte Detection

2.3.1 Introduction

Electrochemistry is an area of science which deals with the transformation of electrical energy into chemical energy and vice versa. These electrical responses are then converted via a physical transducer into an observable response [Crow (1988)]. It should be pointed out that there is a clear difference between biosensor and chemical sensor. Chemical sensors used within biological systems are not regarded as biosensors. The term “bio” is exclusively reserved for the type of recognition element used within the sensor, which

has to be of biological source, e.g. enzymes [Thévenot *et al.* (2001)]. Electrochemical principles are widely used in scientific fields, such as biology (nerve response, cell membrane equilibria, pH dependence of amino acid and protein equilibria, ion-body fluid redox equilibria), chemistry (corrosion) and physics (power supply).

Cyclic Voltammetry

In developing new types of electrodes, it is important to characterise the electrode reaction, as well as the electrode response to the analyte of interest. During electrochemical reactions, the oxidised or reduced species is consumed at the electrode surface, forming a concentration gradient in the solution around the electrode. Because molecules diffuse from areas of high concentration to areas of lower concentration in order to establish equilibrium, the oxidised or reduced species diffuses towards the electrode. The affected region is called the diffusion layer. The diffusion layer increases in thickness over time. The thickness of the diffusion layer also increases with increasing electrode size. The shape of the diffusion layer depends on electrode size, being planar for macroelectrodes and hemispherical for microelectrodes.

A conventional macroelectrode using a standard redox couple generates a peak anodic current (i_a^p) corresponding to a peak oxidation potential (E_a^p) and a peak cathodic current (i_c^p) corresponding to peak reduction potential (E_c^p). An illustration of a generic CV is shown in Figure 2.13.

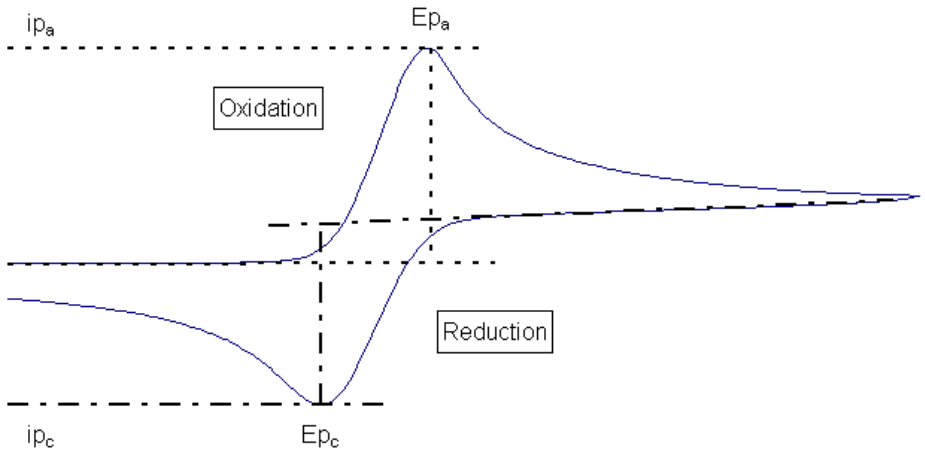

Figure 2.13: Model CV of conventional macroelelectrode in solution containing redox active species

However, due to the increase in mass transfer caused by radial diffusion, microelectrodes produce sigmoidal curves (Figure 2.14). Thus, the shape of the voltammogram provides information about the characteristics of the electrode.

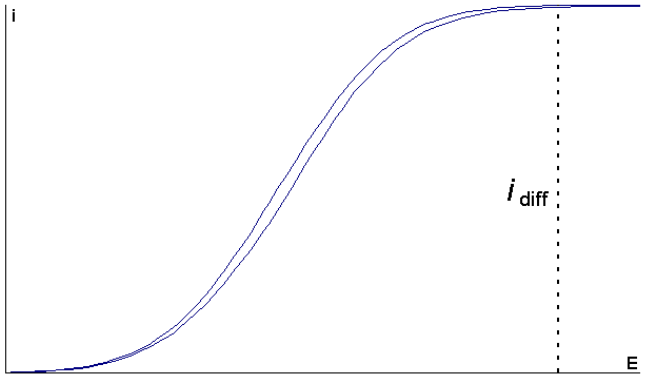

Figure 2.14: Model CV of microelectrode in solution containing redox active species

Cyclic voltammetry (CV) is a common electrochemical tool used to investigate the initial chemical reactions occurring at an electrode surface. CV has been used to determine electron transfer kinetics, e.g. rate constants of thermodynamically reversible redox systems, the rate of chemical reactions for simple systems, and the number and stability of oxidation states. CV has been used to determine the oxidation and reduction characteristics of compounds, and the potential at which oxidation and reduction occur. CV has also been used to identify oxidation and reduction reactions in complex systems containing multiple redox reactions, and to determine whether a reactant adsorbs to the electrode surface or remains in solution.

Finally, CV has been used to define apparent diffusion coefficients and the real surface area of a working electrode [Ho *et al.* 2003; Yamauchi *et al.* 2005]. A thermodynamically reversible redox system can be defined by:

$$O + ne^- \rightleftharpoons R$$

in which the oxidised (O) and reduced (R) species of an electrode reaction are in equilibrium at the electrode surface, and ne^- is the number of electrons required for the reaction. The variation in the ratio of the oxidised and reduced species as a function of potential is the basis of all voltammetric methods. As long as diffusion is the limiting mass transport regime, the CV of a reversible system has a specific and well-defined characteristic. Nernst established that thermodynamically, the probability that a molecule

will be electrolysed as shown in the equation above is given by:

$$E = E_o + \frac{RT}{nF} \ln\left(\frac{aO}{aR}\right)$$

in which E is the potential applied to the electrode surface, E_o is the standard potential, R is the gas constant, T is the temperature, n is the numnber of electrons transferred, F is the Faraday constant, aO and aR are the activities of the relevant species. At low concentrations of the relevant species, the activity coefficients tend to unity and can be replaced by concentrations. If these characteristics do not hold, electron transfer is not reversible on the timescale of the experiment.

In a totally irreversible system, the absence of a reverse peak is obvious. If the electron transfer is insufficient to maintain surface equilibrium with increased mass transport, peak potential varies with the scan rate. In this case, the voltammogram may appear drawn out, as the peak separation increases with increasing scan rate until the reverse peak disappears. Often reactions are reversible at low scan rates and irreversible at high scan rates. The transition state between these two is known as quasi-reversible, in which case the voltammogram shows a blend of characteristics of both systems.

Ferri/Ferrocyanide Redox System

A number of well-known reversible redox systems are considered standard redox couples, including ruthenium(II/III) hexaammine, hexachloroiridate(III/IV) and ferri/ferrocyanide. Ferri/ferrocyanide was used as a redox couple in the present study. The standard potential of ferri/ferrocyanide in relation to the Normal Hydrogen Electrode (NHE) is:

$$[\mathrm{Fe(CN)_6}]^{-3} + e^- \rightleftharpoons [\mathrm{Fe(CN)_6}]^{-4} \qquad E^o = +0.36\ V \text{ vs. NHE}$$

Under standard conditions, this system has fast electron transfer kinetics, is a simple one-electron reaction, and forms well-defined single oxidation and reduction peaks. As the response of this standard redox couple in solution is already well characterised, it can be used to produce predictable cyclic voltammograms. It has specific forms, depending upon the size and type of electrode used.

Some authors have suggested that a passivating layer of Prussian Blue is formed in the ferri/ferrocyanide redox system, or that ferricyanide and/or ferrocyanide ions themselves adsorb on the electrode surface during potential cycling [Beriet *et al.* (1993), Huang *et*

al. (1992), Kunimatsu *et al.* (1989)]. If this is the case, the rate of electron transfer may be suppressed, and the reversible nature of the electron transfer reaction might decrease, resulting in a quasi-reversible reaction. Other researchers found no evidence of adsorbed species on the electrode surface during their experiments [Christensen *et al.* (1988), Emery *et al.* (2005)].

Amperometry

Steady state amperometry is based on the principle that a specific substance oxidises or reduces at noble metal surfaces at a specific potential that is a characteristic of that chemical species. In this mode of operation, an appropriate potential is held constant between the reference and working electrodes to generate a diffusion limiting current. Provided that there is a stable unstirred layer around the electrode sensing tip, the electrochemical reaction produces a current which is directly proportional to bulk analyte concentration. Convective effects can be minimised by covering the electrode with a membrane and by reducing the electroactive surface. Steady state amperometry offers high sensitivity for analyte concentrations as low as 10^{-6} to 10^{-9} M, provided that the magnitude of the potential is sufficient to oxidise or reduce the analyte at the electrode surface.

Electrochemical sensors are designed to function within specific criteria of performance, these include linearity, sensitivity, response time, detection limit, recovery time, reliability, operational lifetime, reproducibility, selectivity and signal-to-noise ratio [Carr *et al.* (2005), Stefan *et al.* (2001), Thévenot *et al.* (2001)]. The baseline current, which is subtracted from the sensor signal, is also an important factor in sensor design. The magnitude of the baseline current depends on the material, geometry and surface area of the electrode, and also on the electrolyte; it is produced by the electrode when a DC potential is applied between the anode and the cathode in electrolyte without the presence of the target analyte.

Figure 2.15 shows a theoretical plot of current output in amperometric measurements which details the sections of the time response of a generic polymer coated sensor until steady state current is reached.

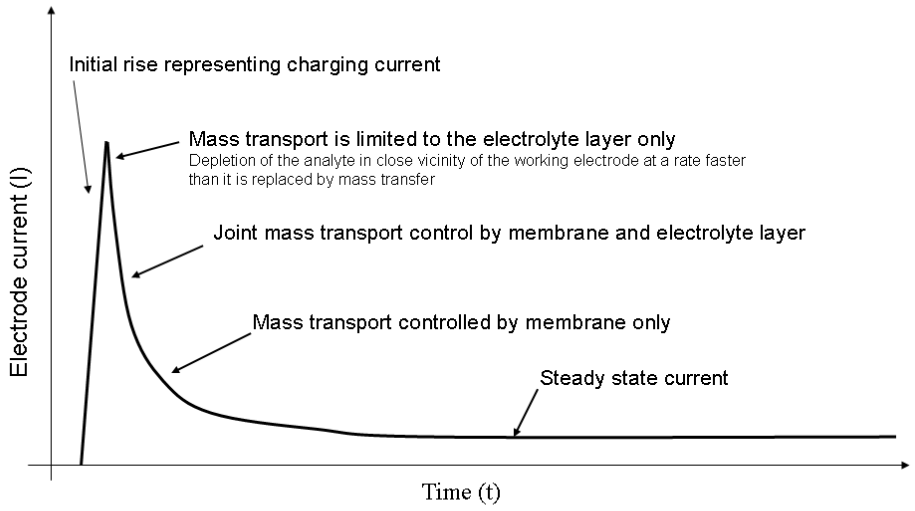

Figure 2.15: Theoretical plot of current output in amperometric measurements of a generic polymer coated sensor until steady state

2.3.2 Microelectrode Characteristics

Microelectrodes have seen widespread use over the past two decades. The definitions of a microelectrode varies, but generally, it is an electrode where surface dimensions are at least one dimension of the order of micrometers smaller than the thickness of the diffusion layer formed on the timescale of the electrochemical experiment [Bard *et al.* (2001)]. However, an electrode with dimensions of ~ 50 μm can be considered as a microelectrode [Imisides *et al.* (1996)]; another term being ultramicroelectrodes, which was defined as an electrode with dimensions smaller than 25 μm [Zoski (2002)]. Microelectrodes are available in different geometries; such as disk, line, cylinder and ring shapes. The most widely used geometry is the disk microelectrode; they are simple to fabricate, easy to maintain and they conform well to diffusion layer theory [Bard *et al.* (2001)]. Due to their small size, microelectrodes offer several advantages, e.g. they can be used *in vivo* and also require only small sample volumes. These properties are especially advantageous for applications in which a microenvironment needs to remain as undisturbed as possible. It is also possible to use the electrodes in solution without electrolyte; because of low currents passing though the cell, higher solution resistances can be tolerated, also reducing the iR drop.

2.3.3 Factors Affecting the Electrode Processes

Thermodynamic and kinetic properties need to be considered in electrochemical reactions. The overall electrochemical reactions taking place at an electrode is governed by the rates of processes such as:

- mass transport to and from the electrode surface
- electron transfer at the electrode surface
- chemical reactions prior to or following electron transfer
- surface reactions, e.g. adsorption, desorption or electrodeposition

Mass Transport

There are three mechanism of mass transport in a solution: migration, convection and diffusion. Convection is the movement of ions and/or molecules in a solution by hydrodynamic transport (thermal effects, stirring). Natural convection is caused by density gradients and forced convection is caused by laminar/turbulent flow and stirring. Migration is the movement of charged ions, cations and anions, in a solution under the influence of an applied potential. Diffusion arises from uneven concentrations between two bulk phases. Entropic forces are the main driving force to smoothen out uneven distributions of concentrations within the solution.

During an electrochemical reaction, the analyte is consumed at the electrode surface and a concentration gradient develops between the electrode and the bulk solution. To re-establish equilibrium, molecules diffuse toward the electrode to replace those being consumed at the electrode surface. However, as these molecules are continuously consumed, equilibrium cannot be established and molecules keep diffusing to this "starved" area maintaining the electrochemical reaction; this area or layer is called the diffusion layer. Fick's First Law determines diffusion of analyte towards a planar electrode surface. It shows that the rate of diffusion is proportional to the surface concentration of the reactant as shown in the following equation:

$$J_o = -D_o \left(\frac{\delta C_o}{\delta X} \right)$$

in which J_o is the flux of a species to the electrode and D_o is the diffusion coefficient of the species and has a negative sign because molecules move always from an area with

higher concentration to an area with lower concentration. C_o is the surface concentration gradient of the analtye and X is the distance from the electrode.

The Cottrell equation describes the change of current as a function of time with a fixed applied potential under diffusion limited conditions (presuming a planar electrode) as such:

$$I = nFAC_o\sqrt{\frac{D}{\pi t}}$$

where I is the measurable current, n is the number of electrons transfered, F is the Faraday constant, A is the surface area of the electrode, D is the diffusion coefficient of the species, t is time and C_o is the concentration of species in the bulk solution. Since conditions are diffusion limited, the surface concentration would be effectively zero and therefore, the measured current can be related to the bulk concentration. At the onset of an electrochemical reaction, the diffusion layer in an unstirred solution grows as a function of time. Initially, the growth of the diffusion layer is similar for micro- and macroelecrodes, however, later the smaller the electrode, the smaller the depth of the diffusion layer at $t > 0$. Consequently, the diffusion gradient and so mass transport is significantly higher at a microelectrode and further enhanced by spherical diffusion. Additionally, steady-state rates of mass transport are more rapidly established [Fisher (1993)].

Electron Transfer

To get a current moving through the cell, a so-called overpotential (η) is required to drive the electrode reaction. With this overpotential, the sum of different terms associated with different reaction steps have to be considered, such as the concentration polarisation (mass transfer polarisation), the activation polarisation (charge transfer polarisation) and the Ohmic polarisation (reaction polarisation).

Concentration Polarisation

In electrochemical reactions, the reactant must be transported from the bulk solution to the electrode surface and then the product has to be transported back into the bulk solution. The rate at which these processes take place may vary considerably and concentration changes in the vicinity of an electrode occur, giving rise to a concentration polarisation effect or mass transfer polarisation. A diffusion layer at the electrode surface will be established, exhibiting a concentration gradient across it. The thickness of this diffusion layer, the Nernst diffusion layer, can vary depending on the nature of the

solution and the electrode. In unstirred conditions, the concentration polarisation will generally increase over time as the concentration gradient tends to develop as reactions proceed. The overall rate of reaction is controlled by the slowest step, either rate of mass transport or charge transfer. Providing that the polarisation potential is sufficiently high, the determining factor will be mass transport to the electrode.

Activation Polarisation

The rate of collission of the electroactive molecule with the electrode surface is determined by the free energy of activation. This can be facilitated by applying an extra voltage, which is termed the charge transfer overpotential or activation polarisation.

Ohmic Polarisation

When a potential of an electrode of interest is measured against a reference electrode, a current is forced through the cell during which the potential will shift/drop in voltage. This ohmic potential drop, also known as iR drop is a measure of the resistance between the surface of the working electrode and the surface of the reference electrode when moving ions through the solution. It should be pointed out that it is a characteristic of the bulk solution and not that of the actual electrode reaction. The effects of this iR drop can be seen in shift of peak potential, decreased current output and increase in peak separation. However, increasing peak separation with increasing scan rate is also a characteristic of a quasi-reversible process.

The iR drop effect can be distinguished by scan rate studies performed using electrolyte solutions with concentration differences of at least one order of magnitude. The same increase in peak separation would then be due to electron transfer kinetics. If the increase in peak separation is less with lower concentrations, this effect is most likely due to iR drop. The iR drop effect can be minimised by using a three-electrode system, operating with high electrolyte concentrations for increased conductivity, placing the reference electrode in close proximity with the working electrode and by using a small working electrode surface area for a decreased current output [Bard *et al.* (2001)]. In an effort to minimise the iR drop, the current output can also be decreased by decreasing the scan rate. In a reversible process the peak current is directly proportional to the square root of the scan rate; therefore, the use of low scan rates will minimize the current flowing though the cell.

2.3.4 Hydrogen Peroxide - Introduction and Motivation

H_2O_2 is a clear liquid, miscible with water and one of the most powerful oxidisers known. Through catalysis, H_2O_2 can be converted into hydroxyl free radicals ($OH^\bullet$), which have reactivity second only to fluorine. Hydroxyl radicals are formed when hyper-reactive thiolgroups or methioine residues are present in a molecule, or if H_2O_2 interacts with free metal ions such as iron [Halliwell *et al.* (2000)].

$$Fe^{2+} + H_2O_2 \rightarrow \text{ intermediate complex} \rightarrow Fe^{3+} + OH^\bullet + OH^-$$

In living organisms, such transition metal ions are usually sequestered and protein-bound so they cannot catalyse free radical reactions *in vivo*. When H_2O_2 is exposed to UV light, it is also converted into a highly reactive hydroxyl radical.

$$H_2O_2 \xrightarrow{\text{UV-light}} 2OH^\bullet$$

H_2O_2 is generated *in vivo* by superoxide dismutase enzymes and non-enzymatically by the dismutation of the superoxide radical ($O_2^{\bullet-}$). It is also directly produced by oxidase enzymes such as glycolate and monoamine oxidase, as well as by the peroxisomal pathway for α-oxidation of fatty acids [De Groot *et al.* (1989)]. Oxidants or stimulators of intracellular generation of reactive oxygen species, such as superoxide anion ($O_2^{\bullet-}$), H_2O_2 and hydroxyl radicals ($OH^\bullet$), are commonly considered as markers for apoptosis and necrosis. Clement *et al.* (1998) found that if certain cell types are exposed to low concentrations of H_2O_2 the intracellular H^+ concentration is elevated causing an acidic environment leading to apoptosis, whereas at higher concentrations of H_2O_2, intracellular alkalinisation is promoted, leading to necrosis. Consequently, a reducing environment giving low H_2O_2 may be needed to induce apoptosis, whereas oxidative stress leads to necrotic cell death [Halliwell *et al.* (2000)]. Low H_2O_2 also promotes caspase activation, which inhibits intracellular $O_2^{\bullet-}$ production, so a defined cellular redox state is likely to be needed for controlling $O_2^{\bullet-}$ production.

Bai *et al.* (1999) found that an overexpression of catalase protected cytosol and mitochondria against cytotoxicity and apoptosis, acting as a sink for H_2O_2, decomposing H_2O_2 into H_2O and O_2. A small percentage of oxygen is reduced enzymatically in the mitochondria to superoxide anion, which then again may be converted enzymatically to H_2O_2. This makes the mitochondria an important source of H_2O_2 and an important

target for oxidative damage, as the only defence against H_2O_2 in the mitochondria is glutathione peroxidase. Other research groups have reported that a high membrane potential in the mitochondria triggers superoxide anion-derived H_2O_2 release [Liu (1997), Lee *et al.* (2002)]. However, Cavazzoni *et al.* (1999) provided evidence that a low membrane potential induces H_2O_2 release. Furthermore, Nohl *et al.* (2005) stated that release of reactive oxidative species (ROS) by the mitochondria is not observed at all. Possible reasons for these varied outcomes could be that the removal of the mitochondria from the natural environment might induce false results, intact mitochondria might have been contaminated with mitochondrial fragments and also varied test methods between researchers makes it difficult to make valid comparisons.

Even though H_2O_2 is a cytotoxic agent, it is essential for the immune system to fend off toxins, parasites, bacteria, viruses and yeasts. Oral bacteria produce H_2O_2, but the amounts have not been elucidated. Exhaled air has been shown to contain H_2O_2 and freshly voided human urine contains substantial quantities of H_2O_2, often exceeding 100 μM. Traces of superoxide dismutase have also been found in urine. It is thought that H_2O_2 is produced in the bladder and that high levels could be advantageous in diminishing infections of the bladder and urinary tract. H_2O_2 could also be involved in regulation of renal function. Diet influences H_2O_2 levels in the human body, but it is also a valuable marker for oxidative stress [Halliwell *et al.* (2000)]. H_2O_2 is also used as an inter- and intracellular signalling molecule [Wang *et al.* (1998), Abe *et al.* (1999)] and it is almost certain that most or even all human cells are exposed to some H_2O_2 [Halliwell *et al.* (2000)].

In modern medicine, monitoring of low levels of H_2O_2 is important as it is considered as a marker for oxidative stress and recognised as one of the major risk factors in progression of disease-related conditions in for example renal disease, cancer and arteriosclerotic vascular disease. Different techniques for measuring H_2O_2 are reported, including fluorescent probes for intracellular H_2O_2 [Royall *et al.* (1993)], a radioisotope technique for H_2O_2 in plasma and whole blood [Varma *et al.* (1991)], electrochemistry using a glassy carbon electrode with incorporated peroxidase [Narasaiah (1994)] and by using platinum electrodes for extracellular H_2O_2 [Test *et al.* (1986)] or blood plasma H_2O_2 determination [Lacy *et al.* (1998a), (1998b)].

Prussian Blue

Prussian Blue (PB), or ferric hexacyanoferrate was first synthesised in Berlin around 1706 and has been traded from around 1709 as a pigment for paints and other colour uses. PB can be synthesised by mixing solutions containing ferric (ferrous) and hexacyanoferrate ions with different oxidation state of iron atoms, such as $Fe^{3+} + [Fe^{II}(CN)_6]^{4-}$ or $Fe^{2+} + [Fe^{III}(CN)_6]^{3-}$. After mixing, the formation of a dark blue colloid is observed.

Chemical and Crystalline Structure

Keggin *et al.* (1936) first investigated on the chemical and crystalline structure of PB using X-ray powder diffraction. PB was found to exhibit a zeolitic nature with a cubic unit cell dimension of about 10.2 Å and channel diameters of about 3.2 Å for both compounds, the so-called soluble $KFeFe(CN)_6$ and insoluble $Fe_4(Fe(CN)_6)_3$ form of PB. These terms, originaly given by dye makers, do not refer to the real solubility in water but rather indicate the ease with which potassium ions disperse into collodial state. Duncan *et al.* (1963) established that PB is indeed $Fe_4^{III}[Fe^{II}(CN)_6]_3$, consisting of alternating iron(II) and iron(III) located on a face centered cubic lattice in a way that the iron(III) ions are surrounded octahedrically by nitrogen atoms and iron(II) ions are surrounded by carbon atoms. An illustration is shown in Figure 2.16:

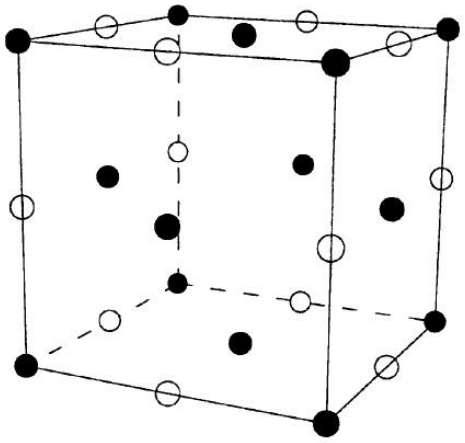

Figure 2.16: PB cubic unit cell according to Keggin *et al.* (1936); • Fe^{3+}, o Fe^{2+}; [adapted from Karyakin (2001)]

Effect of Cations

The ability of cations other than potassium to penetrate the lattice has been studied by many researcher [Ellis *et al.* (1981), Itaya *et al.* (1982), Singleton *et al.* (1967)] and it was found that K^+, Rb^+, Cs^+ and NH^{4+} allow the cyclic electrochemical reactivity of PB whereas Na^+, Li^+ and H^+ are considered as blocking cations. This was explained by their hydrated ionic radii of 1.25, 1.28, 1.19, 1.25 Å respectively and the channel radius of the PB lattice with 1.6 Å.

Electroactivity

The first successfull electrodeposition of PB as electroactive coverage was reported by Neff (1978), in which a platinum foil was used as electrode surface. It was found that PB showed reversible reduction and oxidation by a mechanism which involves the transport of both ions and electrons. For the formation of PB, it was assumd that the soluble salt $KFeFe(CN)_6$ is formed in the presence of excess potassium ions. Other researchers found no evidence of potassium ions in the PB lattice, which led to the conclusion that the insoluble salt is always formed in the deposition reaction [Itaya *et al.* (1982)]. However, potassium ions appeared to be involved in both the reduction and oxidation reactions. Later it was established that insoluble PB is formed initially and converted to the soluble form after being electrochemically cycled in electrolyte containing excess potassium ions [Kellawi *et al.* (1982), Mortimer *et al.* (1984)].

Itaya *et al.* 1984 showed that the reduced form of PB, PW has a catalytic effect for the reduction of H_2O_2 and O_2. It was also found that the oxidised form of PB, Berlin Green, showed a catalytic activity for the oxidation of H_2O_2. Diffraction studies indicated the presence of about eight uncoordinated water molecules per unit cell of PB [Ludi *et al.* (1973), Herren *et al.* (1980)] and it was hypothesised that when for example H_2O_2 penetrates the PB lattice structure, it will be located in the center of each vacancy being surrounded by four divalent high spin iron ions on average. This will then bring about a catalytic reduction of H_2O_2 via a four electron reaction.

The characterisation of PB appeared to be difficult due to it being insoluble and its tendency to form colloids. The impurity of the compositon during traditional synthesis gave subject to varied conclusions. However, PB was found to exhibit a complex structure with variable stoichiometry, depending on the materials and procedures used to crystallise PB. Even though the first successfull electrodeposition of PB as electroactive coverage

was undertaken in 1978, the development of PB modified electrodes for H_2O_2 detection was first announced by Karyakin *et al.* (1994).

Electrochemical Redox-Reaction

The uncertainty of the structure of PB gave rise to uncertainty in the electrochemical reaction taking place at the electrode surface. It is now established that a four-electron reduction takes place in which the oxidised form of PB produces PW and is accompanied with the consumption of alkali metal ions, which is then reoxidised from PW to PB according to the following reactions [Lukachova *et al.* (2003)]:

$$Fe_4^{III}\left[Fe^{II}(CN)_6\right]_3 + 4K^+ + 4e^- \rightleftharpoons K_4Fe_4^{II}\left[Fe^{II}(CN)_6\right]_3 \tag{2.1}$$

However, a large drawback with PB was the loss of its electrochemical stability in neutral and alkaline aqueous media. In addition, PB was found to produce parasitic anodic currents in the presence of O_2 during H_2O_2 reduction [Itaya *et al.* (1984)].

pH Stability

Other researchers [Haghighi *et al.* (2004), Ricci *et al.* (2005), Karyakin *et al.* (1999)] have observed that PB films show decay due to both non-Faradaic (electrolyte and buffer at high pH) and Faradaic processes (due to substrate).

This decay is associated with the presence of hydroxide ions at high pH values and also by OH^- formed during the catalytic cycle. These hydroxide ions are responsible for the cleavage of the PB complex due to the formation of ferric hydroxide [Haghighi *et al.* (2004)] according to:

$$Fe_4^{III}\left[Fe^{II}(CN)_6\right]_3 + 12OH^- \rightleftharpoons 4Fe(OH)_3 + 3\left[Fe^{II}(CN)_6\right]^{4-} \tag{2.2}$$

Decomposition due to Non-Faradaic Process

Fe^{3+} ions are known to coordinate six molecules of water [Karyakin *et al.* (1999), de Mattos *et al.* (2000)]. Even in weak acidic solutions, the coordination sphere may contain OH^-. These hydroxide ions are able to break the Fe-(CN)-Fe bond and PB precipitates can be solubilised in alkaline solutions which was demonstrated by Itaya *et al.* (1986). Therefore, hydroxide ions should be eliminated from the coordination sphere of the iron atoms before deposition of PB in order to diminish the number of defects in the result-

ing polycrystal. This was achieved by increasing the acidity of the initial solution for deposition of PB [Karyakin *et al.* (1999)].

Thus, it was found that if the deposition solution contained a supporting electrolyte of 0.1 M KCl/HCl, PB modified electrodes showed enhanced stability. However, Karyakin *et al.* (1999) found that if the acid concentration was too high, decreased growth rate of the PB layer was observed. This could be due to H^+ acting as blocking cation interfering with the formation of polycrystal formation [Itaya *et al.* (1984), (1986)].

Additionaly, as the PB precipitate contains an average of 14-16 water molecules per unit $Fe_4[Fe(CN)_6]_3$ [Ganguli *et al.* (1983)], it was suggested that this so-called zeolitic water could be irreversibly removed from PB by heat treatment. Indeed, freshly prepared PB modified electrodes showed less stability over dryed electrodes [Karyakin *et al.* (1999)].

Decomposition due to Faradaic Process

During electrochemical H_2O_2 reduction in neutral media, OH^- are formed according to [Karyakin *et al.* (1999)]:

$$\begin{aligned} Fe_4^{III}\left[Fe^{II}(CN)_6\right]_3 + 4K^+ + 4e^- &\rightarrow K_4Fe_4^{II}\left[Fe^{II}(CN)_6\right]_3 \\ K_4Fe_4^{II}\left[Fe^{II}(CN)_6\right]_3 + 2H_2O_2 &\rightarrow Fe_4^{III}\left[Fe^{II}(CN)_6\right]_3 + 4OH^- + 4K^+ \end{aligned} \tag{2.3}$$

with the net reaction being:

$$H_2O_2 + 2e^- \rightarrow 2OH^- \tag{2.4}$$

From the equation above, it is apparent that by breaking up PB, PW can not be formed in the reverse scan. Hence, it is only PW which has catalytic activity towards H_2O_2 reduction. Thus, Karyakin *et al.* (1999) found that the solubilisation of PW in the presence of cations which promote its electroactvity is thermodynamically a viable process. It is therefore necessary to stabilise the pH near the electrode surface during electrocatalytical H_2O_2 reduction. Karyakin *et al.* (1999) found that the addition of 0.05 M phosphate buffer (pH 6) increased the stability of PB dramatically. It was further found [Karyakin *et al.* (2004)] that these mediated electrodes allow low-potential detection with a detection limit of 10^{-8} M and a linear calibration range of 10^{-8} to 10^{-2} M.

Selectivity, Stability and Performance

Curulli *et al.* (2004) assessed the selectivity of PB modified electrodes to H_2O_2 against typical interferents such as uric acid, ascorbic acid and acetaminophen. Additional current outputs were found with ascorbic acid and acetaminophen. Furthermore, PB modified electrodes showed low stability, producing no analytical response after 15 days. This could have been due to storage of the electrodes in phosphate buffer solution at pH 7.4 as PB was found to be less stable in neutral media. These electrodes were also not exposed to elevated temperatures due out depositing procedure, which also could have improved their performance. Moscone *et al.* (2001) achieved high pH stability by depositing PB chemically on graphite powder, however, the sensitivity reported with 45 mA/(M/cm^2) was low. De Mattos *et al.* (2003) found the highest sensitivity (2000 mA/(M/cm^2)) in H_2O_2 detection using gold screen-printed PB modified electrodes, though the linear response and the detection limit was not reported. Karyakin *et al.* (2004) reported the lowest detection limit with 0.01 μm, a linear response up to 100 mM but a low sensitivity of only 60 mA/(M/cm^2) with PB modified glassy carbon electrodes. These findings demonstrate that PB modified electrodes may perform very well in one aspect but are worse in another aspect.

2.3.5 Partial Pressure of Oxygen - Introduction and Motivation

Danneel *et al.* (1897) were possibly the first who reported that O_2 reacts in aqueous solution with negatively charged inert metals, showing a linear relationship between pO_2 and current by using two polarised platinum electrodes. Their discovery fell into disuse as the electrode was rapidly poisoned or coated with proteins when used in biological media, making this method for pO_2 estimation unreliable.

The invention of the dropping-mercury electrode in 1922 by Heyrovsky and the subsequent determination of dissolved oxygen with this electrode led to an increased interest in measuring dissolved oxygen. However, solid metal working electrodes were considered as unsuitable due to electrode poisoning. Blinks *et al.* (1938) showed that platinum does produce good current linearity when used in stirred solutions at fixed polarising potentials for amperometric determination of pO_2 in biological media.

With Clark (1956) introducing a gas-permeable membrane, situated between the liquid sample and the working electrode, the problem of contamination or poisoning of the working electrode was overcome. Also, much lower concentrations of O_2 could be

measured, however, stirring was still required. The introduction of smaller electrodes for intravascular use finally overcame this stirring problem. Reduced cathode diameter reduced the quantity of O_2 consumed by the sensor, thus reducing the response time and also interfering less with the surrounding microenvironment around the sensor.

There are several techniques commonly used for measuring pO_2, *in vitro* via a bench blood-gas analyser, *in vivo* via insertion of an electrochemical sensor into an artery or subcutaneous tissue, or by placing an electrochemical sensor on the skin (transcutaneous) and measuring O_2 diffusion through the skin.

Electrochemical Reaction

There are various schemes on how electrochemical O_2 reduction at -500 to -800 mV versus Ag/AgCl at noble metal surfaces taking place in alkaline media. Either the hydrogen peroxide ion or the hydroxyl ion is proposed as the product of the electrochemical reaction. Simplified reaction schemes are presented as:

$$O_2 + H_2O + 2e^- \rightarrow HO_2^- + OH^- \tag{2.5}$$

$$O_2 + 2H_2O + 4e^- \rightarrow 4OH^- \tag{2.6}$$

The net result of these processes is that the number of electrons involved in the reduction of O_2 can be either 2 or 4. If the hydrogen peroxide ion is produced during reduction of O_2, it can diffuse back to the cathode surface and be reduced to hydroxyl ions, resulting in an elevated current response. This is not the case when a hydroxyl ion is produced directly during reduction of O_2. However, the applied potential, the electrode material, electrode size, membrane material as well as the pH of the electrolyte play part in the reduction process scheme.

Electrochemical Performance

Electrochemical O_2 sensors show good selectivity, sensitivity and fast response times, but protein adsorption is still the major drawback when sensors are used *in vivo*, especially when in contact with blood [Rolfe (1990)]. In contrast, Greenbaum *et al.* (1997) reported constant current-voltage outputs for a period of eight hours when using 21-gauge Pt/Au electrodes in tissue without using a membrane.

Good progress has been made with intravascular and subcutaneous devices for short-

term applications. Zhang *et al.* (1996a) produced a haemocompatible O_2 sensor by applying phospholipid-based copolymer membrane on the sensor tip. In protein solutions, serum and whole human blood, stable current response over a period of 64 hours were reported. Wang *et al.* (2003) investigated on the distribution of pO_2 in the skin of human finger nail folds. Good correlation with experimental and theoretical estimates of pO_2 were achieved.

2.3.6 Interferent Current Responses

H_2O_2 Detection

Electrochemical sensors for monitoring H_2O_2 operate on the principle of oxidising the analyte at the working electrode with a potential in the range of +500 to +700 mV versus Ag/AgCl. Hydrogen peroxide was found to have a diffusion coefficient of $1.6 \times 10^{-9} m^2 s^{-1}$ [Higgins *et al.* (1999)] and assumed to be therefore accessible to the platinum working electrode at significant concentrations. However, other substances e.g. ascorbate, urate and acetaminophen, are also present *in vivo* at sufficiently high concentrations (Table 2.1) and oxidise at the same potential range, causing aditional interfering current responses.

Interferents	Physiological Concentrations	
Ascorbic acid		0.6 - 2 mg per 100 ml (0.034 - 0.1 mM)
Uric acid	Males:	3.5 - 7.2 mg per 100 ml (0.21 - 0.43 mM)
	Females:	2.5 - 6 mg per 100 ml (0.15 - 0.36 mM)
	Children:	2 - 5.5 mg per 100 ml (0.12 - 0.33 mM)

Table 2.1: Physiological concentrations of potential interfering species in amperometric H_2O_2 detection [Ciba-Geigy (1981)]

Ascorbic acid acts as a detoxifying reducing agent in the body by reacting with free radicals and reactive oxygen species. Its two-step oxidation (Figure 2.17) produces dehydroascorbic acid via formation of intermediate ascorbate free radical monodehydroascorbic acid [Szymula *et al.* (2003)]. Electro-oxidation of ascorbic acid results in the liberation of two electrons in a quasi-reversible manner, followed by irreversible chemical reactions [Ernst *et al.* (2001)]. Ascorbic acid has pK_a values of 4.17 and 11.57 and is negatively charged at physiological pH values.

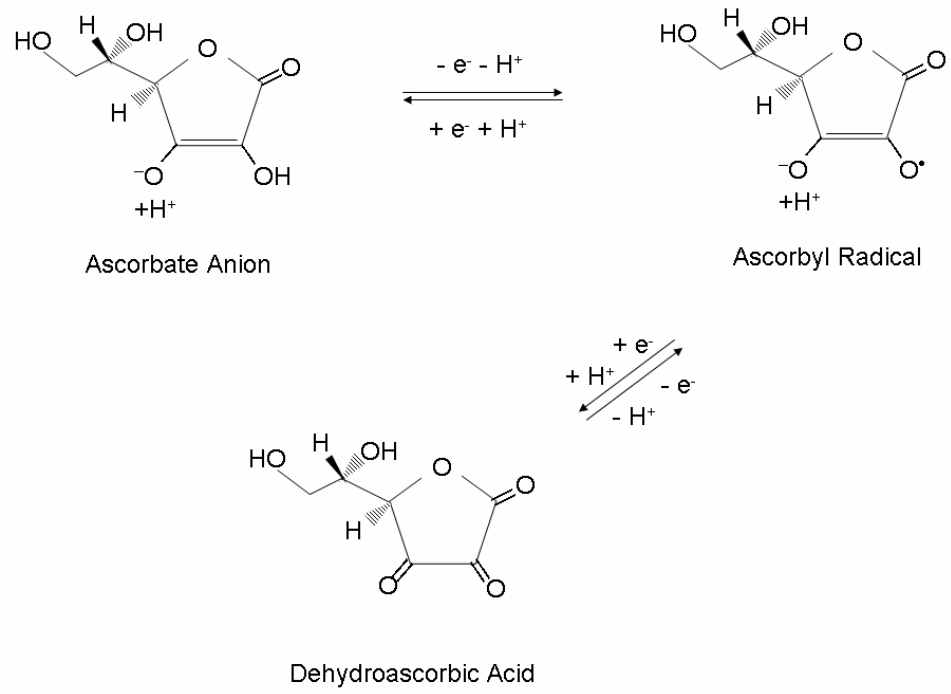

Figure 2.17: Electrochemical oxidation of L-ascorbic acid

Uric acid is a purine and is only slightly soluble in water. Like ascorbate, it is a strong reducing agent. About half of the antioxidant capacity of plasma comes from uric acid. Uric acid has a pK_a of 5.75 and is negatively charged at physiological pH levels. The heterogeneous electrochemical oxidation of uric acid (Figure 2.18) is a quasi-reversible, two-electron transfer process, followed by irreversible chemical reactions, similar to the oxidation pathway of ascorbic acid. Uric acid is initially oxidised into a very unstable anionic quinonoid diimine, which is attacked by water to produce an anionic imine-alcohol. A subsequent ring contraction reaction produces another intermediate diol, which decomposes to allantoin [Goyal *et al.* (1982)]. However, the resulting products are pH-dependent.

Acetaminophen is not a naturally occuring substance in the human body, but the active ingredient in widely used painkillers. So not only does the concentration of acetaminophen vary considerably, but its electrochemical oxidation is extremely pH-dependent. The oxidation at physiological pH levels results in the generation of N-acetyl-p-benzo-quinone imine (NAPQI) [Nematollahi *et al.* (2009)]. This reaction generates two electrons and two hydrogen ions in a quasi-reversible reaction, as illustrated in Figure 2.19.

Most of the relevant interferents are negatively charged molecules such as ascorbate and urate. By using a negatively charged membrane e.g. sulphonated polymers, the interferents are simply repelled [Vaidya *et al.* (1994), Lee *et al.* (2000)]. However, ac-

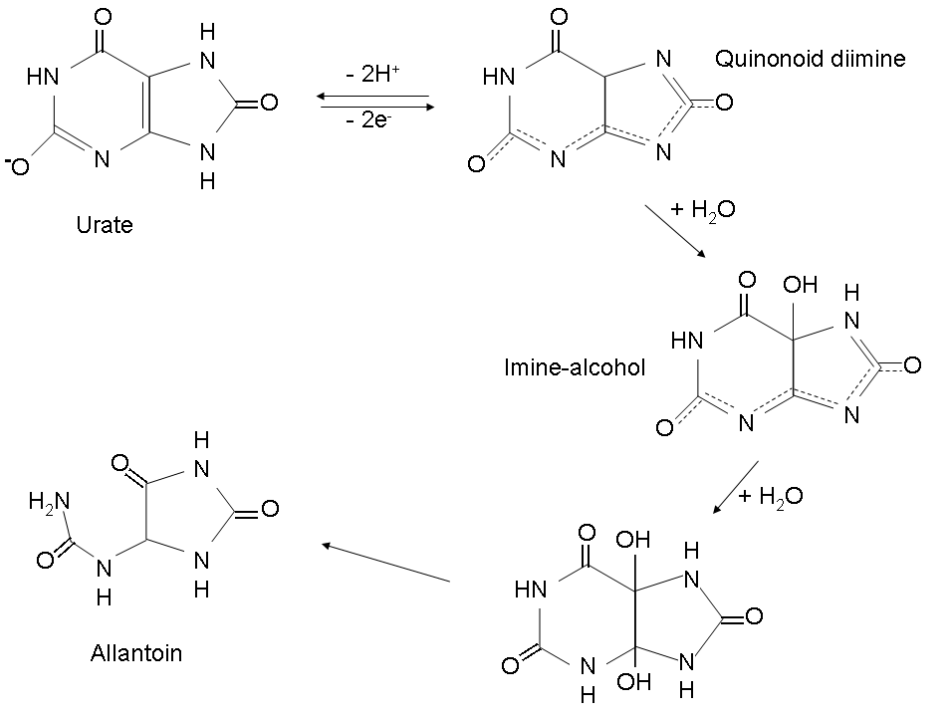

Figure 2.18: Electrochemical oxidation of uric acid

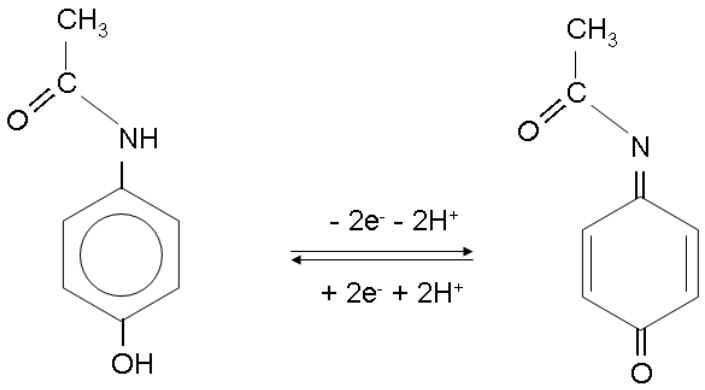

Figure 2.19: Electrochemical oxidation of acetaminophen

etaminophen has no formal charge and can be excluded by using a semi-permeable membrane. Another method to overcome interference is by reducing H_2O_2 at low potentials using for example Prussian Blue [Karyakin *et al.* (2000), Lukachova *et al.* (2003)].

Oxygen Detection

Electrochemical sensors for monitoring pO_2 operate on the principle of reducing the analyte at the working electrode with a potential in the range of -500 to -800 mV versus Ag/AgCl. Amongst the anaesthetic agents, it has been found that nitrous oxide (N_2O) and halothane ($CF_3CHClBr$), used as inhalational agents, are electrochemically active at the polarising voltage window for O_2. The sensor currents generated by these agents give "pseudo-oxygen" currents.

Johnson *et al.* (1974) established that N_2O is reduced on a Pt working electrode only when it was adsorbed to the Pt surface, otherwise no electrochemical reduction takes place. Also, they found that pH and the polarising voltage are connected; the reduction would take place at a polarising potential of -800 mV versus Ag/AgCl at pH 14 or at -650 mV versus Ag/AgCl at pH 10. Since most sensors used in medicine and biology employ Pt electrodes at pH 7, nitrous oxide is not expected to give additional current responses. However, there is still some intermittent interference effect. Albery *et al.* (1978) found that silver ions from the Ag/AgCl reference electrode were plated on to the working cathode during pO_2 measurement, then reducing N_2O giving interfering current responses. These interfering current responses did not occur when the cathode surface was either abraded or cleaned in nitric acid in order to remove these silver deposits.

Halothane is liquid at room temperature and electrochemically active at silver and gold surfaces. It was synthesised in 1951 and is still used as an inhalational anaesthetic agent. The electrochemical sensitivity to halothane depends on the polarising voltage, the electrolyte and the pH. If other materials as working electrode surfaces such as Pt are used, care has to be taken regarding to potential silver contamination of the cathode.

Chapter 3

Materials, Instrumentation and Methods

3.1 Materials

The chemicals used were analytical grade acetone (270236T), tetrahydrofuran (THF, 152476C), n-heptane, dichloromethane (DCM), isopropanol (IPA, 59304), toluene, glycerol, dimethylsulphoxide (DMSO, 28216), hydrochloric acid (1 M, 28507), aluminium oxide (331372Q, Lot K24020272 720) and ethanol, absolute (EtOH, 270236T) as supplied by BDH Chemicals, UK.

Cobalt chloride ($CoCl_2$, 60818), potassium peroxodisulphate ($K_2S_2O_8$, PPDS, P5592), triisobutylaluminium ($[(CH_3)2CHCH_2]_3Al$, TIBA, 257214), sodium hydride, 60% in mineral oil (NaH, 452912), sodium hydroxide pellets ($NaOH \cdot H_2O$, S8045), ascorbic acid (AA, A-1417), N-Acetyl-4-aminophenol (A-5000), potassium ferrocyanide ($K_4Fe(CN)_6$) phosphorus pentoxide (P_2O_5, 04113), sodium dodecyl sulphate (SDS, L6026), Nafion®117 (70160), potassium chloride (KCl, P9333), potassium dihydrogen phosphate (KH_2PO_4, 229806), dipotassium phosphate (K_2HPO_4, 60349), perchloric acid ($HClO_4$, 34288), bovine serum albumin (BSA, 99%, A7638), hexamethyldisilazane (HMDS, H4875) and 1,3 propane sultone (PS, 291250) were of analytical grade and supplied by Sigma-Aldrich, UK.

Urea (51458), potassium permanganate ($KMnO_4$, 60460), sodium hydroxide solution (NaOH, 1 M, 72082), ninhydrin (solid, 72490), hydrogen peroxide (H_2O_2, 30 % v/v, 95302), anhydrous iron(III) chloride ($FeCl_3$, 44943) and ammonium hydroxide solution

(NH_4OH, 1 M, 09859) were of analytical grade and obtained from Fluka Chemicals, UK. Potassium hexacyanoferrate ($K_3Fe(CN)_6$) was of analytical grade and a kind gift of Prof. Karyakin, M.V. Lomonosov Moscow State University, Russia.

For the direct cell contact assay, Dulbecco's Modified Eagle Medium (D-MEM, 21885), penicillin-streptomycin (P/S, PEN-NA/S0890), trypsin (T8003), foetal serum albumin (FSA, 10108-165, 07Q5364F) and murine fibroblast cell line 3T3 (ECACC Ref. No 93061524) was used as obtained from the ICMS, Centre for Academic Surgery, QMUL.

Therminox coversliops (13 mm, 174950, Lot 551810) were obtained from Nalgene Nunc, USA and standard organo-tin doped plasticised PVC (499/400/000, Lot 30375) were obtained from Fisher Scientific UK. Alamar Blue^{TM}(DAL1100, Lot 1454005A) was obtained from Biosource, UK.

Nitrogen, oxygen and helium gas was used as supplied by BOC Gases, UK. Glacial acetic acid (GAA) was supplied by QMUL Chemistry Department which was originally purchased by Hayashi Pure Chemical Ltd., Japan.

Stainless steel tubing (Cr18/Ni10, FE227130), polyester insulated Pt wire (PT00584019) and co-axial cable (123836) were supplied by Goodfellow Cambridge, UK and 2-part epoxy resin (HY1300GB and RX771C/NC) was used as supplied by Robnor Resins, UK. Glutaraldehyde (GA, R1351), sodium cacodylate (R1104), osmium tetraoxide (R1022) and uranyl acetate (R1260A) were obtained from Agar Scientific, UK.

Sterile glassware and disposable plastics were used as appropriate and included standard laboratory glass beakers, microscope slides, tissue culture polystyrene flasks, well plates, centrifuge tubes, pipette tips and other accessories for use in experiments and cell culture. Various suppliers were used (Thermanox®, Gibco®, Falcon^{TM}, Sterilin®, Corning®).

Pelletised PU was of medical grade as supplied by Thermedics, USA and medical grade silicone rubber (SR) was used as supplied by NuSil, UK. Details of these polymer materials are listed in Table 3.1.

Polymer	Trade Name	Description	Composition
PCU	Bionate®	Shore A	MDI/BD/PHEC
PEU	Tecoflex®	Shore A	H_{12}MDI/BD/PTMEG
SR	MED-4211	PartA	Silica, amorphous
SR	MED-4211	PartB	Dimethyl-methylhydrogen siloxane copolymer

Table 3.1: List of polymers including composition used in synthesis

When deionised water is used, it was obtained using an USF Elga Option 3 Water Purifier (10 MΩ). In all cases, stirring and heating were carried out using an IKA Werke magnetic stirrer/heater and polyethylene covered magnetic stirrer bars. Filtering was carried out using Whatman filter paper (Grade 1) and pH monitoring was performed using a Hanna Instruments HI 9024 pH probe. Glassware was cleaned with warm soapy water, rinsed with warm water and then rinsed again with deionised water.

3.2 Instrumentation

3.2.1 Fourier Transform Infra-Red Spectroscopy

FTIR spectra of polymers were obtained using a Nicolet 800 FTIR spectrometer in conjunction with a Mtech Photoacoustic Spectrum (PAS) cell including associated software (OMNIC).

3.2.2 Scanning Electron Microscopy

A JEOL JSM 6300 scanning electron microscope (SEM) from JEOL Ltd., Herts, UK was used.

3.2.3 Static Contact Angle

Static contact angles of polymers were measured by means of a sessile-drop method. The instrument used was an optical contact angle KRÜSS drop shape analysis system DSA100 with a resolution of 0.01 mN/m, an accuracy of ±0.1° and 7-fold zoom optics with stray light compensation.

3.2.4 Thermogravimetric Analysis

Thermogravimetric analysis was performed using TA Universal apparatus Q500 including associated software (Universal Analysis 2000). The following settings were used: N_2 flow rate 60 ml/min, temperature range between 20 and 1000°C with an increase of 50°C/min.

3.2.5 Light Microscopy

A Leica DM IRB microscope including associated digital camera and software from Leica Microsystems (UK) Ltd were used to take digital pictures of polymers including cells. A Motic BA400 microscope including associated digital camera and software was used to take digital pictures of polymers on glass slides.

3.2.6 Spectrophotometry

Spectrophotometeric analysis was performed using Perkin Elmer Lambda 900 UV/Vis including associated software. The scan range was set to 800-300 nm and 6×6 cells with automatic baseline corrections were used.

3.2.7 Potentiostats

A μAutolab Type II potentiostat, a μAutolab multichannel potentiostat with associated GPES software purchased from Windsor Scientific Ltd., UK was used along with a portable potentiostat type PalmSens including Pocket PC with associated software (HP) obtained from Palm Instruments BV, NL.

3.2.8 pH Meter

A Jenway 3310 pH meter purchased from Spectronic Analytical Instruments, Leeds, UK was used for pH measurements.

3.2.9 Multilabel Reader

A Wallace, 1420 Victor^2 Multilabel counter with associated software purchased from Perkin Elmer Life Sciences Ltd was used to measure absorbances at 570 and 600 nm.

3.2.10 Surface Profiler

A Veeco Dektak 3-ST surface profiler with associated software, Version 3.21 was used to measure the thickness of polymers.

3.3 Methods

3.3.1 Synthesis of Polyurethane and Silicone Rubber

PU was made by solution casting procedure *in situ* via a one-step process with and without subsequent phase inversion utilising a non-polar coagulation medium. Phase inverted polyurethane with carbonate moieties in their soft segments are referred as PCU, polyurethane with ether moieties in their soft segments are referred as PEU. A scheme of conventional solvent-cast and phase intered polymers regarding to hard- and soft segment distribution is illustrated in Figure 3.1. SR was made by solution polymerisation *in situ* via a two-step process utilising either non-polar or polar solvent; samples with non-polar solvent were referred to as "SR control" and samples with polar solvent were referred to as "SR modified".

Synthesis of Polyurethane *in situ*

PCU, one-step process

- 1.05 g of pelletised PCU was rinsed in acetone for 15 minutes.
- PCU was then dried *in vacuo* at 80°C overnight.
- 15 ml of THF was pipetted into a glass vial.
- PCU was added slowly to THF under stirred conditions.
- The glass vial was then immediately covered.
- Stirring was continued until pelletised PCU was fully dissolved.

PEU, one-step process

- 1.05 g of pelletised PEU was rinsed in acetone for 15 minutes.
- PEU was then dried *in vacuo* at 80°C overnight.
- 15 ml of DCM was pipetted into a glass vial.
- PEU was added slowly to DCM under stirred conditions.
- The glass vial was then immediately covered.
- Stirring was continued until pelletised PCU was fully dissolved.

Solvent Casting and/or Phase Inversion

- 3 ml of polymer solution was cast onto each clean glass slide of 7.5 × 2.5 cm and immediately covered with a glass lid.
- These cast glass slides were left at room temperature for one minute for polymer formation.
- Then, the cast glass slides were immersed into coagulation medium (heptane) for ten minutes.
- The glass slides with resulting phase-inverted polymers were then removed from the coagulation medium, covered and left to dry at room temperature for 2 days.

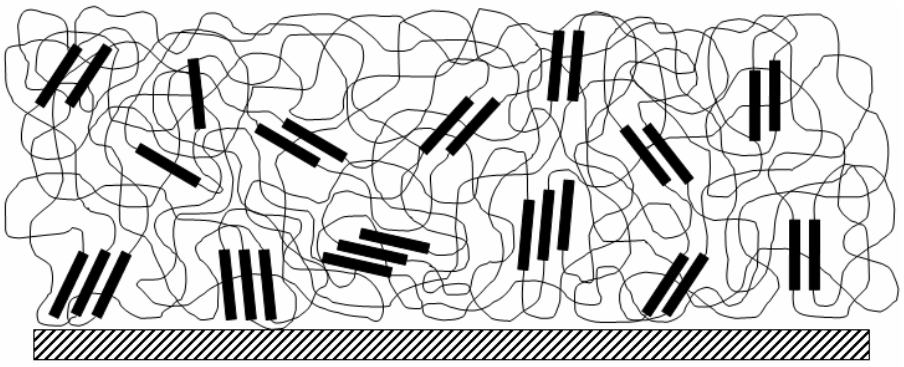

(a) Convential solvent cast PU

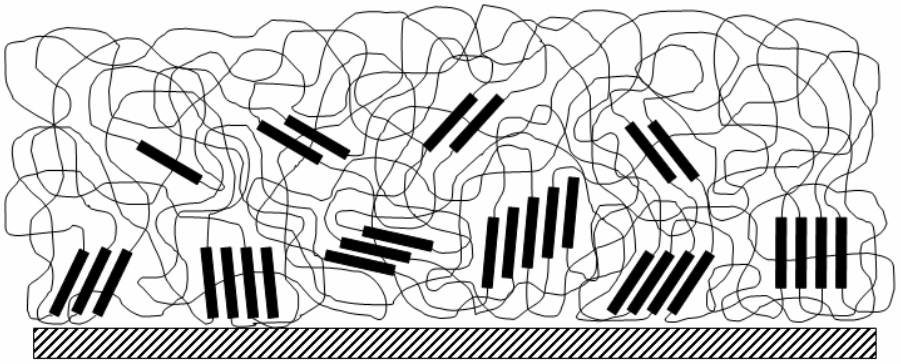

(b) Phase inverted PU

Figure 3.1: Schematic illustration of (a) solvent cast and (b) phase inverted PU (solid rectangles represent hard segments; fine lines represent soft segments)

PU without immersion in coagulation medium were also prepared for reference purposes. In this case, the casting solution was evaporated for one minute and then covered and left to dry for 2 days at room temperature. Films with a thickness of $\sim$ 15 μm were obtained. These coated glass slides were stored prior to use in designated glass-slide boxes free of dust.

Synthesis of Silicone Rubber *in situ*

SR control, two-step process

- 3.75 g of SR Part A was thoroughly mixed at room temperature in 15 ml heptane via vigorous stirring for two hours until fully dissolved.
- 0.375 g of SR Part B was added whilst stirring was maintained for another 5 minutes.
- 2 ml of the polymer mixture was then cast into polypropylene Petri dish and immediately covered and left for 5 minutes in the fume hood at room temperature.
- The lid of the Petri dish was then raised to leave a 2 mm gap for solvent evaporation and left for three hours before being transferred into an oven set at 50°C.
- After 4 hours, the temperature was raised to 100°C and left for one hour to obtain fully cured SR.

By using a non-polar solvent, the non-polar amorphous silica gel (Part A) will form a homogenous mixture. After addition of Part B and applying heat, SR cures in a highly crosslinked manner [Braun et al. (2003)]. See Figure 3.2 for illustration.

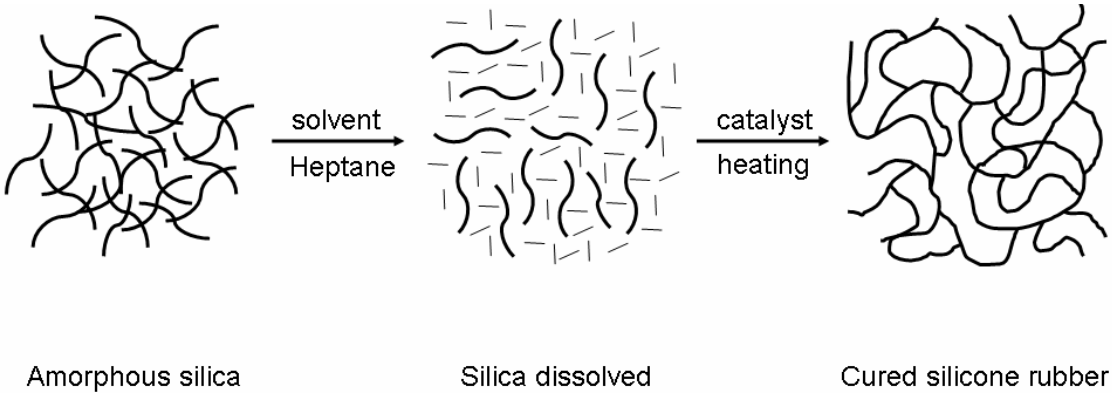

Figure 3.2: Schematic diagram of SR synthesis utilising non-polar solvent

SR modified, two-step process

- 3.75 g of SR Part A was thoroughly mixed at room temperature in 15 ml IPA via vigorous stirring for at least eight hours until fully suspended.
- 0.375 g of SR Part B was added into suspension whilst stirring was maintained for another 15 minutes.

- 2 ml of the polymer suspension was then cast into polypropylene Petri dish and immediately covered and left for 5 minutes in the fume hood at room temperature.
- The lid of the Petri dish was then raised to leave a 2 mm gap for solvent evaporation and left for one hour before transferred into oven set at 40°C.
- After 4 hours, the temperature was increased to 70°C and left in the oven over night.
- The next day, SR was fully cured in the oven set at 100°C for another 2 hours.

By using a polar solvent, the non-polar amorphous silica gel (Part A) does not fully dissolve, instead, a heterogeneous mixture (suspension) is produced. It is hypothesised that the silica monomers will aggregate to clusters which would lead to a lower crosslink density when fully cured. An illustration is shown in Figure 3.3.

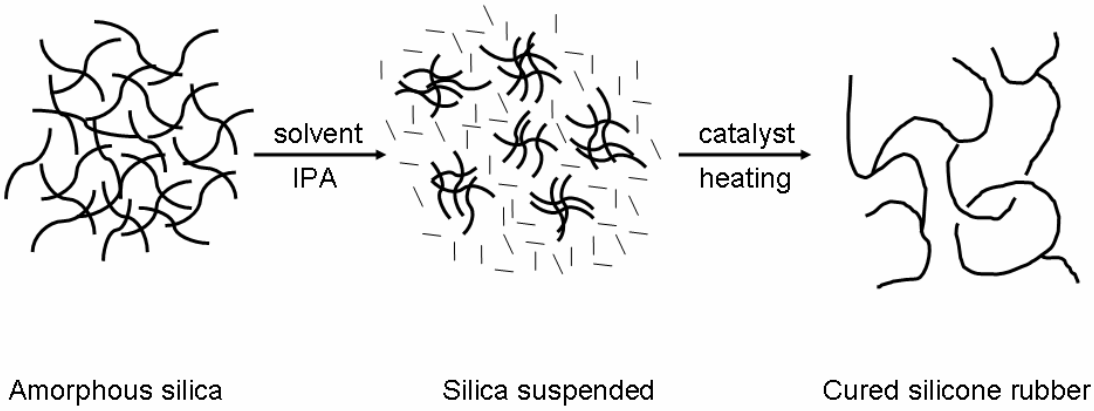

Figure 3.3: Schematic diagram of SR synthesis utilising polar solvent

Polymers with a thickness of ~ 20 μm were obtained and stored at room temperature in Petri dishes individually separated with Whatman filter paper prior to use.

3.3.2 Surface Modification of Polyurethane

Hydroxylation

Solvent-cast PU (Section 3.3.1) was functionalised via hydroxylation in aqueous media utilising PPDS. This was aimed at increasing the surface hydrophilicity and potentially increasing the yield of subsequent grafting reactions [Bamford *et al.* (1996)]. A reaction vessel (Figure 3.4) was designed for these specific reactions and manufactured in-house by Mr. John W. Cowley, a glassblower from the Chemistry Department at QMUL.

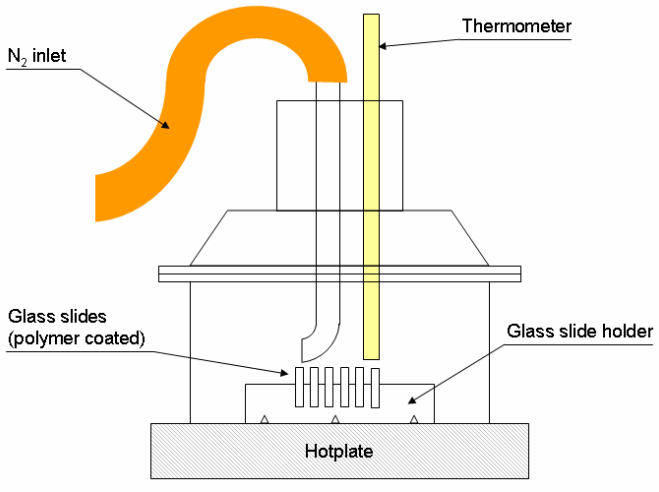

Figure 3.4: Reaction vessel used for surface modification of polymers

Procedure for Hydroxylation

- 6 glass slides holding solvent-cast polymers were dried *in vacuo* at 60°C overnight.
- These glass slides were placed in the reaction vessel containing 200 ml deionised water and continuously purged with nitrogen and stirred at all times.
- The temperature was set to 40°C.
- After 30 minutes, 20 g of PPDS was added and the temperature elevated to 80°C and maintained for 4 hours.
- After the reaction, the polymers were washed copiously with hot distilled water and then dried *in vacuo* at 60°C for at least 24 hours.

Hydroxylated PEU were referred as PEU-OH and hydroxylated PCU were referred as PCU-OH.

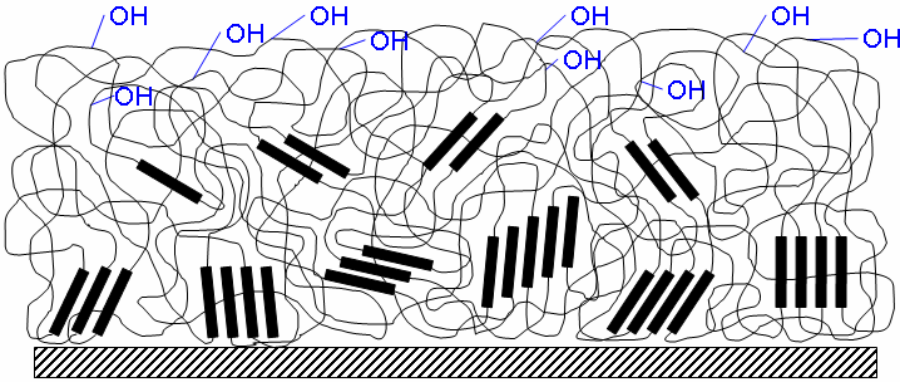

Figure 3.5: Schematic illustration of hydroxylated PU

Procedure for Sulphonation

PU was sulphonated by a two-step procedure. In the first step, the polymer surfaces were functionalised according to the method described in Section 3.3.2 Hydroxylation. The second step used NaH 60% (w/w) in mineral oil and TIBA as the catalyst and PS for surface grafting.

- 0.1 g NaH was rinsed in THF and dried unter nitrogen flow before 25 ml of toluene was added.
- 0.4 g TIBA solution (25 wt. % in toluene) was added with a syringe into the NaH/toluene suspension; the temperature was set to 50°C and stirred for 4 hours under nitrogen purge.
- 6 glass slides holding functionalised polymers were placed into the reaction vessel containing 175 ml toluene; the temperature was set to 80°C and the reaction vessel was purged with nitrogen and stirred at all times.
- After 30 minutes, 25 ml of NaH/TIBA/toluene solution was added with a syringe into the reaction vessel.
- After 15 minutes, 10 g of PS was added.
- After 8 hours, the grafted polymers were removed, thoroughly rinsed in toluene and dried *in vacuo* at 60°C for 24 hours.

Sulphonated PEU were referred as PEU-SO_3 and sulphonated PCU were referred as PCU-SO_3.

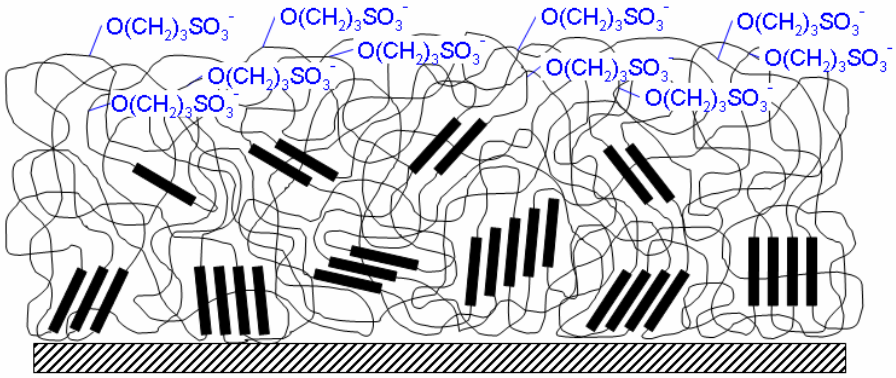

Figure 3.6: Schematic illustration of sulphonated PU

3.3.3 Polymer Characterisation

Amino Acid Assay

The amount of BSA adsorbed onto polymer was determined by means of spectrometry using the ninhydrin method, which is based on the methods established by Moore *et al.* (1954) and Moore (1968).

Preparation of Hydrindantin

- 2 g of ninhydrin was dissolved in 50 ml deionised water at 90°C under stirred conditions.
- 2 g of AA was dissolved in 10 ml deionised water at 40°C under stirred conditions.
- The AA solution is added to ninhydrin solution at 90°C under stirred conditions.
- Without further heating, crystallisation of hydrindantin was allowed to proceed for 30 minutes.
- The suspension was then cooled to room temperature under running tap water and the hydrindantin crystals are filtered off and copiously washed with deionised water.
- The compound was dried overnight over P_2O_5 in a vacuum desiccator protected from light.

Ninhydrin is reduced with ascorbic acid to hydrindantin; a fine white powder with a yield of 94% was obtained; hydrindantin was stored in a dark glass vial at 4°C.

Sodium Acetate Buffer, pH 5.2

- 168 g of $NaOH \cdot H_2O$ was added into 400 ml of deionised water under stirred conditions.
- 293 ml of glacial acetic acid was added when sodium hydroxide pellets were half dissolved while stirring was maintained until fully dissolved.
- This solution was made up to 1 litre and the pH was adjusted to 5.20 $\pm$0.05 with either 0.1 M NaOH or 0.1 M HCl if necessary while monitoring with a pH meter.

This buffer solution was stored at 4°C without preservative.

Ninhydrin Reagent Solution

- 2 g of ninhydrin and 0.3 g of hydrindantin was dissolved in 75 ml DMSO under a stream of nitrogen gas and with stirred conditions.
- 25 ml of sodium acetate buffer was added while stirring and nitrogen bubbling was maintained.

This reagent solution was stored at 4°C prior to use. A fresh solution was prepared for each assay.

Calibration Curve

- 0.5 g BSA (99%) was dissolved in 10 ml deionised water to obtain a standard stock solution of 5% (w/v).
- Serial dilutions were made from this standard solution to obtain concentrations of 5, 10, 15, 25 and 50 μg/ml.
- 0.5 ml of Ninhydrin Reagent Solution and 2 ml of each BSA serial dilution was put into screw-capped test tubes and heated in a boiling water bath for 10 minutes.
- After heating, these tubes were immediately cooled in an ice bath.
- 2.5 ml of absolute EtOH was added into each tube and thoroughly mixed with a Vortex mixer for 30 seconds each.
- The absorbance was recorded with a spectrophotometer in the range of 800-300 nm.

Quantification of Adsorbed Proteins to Polymer Surfaces

- Polymers (1 cm^2) were placed into 24-well plate (Figure 3.7).
- These samples were incubated in aqueous solution containing 5% w/v BSA for a period of 5, 10, 20 and 40 minutes, 1 hour and 24 hours respectively.
- The samples were then rinsed in deionised water.
- Each polymer was incubated in 1 ml of aqueous 2% v/v SDS for 8 hours in order to remove proteins from the polymer surface.
- Protein solutions were placed into screw-capped test tubes and topped up with deionised water to make 2 ml.

- 0.5 ml of Ninhydrin Reagent Solution was added into each of these test tubes and heated in a boiling water bath for 10 minuters.
- After heating, these tubes were immediately cooled in an ice bath.
- 2.5 ml of absolute EtOH was added into each tube and thoroughly mixed with a Vortex mixer for 30 seconds each.
- The absorbance was recorded with a spectrophotometer in the range of 800-300 nm.

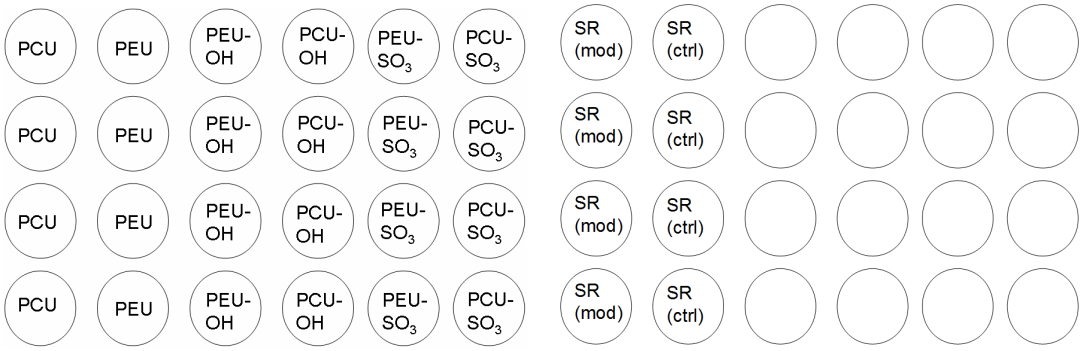

Figure 3.7: Well-plate set-up for protein adsorption study

The test tubes were protected from light throughout the ninhydrin procedure. A calibration curve for absorbency at 570 nm of different solutions of known BSA concentrations was generated. From this curve, the actual amount of proteins adsorbed to the polymers after incubation was determined. Each incubation was performed in quadruplicate in order to allow the monitoring of variability of protein adsorption onto any single polymer sample.

Sessile Contact Angle

The polymers were prepared as follows:

- Samples (1 cm^2) were placed into 24-well plate and incubated in 2 ml of aqueous solution containing 5% w/v BSA for a period of 5, 10, 20, 40 and 60 minutes respectively.
- The polymers were then rinsed in deionised water, placed on glass slides and dried in a vacuum oven set at 60°C for 6 hours.

Contact angle measurements were taken on the air facing surface. All measurements were taken at a controlled temperature of 25°C and 65% relative humidity against

deionised water, glycerol and DMSO using a droplet of 2 μl volume. The contact angles were measured on static drops and read within 1 minute of placing the droplet. Five measurements on different surface sites per sample were taken. For reference purpose, contact angle measurements were also taken with non-protein fouled polymers.

Polymer Film Degradation

Accelerated oxidative degradation of polymers was simulated *in vitro* using a hydrogen peroxide-cobalt chloride system. Cobalt ions catalyse the decomposition of H_2O_2 to create reactive hydroxyl radicals [Schubert *et al.* (1997b)]:

$$Co^{2+} + H_2O_2 \rightarrow Co^{3+} + HO^- + HO^{\bullet}$$

Procedure:

- 24-well plate (same set-up as in Figure 3.7) was rinsed in IPA and polymers (1 cm^2) were placed into well plate.
- 200 ml deionised water and 100 ml H_2O_2 (30%, v/v) was measured and mixed together to obtain 20% H_2O_2 (v/v) solution.
- 0.1 mol (2.598 g) of $CoCl_2$ was added into this H_2O_2 solution; this mixuture was left in fume hood for 2 hours to form free radicals.
- 1 ml of this oxidative solution was placed into each well, the well plate was covered and stored in oven set to 37°C.

The polymers were treated in this oxidative solution at 37°C for up to 21 days. Every 3 days, polymers were retrieved to examine chemical and physical changes and placed in a freshly prepared solution in order to maintain a relative constant concentration of radicals. Each incubation was performed in quadruplicate.

Fourier Transform Infrared Spectroscopy (FTIR)

FTIR spectra of modified and unmodified polymers (1 cm^2) were obtained in the mid infrared region (4000-400 cm^{-1}) at 8 cm^{-1} resolution, using an interferometer mirror velocity of 0.633 cm/s with a modulation frequency of 10 kHz, averaging 256 scans. The sample chamber of the photoacoustic spectrum (PAS) cell was purged with dry helium gas (pre-dried over a column of magnesium perchlorate). A background scan was obtained

prior to each set of tests using a carbon black specimen. According to McClelland *et al.* (2002), Schubert *et al.* (1997a), 5-10 μm depth of the polymer surface is sampled with these settings.

Scanning Electron Microscopy (SEM)

1 cm^2 sections of modified and unmodified polymers were affixed on aluminium stubs provided by the QMUL Materials Department, SEM Unit and gold-sputtered under vacuum for 90 seconds. The surfaces of these samples were then viewed by SEM at a filament voltage of 10 kV.

Thermogravimetric Analysis (TGA)

Small sections ($\sim$ 5-20 mg) of modified and unmodified polymers were cut and placed onto the sample pound. The exact weight of these samples was determined before each measurement. The temperature was increased from 20°C to 1000°C in increments of 50°C per minute.

3.3.4 Electrochemistry

A three-electrode configuration was used due out the experiments comprising of Pt as working electrode, Ag/AgCl as reference and Pt wire as counter electrode unless stated otherwise. Polymer coated needle-type electrodes were fabricated (Section 3.3.5), prepared (Sections 3.3.5 and 3.3.5) and assessed in respect to their performance in amperometric analyte detection (starting from Section 3.3.7). Polymer coatings (PCU, PCU-OH, PCU-SO_3, PEU, PEU-OH, PEU-SO_3 and SR modified) were applied on electrode tips as described in Section 3.3.6. Bare electrodes were also used for reference purposes. For H_2O_2 detection, the working electrode surface (Pt) was additionally modified with Prussian Blue (Section 3.3.7) and compared to non-PB modified, polymer coated and uncoated electrodes. All electrodes were analysed in triplicate.

Preparation of Solutions

Hydrochloric Acid Solution, 0.1 M

10 ml of HCl was added into 1,000 ml volumetric flask and dissolved at room temperature in deionised water to make up 1 litre.

Potassium Chloride Solution, 0.1 M

7.4 g KCl was added into 1,000 ml volumetric flask and dissolved at room temperature in deionised water to make up 1 litre.

Ferrocyanide Solution, 1 mM in 0.1 M KCl

42.24 mg $K_4Fe(CN)_6$ and 0.75 g of KCl was transferred into 100 ml volumetric flask and dissolved at room temperature in deionised water to make up 100 ml.

Ferric Chloride Solution, 0.1 M

0.270 g $FeCl_3$ was added into 10 ml volumetric flask and dissolved at room temperature in 1 M HCl standard solution to make up 10 ml.

Ferricyanide Solution, 0.1 M in 0.1 M KCl

3.293 g $K_3Fe(CN)_6$ and 0.75 g of KCl was transferred into 100 ml volumetric flask and dissolved at room temperature in deionised water to make up 100 ml. This solution was prepared fresh each time.

Potassium Phosphate Buffer Solution, 0.1 M KCl, pH 7.4

- 2.0 M monobasic phosphate stock solution was prepared in 50 ml volumetric flask from 13.61 g KH_2PO_4 anhydrous dissolved in 50 ml deionised water.
- 2.0 M dibasic phosphate stock solution was prepared in 50 ml flask from 17.42 g K_2HPO_4 anhydrous dissolved in 50 ml deionised water.
- 0.1 M buffer working solution was prepared in 1,000 ml volumetric flask from 3.6 ml monobasic phosphate stock solution, 16.4 ml dibasic phosphate stock solution and 7.5 g KCl in deionised water at room temperature to make up 1,000 ml.

These solutions were stored at 4°C. If necessary, the buffer working solution was adjusted to pH 7.4 using stock solutions.

Hydrogen Peroxide Standard Stock Solution, 0.1 M

The actual concentration of H_2O_2 in aqueous solution containing 30 % v/v H_2O_2 was determined by titration with a potassium permanganate solution of known strength.

Theoretically, 113.38 μl of H_2O_2 (30% v/v) was transferred into a 10 ml volumetric flask and buffer solution was added to make up 10 ml. However, the exact amount of H_2O_2 added to obtain a standard stock solution of 0.1 M was determined according to the "real" H_2O_2 concentration. This solution was prepared fresh each time.

Hydrogen Peroxide Standard Stock Solution, 0.001 M

Theoretically, 100 μl of 0.1 M H_2O_2 stock solution was transferred into a 10 ml volumetric flask and buffer solution was added to make up 10 ml. However, the exact amount added was determined according to the "real" H_2O_2 concentration. This solution was prepared fresh each time.

N-Acetyl-4-aminophenol Standard Stock Solution, 0.1 M

151.2 mg of N-Acetyl-4-aminophenol (acetaminophen) was transferred into a 10 ml volumetric flask and buffer solution was added to make up 10 ml. This solution was prepared fresh each time.

L-Ascorbic Acid Standard Stock Solution, 0.1 M

176.1 mg of ascorbic acid was transferred into a 10 ml volumetric flask and buffer solution was added to make up 10 ml. This solution was prepared fresh each time.

Uric Acid Standard Stock Solution, 0.1 M

168.1 mg of uric acid was dissolved in 2 mM ammonium hydroxide solution in the molar ratio of NaOH to UA of 1.7:1 as suggested in literature [Ellerbe *et al.* (1988), Xinhua (2006)]. This stock solution was stored in a dark flask at -20°C and is stable for at least 3 months.

Bovine Serum Albumin Standard Stock Solution, 10 % w/v

1 g of bovine serum albumin (99%) is dissolved in 10 ml potassium phosphate buffer solution (0.1 M KCl, pH 7.4).

3.3.5 Fabrication of Needle-type Electrodes

Stainless steel tubing was cut to about 70 mm length and the ends were smoothened out with emery paper. A polyester insulated platinum wire was inserted into the tubing and

affixed with epoxy resin. A co-axial cable of about 30 cm length was split at both ends and at one of the ends, one of the two exposed wires was attached to the stainless steel tubing and the other wire to the platinum wire from which the insulation was taken off at the end. This construct was housed into a small syringe and affixed with epoxy resin; Figure 3.8 shows an illustration.

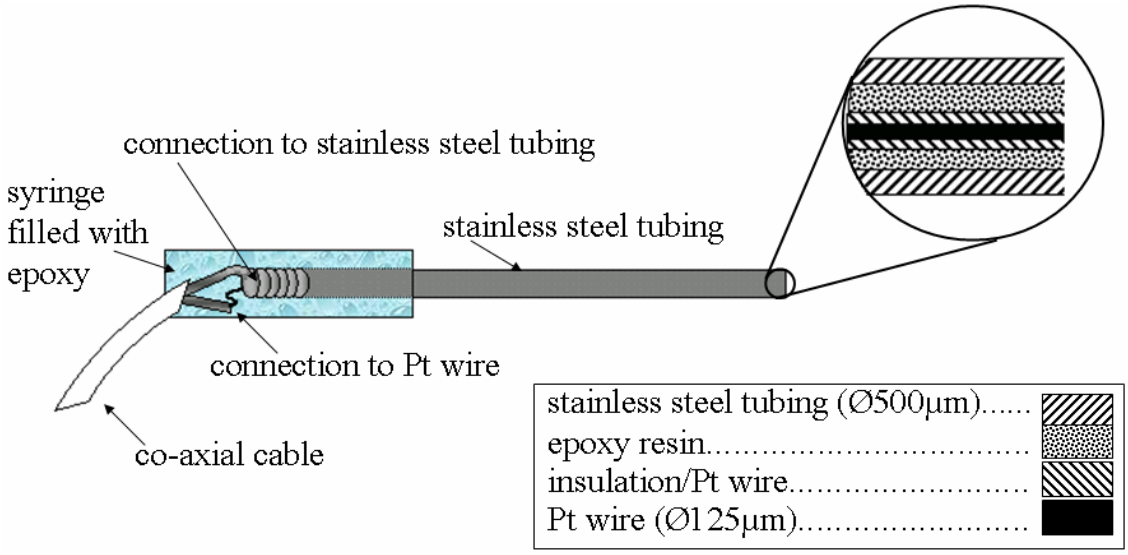

Figure 3.8: Schematic illustration of needle-type electrode

Surface Preparation of Working Electrode

To obtain a smooth and reproducible working electrode surface, the electrode tip was mechanically polished in a slurry of aluminium oxide powder in a figure of eight motion using wet 1200 grade silicon carbide paper. The electrodes where then copiously rinsed in deionised water and sonicated for a few minutes to remove any residual alumina powder [Bott (1997)].

Electrochemical Pre-treatment

Prior to each experiment, the electrode tip was placed in 1 M $HClO_4$ and a switching potential in the range of -0.25 to 1.5 V versus Ag/AgCl was applied with a scan rate of 0.1 V/sec. This treatment serves to regenerate a reproducable electroactive surface free of residual impurities [Ho *et al.* (2003)].

A typical scan of a needle-type electrode with a clean Pt surface is illustrated in Figure 3.9. The chemical processes occurring at the electrode surface with cathodic peaks at $< +0.1$ V are adsorption and desorption of hydrogen on the Pt electrode. The

anodic peaks at $> +0.5$ V are ascribed to the surface oxide formation and the cathodic peaks at $\sim +0.4$ V are ascribed to the surface oxide reduction. The evolution of hydrogen and oxygen takes place at < -0.2 V and > 1.25 V, respectively.

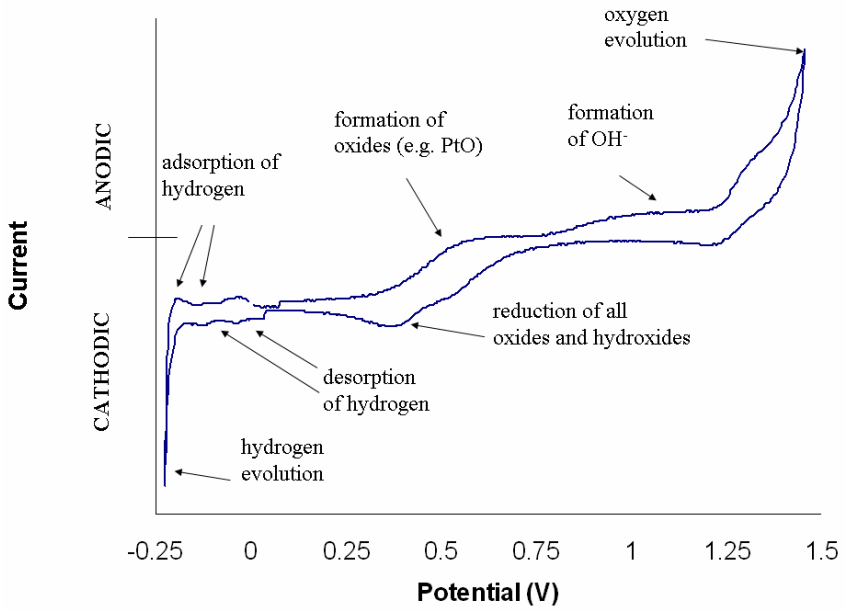

Figure 3.9: Typical CV of a clean Pt electrode surface (vs. Ag/AgCl; 100 mV/s; solution phase: 1 M $HClO_4$)

3.3.6 Prussian Blue Formation

Needle-type electrodes were prepared and pre-treated according to Sections 3.3.5 to 3.3.5. The Pt working electrode was electropolymerised with PB via cyclic voltammetry, using a two-step method modified from that reported by Karyakin *et al.* (1999).

First Step/Deposition:

The electrode tips were immersed into growth solution of

- 160 μl of 0.1 M $FeCl_3$ in 1 M HCl
- 160 μl of 0.1 M $K_3Fe(CN)_6$
- 3640 μl of 0.1 M HCl/KCl

and cycled with a switching potential of +0.75 to +0.4 V (vs. Ag/AgCl) at a scan rate of 40 mV/s for 8, 12 and 16 cycles respectively. After formation of the PB precipitate (film growth), electrodes were placed in a vacuum oven set at 65°C and dried for 4 hours.

Second Step/Activation:

The electrodes were then activated in 0.1 M HCl/KCl with a switching potential of +0.35 to -0.05 V at a scan rate of 50 mV/s for 25 cycles or until stable voltammogram was obtained. With this activation step, the formation of a polycrystalic PB in the presence of counter ions K^+ is completed. These electrodes were then placed in a vaccuum oven set at 100°C and dried for 1 hour before stored in designated boxes prior use.

All experiments were carried out at room temperature (25°C) in non-stirred conditions using an experimental set-up as illustrated in Figure 3.11. The solutions for growth and activation were purged with nitrogen for 30 minutes prior to use.

PB Stability Testing

It has been reported that the stability of the electrocatalytic PB layer was compromised at potentials more negative than the PB/PW redox potential [Itaya *et al.* (1984)]. Karyakin *et al.* (1999) suggested a method for stability testing by applying a cathodic potential of -50 mV (vs. Ag/AgCl) to the PB modified electrode.

In this study, accelerated degradation of PB was simulated by applying -50 mV (vs. Ag/Agcl, 0.1M HCl/KCl) to the PB modified electrode for 300 seconds. CVs were taken before and after degradation as described in Section 3.3.6, *Second Step/Activation*. The peak currents and the potential separation was compared before and after degradation.

Polymer Coating

PU solutions and SR suspension were prepared and dried as outlined in Section 3.3.4. Instead of solvent-cast on glass slides, polymers were applied by dipping the electrode tips into these solutions. Surface modifications on PU coated needle-type electrodes was also undertaken using the same procedure as described in Section 3.3.1. A separate glass vessel (Figure 3.10) to accommodate needle-type electrodes was designed for these specific reactions. This reaction vessel was manufactured in-house by Mr. John W. Cowley, a glassblower in the Chemistry Department at QMUL. These coated and/or modified electrodes were stored in designated boxes free of dust prior use.

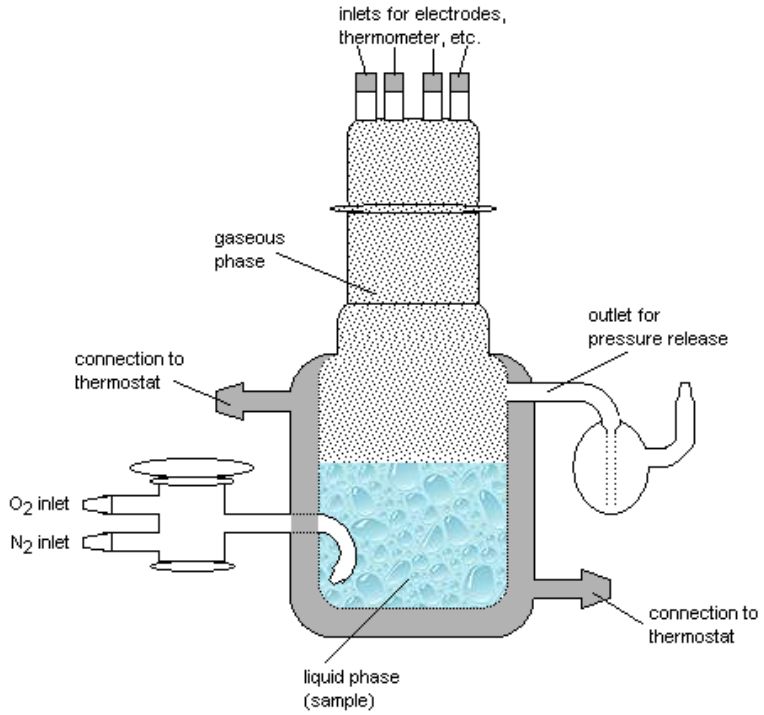

Figure 3.10: Glass vessel to accomodate needle-type electrodes

3.3.7 Electrochemical Performance

Conditioning of Needle-type Electrodes

Prior to amperometric analyte detection, a Clark-type measuring chamber (Figure 3.11) was connected to an external circulating thermostat (set to 25°C). 5 ml of phosphate buffer solution was placed into sample chamber and left for about 30 minutes under stirred conditions to reach set temperature. Pre-treated needle-type electrodes (Sections 3.3.5 to 3.3.6) were placed into this sample chamber.

For O_2 measurements, a two-electrode set-up was used in which the Pt working electrode was polarised with a potential of -650 mV versus stainless steel as pseudo-reference [Whalen *et al.* (1980)]. H_2O_2 detection was performed via three-electrode set-up as outlined in Section 3.3.4. PB modified Pt electrodes were polarised with 0 mV, non-PB modified Pt electrodes were polarised with +650 mV both versus Ag/AgCl. The current response was recorded electronically; this procedure was performed until a stable background current was established.

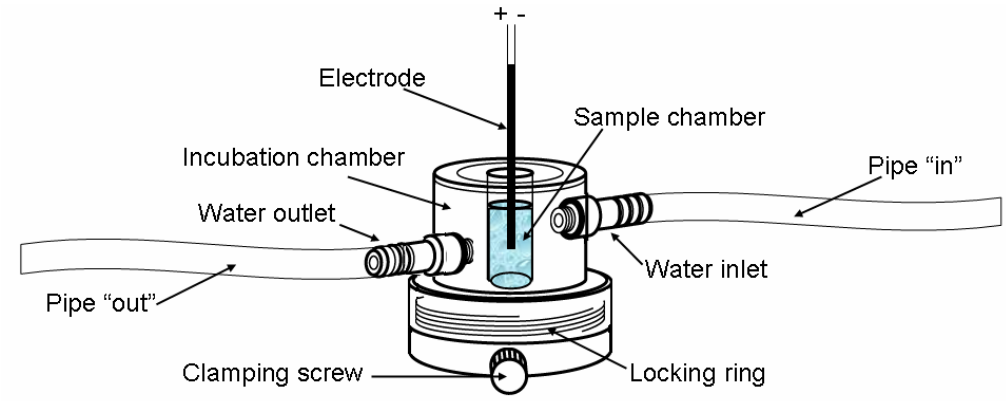

Figure 3.11: Generic electrode set-up for temperature controlled measurements using Clark-type electrode as measuring chamber [adapted and modified from operational manual of dissolved oxygen electrodes supplied by Rank Brothers Ltd., Cambridge, UK]

Calibration of Needle-type Electrodes

H_2O_2 Detection:

After conditioning (Section 3.3.7), calibration was performed by step-concentration addition of H_2O_2 standard stock solution (0.001 M) in 5 ml buffer solution to obtain concentrations of 1, 5, 10, 15, 20, 25, 30, 35, 40, 45, 50 μM and additionally from 50 to 200 μM in 10 μM steps. For higher concentrations, the calibration was performed by step-concentration addition of H_2O_2 standard stock solution (0.1 M) to obtain solutions with the concentrations of 1, 2.5, 5, 7.5 and 10 mM.

In order to maintain a constant volume, the corresponding volume to be added from the H_2O_2 stock solution was removed from the bulk solution before each analyte injection. Each measurement was taken in triplicate.

O_2 Detection:

For calibration purposes, an airtight vessel was required in which the oxygen concentration could be readily altered to different, well defined levels. Readily available plastic tubing material and plastic syringes from Royal London Hospital, Whitechapel were used. The design developed was based on commercially available single mixing stopped-flow cells. The operation of this "Stop-Flow-Cell" (Figure 3.12) was conducted under temperature controlled conditions of 25°C.

The electrodes were conditioned as outlined in Section 3.3.7. In the meantime, PBS was placed in a glass vessel (Figure 3.10) and de-oxygenated by flushing with nitrogen

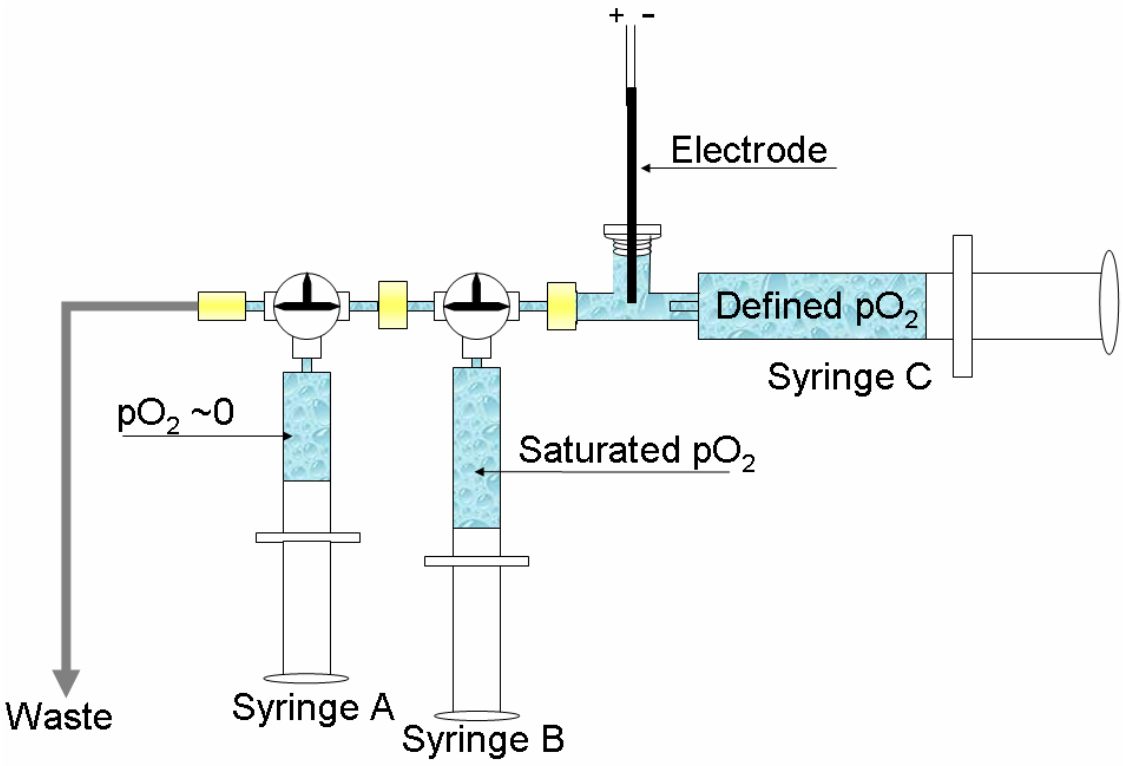

Figure 3.12: Schematic illustration of "Stop-Flow-Cell" for calibration purposes of needle-type electrodes for measuring pO_2

gas for 30 minutes. In a separate, identical glass vessel (Figure 3.10), PBS was flushed with O_2 gas for 30 minutes for oxygen saturation. The de-oxygenated PBS was placed into syringes A and C and the cell was then flushed through with this solution, keeping a remainder of 50 ml within the construct. The conditioned electrode was placed into this assembly, whilst maintaining the connection to the potentiostat.

Once the background current stabilised, oxygen saturated phosphate buffer solution was added via syringe B in 0.75 ml steps. Before each addition, the corresponding volume (0.75 ml) was first removed with separate syringe to maintain the overall volume. These buffer samples were then submitted to pO_2 determination using an in-house blood gas analyser. The pO_2 values differed only by about ± 0.1 kPa, demonstrating the air tightness of this construct. Each time 0.75 ml of oxygen saturated buffer was added to the construct, it was thoroughly mixed with separate syringe.

Analyte Selectivity of H_2O_2

Electrodes were treated and conditioned according to Sections 3.3.5 to 3.3.7, including and excluding Section 3.3.6. Then 5 μl of ascorbic acid stock solution was added to

5 ml buffer solution to obtain a concentration of 0.1 mM. When the current response was stable, another 45 μl of ascorbic acid solution was added to obtain a concentration of 1 mM. The electrode was then removed and thoroughly rinsed in deionised water before being placed in fresh buffer solution (5 ml). This process was repeated with uric acid and acetaminophen of the same concentration.

To simulate a real environment, this process was also conducted with buffer solution containing H_2O_2 (0.1 mM) including all of the interferents at expected average physiological values (0.4 mM uric acid + 0.1 mM ascorbic acid + 0.1 mM acetaminophen). To maintain volume and concentration at desired levels, the corresponding volume to be added was removed from the bulk solution before each analyte injection. Each measurement was taken in triplicate.

Electrode Fouling

The electrodes were treated and conditioned according to Sections 3.3.5 to 3.3.7, including and excluding Section 3.3.6. Hydrogen peroxide stock solution was added to buffer solution to obtain a concentration of 0.05 mM. Once the current response was stable, 2.5 ml were removed and replaced by 2.5 ml BSA stock solution to obtain a protein concentration of 5 % w/v. The current response was monitored for twenty four hours and related to the current response before protein exposure. The same measurements were also conducted with a H_2O_2 concentration of 5 mM and 5 % w/v BSA. All measurements were taken in quadruplicate.

3.3.8 Cell Work

Polymers, modified and unmodified, described in Section 3.3.1 onwards were evaluated regarding cell-material interactions. The level of cell attachment including growth and spread was assessed. This work was conducted at the Institute of Cell and Molecular Science (ICMS), London.

The test chosen was the direct cell contact assay according to ASTM F813-83 using a murine fibroblast cell line. Cell viability and proliferation was assessed quantitatively via resazurin-based dye reduction (AlamarBlue^{TM}) and supplemented via qualitatively visual observation of cell morphology using an inverted light microscope.

Preparation of Solutions

Cell Culture Media

Dulbecco's Modified Eagle Medium and small centrifuge tubes of FBS and P/S were placed in a water bath set to 37°C. After 15 minutes, the medium bottle and the tubes were wiped with aqueous EtOH (70% v/v) and placed in laminar flow hood. 55 ml of medium were removed and replaced by 50 ml of FBS solution (10 %) and 5 ml of P/S solution (1 %).

Washing Medium

Dulbecco's Modified Eagle Medium

Cyropreservation Mixture

8 ml washing medium and 2 ml of DMSO were added into a 10 ml centrifuge tube and thoroughly mixed.

Alamar Blue^{TM}Solution

45 ml of cell culture medium was placed into screw-cap vial and 5 ml of Alamar Blue^{TM}was added to obtain a concentration of 10% (v/v).

Procedures for Cell Culturing

Thawing of Frozen Cells

The cryogenic vial (2 ml tube) containing frozen cells was taken out of the liquid nitrogen storage tank and gently defrosted by first warming it in the hands for a few minutes; it was then placed into a water bath set at 37°C to thaw quickly.

Cell Culture

- 9 ml of washing medium was placed into 20 ml centrifuge tube and the 1 ml defrosted cell suspension was added and well mixed.
- This suspension was centrifuged at 1000 rpm for 3 minutes before washing solution was dispensed.

- 10 ml of washing solution was then added and cells were re-dispensed and centrifuged before washing solution was dispensed. This washing process was repeated three times.
- 10 ml of cell culture media was then added to the centrifuged cells and well mixed before being placed in a cell culture flask.
- The cell culture flask was placed in an incubator (37°C/10% CO_2).

Cell Harvesting and Splitting

- Used cell culture medium was aspirated.
- Remaining cells were rinsed once with washing solution.
- 5 ml trypsin was added into cell culture flask.
- The flask was then gently swayed to ensure even coverage of trypsin and placed into incubator (37°C) for about 8 minutes or until cells become rounded and loosen from the surface of the flask.
- This suspension was transferred into centrifuge tube and centrifuged for 3 minutes at 1000 rpm after which the solution was suspended.
- The remaining cells were well mixed with washing solution, centrifuged for 3 minutes at 1000 rpm and the remaining solution was dispensed. This process was repeated three times.
- The supernatant was then finally replaced with 10 ml of cell culture media and well aspirated with the cells.
- Into each cell culture flask, 2 ml of the final cell suspension was added and placed into incubator (37°C/10% CO_2).

Cell Counting

A haemocytometer was used to determine the amount of cells present per millilitre cell suspension. This is a specially designed glass slide with a 0.1 mm^3 chamber and a counting grid (Figure 3.13). The haemocytometer was stored in an aqueous EtOH solution (70% v/v) when not in use.

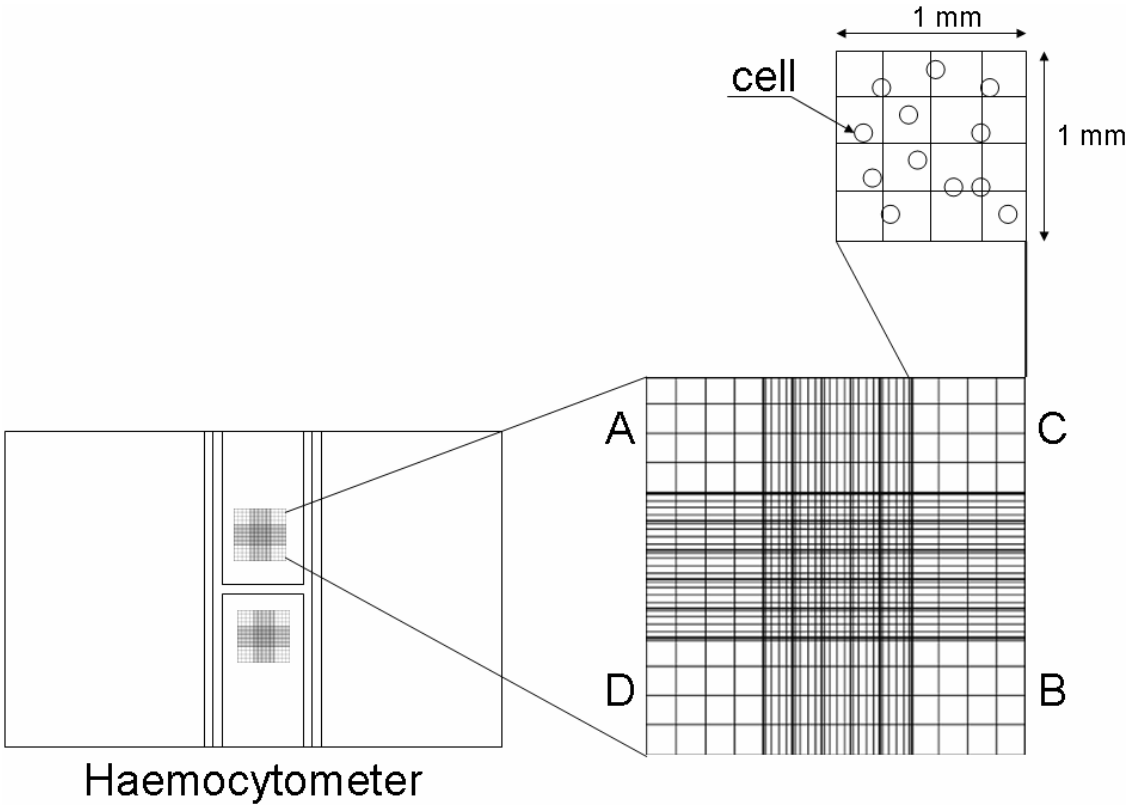

Figure 3.13: Illustration of haemocytometer layout

Procedure:

- The shoulders of the haemocytometer were moistened and the coverslip was affixed using gentle pressure and small circular motions.
- Harvested cell suspension (Section 3.3.8) was well mixed before 10 μl were placed on the edge of the haemocytometer using a pipette.
- A microscope was used to focus on the grid lines within one chamber. 16 squares should be visible per chamber; the cells were counted within this area.
- This was repeated for the three remaining chambers and the average amount of cells was calculated.

Cryopreservation of Cells

- 0.5 ml harvested cell suspension (Section 3.3.8) was placed into 2 ml cryocenit vial.
- 0.5 ml of cryopreservation mixture (Section 3.3.8) was added and carefully mixed.

- Cryocenit vials were wrapped in several layers of tissue and stored at 4°C for 2 hours before placed into freezer set at −70°C for 24 hours.
- Cyrocenit vials were then unwrapped and placed into liquid nitrogen storage.

Cytotoxicity Testing

3T3 fibroblast cells were grown in direct contact with polymers and cytotoxicity testing was conducted using Alamar Blue™. Both positive (PC) and negative (NC) toxicity control samples were also included for reference purposes.

Polymers (Sections 3.3.1 to 3.3.2) and PC strips were cut into 1 cm^2 sections and placed in well plates including NC cover slips. The 24-well plate set-up is illustrated in Figure 3.14, in which PC stands for positive control, NC for negative control, M+C stands for cell culture medium including cells and M for cell culture medium only.

The results were calculated according to how much dye had been reduced by the cells over a set time period.

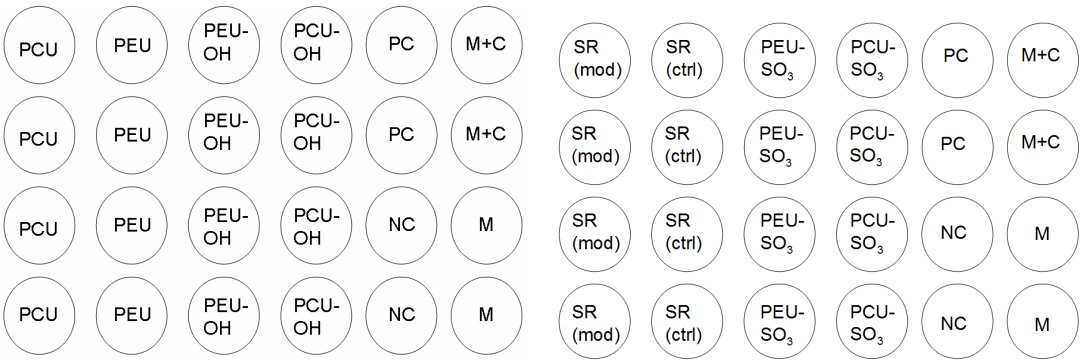

Figure 3.14: Well plate set-up for cytotoxicity testing

Seeding of Cells on Polymers

Polymers (Figure 3.14) were soaked in aqueous EtOH (70% v/v) over night for sterilisation. The sterilising solution was aspirated and the well plates were then left to dry in tissue culture fume hood under sterile conditions for 6 hours. A 3T3 fibroblast cell line was prepared and counted as stated in Section 3.3.8. The cells were then deposited on the centre of each polymer to obtain a cell density of $1x10^4$ cells per well. These seeded well plates were placed into incubator (37°C/10% CO_2) for 24 hours to allow the cells to attach to the surface.

Alamar Blue™ Assay

Alamar Blue™, a non-toxic aqueous dye, was used to asses the viability and proliferation of 3T3 fibroblasts seeded on polymeric materials. The examination time points were set after 24, 48, 72, 96 and 168 hours of initial cell incubation.

Procedure:

- Cell culture medium was aspirated.
- Remaining seeded polymers were rinsed once with washing medium.
- Washing medium was aspirated and 1 ml of Alamar Blue™ solution (Section 3.3.8) was added into each well.
- The well plate was then placed into incubator (37°C/10% CO_2) for four hours.
- 50 μl of this dye solution was removed from each well and placed into a 96 well plate.
- The absorbance was measured spectrophotometrically at 570 and 600 nm with a well plate reader.
- The rest of the dye containing medium was aspirated and each well was rinsed once with washing medium.
- 1 ml of fresh cell culture medium (Section 3.3.8) was added into each well.
- Wells were placed into incubator (37°C/10% CO_2).

The morphology of the cells was examined after each AlamarBlue™ incubation using an inverted light microscope from which digital images were taken. The dye absorbencies were calculated and plotted into graph format showing how much dye had been reduced by the cells.

Cell Fixation for SEM Analysis

All biological samples were prepared using the method which has been established by Nation (1983) as a standard protocol for biological samples. This method utilises hexamethyldisilazane (HMDS), which allows air drying of cells as opposed to critical point drying.

Procedure:

Following cell seeding and attachment on polymers (same set-up as illustrated in Figure 3.14), samples were cooled and stored at 4°C for thirty minutes. The cell culture medium was removed and replaced with 1.5% (v/v) glutaraldehyde (GA) buffered in 0.1 M sodium cacodylate (pH 7.2). This fixative was prepared by mixing equal volumes of 3% (v/v) GA with 0.2 M sodium cacodylate. The 0.2 M buffer was prepared by dissolving 4.28 g of sodium cacodylate in 100 ml of de-ionised water and the pH was adjusted to 7.3 by drop-wise addition of 5 M HCl.

This was a primary fixation step and samples were stored in this solution for at least two hours at 4°C before proceeding to the next step. Samples were washed twice for five minutes in 0.1 M sodium cacodylate and then treated with 1% osmium tetraoxide buffered in 0.1 M sodium cacodylate for one hour at room temperature. The samples were then washed three times (five minutes each time) with 0.1 M cacodylate buffer. The samples were then dehydrated with EtOH with increasing concentration (20, 30, 50 and 70% v/v) in two cycles for each concentration (five minutes each time). The samples were then treated with 0.5% uranyl acetate dissolved in 70% (v/v) EtOH for 30 minutes before two 10 minute washes in each of 90% (v/v) and 100% (v/v) EtOH. The fixed and dehydrated cells were finally submerged in HMDS and allowed to fully air-dry over night. Once dry, the samples were then mounted on aluminium stubs, gold-sputtered under vaccuum for 90 seconds and viewed under field-emission microscope.

3.4 Source Addresses

- BDH Chemicals, Poole, Dorset, UK.
- BOC Gases, Priestley Road, Surrey Research Park, Surrey, GU2 7XY, UK
- Fisher Scientific, Bishop Meadow Road, Loughborough, LE11 5RG, UK
- Fluka Chemicals, The Old Brickyard New Road, Gillingham, SP8 4JL, UK
- Goodfellow Cambridge Ltd., Ermine Business Park, Huntingdon, PE29 6WR, UK
- Institute of Cell and Molecular Science, Barts and The London School of Medicine and Dentistry, The Blizard Building, 4 Newark Street, London E1 2AT, UK
- JEOL UK Ltd., JEOL House, Silver Court, Welwyn Garden City, AL7 lLT, UK

- KRÜSS GmbH, Borsteler Chaussee 85-99a, 22453 Hamburg, Germany
- Leica Microsystems Ltd., Davy Avenue, Knowhill, Milton Keynes, MK5 8LB, UK
- Merck Chemical Ltd., Boulevard Industrial Park, Padge Road Beeston, Nottingham, NG9 2JR, UK
- Millipore S. A. S. - Molsheim, BP 116, 67124 Molsheim Cedex, France
- Motic Microscopes, Saracens House, 25 St. Margarets Green, Ipswitch, IP4 2BN, UK
- NuSil, Unit 2, Network 4, Cressex Business Park, High Wycombe, HP12 3RF,UK
- Palm Instruments BV, Dr. Kees van Velzen, Ruitercamp 119, 3992 BZ Houten, NL
- Perkin Elmer Life Sciences Ltd., 204 Cambridge Science Park, Cambridge, CB4 0GZ, UK
- Robnor Resins Ltd., Hunts Rise, South Marston Park, Swindon, SN3 4TE, UK
- Royal London Hospital, Whitechapel Road, Whitechapel, London E1 1BB, UK
- RS Components Ltd., PO Box 99, Corby, NN17 9RS, UK
- Sigma-Aldrich Company Ltd., Fancy Road, Poole, BH12 4QH, UK
- TA Instruments-Waters LLC, 109 Lukens Drive, New Castle, DE 19720, US
- VWR International Ltd., Merck House, Poole, BH15 1TD, UK
- Windsor Scientific Ltd., 264 Argyll Avenue, Slough Trading Estate, Slough, SL1 4HE, UK

3.5 Calculations / Statistical Analysis

Cyclic Voltammetry

The voltage separation between the current peaks for reversible reaction under standard conditions is given by:

$$\Delta \mathrm{E} = E_p^a - E_p^c = \frac{59}{n} mV \tag{3.1}$$

where ΔE stands for peak separation, E_p^a and E_p^c are anodic and cathodic peak potentials, respectively, and n is the number of electrons appearing in the half-reaction for the redox couple. The ratio of the peak currents is unity, and can be expressed as:

$$\frac{i_p^a}{i_p^c} = 1 \tag{3.2}$$

in which i_p^a and i_p^c stand for anodic and cathodic peak currents, respectively. For diffusion-limited current, the peak current is proportional to the square root of the scan rate:

$$i_p \propto \sqrt{v}. \tag{3.3}$$

If the redox peak is relatively broad, and the peak potential is difficult to determine, it is more convenient to report the potential at half-peak current, i.e. the half-peak potential, $E_{p/2}$. The polarographic $E_{1/2}$ value is located about midway between E_p and $E_{p/2}$, and the Nernstian wave for a reversible reaction is given by the following equation:

$$E_p - E_{p/2} = 2.2\frac{RT}{nF} = \frac{56.5}{n} \text{ mV at } 25^\circ\text{C} \tag{3.4}$$

where E_p (V) is the peak potential and is independent of the scan rate, $E_{p/2}$ (V) is the half-peak potential, R is the universal gas constant (8.314472 J/K mol), T is the absolute temperature in Kelvin, and F is the Faraday constant (96485 C/mole).

The amplitude of the oxidation peak in a CV for a reversible system is directly proportional to the analyte concentration of the redox couple, as described by the Randles-Sevčik equation:

$$i_p = (2.69 \times 10^5) n^{3/2} A C D^{1/2} v^{1/2} \text{ at } 25^\circ\text{C} \tag{3.5}$$

where i_p is the peak current (A), n is the number of electrons, A is the electrode area (cm^2), C is the concentration of the electrocactive species in the bulk solution (mol/cm^3), D is the diffusion coefficient (cm^2/sec) and v is the scan rate (V/sec). The unit of the constant is $C/mol^{1/2}v^{1/2}$.

Prussian Blue

The PB coverage (Γ) on the electrode surface was determined by manually integrating the area of the cathodic peak under voltommetric I-E curves using the following equation:

$$Q = nAF\Gamma \tag{3.6}$$

where Q is the total charge (C), n is the number of electrons, A is the surface area (cm^2) and F is the Faraday constant (96485 C/mole). The units of surface coverage (Γ) is expressed in mole/cm^2. A transfer of four electrons per unit cell of Prussian Blue was presumed [Hazen *et al.* (2003), Itaya *et al.* (1984)]. Assuming a uniform distribution of the deposited film, the thickness (L) of the PB film was determined with equation (Hazen *et al.* (2003):

$$L = \Gamma M_V \tag{3.7}$$

in which M_V stands for molar volume, which is given as 677 cm^3/mole. The unit for film thickness is expressed in cm.

Amperometry

Statistical regression analysis provides a robust technique for fitting a line of best fit through a series of data points (x,y). The equation for this line of best fit is given by

$$y = ax + b \tag{3.8}$$

where $a = \Sigma(x - \bar{x})(y - \bar{y})/\Sigma(x - \bar{x})^2$ and $b = \bar{y} - a\bar{x}$. The values for a and b will vary, dependant upon the values of the data points (x,y). The best statistic for summarising the quality of the line of best fit for any set of data points is R^2 (also known as the coefficient of determination). A value of 1 for R^2 indicates that the data points (x,y) have a perfect linear relationship. The R^2 statistic is defined as

$$\frac{SS_R}{SS_T}$$

where $SS_T = \Sigma(y - \bar{y})^2$, $SS_R = \Sigma(\hat{y} - \bar{y})^2$ and $\hat{y}$ is the predicted value of y, obtained from equation (3.8) when a and b have been calculated.

The performance characteristics of the needle-type electrodes were determined using linear regression and correlation analyses. Linearity of the sensor was determined as the

fit of each calibration curve to a straight line, using the correlation coefficient, R^2. The sensitivity was defined as the change in current per unit analyte concentration, calculated as the slope of the line of best linear fit.

The response time (T_r) was defined as the difference between the time at which an analyte was introduced (T_0) and the time at which it returned to steady state (T_a):

$$T_r = T_a - T_0. \tag{3.9}$$

The limit of detection (LOD) was derived from the smallest measure (x_L) that can be detected with reasonable certainty for a given analytical procedure [McNaught *et al.* (1997)]:

$$x_L = x_{\text{bl}} + k s_{\text{bl}} \tag{3.10}$$

in which x_{bl} stands for the mean of blank measurements, s_{bl} the standard deviation of blank measurements and k is defined as the numerical factor chosen acording to the confidence level desired.

The reproducibility (RSD) is a measure of the scatter/drift in a series of results (s_X) performed over a period of time for analyte concentrations within the linearity range [Thévenot *et al.* (1999)]. RSD indicates the reproducibility of one sensor (RSD_1) in comparison with a batch of five different sensors (RSD_5):

$$RSD(\%) = \frac{s_X \times 100}{\bar{X}} \tag{3.11}$$

where $\bar{X} = \Sigma X_i/n$ and $s_X = \Sigma(X_i - \bar{X})^2/(n-1)$.

The long- and short term stability of a sensor gives an indication on a sensor's current output when the sensor was used continuously within the linear concentration range over a certain period of time; short-term being operational stability and long-term being storage stability:

$$T_{LX} = \frac{s_X \times 100}{X}. \tag{3.12}$$

Selectivity (i_s), expressed as the percentage of variation of the sensor output, was determined by the ability of a sensor to reject current responses (X_i) to chemical species other than the target analyte (X):

$$i_s = \frac{X - X_i}{100}. \tag{3.13}$$

Chapter 4

Development and Characterisation of Polymers

4.1 Introduction

The first project objective was to synthesise and modify PU and SR as coating materials for amperometric needle-type electrodes. The two main goals were:

- to develop effective surface modification methods for PU in order for these modifications to be performed on polymers already attached to needle-type electrodes;
- to develop effective bulk modification for SR to achieve permeability to H_2O_2.

To accomplish these goals, the polymers would be required to retain their adherence properties to the sensing device, as well as to maintain the activity of the sensing part of the electrode throughout the modification process and thereafter. The prepared polymers would also be required to maintain their mechanical integrity and functionality in prolonged measurements. These materials have to be non-toxic to cells, albeit effectively suppressing cell attachment and growth.

In this Chapter, synthesis and modification methods of PU and SR are presented. The characteristics of the obtained polymers were investigated in terms of surface chemistry and surface structure, thermal stability, wettability and protein adsorption, degradative stability and cytotoxicity.

4.2 Polyurethane

Preliminary experiments involved the synthesis of polyurethane (PU) performed *in situ* by solvent-casting procedure in a one-step process. The resulting polymers contained either carbonate (PCU) or ether (PEU) moieties in their soft segment. It was found by other researchers [Kiremitçi *et al.* (1990), Kruczek *et al.* (2003), Lamba *et al.* (1998)] that the hard and soft segment distribution on the surface of the polymer can be altered by utilising a coagulation medium of specific polarity. This process is referred to as the phase inversion method. The methodology for the preparation of phase inverted PU used in this study was modified from a method reported by Huang *et al.* (1999). The differences to this method were as follows:

- Phase inversion was performed in non-polar coagulation medium.
- Lower polymer concentration was used.
- PUs differed in hard and soft segments.
- PUs had similar hard and soft segment ratios (HS-ratio).
- Polymers were prepared and dried at room temperature under normal atmospheric pressure.

These modifications were thought to result in an increased soft segment ratio on the surface of these polymers, which would be beneficial to further surface modifications, such as hydroxylation and sulphonation. In this section, phase inverted and conventional solvent cast PU were compared regarding to surface composition. Further surface modification of phase inverted polymers were assessed regarding their effectiveness and (bio)stability by means of Photoacoustic Fourier Transform Infrared Spectroscopy (PA-FTIR), Thermogravimetric Analysis (TGA), Contact Angle measurements (CA), Scanning Electron Microscopy (SEM), inverted microscope, protein adsorption and cytotoxicity. In Table 4.1, the chemical components including selected characteristics of PU and solvents used in this study are listed.

4.2.1 FTIR Analysis

FTIR spectra for conventional solvent cast and phase inverted PU were taken and analysed with respect to their characteristic frequencies using general reference texts [Bower

	Polyether Urethane (PEU)			Polycarbonate Urethane (PCU)		
Hard segment	H_{12}MDI/BD			MDI/BD		
Soft segment	PTMEG			PHEC		
HS-ratio	30/70			35/65		
Solubility parameter (cal/cm^3)	H_{12}MDI	8.98	*	MDI	13.95	*
	BD	11.00	*	BD	11.00	*
	PTMEG	7.09	**	PHEC	6.75	**
	DCM	9.93	***	THF	9.52	***
	n-Heptane	7.40	***	n-Heptane	7.40	***

Table 4.1: Characteristics of components for solution polymerisation of PU [adapted from Huang *et al.* (1997) *; Yang *et al.* (1999) ** and Burke (1984) ***]

et al. (1992), Coates (2000), Cross *et al.* (1969)]. The observed spectra displayed peak positions that correlated well with studies reported previously by various researchers [Christenson *et al.* (2004a), Korematsu *et al.* (2002), McCarthy *et al.* (1997), Zhang *et al.* (2003)]. During the phase inversion process in this study, the polymers were exposed to non-polar coagulation medium. During this process, the relative non-polar soft segments are expected to arrange themselves towards the surface whereas the relative polar hard segments subsequently will arrange themselves away from the surface. This should be reflected in the FTIR spectra. The peak assignments for polycarbonate urethane (PCU), conventional solvent cast and phase inverted, are tabulated in Table 4.2; Table 4.3 displays the corresponding values for polyether urethane (PEU). The full spectra of these polymers are illustrated in Figure 4.1 for PCU and Figure 4.2 for PEU.

The FTIR spectra of conventional solvent cast and phase inverted PCU (Figure 4.1) show the amino (N-H) vibration bands at 3200-3500 cm^{-1}, methylene (CH_2) bands at 2800-3030 cm^{-1}, carbonyl (C=O) bands at 1670-1770 cm^{-1}, specific urethane bands at 1300-1620 cm^{-1}, carbonate (C-O-C) stretch located at 1160-1300 cm^{-1} and urethane interface bands (C-O-C of C-O-C=C) at 1050-1100 cm^{-1}.

The FTIR spectra of conventional solvent cast and phase inverted PEU (Figure 4.2) show the N-H bands at 3200-3500 cm^{-1}, CH_2 bands at 2750-3030 cm^{-1}, C=O stretching regions at 1650-1750 cm^{-1}, specific urethane bands at 1200-1620 cm^{-1}, aliphatic ether (C-O-C) stretch located at 1100-1150 cm^{-1} and urethane interface bands C-O-C of C-O-C=C at 1070-1100 cm^{-1}.

The peaks for solvent cast and phase inverted PU in each spectrum appear to be relatively similar. Differences in the heights of various peaks is a strong indication of changes in surface composition of PU [McCarthy *et al.* (1997)]. In this study these

Peak assignments (cm^{-1})	Mode	Relative Intensity	Solvent cast	Phase inverted
N-H				
nonbonded	v	m	3334	3334
H-bonded	v	sh	3323	3323
C-H in CH_2				
asymetric	v	s	2939	2939
symetric	v	s	2862	2862
C=O				
carbonate nonbonded	v	vs	1743	1743
carbonate H-bonded	v	sh	1722	1722
urethane H-bonded	v	s	1701	1701
C=C				
aromatic ring	v	m	1597	1597
C-N & N-H				
amide	δ	s	1533	1533
C-H in CH_2				
bending, very strong	δ	m	1458	1458
C-C				
aromatic ring	v	m	1414	1414
C-N & N-H	v	m	1309	1309
C-O-C of C-O-C=C				
carbonate	v	vs	1259	1259
C-N	δ	sh	1223	1223
C-O	v	w	1111	1111
C-O-C of C-O-C=C				
urethane	v	m	1080	1080
C-H				
aromatic ring	β	w	1018	1020
Butadiene segment				
trans-1,4 form	v	w	964	964
C-H				
aromatic ring	γ	w	793	793

Table 4.2: Observed infrared band positions for conventional solvent cast and phase inverted PCU; where in Mode, v = vibration, β = in plane bending, γ = out of plane bending, δ = bending, and in Relative Intensity, w = weak, m = medium, s = strong, vs = very strong, sh = shoulder

Peak assignments (cm^{-1})	Mode	Relative Intensity	Solvent cast	Phase inverted
N-H				
nonbonded	v	w	3446	3446
H-bonded	v	s	3321	3319
C-H in CH_2				
asymmetric	v	s	2933	2933
asymmetric/symmetric	v	s	2854	2854
symmetric	v	w	2796	2796
C=O				
urethane nonbonded	v	s	1734	1734
urethane H-bonded	v	vs	1703	1703
associated amides	v	sh	N/A	N/A
C-N & N-H				
amide	δ	s	1533	1533
C-C				
aromatic ring	v	m	1414	1414
CH_2				
$\alpha-CH_2$ ether	w	w	1367	1367
C-N & N-H	v	m	1321	1321
C-O	v	sh	1246	1246
C-N	δ	s	1223	1223
C-O-C				
aliphatic ether	v	vs	1113	1113
C-O-C of C-O-C=C				
urethane	v	vs	1080	1080
Butadiene segment				
trans-1,4 form	v	w	972	972
C-H				
aromatic ring	γ	w	781	781

Table 4.3: Observed infrared band positions for conventional solvent cast and phase inverted PEU; where in Mode, v = vibration, γ = out of plane bending, δ = bending, w = wagging and in Relative Intensity, w = weak, m = medium, s = strong, vs = very strong, sh = shoulder

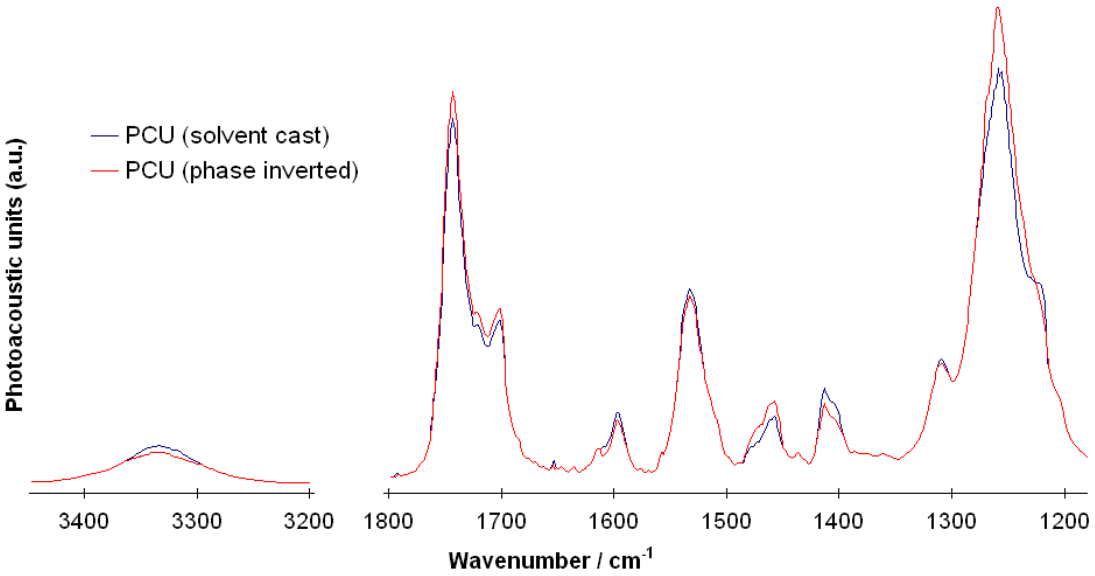

Figure 4.1: FTIR spectra of PCU, solvent cast and phase inverted

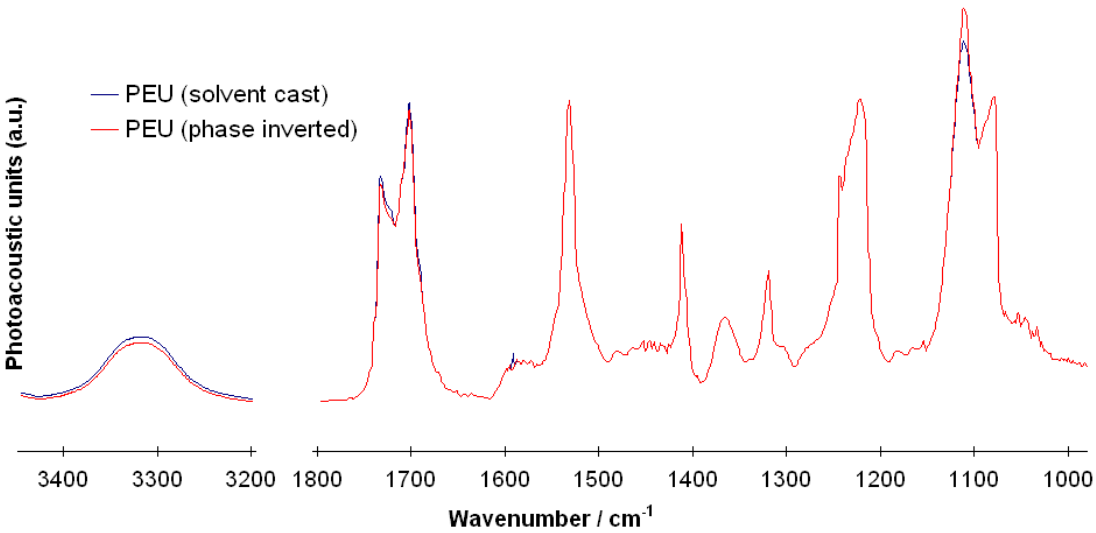

Figure 4.2: FTIR spectra of PEU, solvent cast and phase inverted

differences are associated with soft segment enrichment on the surface which was induced by phase inversion. More specifically, peak height changes of certain bands were observed; in particular the amino and carbonyl bands, the carbonate vibration bands (for PCU) and the aliphatic ether bands (for PEU). The peak height differences from these spectra were calculated and are presented in Figure 4.5. Since a low polymer concentration was used in this study, the decreased polymer content in the solvent would keep the polymer chains more mobile than more highly concentrated polymer solutions. This may have made the phase inversion process more effective.

Surface hydroxylation and sulphonation

Once the surface of PU was optimised regarding to soft segment enrichment, surface modification was investigated. In this section, PU was subjected to surface hydroxylation using potassium peroxodisulphate (PPDS). Sulphonate groups were then incorporated as side chains on the hydroxyl functional groups located at the polymer surface by subjecting hydroxylated PU to sodium hydride (NaH), triisobutylaluminium (TIBA) and 1,3 propane sultone (PS). The methodology for surface-hydroxylation of PU used in this study was modified from a method outlined by Bamford *et al.* (1994) and performed under multiple conditions: varying concentrations, time, and temperature. Using PPDS with a concentration of 10% w/v with temperatures of first 40°C and then 80°C over 4 hours gave the best results (Section 3.3.2).

A new methodology for sulphonation of functionalised PU was proposed and attempted under multiple conditions: varying concentrations, time, temperature and solvent. Using the initiator NaH/TIBA in the ratio of 1:1 and 5% w/v 1,3 propane sultone in the presence of toluene at 80°C gave the best results (Section 3.3.2). The full FTIR spectra are illustrated in Figure 4.3 for PCU and in Figure 4.4 for PEU. The observed spectra display peak positions that correlate well with that of spectra illustrated in Figure 4.1 and Figure 4.2.

However, differences in peak heights are observed compared to surface-modified and unmodified phase inverted polymers. These can be seen with N-H at 3200-3500 cm^{-1}, C=C at 1580-1630 cm^{-1} for PCU, C=O bands at 1670-1770 cm^{-1} for PCU and 1650-1750 cm^{-1} for PEU, C-O-C (PCU) at 1160-1300 cm^{-1} and C-O-C (PEU) at 1100-1150 cm^{-1}. New peaks are observed at 1041 cm^{-1} and 1182 cm^{-1} for PCU, 1049 cm^{-1} and 1182 cm^{-1} for PEU. These appearances confirmed the presence of sulphonate groups

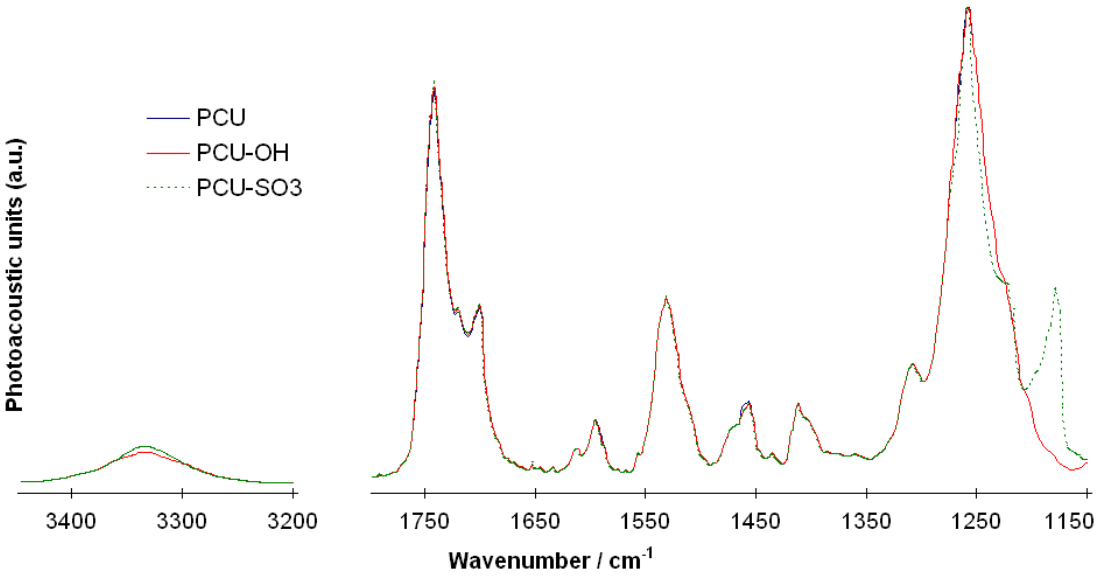

Figure 4.3: FTIR spectra of phase inverted, hydroxylated and sulphonated PCU

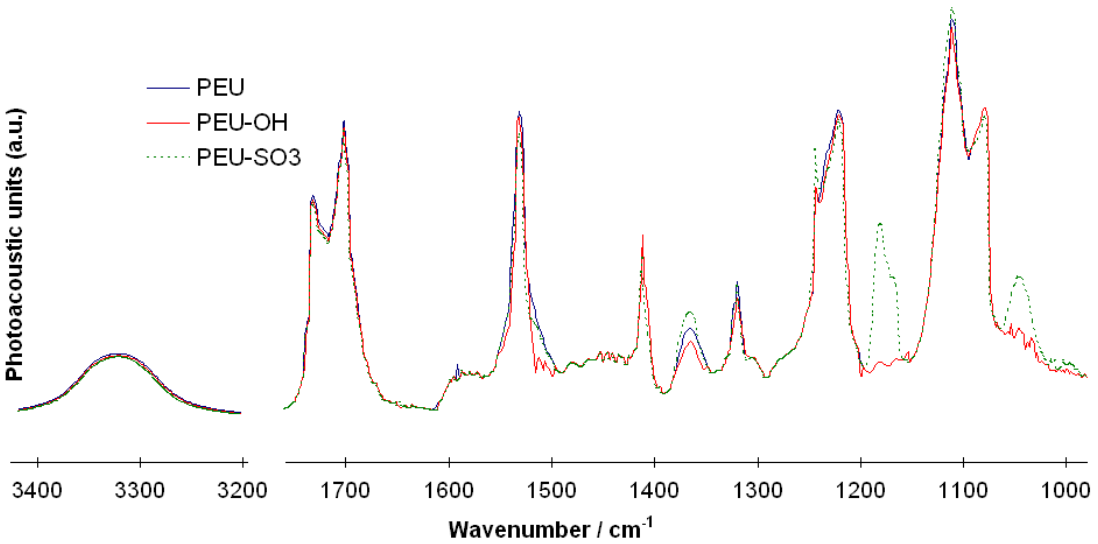

Figure 4.4: FTIR spectra of phase inverted, hydroxylated and sulphonated PEU

grafted onto the polymer surface [Keogh *et al.* (1996); Yuan *et al.* (2003); Jiang *et al.* (2004)] with procedure outlined in Section 3.3.2. The relative peak differences for modified and unmodified PU in relation to conventional solvent-cast PU were calculated from PA-FTIR scans and are illustrated in Figure 4.5. Overall, surface modifications such as hydroxylation and sulphonation, showed with only minor peak height differences, that the phase inversion process was stable and did not cause the hard and soft segments to rearrange.

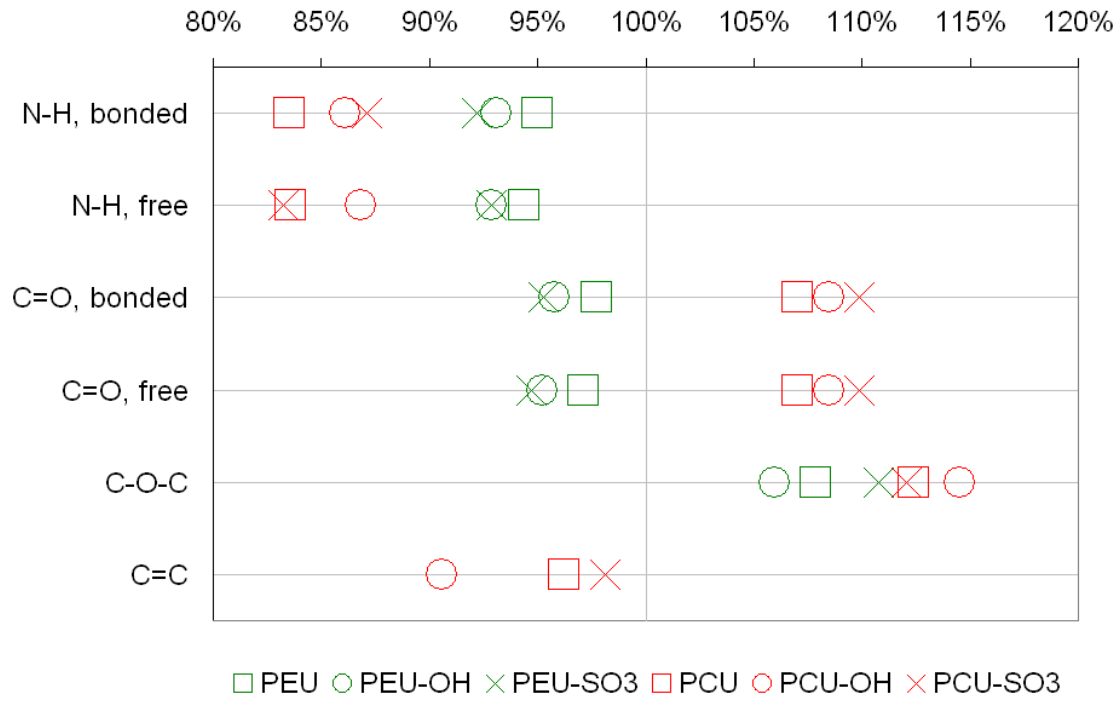

Figure 4.5: Relative peak height differences (expressed in percentage) of phase inverted, hydroxylated and sulphonated PU in relation to conventional solvent cast PU (taken as 100%)

In Figure 4.5 it is possible to note that for PCU, the peak heights of N-H and C=C decreased whereas the peak heights of C=O and C-O-C increased in comparison with conventional solvent-cast PCU. For PEU, the peak heights of N-H and C=O decreased, whereas that of C-O-C increased. This was observed for both unmodified and surface modified PU. However, the peak height differences are more apparent with PCU, including most surface modified polymers of both types.

N-H (bonded and free) are located in the hard segments of both polyether and polycarbonate urethane. With induced phase separation, the hard segments retreat away from the surface, causing this peak intensity to decline in comparison with conventional solvent-cast PU, as seen in Figure 4.5. The C=C stretch is located in the core of the hard

segments of the MDI ring structure of PCU and shows a decreased vibration band. This is further evidence that the hard segments of PCU retreated away from the surface.

C=O (bonded and free) are located at the interface of the hard and soft segments. Due to this location, the peak height decline of phase inverted polymers is clearly apparent as shown in Figure 4.5, but not as pronounced as for bonding located within the hard segments, such as N-H. In PCU, C=O bonds are located within the carbonate soft segments. Therefore, these peak heights show an expected increase with soft segment enriched surfaces compared to conventional solvent-cast polymers. The C-O-C bonds are either the aliphatic ether soft segments (in PEU) or the carbonate soft segments (in PCU). The increased intensity for both PCU and PEU verifies that these compounds have migrated to the surface.

Overall, PCU shows a much greater difference in peak height in comparison to PEU. This can be explained by differences in polarity of the casting solution and the coagulation medium in connection with hard and soft segments. The casting solution used for PEU is of non-polar nature. When the cast PU is dipped in non-polar coagulation medium, the residual solvent within the polymer matrix will simply mix with the coagulation medium. The effect will be that the relatively polar hard segments are reinforced to sequester away from the surface. This can be clearly seen with peak height differences of phase inverted compared to conventional solvent-cast polymers (Figure 4.5).

The casting solution of PCU is of moderate polarity. Upon the association of these polymers with the non-polar coagulation medium, the residual solvent within the polymer matrix will not mix. The hard segments will then sequester away from the surface and the residue of the moderate polar solvent will be adsorbed onto the relatively polar hard segments. Once the non-polar coagulation medium is evaporated, the residual moderate polar casting solution will then evaporate. The residual casting solution will keep the hard segments mobile enabling them to readily rearrange and form stronger bonds within the hard segment matrix upon evaporation of the casting solution. This can be seen with more pronounced peak intensity differences for hard and soft segments in PCU compared to PEU (Figure 4.5).

Hard-/Soft segment Ratio (HS-Ratio)

The hard and soft segment ratio (HS-ratio) of these different PU is another significant factor in the peak height differences seen here. This ratio is affected by the interaction of

N-H groups with C-O-C groups and can be evidenced by peak intensity differences. The degree of phase inversion in relation to soft segment enrichment and surface modification is now quantified by the change in hard- and soft segment (HS) ratio (N-H/C-O-C). The calculated values are illustrated in Table 4.4.

	Solvent cast	Phase inverted	Hydroxylated	Sulphonated
PCU	0.21	0.16	0.16	0.16
PEU	0.42	0.37	0.37	0.35

Table 4.4: HS-ratio (N-H/C-O-C) of modified and unmodified PU

The results in Table 4.4 clearly demonstrate a difference in HS-ratio for both PCU and PEU between solvent cast and phase inverted polymers. This further quantifies a successful phase separation taking place after phase inversion with the hard segments retreating away from the surface (Figure 3.1). Furthermore, the HS-ratio of hydroxylated PCU and PEU shows no difference to their unmodified, phase inverted counterparts; the same is also true for sulphonated PCU. The HS-ratio of sulphonated PEU is slightly lower than that of either phase inverted and hydroxylated PEU. However, this is further evidence that the surface modification processes did not compromise the initial phase inversion process, demonstrating that the hard- and soft segments did not rearrange, and confirming stability.

Hydrogen Bonding Index (HBI)

Chemical properties regarding the strength of interpolymer bonding can be addressed by means of the hydrogen bonding index [Huang *et al.* 1997]. Hydrogen bonding is evident by more organised micro domains within the polymer matrix and is apparent in an interchange between hydrogen- and non-hydrogen bonded absorbences. The main participants in hydrogen bonding for polymers used in this study are proton donor groups (N-H) and proton acceptor groups (C=O, C-O and C-O-C). In Figures 4.1 to 4.4 two absorption bands are observed for N-H and C=O related to hydrogen- and non-hydrogen bonded forms; these are listed in Tables 4.2 and 4.3. For the identification of the average strength of interpolymer hydrogenbonds, the hydrogen bonding index (HBI) values were quantified by differences in N-H/C=O ratio. The calculated HBI values are illustrated in Table 4.5.

HBI values > 1 indicate that there is more hydrogen bonding than non-hydrogen bonding present. Hence, the higher the HBI values the stronger is the hydrogen bonding

		Solvent cast	Phase inverted	Hydroxylated	Sulphonated
PCU	N-H	0.92	0.92	0.91	0.97
	C=O	0.45	0.45	0.45	0.45
PEU	N-H	1.97	1.98	1.97	1.95
	C=O	1.27	1.28	1.28	1.28

Table 4.5: HBI of modified and unmodified PU with N-H being the proton donor and C=O the proton acceptor group

between the chemical groups. The HBI values in Table 4.5 show a much higher value for PEU compared to PCU. This implies that there is more, stronger hydrogen bonding present in PEU compared to PCU.

PEU used in this study is made up of H_{12}MDI, and PCU of MDI; both of these hard segments are comprised of two symmetric ring structures. This facilitates tight packing within the polymer matrix, thus allowing hard segments to readily order and phase separate. However, hydrogenated MDI is an aliphatic molecule and may have multiple conformations. These differing conformations may sterically hinder the process of hydrogen bonding between the H_{12}MDI segments, resulting in microdomains which are less well ordered than that of MDI hard segments [Lamba *et al.* (1998)]. Therefore, this would imply that the HBI values for PEU should be lower than that of PCU. However, this was not found in this study.

When examining the soft segments, the carbonate constituent (PHEC) can undergo hydrogen bonding with the hard segments as well as intermolecular interaction between soft segments, whereas PTMEG undergoes hydrogen bonding predominantly with the hard segments. However, according to Yang *et al.* (1999), the conjugated planar configuration of the soft segment in PCU prevents the C=O bond from rotating due to steric hindrance. This effect appears to have a large impact, which is reflected in lower HBI values of PCU as seen in Table 4.5.

Table 4.5 shows only minor differences in HBI values between solvent cast and phase inverted polymers. Huang *et al.* (1999) reported on phase inverted PEU, albeit with varied hard segment content in the bulk of 33, 51, and 61 weight percent. However, the HBI value increased only by an average of about 0.11 points per ten percent hard segment increase. It was concluded in that paper that larger HBI values are an indication of changed hard segment distribution on the surface of the polymer. Hence, more N-H and C=O groups are then hydrogen bonded. In the present study, the hard segment content in the bulk was not varied and therefore, possible differences in HBI can only

be due to migration of hard and soft segments within the polymer matrix. Hence the differences in HBI values calculated from FTIR spectra (Figures 4.1 and 4.2) are less pronounced.

Overall, the observed relative peak height differences and the hard and soft segment ratios showed that the polymers prepared with the phase inversion method resulted in a PU with a much higher amount of soft segments on the surface compared to conventional solvent cast PU. Furthermore, the strength of the hydrogen bonding was not compromised, as seen with nearly identical HBI values for phase inverted in comparison with surface modified polymers in Table 4.5.

4.3 Silicone Rubber

Preliminary experiments involved the synthesis of silicone rubber (SR) performed *in situ* by solution polymerisation in a two-step process. A two-part elastomer compound was used as obtained from NuSil Technology, USA. Part A (amorphous silica) consists of 25% synthetic amorphous silica, Pt-based catalyser and inhibitor; Part B consists of 20% dimethyl,methylhydrogen siloxane (DMMHS) copolymer. These components have been mixed in specified proportions according to product profile (MSDS) and pre-established recipe kindly supplied by Dr. Derek Williams-Wynn, Polymer Systems Technology Ltd., UK. The sample polymers obtained via this procedure are referred to as SR control.

The methodology for the preparation of modified SR was changed from the above supplied method (Section 3.3.1) in the following ways:

- Part A was mixed in polar solvent over night.
- Part B was added to suspension and thoroughly mixed.
- Curing was performed in 3 temperature zones for prolonged periods of time.

Silicone Rubber obtained with modified procedure are referred to as SR modified.

Two different solvents were used in this study, heptane (SR control) and isopropanol (SR modified). These solvents were selected for their contrasting properties: heptane belongs to the family of alkanes, is non-polar and has a boiling point of 98.42°C; isopropanol belongs to the family of alcohols, is polar and has a boiling point of 82.3°C. It was hypothesised that by using a polar solvent, the non-polar silica monomers would aggregate to clusters, leading to a lower crosslink density when fully cured. Furthermore,

the hydrophobic methyl groups within the silicone matrix will reorientate away from the air interface when in contact with the hydrophilic solvent. This will increase the hydrophilicity of the polymer surface. The lower crosslink density concomitant with the induced hydrophilicity should then allow small hydrophilic molecules, such as H_2O_2, to penetrate across the polymer network. A requirement for amperometric analyte detection which will be examined in detail in Chapter 6.

In this section, SR control and SR modified are analysed in terms of chemical properties and surface morphology to determine whether they are good candidates for coating material of needle-type electrodes in amperometric analyte detection for H_2O_2 and dissolved O_2 as target analytes.

4.3.1 FTIR Analysis

FTIR spectra for SR control and SR modified polymers were taken and analysed for their characteristic frequencies using general reference texts [Bower *et al.* (1992), Coates (2000), Cross *et al.* (1969)]. The observed spectra display peak positions that correlate well with studies reported previously by various researchers [Chen *et al.* (2005), Chung *et al.* (2007), Völcker *et al.* (2001)]. The peak assignments for these polymers are tabulated in Table 4.6. The full spectra of these polymers are illustrated in Figure 4.6.

Peak assignments (cm^{-1})	Mode	Relative Intensity	SR control	SR modified
C-H in CH_2				
asymmetric	v	s	2962	2962
asymmetric/symmetric	v	m	2904	2904
CH_3				
deformation in $SiMe_2$	v	m	1412	1412
CH in Si-CH_3				
in plane bending	δ	s	1261	1261
Si-O-Si				
asymmetric	v	s	940-1240	940-1230
Si-CH	δ	m		910
Si-C		s	867	860
CH in H_3C-Si-CH_3				
plane swing	p	s	813	817 / 798
CH_2				
rocking	v	w	650-720	650-730

Table 4.6: Observed infrared band positions for SR control and SR modified; where in Mode, v = vibration, δ = bending, p = in plane bending or rocking, and in Relative Intensity, w = weak, m = medium, s = strong

The FTIR spectra (Figure 4.6) of SR modified shows C-H vibration bands of the

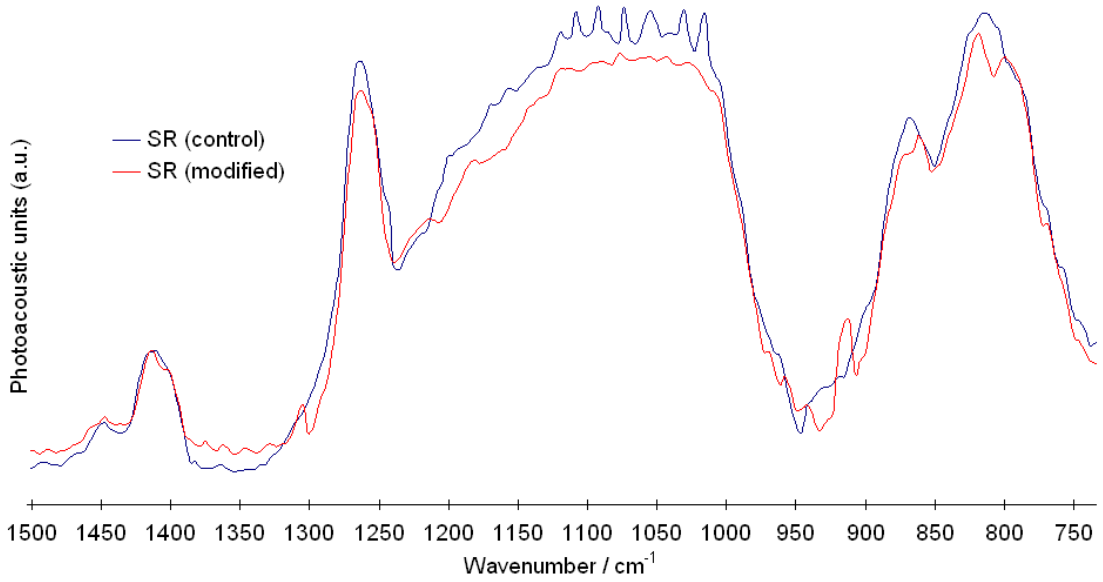

Figure 4.6: FTIR spectra of SR control and SR modified

methylene (CH in CH_2) groups at 2940-3000 cm^{-1} (asymmetric) and 2890-2930 cm^{-1} (asymmetric/symmetric), the CH_3 deformation bands are at 1390-1430 cm^{-1}, the CH groups of the silicone are at 1240-1300 cm^{-1}, the siloxane (Si-O-Si) groups are at 940-1240 cm^{-1}, a new vibration band of Si-CH appeared at 906-933 cm^{-1}, the Si-C are at 852-906 cm^{-1}, the CH in H_3C-Si-CH_3 are at 740-852 cm^{-1} and the CH_2 bands are at 650-730 cm^{-1}.

SR control sample shows C-H stretching at 2930-3020 cm^{-1} (asymmetric) and 2890-2920 cm^{-1} (asymmetric/symmetric), the CH_3 deformation bands are at 1380-1440 cm^{-1}, the CH groups of the silicone are at 1230-1340 cm^{-1}, the siloxane (Si-O-Si) groups are at 940-1230 cm^{-1}, the Si-C are at 852-920 cm^{-1}, the CH in H_3C-Si-CH_3 are at 740-852 cm^{-1} and the CH_2 bands at 650-720 cm^{-1}.

The peaks in each spectrum appear to be relatively similar; however, there are small changes in the vibration bands between 940-1240 cm^{-1}, which can be ascribed to the Si-O-Si stretching. SR modified shows a decreased intensity compared to the control sample, which is an indication of a less tight siloxane network due to fewer crosslink sites (Figure 3.3 and Figure 3.2). The new vibration band for modified SR at 910 cm^{-1}, assigned to Si-CH and the multiple peak formation at 740-852 cm^{-1} for CH in H_3C-Si-CH_3 compared to a single peak with the control sample strongly suggests unreacted silicone sites. This can be attributed to the polar solvent used for the synthesis of modified SR. The non-polar silica gel forms a suspension with the polar solvent, in which the silica

monomers aggregate to clusters instead of forming a homogeneous mixture. This then is reducing the crosslink density leaving unreacted silicone sites within the polymer matrix.

These results confirm the hypothesis of changed crosslink density induced by polar solvent which should allow the permeation of H_2O_2 across the polymer matrix. This would be of particular advantage in amperometric analyte detection and is examined in detail in Chapter 6.

4.4 Thermogravimetric Analysis

TGA is performed on samples to determine changes in weight in relation to changes in temperature. Such analysis relies on three measurements: weight, temperature, and temperature change. As weight loss curves look similar, an additional derivative weight loss curve is used to define the point at which weight loss is most apparent. All samples in this study were examined regarding their thermal endurance; the results are tabulated in Table 4.7. The thermal degradation profile for PCU is illustrated in Figure 4.7, that of PEU in Figure 4.8, and that of SR in Figure 4.9.

	Onset (°C)	Inflection Point (°C)	Weight Loss (%)
	First Step		
PCU	297±1.9	304±2.4	61±0.2
PCU-OH	332±2.6	340±6.9	89±2.6
PCU-SO_3	321±2.4	348±4.3	91±1.9
PEU	309±3.5	339±1.4	34±1.6
PEU-OH	310±0.7	337±0.9	34±0.9
PEU-SO_3	306±0.8	330±1.0	36±0.6
SR (modified)	152±3.5	217±7.7	4±0.3
SR (control)	155±3.7	220±4.6	2±0.9
	Second Step		
PCU	422±2.2	465±0.3	35±0.6
PCU-OH	452±3.9	485±4.5	9±2.9
PCU-SO_3	463±2.4	481±2.5	7±2.0
PEU	389±1.6	395±0.6	68±1.0
PEU-OH	382±0.1	396±0.2	68±0.9
PEU-SO_3	385±1.0	395±0.3	66±0.8
SR (modified)	594±0.3	648±1.4	45±0.4
SR (control)	594±0.8	664±2.7	42±0.5

Table 4.7: TGA data of phase inverted, hydroxylated and sulphonated PU including SR (modified and control)

Figure 4.7 shows two distinct regions, indicating two-step degradation processes for PCU (modified and unmodified): the weight loss after the first step is 61% for PCU

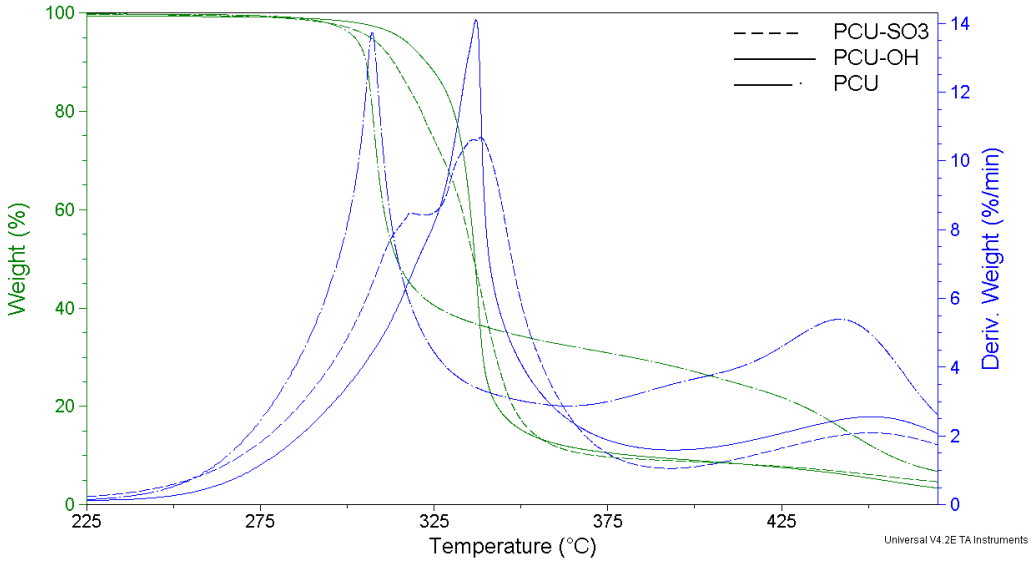

Figure 4.7: TGA curve and relative derivative weight loss for phase inverted, hydroxylated and sulphonated PCU

at a temperature of 296-304°C; 89% for PCU-OH (332-340°C); 91% for PCU-SO_3 (320-348°C). After the second step, the weight losses are: 35% for PCU (421-465°C); 9% for PEU-OH (451-485°C); 7% for PEU-SO_3 (462-480°C).

The multi-step degradation process as seen in this study (Figure 4.7) has also been found by Petrovic *et al.* (1994) in which segmented PU of varied HS-ratios were compared. They found that at initial stages of degradation, the weight loss was dominated by the hard segments. Oezdemir *et al.* (2007) found that pristine PCU starts to degrade at a temperature of 266°C, compared to 296°C in this study. As the chemical compounds were not specified in their study, it can be assumed that the type of hard segments and the HS ratio is responsible for this difference.

The thermal degradation curve for unmodified PCU shows a different weight loss profile compared to its surface modified counterpart. The two-step profile is shifted to higher temperatures after surface modification and is in the following order: PCU > PCU-OH > PCU-SO_3. This indicates that compounds are released at higher temperatures which might be attributed to stronger intermolecular bonding. It is assumed that minor changes in hydrogen bonding of N-H (see also HBI values in Table 4.5) may have caused the temperature shift, as there was more energy required to break these bonds.

The shoulder on the first step of degradation, as seen in the derivative weight loss peak

for sulphonated PCU, can be attributed to chain scission of the additional sulphonated groups. The additional groups on the polymer surface induce changes in molecular weight and molecular weight distribution compared to non-modified PCU, hence the changed weight loss profile (Figure 4.7). Furthermore, the weight loss after the second step is highest at 35% with PCU whereas modified PCU shows a final weight loss of $< 10\%$.

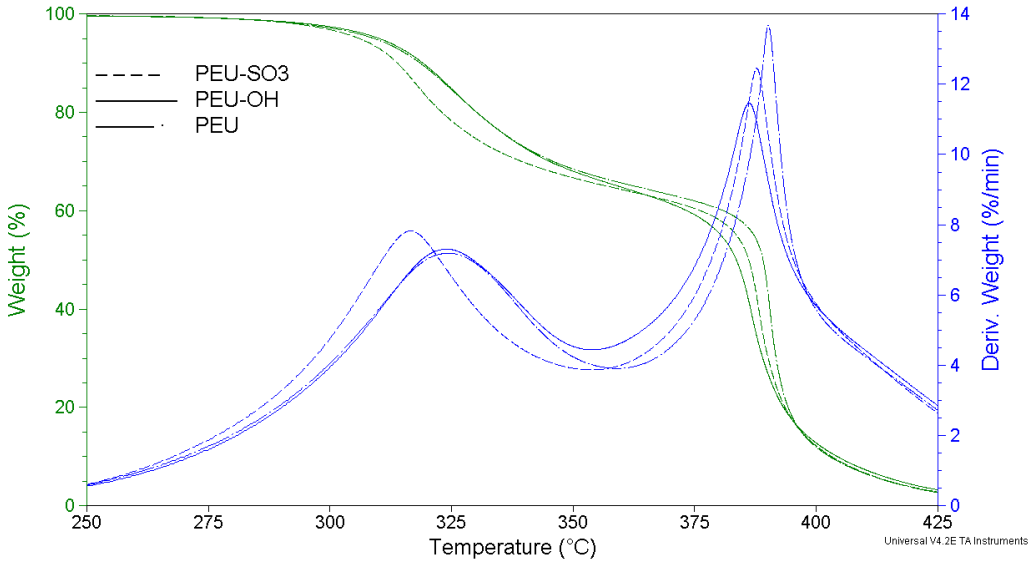

Figure 4.8: TGA curve and derivative weight loss for phase inverted, hydroxylated and sulphonated PEU

Figure 4.8 shows two distinct regions indicating two-step degradation processes for PEU (modified and unmodified): the weight loss after the first step is 34% for PEU at temperature of 308-339°C, 34% for PEU-OH (309-337°C); 36% for PEU-SO_3 (305-330°C). After the second step the weight losses are: 68% for PEU (388-395°C); 68% for PEU-OH (388-395°C); 66% for PEU-SO_3 (385-395°C).

However, the two-step thermal degradation curves for PEU (surface modified and unmodified) show similar profiles. PEU and PEU-OH showed nearly identical values at the first degradation step, whereas for PEU-SO_3 the weight loss was slightly higher with the onset and inflection point temperature being slightly lower. At the second degradation step, surface modified PEU showed less weight loss at slightly lower temperatures. This indicates that compounds are released at lower temperatures.

Guignot *et al.* (2001) coupled TGA with FTIR studies to analyse the thermal degradation of PEU of similar chemical compositions to those used in this study. This confirms

the findings of Petrovic *et al.* (1994) in which the first degradation step was mainly attributed to the hard segments while the second step was mainly related to the soft segments. However, Guignot *et al.* (2001) reported a weight loss in the first step of 71% with a broad temperature range of 148°C, whereas in this study 34-36% weight loss at a more narrow temperature range (8-25°C) was found in the first step. Thermal treatment of PU induces scission of urethane linkages in macromolecular chains to give the former isocyanate. It has been found that this reaction becomes irreversible at higher temperatures, but can be reversible by rearrangements of neighbouring isocyanates at lower temperatures [Gupta *et al.* (2003), Lamba *et al.* (1998)]. The narrow temperature bandwidth found in this study, at which these chain scission reactions take place, suggests a complete degradation of urethane linkages within the first step.

The second degradation step shows a higher weight loss in a short temperature range of about 7-10°C, compared to that found by Guignot *et al.* (2001) with 25°C. This could be attributed to a more complete degradation without the formation of intermediate chemical groups due to lower scanning rate used in this study.

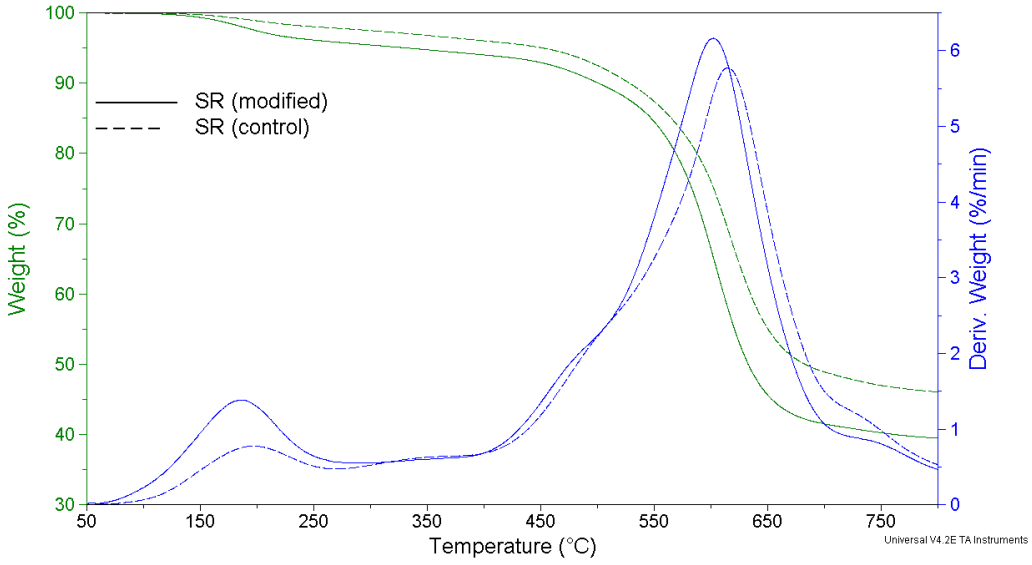

Figure 4.9: TGA curve and derivative weight loss for SR (modified and control)

Figure 4.9 shows two distinct regions indicating two-step degradation processes for SR (modified and unmodified): the weight loss after the first step is 3.79% for SR (modified) at temperature of 151-217°C; 1.9% for SR (control) (154-220°C). After the second step, the weight losses are: 44.9% for SR (modified) (594-648°C); 42.31% for SR (control)

(593-664°C).

The thermal degradation of SR (modified and control sample) show similar degradation profiles. The first step can be attributed to chain scissions of methylene bondings within the crosslinked silicone network. The second step is related to the splitting of main chains, the siloxane groups and any remaining methylene bondings. This peak appears at a broad temperature bandwidth and is an indication of incomplete degradation. This can also be seen with the results displayed in Table 4.7.

SR used in this study is a two-part elastomer, which is chemically crosslinked via addition cure involving platinum catalysed addition of silylhydride to the unsaturated side of a vinyl group. During thermal degradation, residual platinum compound would catalyse the formation of inter- and intramolecular methylene-bridges, which then reduces the potential for thermal degradation [Timpe (2007)]. This can be seen in Figure 4.9 with a maximum weight loss of 49% for modified SR and 44% for SR control.

4.5 Contact Angle Analysis

Contact angle measurements in this study were employed to monitor the surface properties of polymers, such as the degree of wetting, surface free energy, dispersive and polar surface free energies. These properties are said to have an influence on protein adsorption and cell adhesion on polymer surfaces [Smith *et al.* (2002), Wu *et al.* (2005)], which are the subject of study in the next sections of this Chapter. Table 4.8 shows the experimental contact angle data for all probe liquids used. The indicated errors are the standard deviations of measurements taken in triplicate.

Test Sample	$\theta W(^\circ)$	$\theta G(^\circ)$	$\theta DMSO(^\circ)$
PCU	86±0.4	79±1.0	57±1.0
PCU-OH	84±1.7	76±0.4	48±3.2
PCU-SO_3	84±0.5	78±1.2	53±4.4
PEU	89±2.4	80±0.4	57±0.3
PEU-OH	75±1.4	76±0.6	43±1.3
PEU-SO_3	71±0.8	68±0.9	40±1.0
SR (modified)	100±2.9	110±0.5	82±1.4
SR (control)	115±0.2	111±0.6	82±2.2

Table 4.8: Contact angle measurements in water (W), glycerol (G) and dimethyl sulphoxide (DMSO) of phase inverted, hydroxylated and sulphonated PU including SR (modified and control)

Both SR (modified and control) show the highest contact angle for all of the probe liq-

uids as expected, hence the highest hydrophobicity. However, SR control exhibits higher contact angle data compared to SR modified, which was most noticeable with water as probe liquid. This was thought to be due to the polar solvent used for preparation of modified SR, causing the hydrophobic components to retreat into the bulk during solvent evaporation, making the polymer surface less hydrophobic. For SR control, a non-polar solvent was used resulting in an even mixture of all of the hydrophobic components within the bulk and the surface and is reflected with contact angle data illustrated in Table 4.8. Zhang *et al.* (1996) reported in their study that a more hydrophobic characteristic may also be due to the surface concentration of the hydrophobic processing aid and the silicone oil present in SR. These additional hydrophobic substances contribute to a more hydrophobic surface characteristic, which is more apparent with unmodified SR due to polymer-solvent interactions (Figure 3.2) during curing process and as seen in contact angle data obtained in this study.

Unmodified PEU shows in comparison with PCU only slightly higher contact angle data (Table 4.8), which is most apparent with water as probe liquid. This is in accordance with Yang *et al.* (1999) in which it was found that PCU rather than PEU does not in itself produce a more hydrophilic surface. It was further suggested that the carbonate structure in the soft segment has inherently lower chain mobility due to steric hindrance compared to that of the ether soft segment. This is related to the Van der Waals volume of 18.9 cm^3/mol to that of a carbonate group compared to 5.0 cm^3/mol for an ether group. Therefore the molecules on the surface of PEU are able to rearrange themselves more readly once in contact with probe liquids used for contact angle measurements, hence differences in hydrophilicity are not apparent as seen with data obtained in this study.

Hydroxylation and sulphonation of PCU showed no differences in contact angle data (Table 4.8) compared to their unmodified counterpart. This was unexpected as these hydrophilic surface groups should be reflected with higher wettability. However, surface free energy parameter as calculated and illustrated in Figure 4.13 are suggesting an even decreased polarity with hydrophilic surface functional groups. A possible reason for this phenomenon could be that the surface groups may have reorientated into the bulk. This was also found by Yang *et al.* (1999), in which differences in chain mobility of the soft segments, hence steric effect was thought to be the main reason. Hydroxylated PEU appeared to induce higher wetting behaviour compared to unmodified PEU, though more

apparent with sulphonated PEU. This was in accordance with that reported by Zhang *et al.* (2003). The opposed findings of apparent hydrophilicity and polarity with surface modification of these two PU would confirm the steric effect the carbonate soft segment has regarding to its orientation compared to the ether soft segment.

4.6 Protein Adsorption

The amount of adsorbed protein was determined quantitatively using the ninhydrin method as outlined by Moore *et al.* (1954). The experimental data are presented in Figures 4.10 to 4.12 as the amount of protein adsorbed per unit surface area (cm^2) on polymeric materials. Analysis of protein adsorption, using any method, can lead to highly variable data due to the large number of possible conformations and orientations of the proteins over the polymer surface. Such variable data has been noted by, for example, Castner *et al.* (2002), Elbert *et al.* (1996), Green *et al.* (1997), Sun *et al.* (2003), and was also observed in this study. Consequently, it is the trends of the results which are of primary interest in this Chapter. In addition, Chapter 6 meanwhile focuses on the effects of protein adsorption in electrochemical analyte detection.

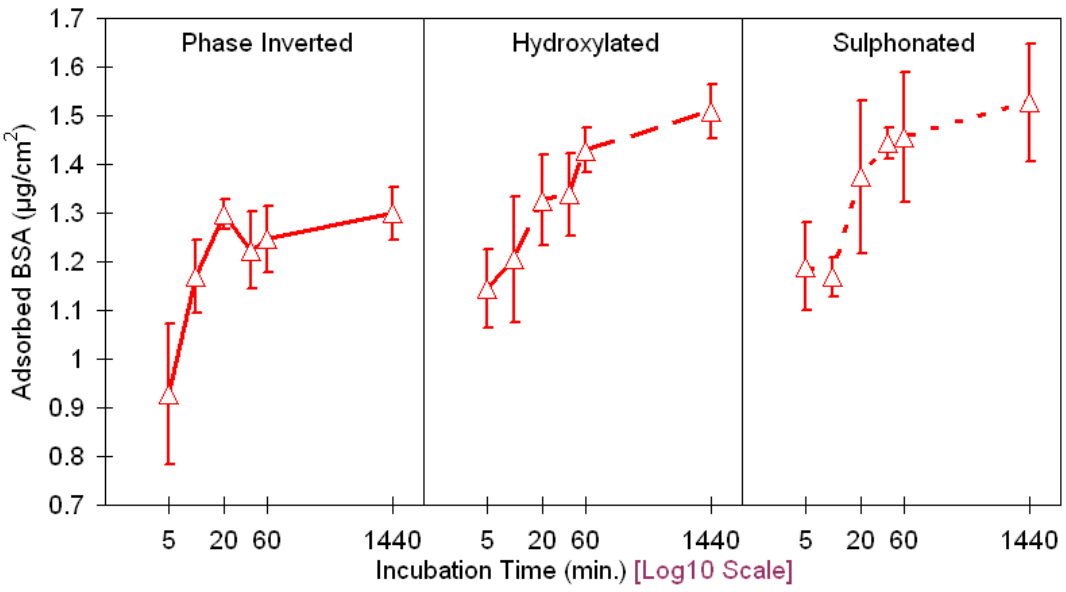

Figure 4.10: Adsorbed BSA of phase inverted, hydroxylated and sulphonated PCU

Figure 4.10 shows the amount of BSA adsorbed on the surfaces of surface modified and unmodified PCU. Unmodified PCU appears to adsorb faster during the first twenty minutes of protein exposure, after which it stays essentially constant (up to the maximum

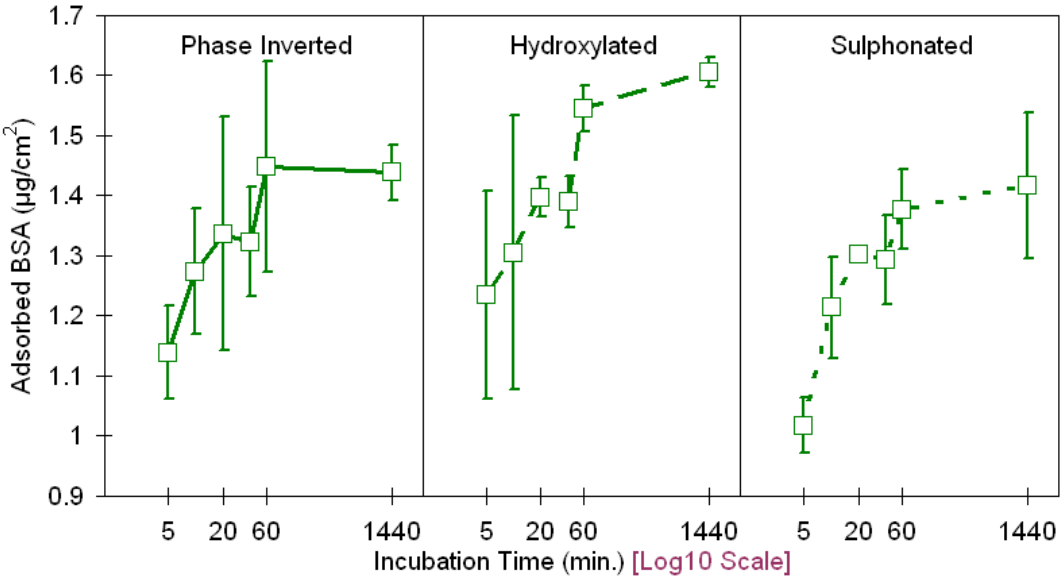

Figure 4.11: Adsorbed BSA of phase inverted, hydroxylated and sulphonated PEU

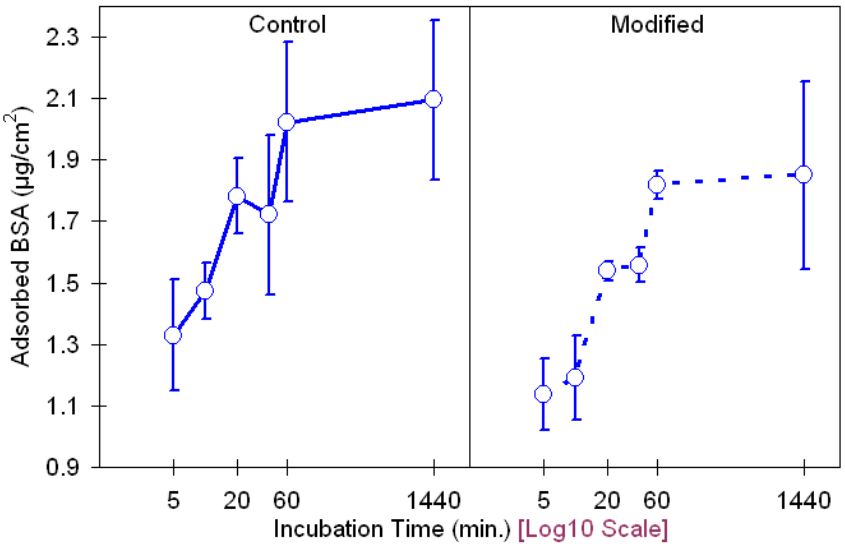

Figure 4.12: Adsorbed BSA of SR (control and modified)

24 hour reading). Conversely, both surface modified polymers have a much higher initial adsorbtion, and continue increasing across the whole 60 minute period. The next 23 hours showed only a slight increase in protein adsorption. PEU, modified and unmodified (Figure 4.11) showed the same trend. However, sulphonated PEU showed the lowest protein adsorption compared to unmodified and hydroxylated PEU.

As seen with PU, protein adsorption for both control and modified SR increased rapidly over the course of the first sixty minutes, which then seemed to stabilise showing only a low increase over the next 23 hours. Nevertheless, modified SR has a much lower initial protein adsorption compared to its unmodified counterpart. Green *et al.* (1997) examined the kinetics of protein adsorption and found that initially proteins adsorb rapidly until saturation of the surface occurs upon the formation of a monolayer. They also found that once the substrate was saturated, no further adsorption in the form of multi-layers occurred regardless of albumin solution concentration. Park *et al.* (2003) reported the theoretical amount of albumin in a monolayer state to be about 1-2 $\mu g/cm^2$. The results in this study suggest a similar response regarding to the adsorption profile, however, the formation of a monolayer could not be confirmed.

Protein adsorption was observed for all polymers and was most apparent with SR. As adsorbed species to the surfaces of polymeric materials used for electrochemical sensing devices may impose a major limitation to their sensitivity and accuracy [Wisniewski *et al.* (2001), Sun *et al.* (2003)], the effect of protein adsorption on polymer coated needle-type electrodes will be further investigated in electrochemical application in Chapter 6. For a better understanding of the adsorption behaviour of proteins on polymers developed in this study, the total surface free energy, including the polar and dispersive components, were estimated using the Extended Fowkes Method [Krüss (2003)]. This method required the use of three different probe liquids to be used; hence the contact angles before and after protein exposure at different time intervals were measured. The surface tension parameter of the probe liquids, which were used in the calculations, are presented in Table 4.8. The surface tension parameters for each of the polymers, modified and unmodified, are displayed in Figure 4.13 (repeat data ranges shown by error bars).

Overall, it is seen in Figure 4.13 that within each polymer the trend of total surface free energy is similar. Furthermore, as expected with hydrophobic polymers, the dispersive components are the dominating proportion. However, PCU showed increased polarity upon prolonged protein exposure.

Probe Liquid	γ (mN/m)	γ^{LW} (mN/m)	γ^{AB} (mN/m)	γ^{+} (mN/m)	γ^{-} (mN/m)
Water	72.80	21.80	51.00	25.50	25.50
Glycerol	64.00	34.00	30.00	3.92	57.40
Dimethyl sulphoxide	44.00	36.00	8.00	0.50	32.00

Table 4.9: Surface tension parameters of test liquids used in contact angle measurements. Surface free energy (mN/m): γ = total, γ^{LW} = Disperson, γ^{AB} = Polar, γ^{+} = Acid, γ^{-} = Base [adapted from Rankl *et al.* (2003)].

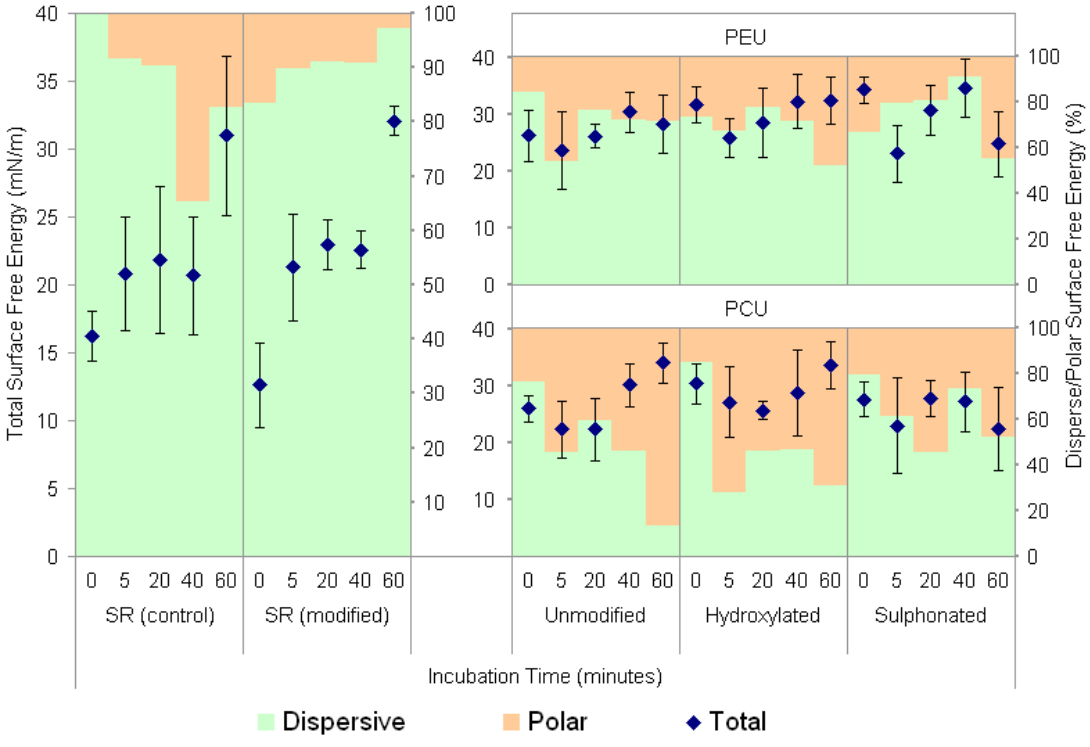

Figure 4.13: Surface free energy parameters of phase inverted, hydroxylated and sulphonated PU including SR (modified and control) before and after protein adsorption

Both control and modified SR showed a moderate increase in the total surface tension after initial protein adsorption, followed by a period of apparent stability before a sharp increase toward the last measured point. For any system it is desirable to be in a low energy level; the higher the surface energy of a material, the greater the motivation for reducing the energy level. Polymers used in this study would have to adsorb substances with lower surface energy to obtain desirable lower interfacial energy. In addition, it can be seen that before protein adsorption, SR control is composed entirely of dispersive components whereas modified SR showed a relative polar contribution of 10 %. This is mainly due to the hydrophobic silicone methyl groups within SR which are able to reorientate away from the air interface during the curing process using a hydrophilic solvent. Hence the appearance of polar components in contrast to the control sample, as confirmed with contact angle data (Table 4.8).

Upon prolonged protein exposure, the polar component of modified SR appeared to have decreased unlike the control sample. This is mainly due to the conformation and orientation of the proteins themselves, which largely depend on the surface properties of the absorbent polymer [Castner *et al.* (2002)]. In this case, during protein exposure, the proteins will orientate themselves such that the hydrophilic groups are in contact with the polymer surface, whereas the hydrophobic groups are facing away from the polymer surface. Hence the reduced polarity which becomes more apparent with prolonged exposure time, as seen with data obtained. For the more hydrophobic SR (control), the protein will orientate itself such that the hydrophobic groups are in contact with the polymer surface and the hydrophilic groups are facing upwards, as indicated in Figure 4.13. Hence, the differences in polar and dispersive components of both SR is a measure of the conformation and orientation of the proteins adsorbed to the surface, since the hydrophilicity of the upper most surface (proteins in this case) is measured, and not that of the underlying polymer.

This confirms that the modification procedure as outlined in Section 3.3.1 resulted in increased polarity when compared to the conventional preparation method. This increased polarity gave lower protein adsorption for unmodified SR; however, the total surface free energy remained virtually unchanged upon protein adsorption for both SR.

The total surface free energy of PEU before protein adsorption showed an increased value for both surface modifications as well as an increase in the polar component in the order PEU > PEU-OH > PEU-SO_3, as expected. However, after protein adsorp-

tion, unmodified and hydroxylated PEU showed very little changes in total surface free energy over the whole time frame of protein exposure. Sulphonated PEU decreased in total surface free energy after initial protein adsorption, increased with prolonged protein exposure and then showed an apparent drop towards the last measuring point. Modified and unmodified PCU showed very little differences in total surface free energy before protein adsorption whereas with prolonged protein exporsure, these values indicate a slight increase for unmodified and hydroxylated PCU and may suggest a slight decrease for sulphonated PCU.

The polar component of the total surface free energy was with unmodified PEU after 5 minutes protein exposure the highest whereas surface modified PEU showed after 60 minutes a peak value. Differences in polarity with prolonged protein exposure were also seen with SR for which the reason was thought to be in protein conformation and orientation when adsorption to the polymer surface takes place. Interestingly, for modified and unmodified PCU, the polar component showed a sharp increase with prolonged protein exposure. This can not only be explained with conformation and orientation of the proteins, but also due to the reorientation of the soft segments including the surface functional groups within the polymer matrix. The covalent attachment of hydrophilic functional groups on the surface of hydrophobic polymers, such as OH^- and SO_3^- should be reflected with an increase in wettability and polarity. This is the case with PEU, but can not be seen with PCU. A similar phenomenon was seen in studies conducted by Yang *et al.* (1999), in which differences in chain mobility of the soft segments including steric effect was thought to be the main reason.

4.7 Degradation

Any type of polymer modification may induce significant loss of mechanical and chemical properties. PU is known to be susceptible to oxidation, though different soft segments show more or less extended biostability. Carbonate soft segments are said to be more stable compared to ether in PU [Mathur *et al.* (1997)]. In this section, degradation of surface modified PEU and PCU are examined and compared to untreated control samples. Treatment of polymers with a hydrogen peroxide-cobalt chloride system is a common method to reproduce the chemical and physical characteristics of degradation at an accelerated rate [Christenson *et al.* (2004a), Schubert *et al.* (1997)]. Surface modified and unmodified PU were treated with this oxidative solution for 21 days at 37°C. The

proposed degradation mechanisms are illustrated in Figures 2.7 to 2.9.

Characteristic FTIR spectra of phase inverted and surface modified PU before and after degradation are illustrated in Figures 4.14 to 4.19. The extent to which hard- and soft segment degradation occurred is illustrated in Figure 4.20 with relative hard and soft segments remaining over the 21 day period.

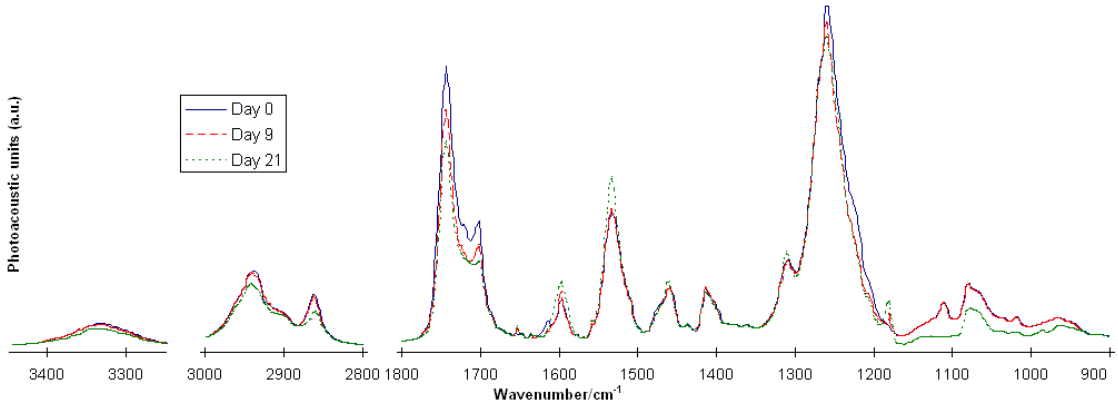

Figure 4.14: FTIR spectra of PCU of undegraded control sample (Day 0) and with increasing degradation times after 9 and 21 days

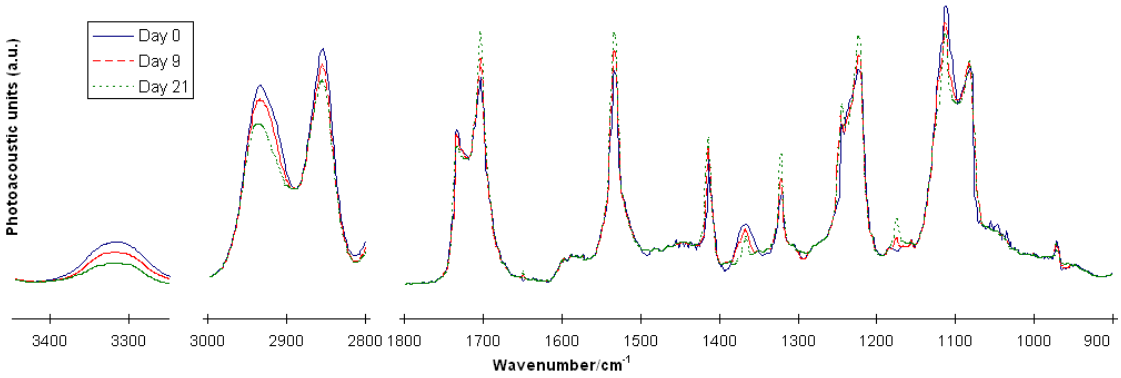

Figure 4.15: FTIR spectra of PEU of undegraded control sample (Day 0) and with increasing degradation times after 9 and 21 days

Hard Segment Degradation

The N-H groups are located within the core of the hard segments and are not degrading as such. However, the molecules located adjacent to these N-H groups would show chain scission during oxidative attack. This has an effect to the hydrogen bonding of the hard segments, and is visible in changes of peak intensities of hydrogen bonded and non-

hydrogen bonded N-H groups. The peak intensities for PCU and PCU-OH of hydrogen bonded (3323 cm^{-1}) and non-hydrogen bonded (3334 cm^{-1}) N-H stretches in this study - as illustrated in Figures 4.14 to 4.18 - showed similar degradation profile over the 21 day period compared to the non-degraded reference sample. However, hydrogen bonded and non-hydrogen bonded N-H stretches in sulphonated PCU showed an increased intensity up to day 6, which was followed by a steady decrease of intensity over 21 days. The peak intensities of hydrogen bonded (3323 cm^{-1}) and non-hydrogen bonded (3334 cm^{-1}) N-H stretches for both, phase inverted and hydroxylated PEU - as illustrated in Figures 4.15 to 4.19 - showed a decreased intensity over the 21 day period, however, that of unmodified PEU was more pronounced. The degradation profile for sulphonated PEU showed an apparent increase in intensity in both, hydrogen bonded and non-hydrogen bonded N-H peak intensities until day 3 and thereafter a steady decrease over 21 days.

The molecules closest to the surface will degrade first under oxidative attack. This will mean for the phase inverted polymers in this study, that the soft segments degrade first, leading to a decreased amound of soft segments on the surface concomitand with an increased molecular mobility of the soft segments overall due to chain scission during degradation. With decreased amound of soft segments, the sampling depth can go deeper, measuring further into core of the hard segments showing an artificial increase in hard segments. The apparent increase in hard segment from initial in some samples can also be explained with the depth of degradation, which is assumed to be in the order of 10 μm [Schubert *et al.* (1997), Wu *et al.* (1994)]. With continued oxidative attack, the hard segments will undergo chain scission (Figure 2.9), leading to decrease peak intensity of hydrogen bonded and non-hydrogen bonded N-H groups as seen in FTIR spectra illustrated in Figure 4.14 to 4.19. However, isolated hard segments in the soft segment phase, in this study non-hydrogen bonded N-H, were said to be particulary prone to degradation. Christenson *et al.* (2004) reported a 42 % loss over 24 days of the free urethane carbonyl peak. The results in this study show that hydrogen bonded hard segments are less accessible to degradation due to their location and the crystalline structure of the hard domains. The hard segments dispersed in the soft segment phase and at the interphase region show with a higher intensity loss that they are more vulnerable to degradative attack.

The amide (C-N & N-H) stretches at 1533 cm^{-1} in PCU showed a stable intensity of up to 9 days whereas those of hydroxylated and sulphonated PCU gradually increased.

This was then followed by a sharp increase in peak intensity over the total of 21 days. The amide stretches C-N at vibration band 1223 cm^{-1} for all PCU, phase inverted and surface modified, showed initially a sharp decrease in intensity which then appeared to plateau out towards the end of the 21 day degradation period. The amide stretches (C-N & N-H) at 1533 cm^{-1} for all PEU, phase inverted, hydroxylated and sulphonated, showed a gradual increase in peak intensity over the 21 day degradation period. The sulphonated PEU showed with 10% the loweste intensity increase whereas phase inverted PEU exhibited with a 24% increase the highest peak intensity change. The amide stretches C-N at vibration band 1223 cm^{-1} for all PEU, phase inverted and surface modified, showed a gradual decrease in intensity over the 21 day degradation period.

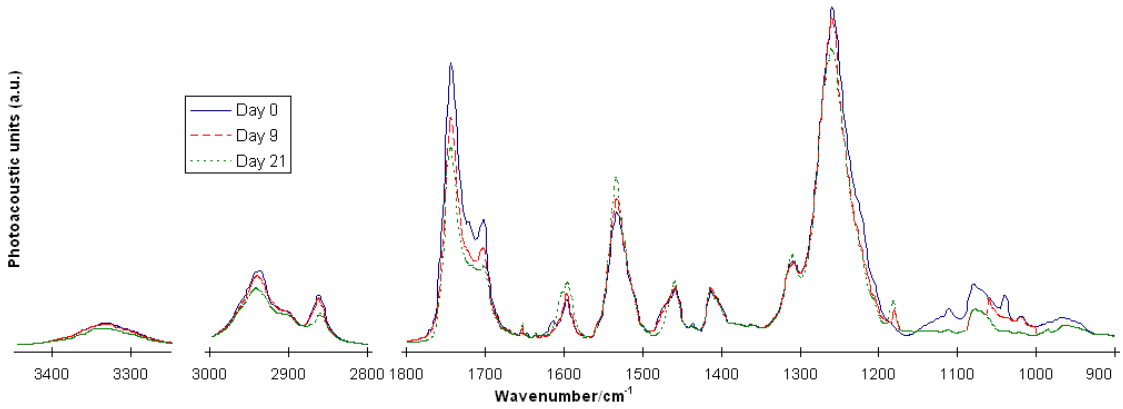

Figure 4.16: FTIR spectra of PCU-OH of undegraded control sample (Day 0) and with increasing degradation times after 9 and 21 days

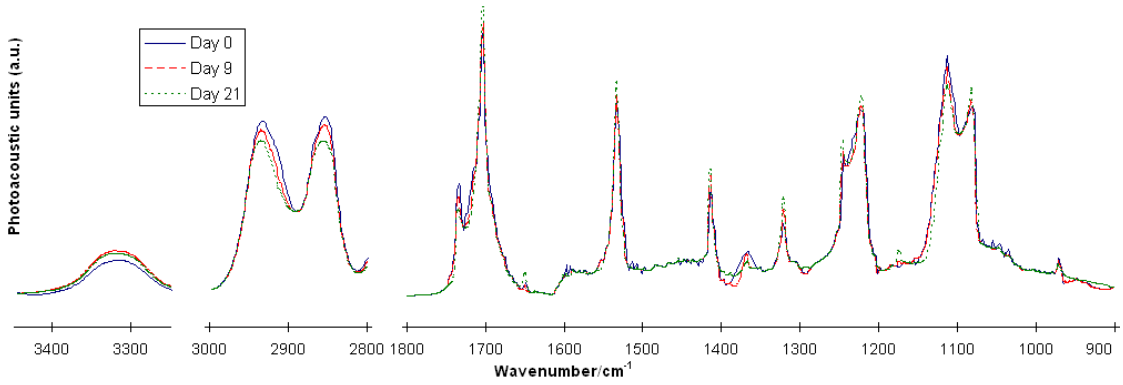

Figure 4.17: FTIR spectra of PEU-OH of undegraded control sample (Day 0) and with increasing degradation times after 9 and 21 days

A new peak at 1650 cm^{-1} was observed in the spectra of degraded PCU, which was

assigned to free aromatic amines (N-H). Additionaly, a new peak at 1650 cm^{-1} was observed in the spectra of hydroxylated and sulphonated PEU with prolonged degradation, but was not evident in phase inverted PEU. This new peak was thought to be the degradation product of that of the amide stretches C-N & N-H at 1533 cm^{-1}. These findings correlate with data of Christenson *et al.* (2004a) in which no evidence of this new peak in spectra of degraded PEU, but in that of degraded PCU was found; the new peak was attributed to chain scission of the hard segment.

Hydrogen bonded C=O stetches (1703 cm^{-1}) are identified with the hard domains [Christenson *et al.* (2004)], it can be seen with the results obtained in this study that all PU are susceptible to hard segment degradation. However, phase inverted PEU showed with 17 % the highest loss of intensity compared to that of 9 % for hydroxylated and sulphonated PEU. Hydroxylated PCU showed with 20 % the highest loss of intensity compared to that of 15 % for phase inverted and sulphonated PCU respectively.

Non-hydrogen bonded C=O stretches (1734 cm^{-1}) are located either at the interphase of hard- and soft segments or dispersed in the soft segment phase. Therefore, Christenson *et al.* (2004) assigend a decrease of the non-hydrogen bonded C=O bands to soft segment carbonate carbonyl chain scission. The peak intensity decreases found in this study with 10-17 % for PEU are similar than those of the hydrogen bonded C=O with 9-17 %. The peak intensity decreased with 7 % for both, phase inverted and sulphonated PCU compared to that of hydroxylated PCU with 19 % suggest that the hydroxylated version of this polymer shows the highest susceptibility to degradation.

Soft Segment Degradation

The carbonate soft segment in C-O-C (1259 cm^{-1}) stretches for phase inverted, hydroxylated and sulphonated PCU showed similar degradation profile via peak intensity decrease over 21 days. However, hydroxylated PCU showed a more rapid peak intensity loss compared to the phase inverted and sulphonated counterpart. The peak intensity of the C-O-C (1113 cm^{-1}) vibration band for phase inverted, hydroxylated and sulphonated PEU showed a gradual decrease in peak intensity over 21 days with a slighly higher intensity loss for sulphonated PEU. This was in accordance to what was found in degradation studies of Christenson *et al.* (2004), in which a decrease in peak height of conventional solvent cast PEU and PCU over a degradation period of 24 days was observed. These decreased intensities were attributed to chain scission of the aliphatic ether soft segment

(PEU) and carbonate oxygen linkage (PCU) via oxidation.

For phase inverted and hydroxylated PEU, a new peak appeared at 1174 cm^{-1} vibration band, which is assigned to branched ether. These changes in intensity are an indication of abstraction of a polyether α-methylene hydrogen atom by oxygen radicals causing crosslinking of the PU. Additionally, for phase inverted and hydroxylated PCU, a new peak was observed at 1180 cm^{-1} vibration band, which was previously correlated only with cross-linking of PEU [Christenson *et al.* (2004b)]. However, the decreased peak intensities of the C-O-C soft segment observed with these polymers showed evidence that the oxidative environment produced chain scission and cross-linking of the soft segment with the formation of a branched ether. A similar observation with both sulphonated PEU and PCU was not possible because of overlapping bands with those of SO_3 peaks at 1182 cm^{-1} vibration band.

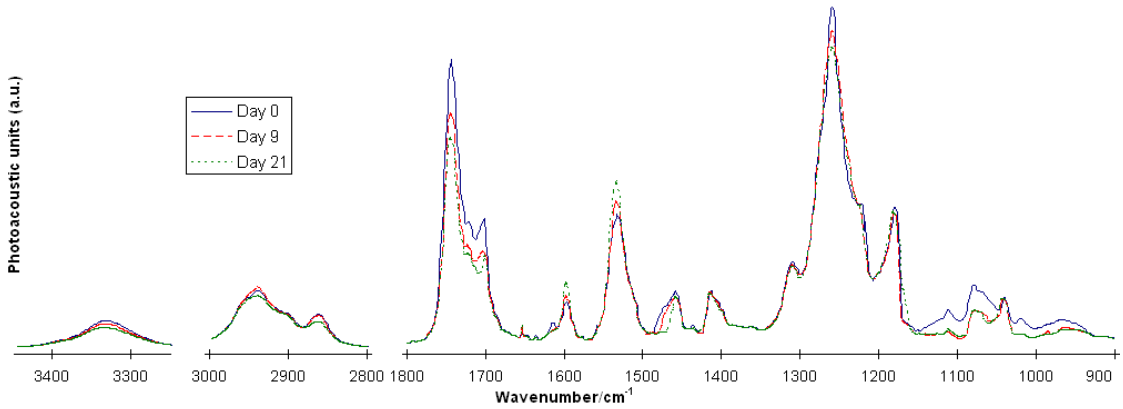

Figure 4.18: FTIR spectra of PCU-SO_3 of undegraded control sample (Day 0) and with increasing degradation times after 9 and 21 days

Overall, soft segment degradation underwent a relatively steady decrease over the 21 day period for both types of PU including the surface modified versions (Figure 4.20). Though the rate of soft segment loss was initially higher for PEU but after a 12 day period relatively similar for both PUs. Similar observations were made by Christenson *et al.* (2004a) in which 10 % loss of polycarbonate and 22 % loss of polyether was detected after 12 days concomitant with a parallel rate of soft segment loss for both PEU and PCU. The more prominent soft segment loss was thought to depend on the soft segment chemistry.

These results show that although both PEU and PCU underwent some hard segment degradation, PCU appeared to exhibit more hard segment degradation. The soft segment

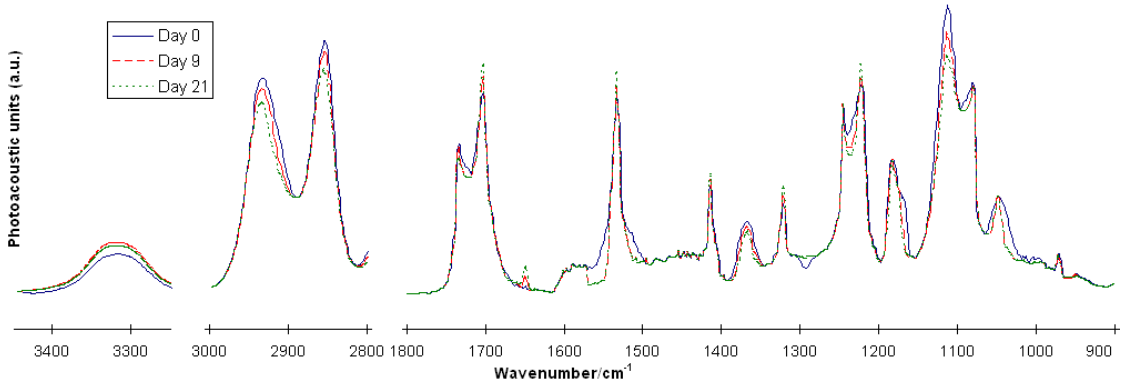

Figure 4.19: FTIR spectra of PEU-SO_3 of undegraded control sample (Day 0) and with increasing degradation times after 9 and 21 days

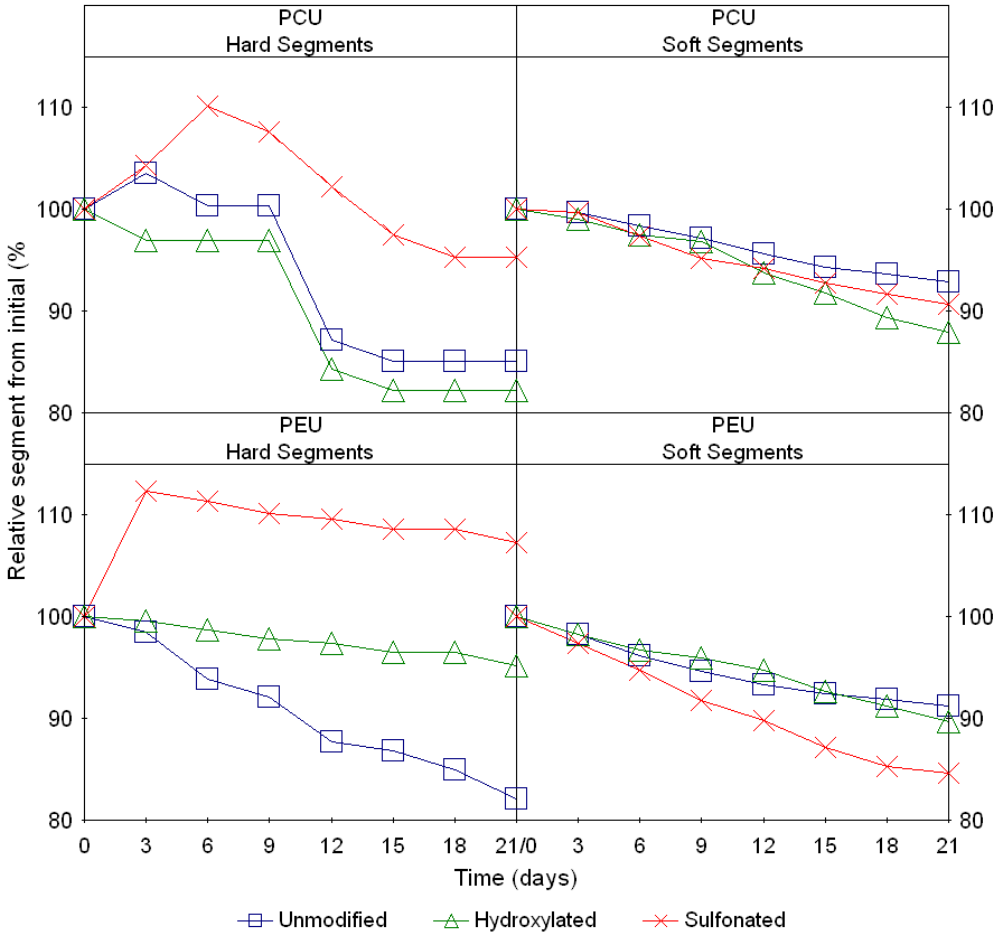

Figure 4.20: Relative hard and soft segment remaining from initial for PEU and PCU (modified and unmodified).
The extent of the soft segment degradation was made on the basis of percent change in the 1113 cm^{-1} *ether band of PEU and the 1259* cm^{-1} *carbonate band of PCU relative to the untreated control. That of the hard segment degradation was made on the basis of percent change in the N-H vibration bands at 3323* cm^{-1} *hydrogen bonded and 3334* cm^{-1} *non-bonded (PCU) and 3321* cm^{-1} *hydrogen bonded and 3446* cm^{-1} *non-bonded (PEU).*

degradation of that of PCU showed better degradative stability than PEU, confirming the notion that PCU is more biostable [Christenson *et al.* (2004a), Tanzi *et al.* (1997)]. Furthermore, surface modifications showed only a minor decrease in degradation compared to their unmodified counterpart, showing that the chemical properties were not impinged with these modifications.

4.8 Scanning Electron Microscopy

The surface topography (visible changes) of PU and SR (modified and unmodified) was examined to assess microstructural changes owing to biodegradation. SEM images were evalutated regarding to physical appearances in comparison to their non-degraded counterparts.

Unmodified PCU (Figure 4.21) appeared to be smooth, showing no signs of physical changes of the surface throughout a 9 day period. However, after 15 days, the surface showed small distorted sections. After day 21, signs of superficial furrowed areas were visible. Undegraded hydroxylated PCU (Figure 4.22) showed a smooth surface. After 3 days of degradation, the surface appeared to show distorted areas suggesting undulating contours. After 9 days the surfaces show a dimpled texture. These dimples appeared to be more dominant after 15 days; after 21 days mild etching and localised pitting also occurred. Undegraded sulphonated PCU exhibited a smooth and even topography. After 3 days of degradation, the surface showed strong undulating contours in the form of wavelike ripples. After 9 days, fissures and sectional damage (pitting) was clearly visible. After 15 days, the surface appeared to be eroded over the entire area, exposing superficial concavities. At day 21, the surface appeared heavily eroded exposing cavities which might then lead to fracture and pitting.

Surface of unmodified PEU (Figure 4.24) showed localised particles, which may be attributed to dust entrapped on the surface during gold sputtering. Apart from that, the surface was smooth, showing no signs of distortion nor sectional damage. After day 3, the surface appeared to expose concavitational pitting. At day 9, strong wavelike ripples may suggest distortion and/or swelling concomitant with reorientation of molecules within the polymer matrix. This was more apparent at day 15, suggesting sectional fissure. After day 21, the surface appeared to be flat, not showing any waves. However, the fissure penetration was deeper. Undegraded hydroxylated PEU showed a smooth surface. After day 3, signs of undulating contours were visible. After day 9, the surface appeared to

be more distorted showing extruding gouges. At day 15, decay of the surface may be suggested due to eroded sectional damages. After day 21, the surface showed wavelike ripples, with signs of superficial pitting. Undegraded sulphonated PEU (Figure 4.26) exhibited a smooth surface, not showing much changes of the topology after day 3. After day 9, worn away parts suggesting localised eroded sections are apparent, which manifested themselves more at day 15. Furthermore, pitting and sectional damage (gouges) were clearly visible. These cavities appeared to have lifted up after 21 days, suggesting fissure underneath.

SR control did not show any signs of surface degradation including distortion or rippling at day 0 and day 3. At day 9, there may have been sections of apparent erosion noticeable; however the surface did not show any changes throughout the 21 days of degradation. This may suggest that these particles are attributed to trapped dust before gold sputtering. SR modified (Figure 4.28) appeared to have no different over the whole 21 day period of degradation study. Some sections with extruding, possibly eroded particles were visible, however, as these contours did not get manifested, it might be attributed to entrapped particles during gold sputtering.

Overall, SR (control and modified) showed scarcely any changes in relation to surface degradation throughout the testing period. PCU showed much less degradative surface changes compared to PEU. This is in agreement to findings made by Christenson *et al.* (2004a) and Tanzi *et al.* (1997). However, hydroxylated PCU showed a dimpled texture which can be mainly attributed to swelling rather than degradation itself, as after 21 days there was only minor pitting apparent. According to these findings, surface modification resulted in only slightly more visible changes due to oxidative degradation of hard and soft segments compared to their unmodified counterpart.

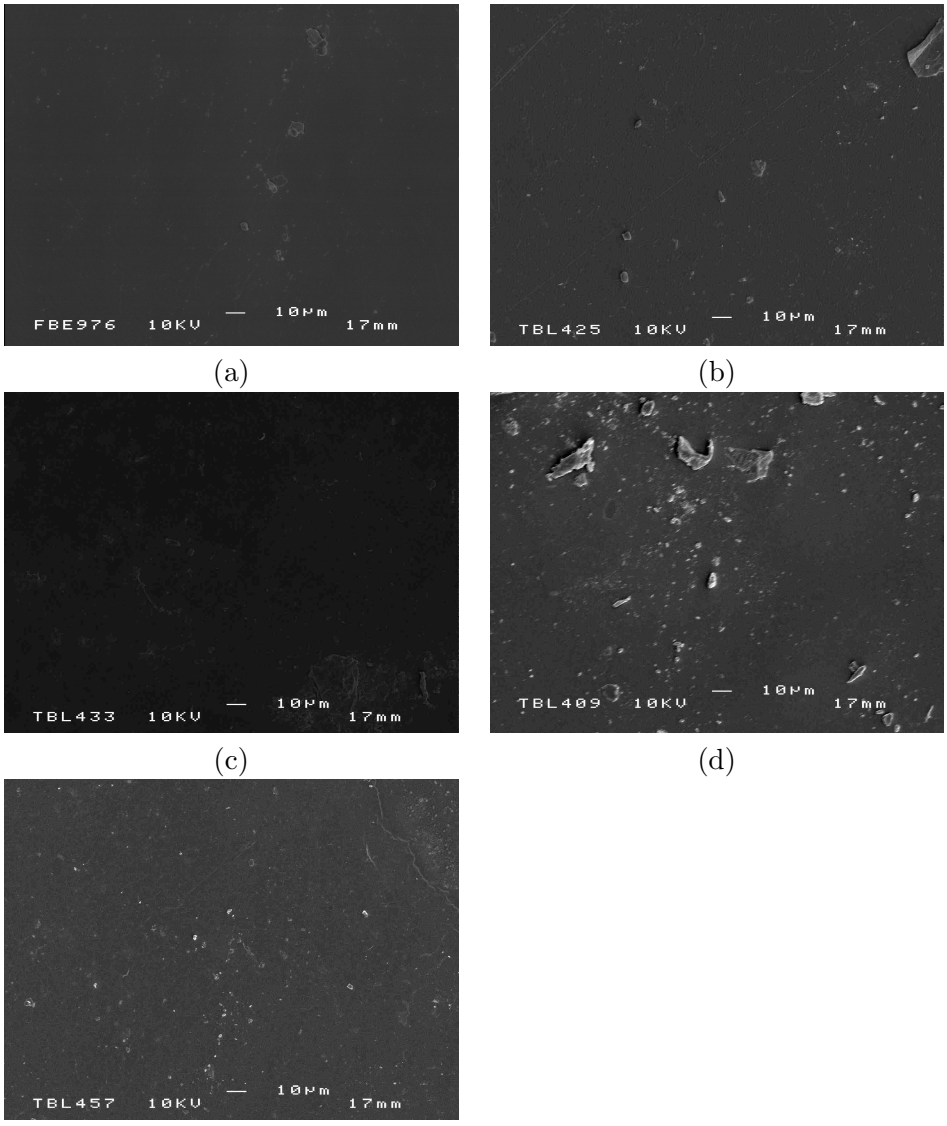

Figure 4.21: SEM micrographs viewing degradation of PCU (a) undegraded control (b) 3 days (c) 9 days (d) 15 days (e) 21 days

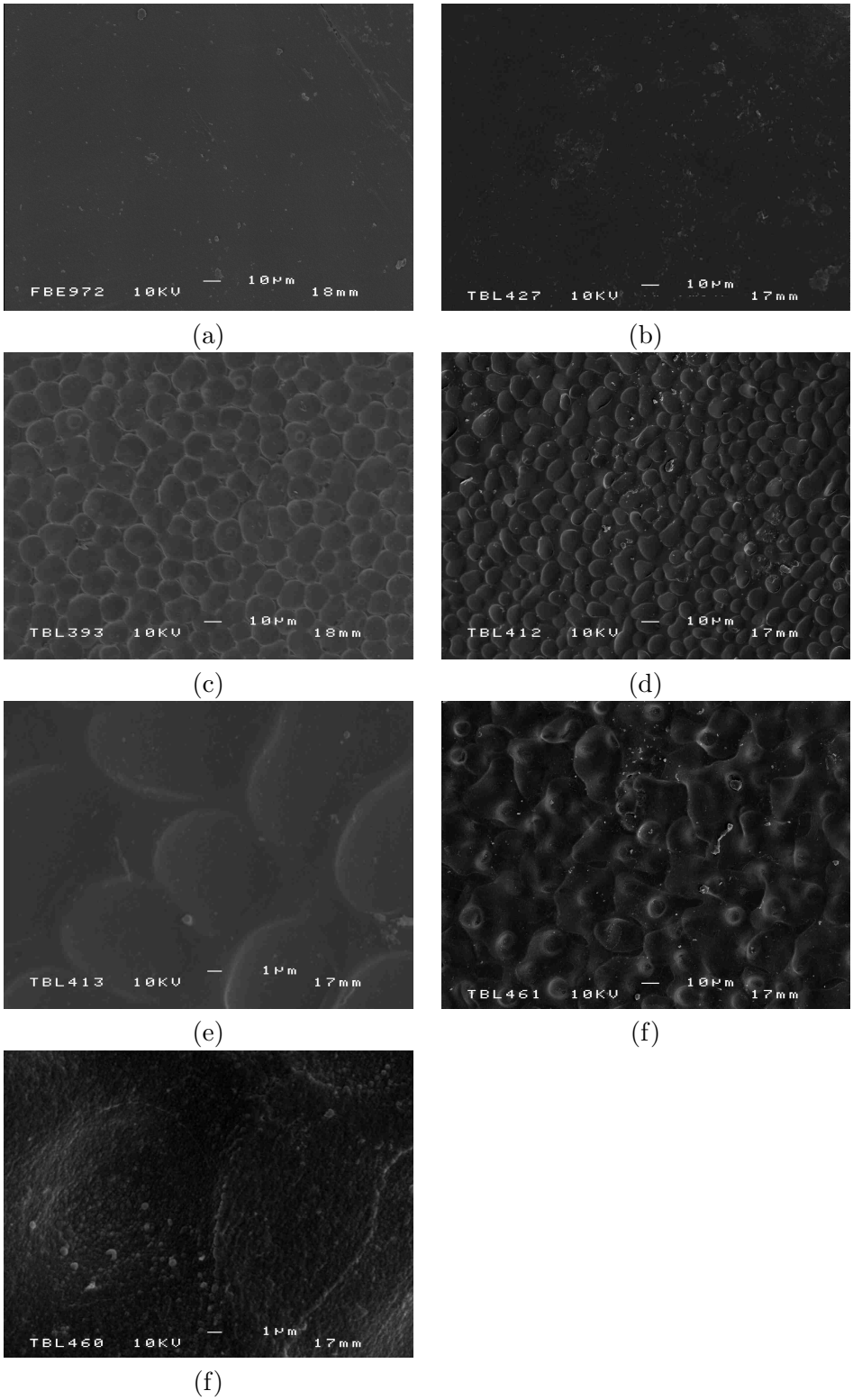

Figure 4.22: SEM micrographs viewing degradation of PCU-OH (a) undegraded control (b) 3 days (c) 9 days (d) 15 days (e) 15 days closeup (f) 21 days (g) 21 days closeup

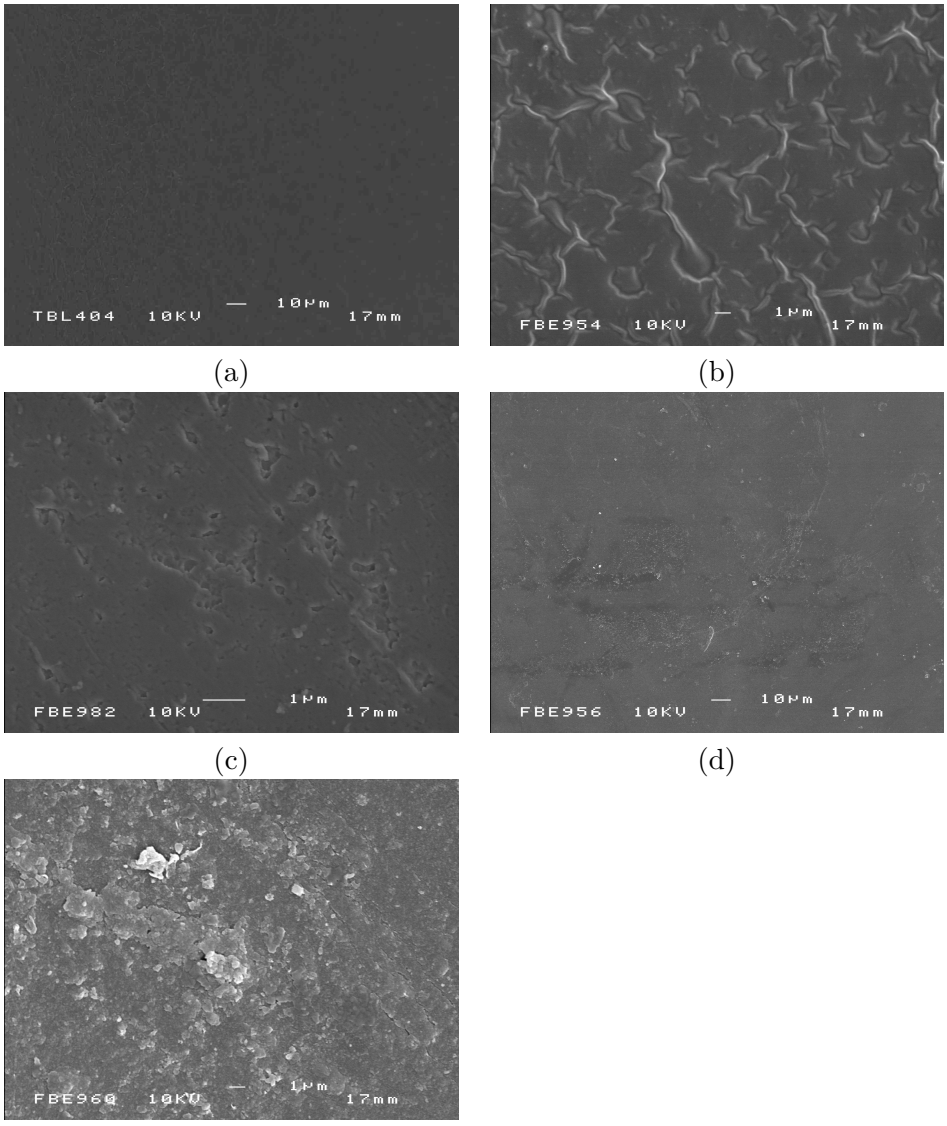

Figure 4.23: SEM micrographs viewing degradation of PCU-SO_3 (a) reference (b) 3 days (c) 9 days (d) 15 days (e) 21 days

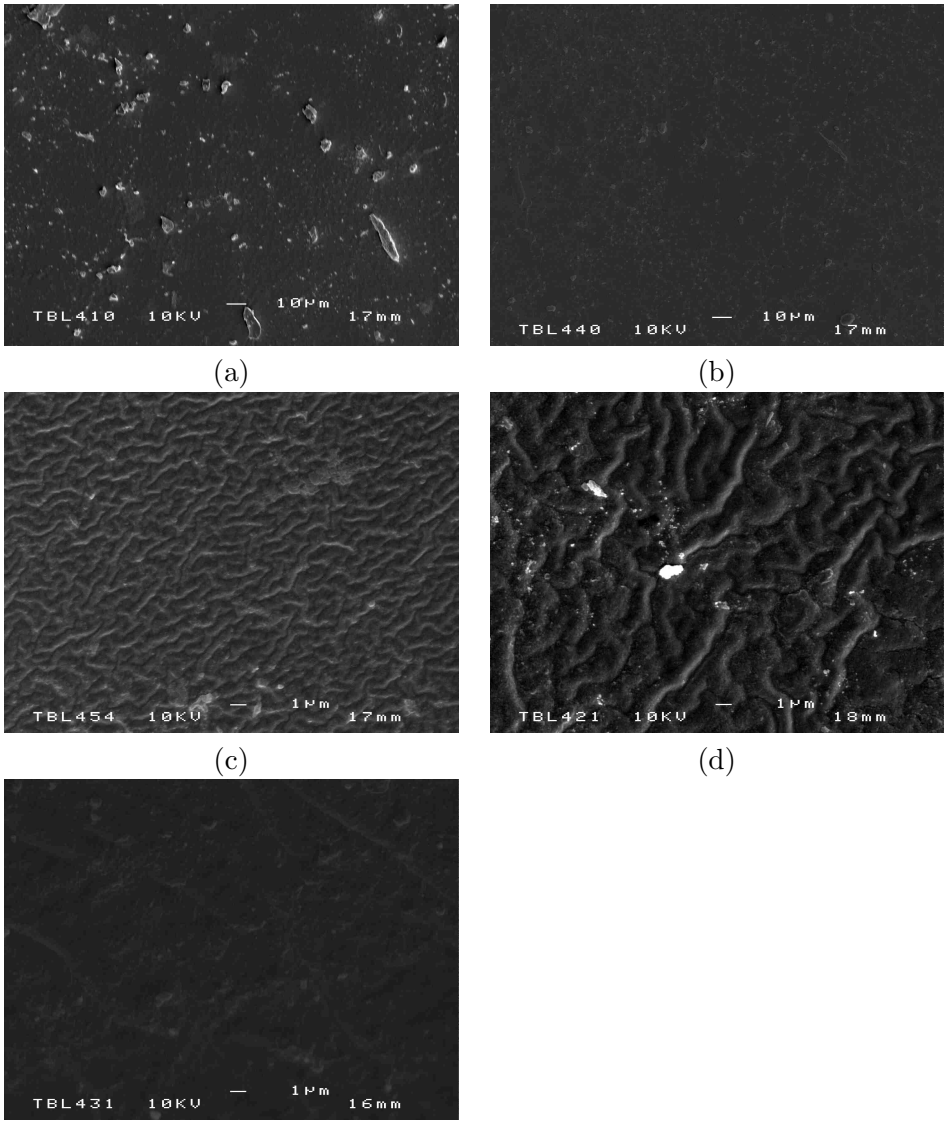

Figure 4.24: SEM micrographs viewing degradation of PEU (a) reference (b) 3 days (c) 9 days (d) 15 days (e) 21 days

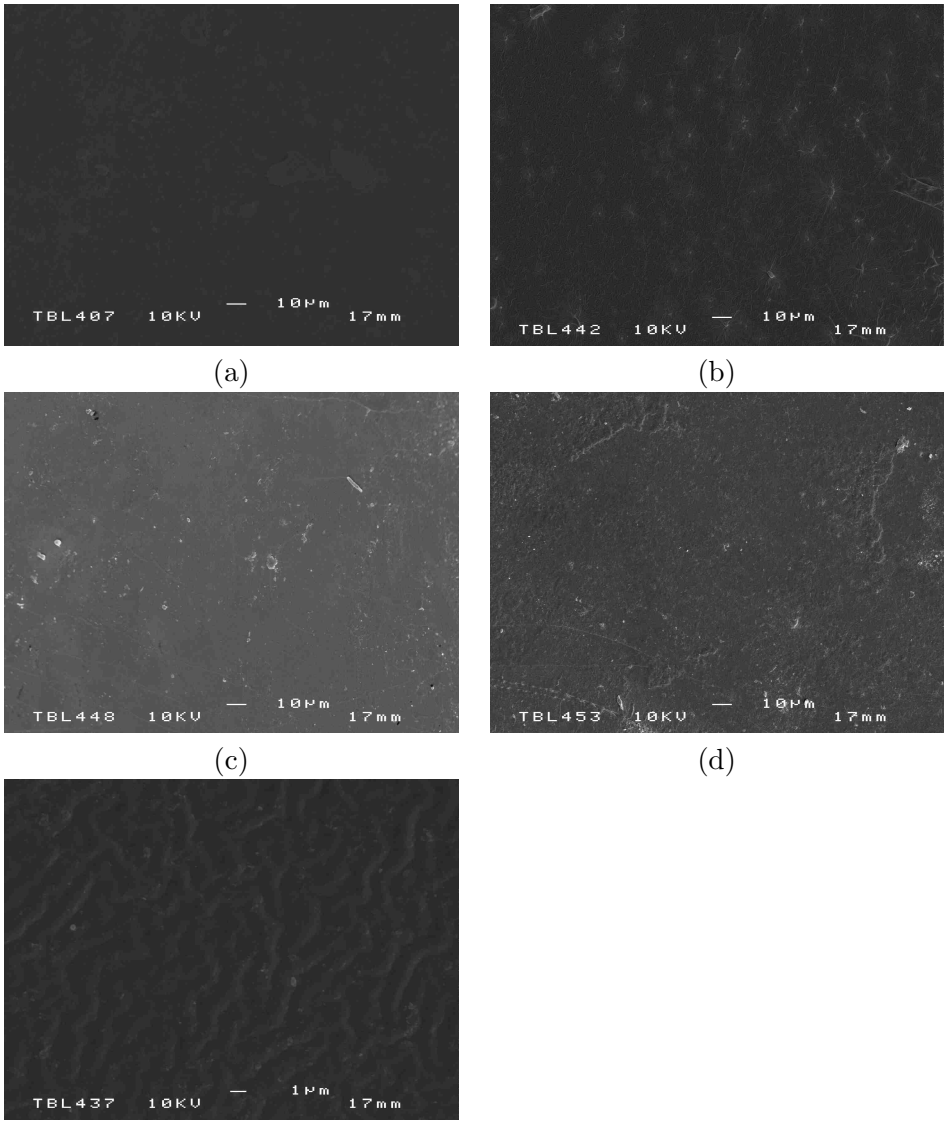

Figure 4.25: SEM micrographs viewing degradation of PEU-OH (a) reference (b) 3 days (c) 9 days (d) 15 days (e) 21 days

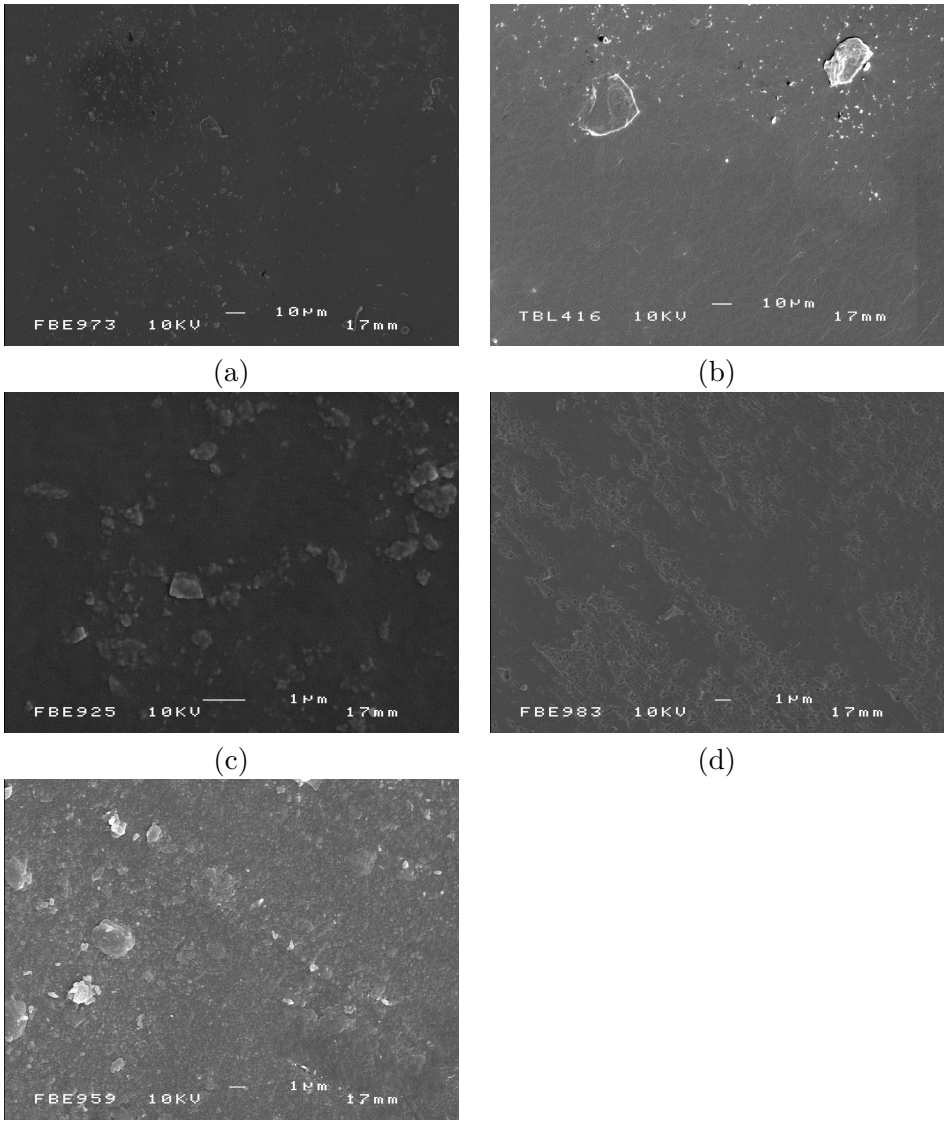

Figure 4.26: SEM micrographs viewing degradation of PEU-SO_3 (a) reference (b) 3 days (c) 9 days (d) 15 days (e) 21 days

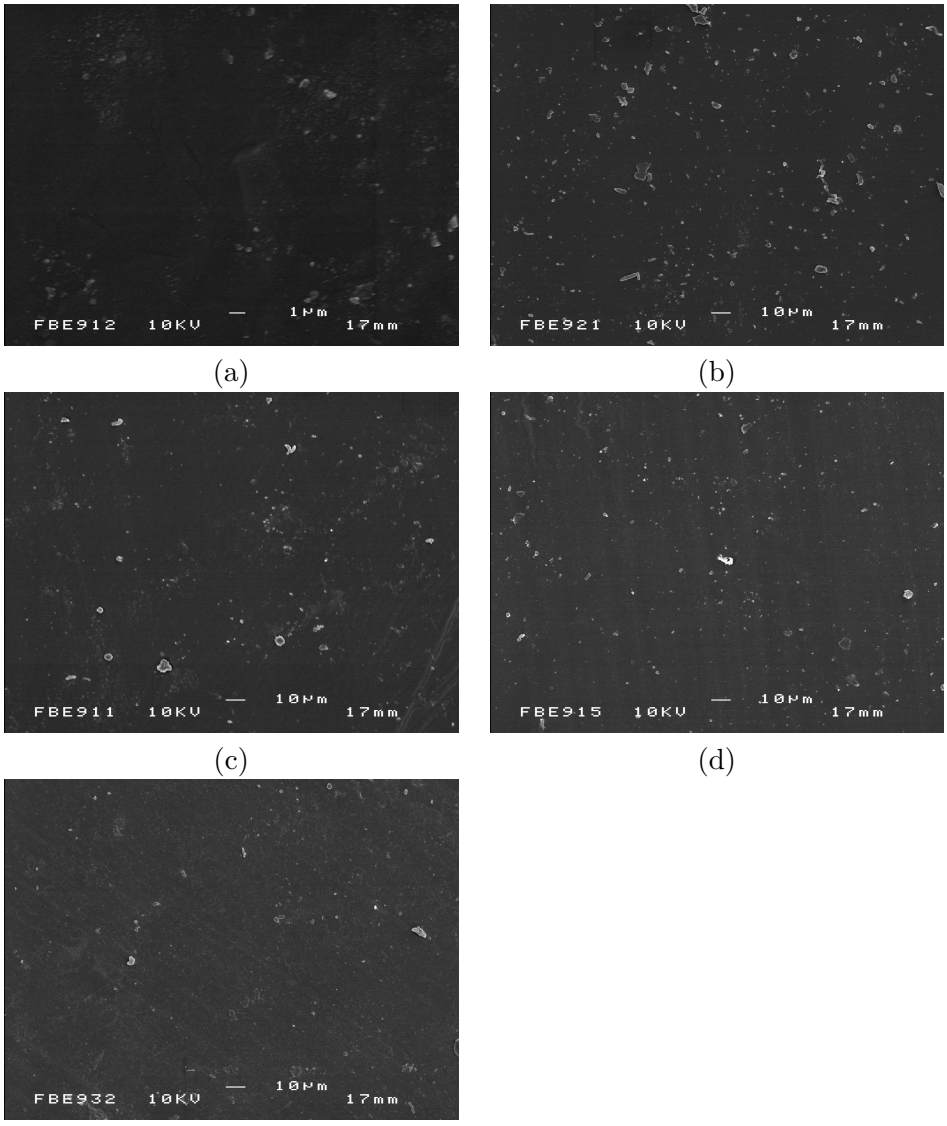

Figure 4.27: SEM micrographs viewing degradation of SR (control) (a) reference (b) 3 days (c) 9 days (d) 15 days (e) 21 days

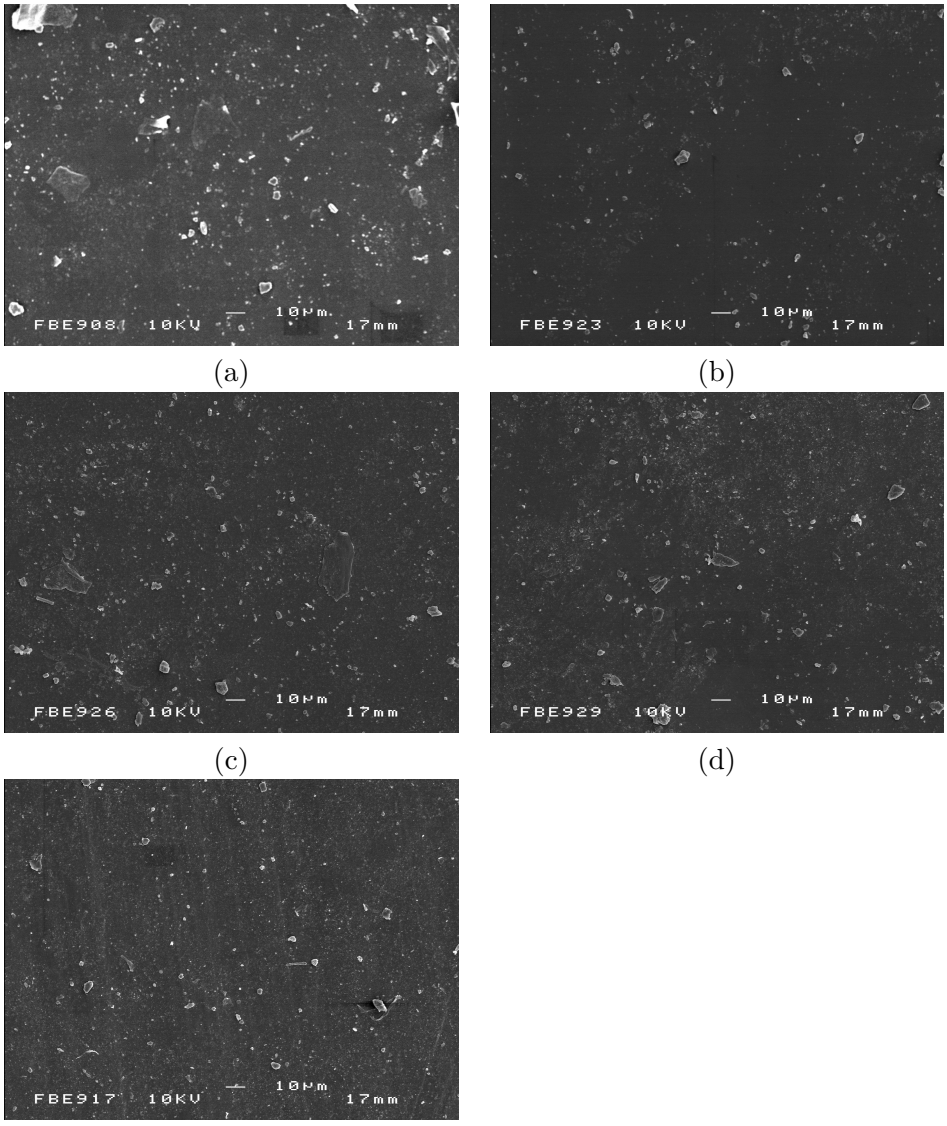

Figure 4.28: SEM micrographs viewing degradation of SR (modified) (a) reference (b) 3 days (c) 9 days (d) 15 days (e) 21 days

4.9 Cytotoxicity

In this section, *in vitro* cell toxicity evaluation was conducted to assess biocompatibility. The level of cell attachment, including growth and spread, provides a good indication on how materials perform in their intended environment, and hence will provide an insight into cell-material interactions. The test chosen is the direct cell contact assay using 3T3 mouse fibroblasts. Cell viability and proliferation was assessed quantitatively via resazurin-based AlamarBlue^{TM} dye reduction and supplementary qualitatively via visual observation of cell morphology.

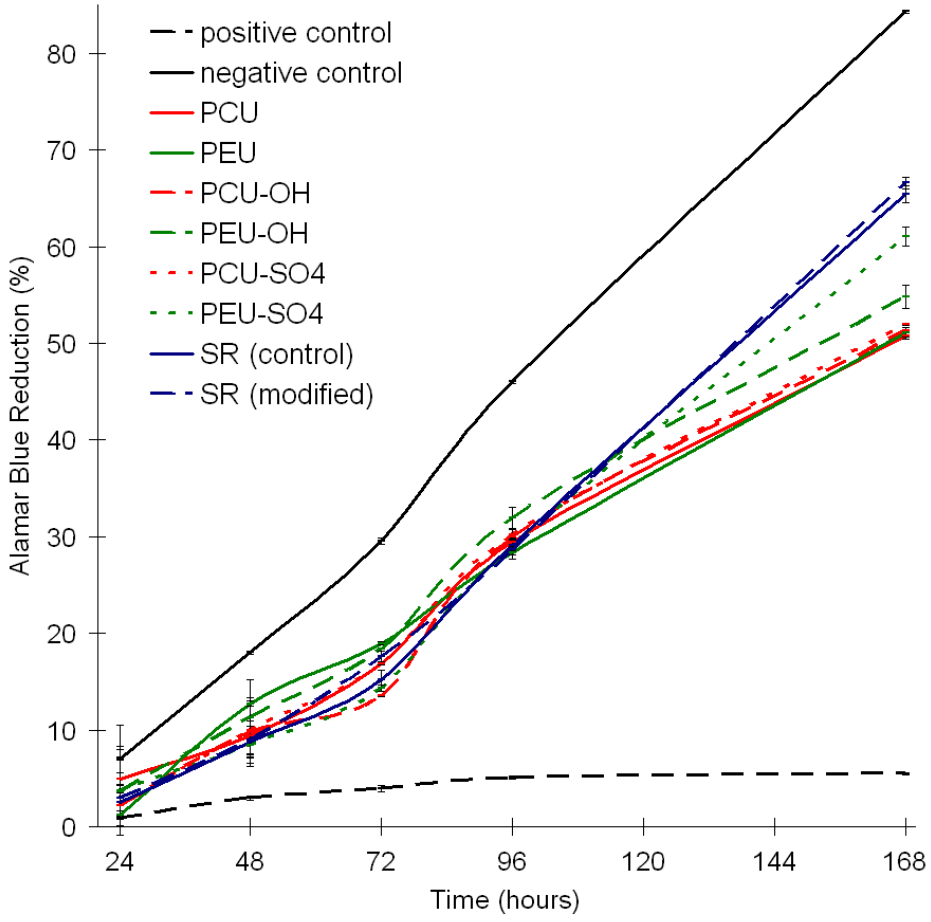

Figure 4.29: AlamarBlue^{TM} reduction on modified and unmodified polymers including positive and negative control samples during set time course

A comparison of AlamarBlue^{TM} reduction over the time frame of 24, 48, 72, 96 and 168 hours is illustrated in Figure 4.29. Measurements at each time point showed the mean of four replicate samples with 95 % confidence intervals. The negative toxicity control sample with Thermanox cover slip in the presence of cells showed an AlamarBlue^{TM} re-

duction of about 85 % and the positive toxicity control sample including cells showed a baseline level of about 5 % of metabolic activity after 168 hours incubation time. The presence of samples containing different variations of PU showed between 50-60 % of AlamarBlue^{TM} reduction at the end of testing. SR showed a slightly higher cell activity over 24 hours of AlamarBlue^{TM} incubation after 168 hours of about 65 %.

Figures 4.30 to 4.32 illustrated the visual observations of cell attachment, growth and spread after 168 hours of cell incubation on selected materials. Cells grown on the negative toxicity control sample (Figure 4.30 (c)) were seen to have adhered after 24 hours and were nearly fully confluent after 168 hours. The cells exposed to SR (Figure 4.30 (a) and (b)) showed attachment and growth in a similar manner to the negative toxicity control sample, yet SR (modified) appeared to promote slightly less cell growth compared to its reference sample. Also, the cells appeared more spread with samples of SR (modified).

PCU, Figure 4.31 (a), showed moderate cell spread and growth compared to the negative toxicity sample; however, some cells appeared to be of rounded morphology which is a sign of cell death. Its hydroxylated counterpart (Figure 4.31 (b)) showed promoted cell growth and spread with the formation of islands of clustered cells. Sulphonated PCU (c) showed the highest cell growth and spread overall. However, the appearance of some rounded cells (Figure 4.31 (c)) may suggest diminished cell activity.

PEU, Figure 4.32 (d) showed cell growth in a similar fashion to PCU (Figure 4.31 (a)). The hydroxylated version of PEU (Figure 4.32 (e)) showed some cells of rounded morphology and appeared to exhibit reduced cell adhesion and spreading. The sulphonated version (Figure 4.32 (f)) of this polymer showed cell growth similar to its unmodified counterpart. However, the cells were seen to be more spread, containing some rounded cells.

The cell attachment, including growth and spread (qualitative) observed for SR is in direct corroboration with data obtained from AlamarBlue^{TM} reduction (quantitative), showing the highest cell proliferation of all of the tested materials. Also, unmodified PU showed the lowest levels of cell proliferation according to data shown in Figure 4.28 which is in confirmation with visual observation via inverted microscope (Figure 4.29). Hydroxylated PU appeared to exhibit a clearly enhanced cell spread and growth compared to its sulphonated counterpart when examined visually, regardless of the type of soft segment present. Cell proliferation assessed via AlamarBlue^{TM} reduction showed enhancements with modified PEU compared to modified PCU.

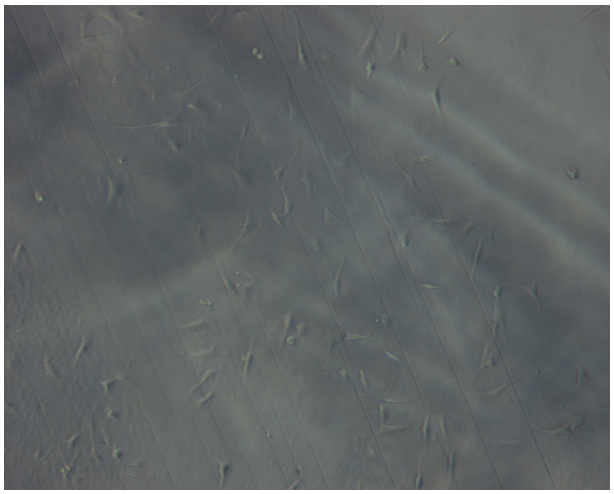

(a) SR (modified)

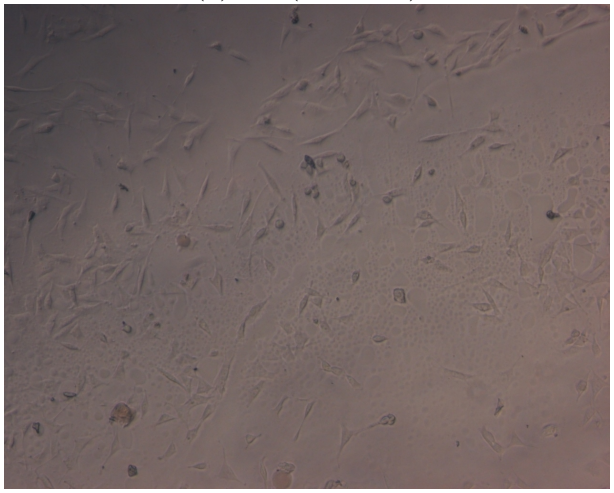

(b) SR (control)

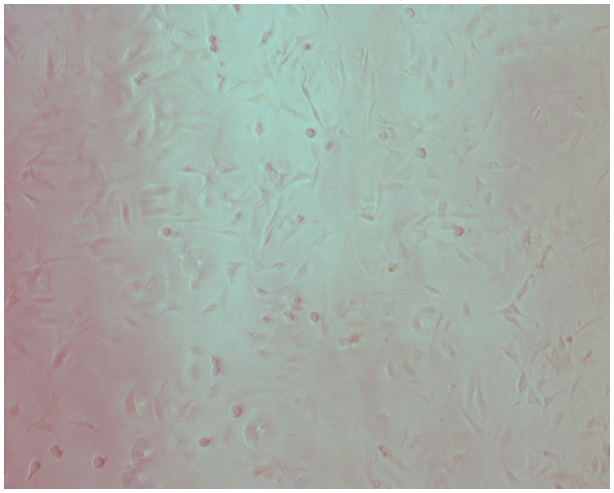

(c) Negative toxicity control

Figure 4.30: Images containing 3T3 fibroblast cells grown on SR (modified and control) including negative control after 168 hours incubation

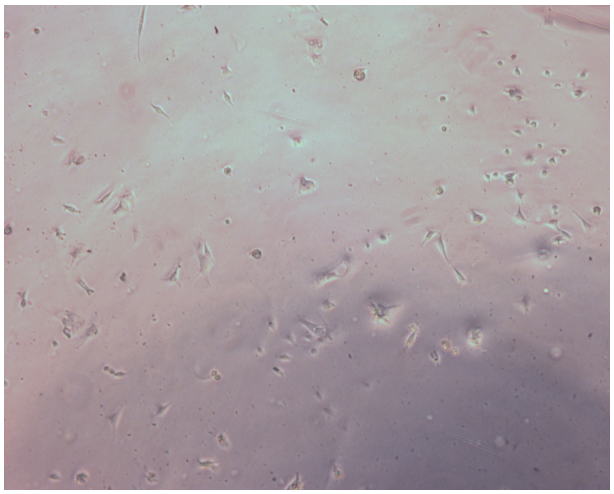

(a) PCU

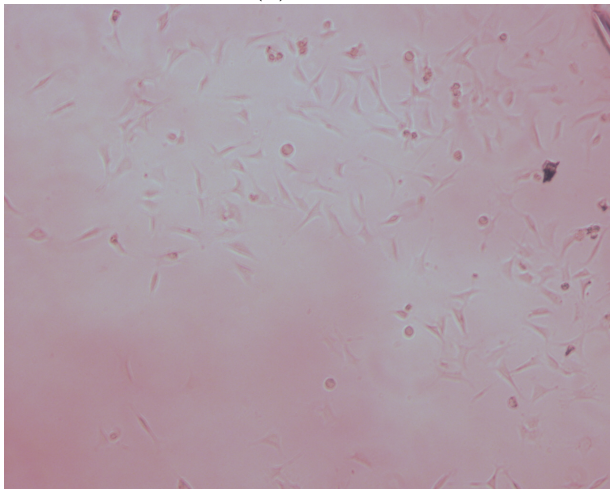

(b) PCU-OH

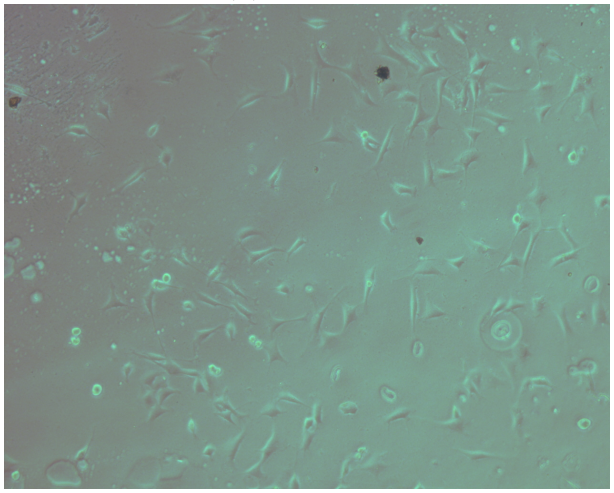

(c) PCU-SO_4

Figure 4.31: Images containing 3T3 fibroblast cells grown on phase inverted, hydroxylated and sulphonated PCU after 168 hours incubation

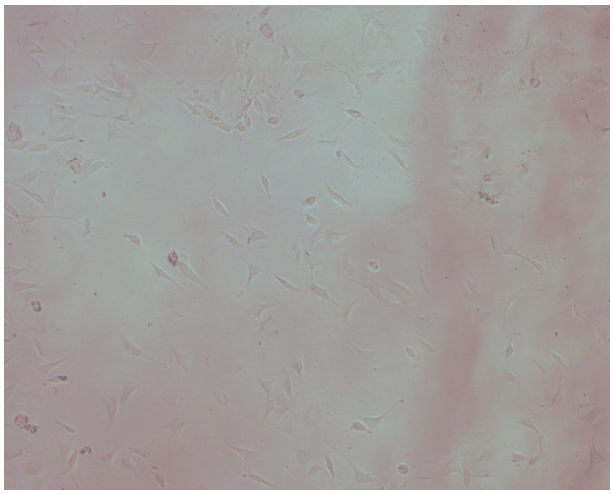

(a) PEU

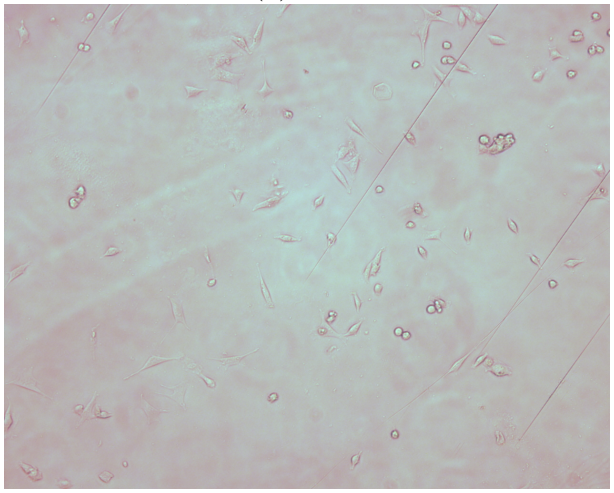

(b) PEU-OH

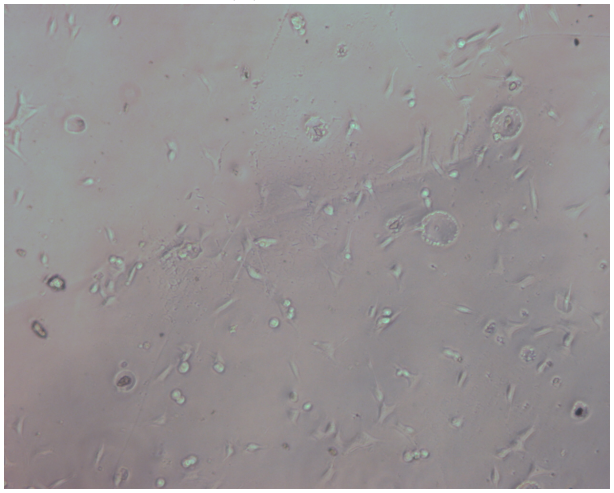

(c) PEU-SO_4

Figure 4.32: Images containing 3T3 fibroblast cells grown on phase inverted, hydroxylated and sulphonated PEU after 168 hours incubation

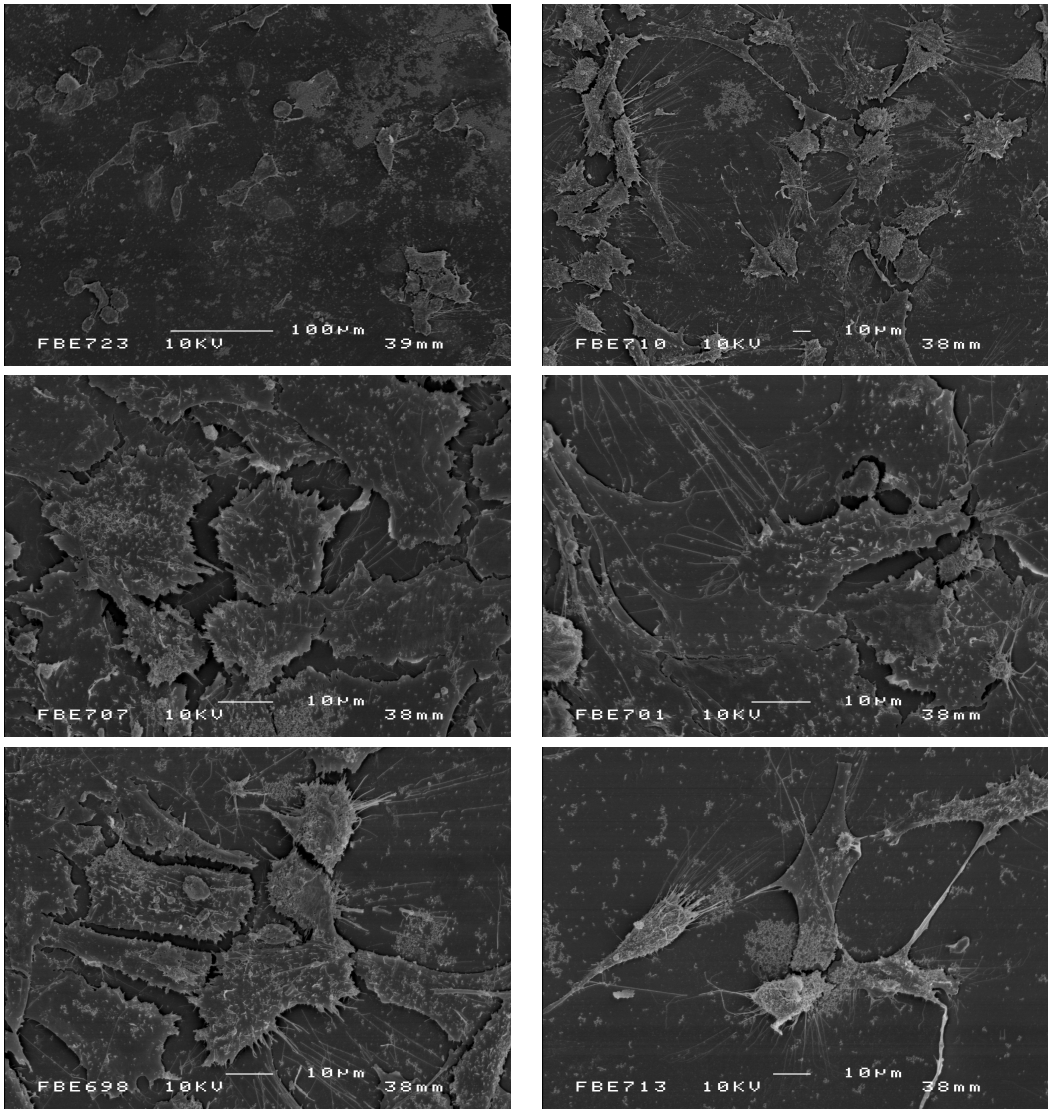

Figure 4.33: SEM micrographs of 3T3 fibroblast cells grown on selected polymer surfaces after 168 hours incubation

The SEMs in Figure 4.33 are representive for all of the polymers, modified and unmodified, as there was no distinct difference to be seen. However, it shows that cells attach and proliferate on all polymers (see also Figures 4.30 to 4.32) to the extent of not becoming confluent even after 168 hours of incubation.

Overall, these results demonstrate that cell adhesion and proliferation occurred on all tested materials with a slight preference to SR; however, the cell spread and growth did not seem to be encouraged nor discouraged. It can be further concluded that these polymers are not likely to be toxic to cells in the short-term.

4.10 Summary

- Effective phase inversion at PU was confirmed by definite soft segment enrichment at the surface.
- Surface modification at PU and bulk modification with SR did not cause detrimental chemical or physical effects at polymers.
- The new method for surface sulphonation was successful.
- SR modification led to a lower crosslink density and reduced hydrophobicity compared to conventional SR.
- Protein adsorption was not compromised with modified polymers and showed less inital adsorption specifically at sulphonated PEU and SR modified polymers.
- Cell adhesion and proliferation showed that all polymers were non-toxic to cells in short term.
- Cell spread and growth on modified polymers did not seem to be encouraged nor discouraged, suggesting bioinert properties.

Chapter 5

Synthesis of Prussian Blue on Pt Electrodes

5.1 Introduction

As stated in Chapter 1, needle-type electrodes were chosen as the tool for analyte concentration measurement in this study. These electrodes require only readily available materials and are therefore cheap in production; they can be fabricated to any size, shape and choice of material; they are small in diameter, therefore requiring only small sample volumes for assay.

At this stage, these electrodes were fabricated with Pt as working electrode. Basic electrochemistry was determined using cyclic voltammetry with ferri/ferrocyanide as a model system. This allowed a vital insight into whether these electrodes performed according to theory. As these electrodes will be used in electroanalysis, it is preferable to improve the selectivity and sensitivity to H_2O_2. To achieve this, the sensing tip was chemically modified with Prussian Blue as an electrocatalyst for H_2O_2 reduction, allowing operation at low polarising voltage.

The main objective of this Chapter is to detail the fabrication of these functional electrodes and their modification with Prussian Blue. Furthermore, these modified electrodes are designed to operate in neutral aqueous media.

5.2 Characterisation of Needle-type Electrodes

Needle-type electrodes used in this study with Pt working electrodes of 0.125 mm in diameter do not encompase true microelectrode standards due to their size [Winlove *et al.* (1993)]. Therefore, the electrochemical response of the electrodes to a standard redox couple was related to the response of conventional macroelectrodes. CVs in potassium ferrocyanide were produced with varied scan rates for each of the electrodes as illustrated in Figure 5.1.

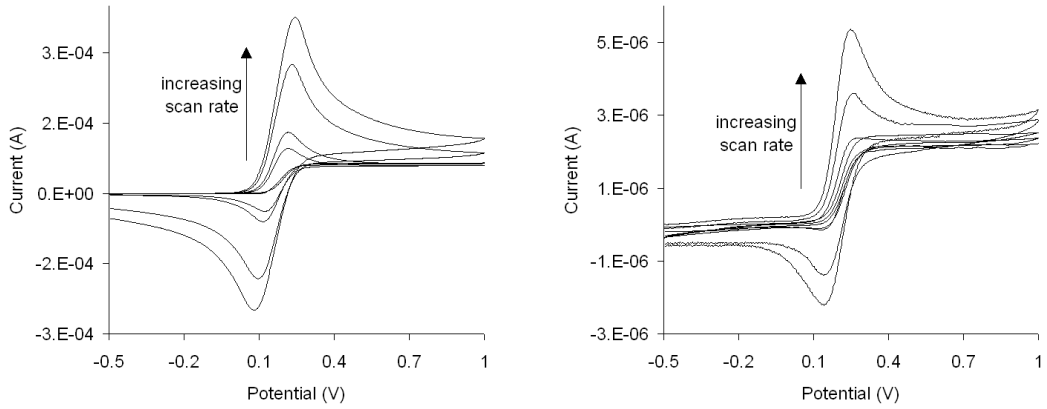

Figure 5.1: CVs for (a) conventional macroelectrodes, 2 mm in diameter, and (b) needle-type electrodes, 0.125 mm in diameter; (in 1 mM $K_4Fe(CN)_6$ vs. Ag/AgCl; electrolyte: 0.1 M KCl)

All of the CVs showed good reproducibility at varied scan rates, with similar forward and back scans, indicating thermodynamic reversibility. During electrochemical reactions, the oxidised or reduced species are consumed at the electrode surface and a concentration gradient is formed around the electrode. As molecules diffuse from an area of high concentration into an area of lower concentration to establish equilibrium, the oxidised or reduced species will diffuse towards the electrode. The region affected by this reaction is called the diffusion layer. This diffusion layer extends in depth over time in unstirred solution and the larger the electrodes, the greater is the depth of this diffusion layer. As shown in Figure 5.1, with increased scan rates, both types of electrodes produced increased peak heights. This indicates that the initial growth of the diffusion layer and the diffusion profile occurs in a smilar fashion regardless of diameter. On the anodic scan, the rate at which the analyte is consumed increases with polarising voltage, causing local concentration depletion. Limited rate of mass transport causes the current to decrease after the initial rise. On the cathodic scan, the oxidised species remains close to the

electrode surface and can be reduced until depletion occurs, so producing a peak. The current then flows in the opposite direction. The macro- and needle-type electrodes produced similar responses, because initially the diffusion layer for both electrodes is smaller than the surface area of the working electrode, and planar diffusion dominates in both cases [Imisides *et al.* (1996)]. This behaviour remained similar for both, macro- and needle-type electrodes at high scan rates.

However, at lower scan rates different mass transport behaviour was seen. The macroelectodes produced peak-shaped curves, although the peaks were less dominant than at the higher scan rates, because the analyte had more time to diffuse to and from the electrode surface. Therefore, the current on the forward scan is maintained to a greater degree after the initial rise, with similar behaviour in the opposite scan. For the macroelectrodes, planar diffusion still dominates at the lower scan rates, and in order to maintain the rate of mass transport, the diffusion layer has to extend further into the bulk solution. Therefore, this changes the concentration gradient, hence slower mass transport.

For the needle-type electrodes at lower scan rates, the diffusion layer extends into the bulk solution in a non-linear way, with edge effects dominating [Howell (1987)]. The diffusion profile becomes hemispherical, causing a greater relative transport of electroactive species to the electrode surface. Therefore, higher flux is maintained for the needle-type electrodes than for the macroelectrodes, and the shape of the curve is sigmoidal rather than peak-shaped. This is indicating steady-state behaviour, since the rate of mass transport is able to keep up with the rate of electron transfer. The absence of a current flow in the cathodic direction is caused by the higher relative mass transport, enabling the products of the oxidation reaction to diffuse away more readily before they can be reduced. The voltage separation (ΔE) between the peak currents was determined for different scan rates for the macro- and needle-type electrodes from the CVs shown in Figure 5.1 and are illustrated in Table 5.1. The macroelectodes gave relatively constant voltage separation over the range of scan rates, while the voltage separation for the needle-type electrodes decreased the lower the scan rates (Table 5.1). A change in peak potential with varying scan rate reflects the response of the electrode to changes in mass transport conditions. For a reversible reaction, the peak potential should remain constant despite a change in scan rate, as seen with the macroelectrodes. For an irreversible reaction, the peak potential shifts as the scan rate changes. A fast scan rate allows less time to reach equilibrium at the electrode surface, and a reversible reaction may appear quasi-reversible, as seen

with the needle-type electrodes.

Scan Rate (mV/s)	Needle-type electrode ΔE (V)	Macroelectrode ΔE (V)
100	0.105	0.096
50	0.102	0.083
10	0.082	0.093
5	N/A	0.093
1	N/A	0.095

Table 5.1: Voltage separation (ΔE) between the peak currents at different scan rates for conventional macroelectrodes and needle-type electrodes

Theoretically, ΔE for thermodynamically fully reversible redox systems in a one-electron reaction, such as the ferri/ferrocyanide redox couple, should be 59 mV [Chapter 3, Equation 3.1]. In practice, peak separation values between 60 and 70 mV are commonly regarded as indicating reversibility [Petrovic (2000)]; values of around 100 mV may be regarded as quasi-reversible systems [Bard *et al.* (2001)]. However, the measured values as seen in Table 5.1 may be on the higher end, possibly due to uncompensated solution resistance and non-linear diffusion.

The Randles-Sevčik equation [Chapter 3, Equation 3.5] predicts that the peak current of a reversible redox process should be linearly proportional to the square root of the scan rate. The linear regression analysis of the peak currents shows this relationship for both the macroelectrodes (Figure 5.2(a)) and needle-type electrodes (Figure 5.2(b)). The peak current ratio of the cathodic and anodic peak currents may also be used to determine reversibility of a redox reaction [Chapter 3, Equation 3.2]. The nearly identical slopes from the regression lines indicate that the peak current ratio is approximately one. These results provide further evidence that the behaviour of both the macro- and needle-type electrodes is reversible and diffusion-limited.

The apparent diffusion coefficient with ferri-/ferrocyanide redox system for needle-type electrodes was calculated using the CVs (Figure 5.1(b)) and determined to be 7.38×10^{-6} (± 0.177) cm^2/sec. This compares favourably with literature values of 7.6×10^{-6} cm^2/sec [Bard *et al.* (2001)] and 7.26×10^{-6} cm^2/sec [Konopka *et al.* (1970)] for 1 mM ferri/ferrocyanide in aqueous media of 0.1 M and 1 M KCl, respectively. From the Randles-Sevčik equation, the area of the working electrode can also be calculated [Yamauchi *et al.* (2005)]. Using the apparent diffusion coefficient of 7.38×10^{-6} cm^2/sec, the effective (functional) surface area of the needle-type electrode was calculated to be 0.0227 ($\pm$ 0.00165) mm^2, however, the geometric surface area was calculated to be 0.0123 mm^2.

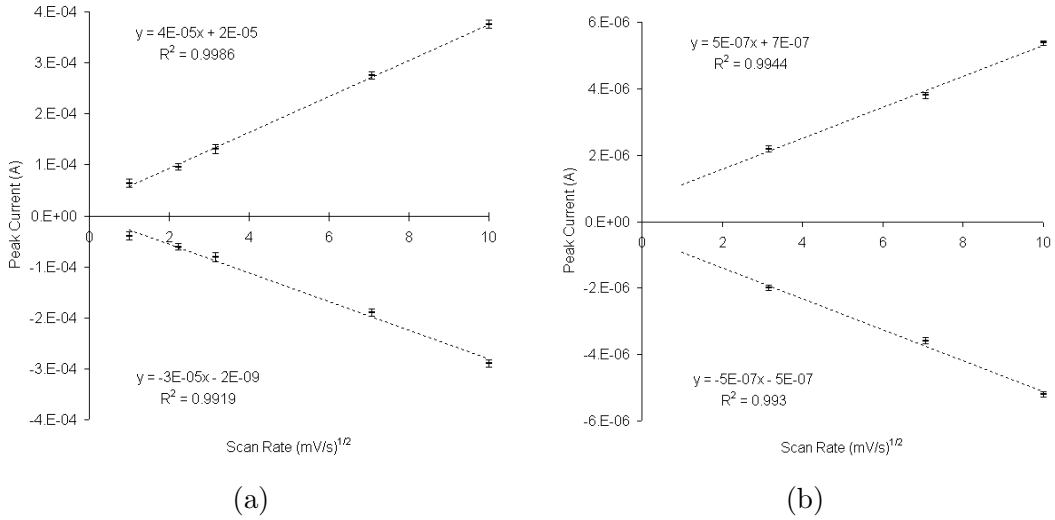

(a) (b)

Figure 5.2: Cathodic and anodic peak current dependence on scan rate for (a) macroelectrodes and (b) needle-type electrodes (in 1 mM $K_4Fe(CN)_6$ vs. Ag/AgCl; electrolyte: 0.1 M KCl)

The reason for the discrepancy in surface area is most likely due to the manufacturer's accuracy, a relatively rougher surface due to the polishing and possibly a slight tilt during polishing.

These results show that needle-type electrodes display microelectrode behaviour, despite the relatively large size of the working electrode. This is more apparent with higher scan rates, therefore the needle-type electrodes can be regarded as quasi-microelectrodes. For microelectrodes, the double-layer charging current decreases more rapidly than the diffusion current, leading to an improved Faradaic/non-Faradaic current ratio [Bard *et al.* (2001)]. The improved ratio increases the sensitivity of the electrode, allowing lower concentrations to be measured.

5.3 Synthesis of Prussian Blue

5.3.1 Introduction

Ferric hexacyanoferrate, also known as Prussian Blue (PB), was electropolymerised onto platinum electrodes. This mediator was selected because it offers improved performance in H_2O_2 sensing regarding selectivity and sensitivity. PB has been used successfully with glassy carbon substrates. However, low stability of PB on platinum has been reported [Ricci *et al.* (2005)]. Therefore, the methodologies for electro-deposition of PB in this study were modified from a method reported by Karyakin *et al.* (1999). The following

changes were made:

- PB was deposited on Pt instead of glassy carbon.
- The electrode was electrochemically pre-treated by potential cycling in 1 M $HClO_4$ from -0.25 to +1.5 V versus Ag/AgCl at a scan rate of 0.1 V/sec.
- A more concentrated growing solution was used: 0.1 M of $FeCl_3$ and $K_3Fe(CN)_6$ instead of 2 mM of each.
- Before activation, electrodes were placed in vacuum oven at 65°C over night.
- PB modified electrodes were activated with a switching potential of +0.35 to -0.05 V versus Ag/AgCl instead of using a fixed potential.

It was hypothesised that with these modifications, a more dense and even coverage of PB could be achieved, resulting in an increased stability. This section will cover the growth and activation towards optimisation of PB on platinum and will show results relating to the assessment of the stability and the pH effect.

5.3.2 Influence of Number of Cycles during PB Growth

Initially, cyclic voltammetry was employed to deposit PB onto platinum electrodes. The main criterion was to optimise film thickness so as to maintain a dense and stable poly-crystalic conducting PB layer. This was done by varying the number of sweeps during cyclic voltammetry.

Figure 5.3 shows the CVs for varied scans during the growth process. The CV at 8 growing cycles showed a sharp current increase between +0.4 and +0.45 V. Then the current increased at a lower rate, rising up towards +0.75 V. The CVs at 12 and 16 cycles showed a sharper current rise with increasing potential between +0.4 and +0.55 V, a plateau between +0.55 and +0.65 V followed by a current increase towards +0.75 V. However, the voltammogram at 12 growing cycles showed the highest current increase with increased potential and a narrow shape whereas that of 16 cycles was very broad. This was thought to be caused be the every increasing thickness of the PB layer as a function of time/cycles. So eventually, the layer of PB will have reached a level of thickness in which the current flow appears to be suppressed. Nevertheless, the shape of the curves (Figure 5.3) regarding current increase with increasing potential is an indication

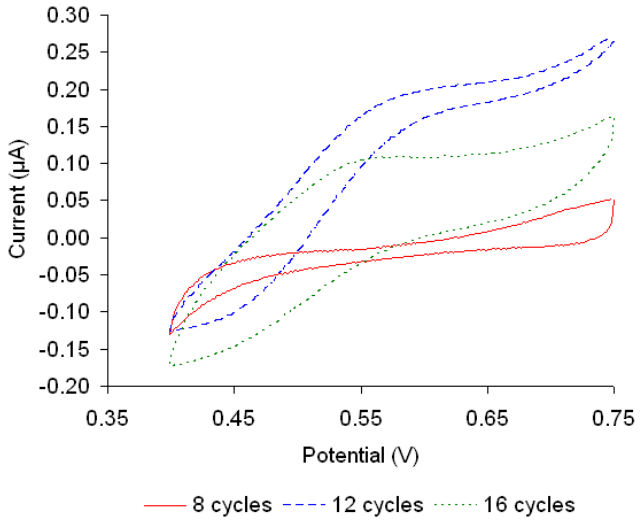

Figure 5.3: CV of PB growth at Pt electrode with 8, 12 and 16 growing cycles (in 0.1 M $FeCl_3/K_3Fe(CN)_6$; vsȦg/AgCl; 40 mV/s; electrolyte: 0.1 M HCl/KCl

of successful precipitation of PB on the Pt surface. Also, the formation of a PB layer could be observed visually via dark-blue colouration.

Pharr *et al.* (1997) found that large spacing of the hexacyanoferrate complex (Figure 2.16) results in a zeolite-type nature, with the interstitial spaces and many lattice sites filled with water molecules and electrolyte ions. Ganguli *et al.* (1983) found that Prussian Blue precipitate contains an average of 14 water molecules per unit $Fe_4[Fe(CN)_6]_3$ and indicated that some portion of water could be irreversibly removed by exposing PB to elevated temperatures. Much research was focused on the heating of polycrystaline PB and its increased stability [de Mattos *et al.* (2000b), Karyakin *et al.* (1999), Ricci *et al.* (2003a)]. However, an additional drying step after electrochemical cycling for precipitate PB formation prior to the subsequent activation step has not previously been reported. The strategy in here was to remove excess water at an earlier stage, to aid the formation of a more compact and stable PB layer. Thus, PB modified platinum electrodes were heated (Section 3.3.6) and then submitted for electrochemical activation. The CVs for PB activation are displayed in Figure 5.4 for 8 growing cycles, in Figure 5.5 for 12 growing cycles and in Figure 5.6 for 16 growing cycles. The respective insets within the graphs show the growth tendency of the peak current in anodic and cathodic direction with increasing number of cycles. All of these scans regardless of the number of growing cycles show typical redox peaks for the electrochemical polymerisation of PB, which are as expected near 0.2 V. The numerical values are listed in Table 5.2. These redox peaks increase gradually by size with increasing number of cycles. Up to a certain point,

the peak current does not increase by much with further scans, demonstrating that a conducting polycrystalic PB layer is formed.

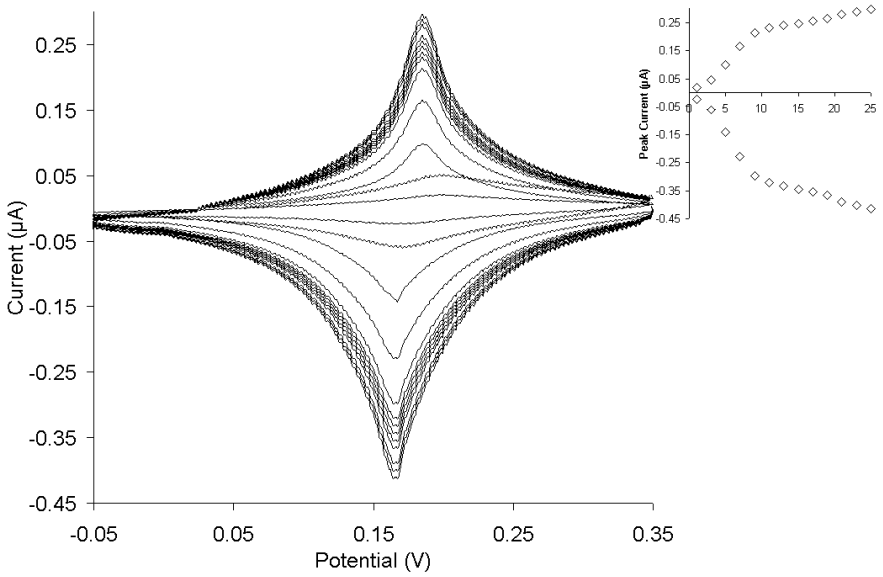

Figure 5.4: CV of a Pt electrode after 8 growing cycles during PB activation (vsȦg/AgCl; 40 mV/s; 25 cycles; electrolyte: 0.1 M HCl/KCl)

The CVs after 8 and 12 growing cycles show sharp peaks, whereas the peaks after 16 growing cyles show an overall broad profile. In general, a sharp peak is an indication of fast electron transfer wheras a broad peak shows reduced electron transfer which could be an indication of a less reversible system. Hence, the peak would then also be drawn out with increasing number of scans, resulting in an ever increasing peak separation. The peak separation (ΔE_p) illustrated in Table 5.2 shows that after 16 growing cycles it is with 110 mV much higher than that of 8 growing cycles with 10 mV and that of 12 growing cycles with 60 mV. An increased ΔE_p with increased growing cycles, hence increased PB surface coverage was also found in studies by various researcher [De Mattos *et al.* (2000), Haghighi *et al.* (2004), Ricci *et al.* (2002)] and was explained by higher capacitive currents due to film thickness which resulted in a less readily and less reversible redox reaction of the PB layer. However, the scans in this study show that a reversible redox interconversion of Prussian Blue and Prussian White, the oxidised and reduced forms respectively, does occur for all of these electrodes.

5.3.3 Chemical Synthesis

Prussian Blue was also chemically deposited on platinum electrodes by immersing the electrode tip into growing solution of varied concentrations and for varied time intervals.

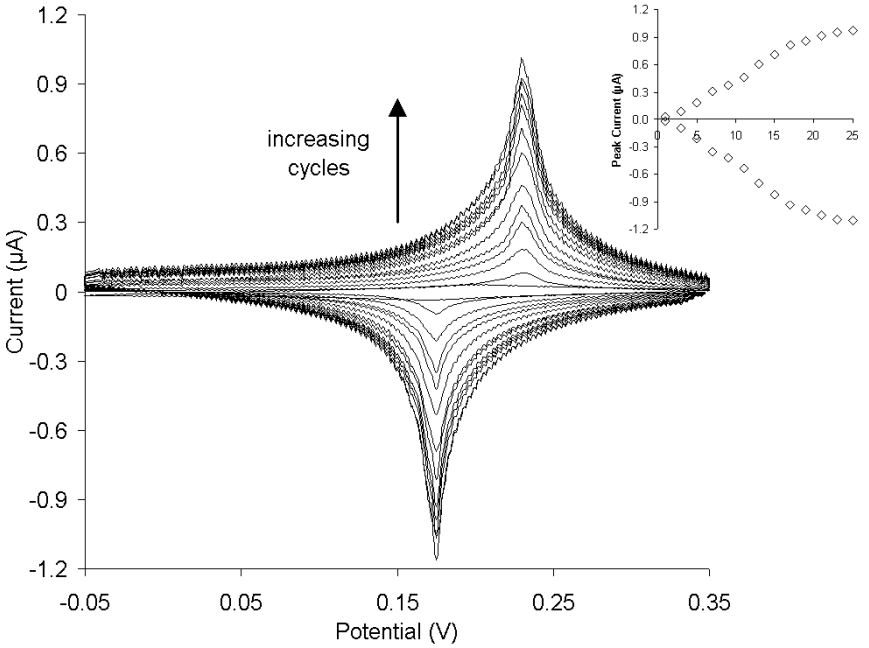

Figure 5.5: CV of a Pt electrode after 12 growing cycles during PB activation (vs. Ag/AgCl; 40 mV/s; 25 cycles; electrolyte: 0.1 M HCl/KCl)

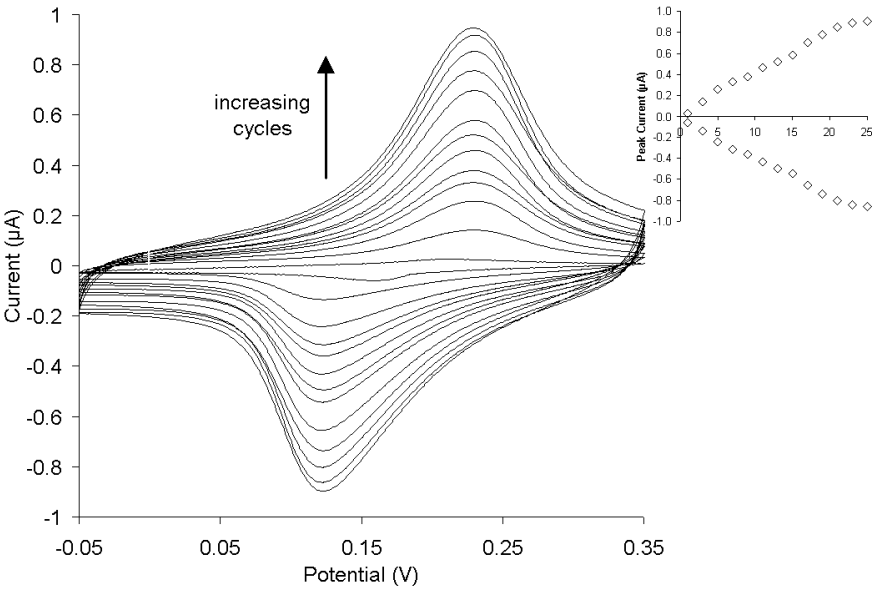

Figure 5.6: CV of a Pt electrode after 16 growing cycles during PB activation (vs. Ag/AgCl; 40 mV/s; 25 cycles; electrolyte: 0.1 M HCl/KCl)

This method is based on spontaneous reaction between ferric chloride and potassium ferricyanide [Moscone *et al.* (2001), Ricci *et al.* (2003)]. PB precipitation proceeded immediately upon immersion, which could be observed visually by darkening of the solution in the area around the electrode tip. However, electrodes placed into this solution for the same time frame under the same conditions produced films of considerably varied electrochemical activity and varied stability. Therefore, no further investigation was undertaken with these samples.

5.3.4 Assessment of PB Stability on the Number of Growing Cycles

One of the main problems with the use of PB in electroanalysis is the stability of the electrocatalytic layer. Karyakin *et al.* (1999) suggested a method for stability testing in which cathodic potentials (-50 mV) were applied. This method was taken up by other research groups and was referred to as "conditioning" [de Mattos *et al.* (2000a), Ricci *et al.* (2003b)] or "activation" [de Mattos et al. (2000b)]. However, this is merely a stability test under accelerated aging conditions, since by holding PB at a potential which is more negative than the PB/PW redox potential, PW was reported to become partially soluble [Itaya *et al.* (1984)].

In this section, the effect of the number of growing cycles on the stability of PB is investigated. This allowed the ideal number of cycles for PB film growth to be identified. In Figures 5.7 to 5.9, the CVs are illustrated before and after PB modified electrodes were exposed to the cathodic potential. The peak-to-peak currents for 8 (Figure 5.7) and 16 growing cycles (Figures 5.9) showed both greatly reduced peak currents after exposure to aging conditions. The peaks with 8 growing cycles changed from a sharp and narrow to that of a flat and rounded shape. The peak currents with 16 growing cycles showed however only changes in peak sizes. Current decrease and broadening of peaks is associated with reduced electroactivity, which would indicate a less compact and uneven PB layer on the electrode surface [Karyakin *et al.* (1999)]. However, the CV for 12 growing cycles in Figure 5.8 showed no significant changes in peak size and shape. Only a minor decrease can be seen in the cathodic peak current and even less decrease in the anodic region, hence good stability of the PB layer.

Relative peak currents (I_p), peak potentials (E_p) including peak separations (ΔE_p) were determined from CVs as shown in Figures 5.7 to 5.9 and are tabulated in Table 5.2. The cathodic potential, which corresponds to the redox state of PW [Karyakin

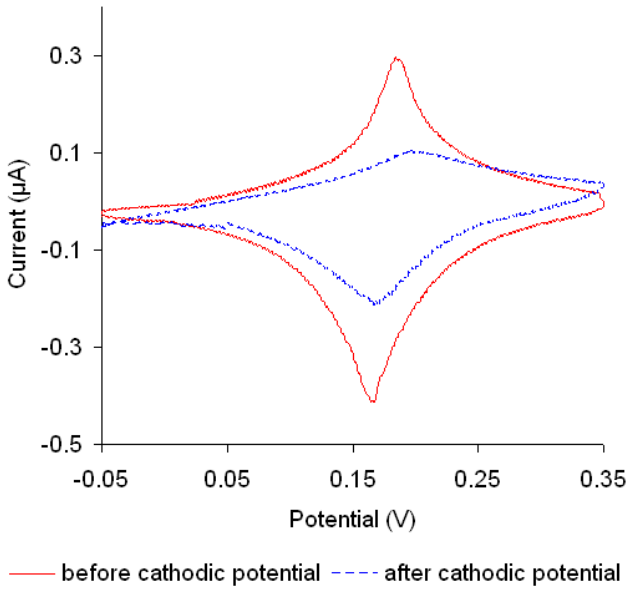

Figure 5.7: CV before and after cathodic potential of -50 mV/300 sec.; growing procedure: 8 cycles (vs. Ag/AgCl; 50 mV/s; 50 cycles; electrolyte: 0.1 M HCl/KCl)

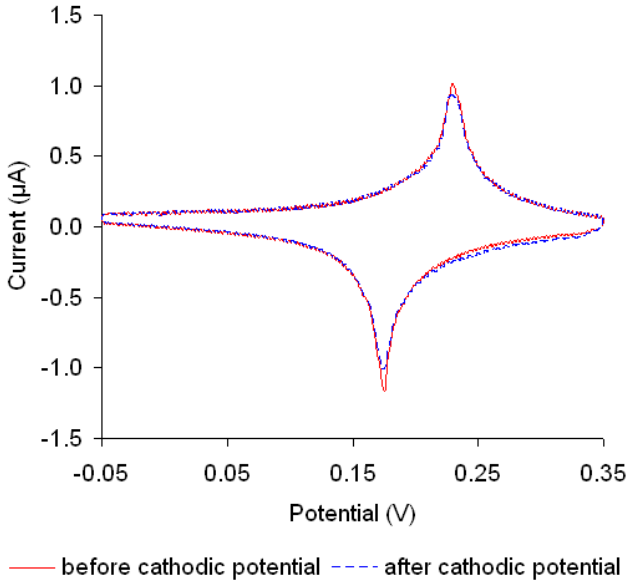

Figure 5.8: CV before and after cathodic potential of -50 mV/300 sec.; growing procedure: 12 cycles (vs. Ag/AgCl; 50 mV/s; 50 cycles; electrolyte: 0.1 M HCl/KCl)

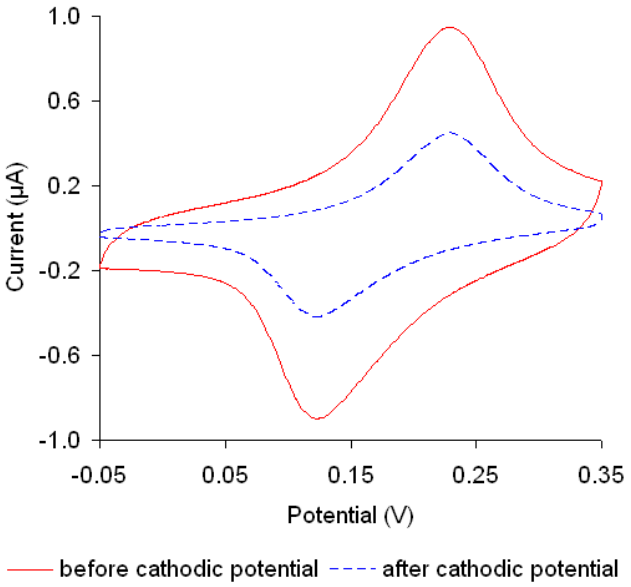

Figure 5.9: CV before and after cathodic potential of -50 mV/300 sec.; growing procedure: 16 cycles (vs. Ag/AgCl; 50 mV/s; 50 cycles; electrolyte: 0.1 M HCl/KCl)

et al. (1999)], showed a reduced current output for all of the PB modified electrodes regardless of the number of growing cycles. However, the cathodic peak current showed a decrease of 13 % for 12 growing cycles and about 50 % decay for 8 and 16 cycles. The anodic potential (redox state of PB) showed with 7 % for 12 growing cycles and for those with 8 and 16 cycles of $>$ 50 % decrease a similar trend. The reduced current output, hence reduced electroactivity of PB strongly suggests a loss of the inorganic polycrystal from the electrode surface. However, the electrode with 12 growing cycles showed a much enhanced stability compared to those with 8 and 16 growing cycles. Curulli *et al.* (2004) reported on 40 % loss of electroactivity after 3 days cycling of PB modified Pt electrodes for 3 consecutive cycles each day and a complete loss of activity after 7 days. In analogy work with glassy carbon electrodes, Karyakin *et al.* (1999) found no loss of peak-to-peak current after prolonged stability testing. However, the experimental conditions varied and a comparison is difficult to make.

ΔE_p was found to be 60 mV with 12 growing cycles and showed no changes before and after stability testing. However, ΔE_p for 8 and 16 growing cycles was found to be shifted by 20 mV after exposure to aging conditions. These changes in peak potential indicates that the electrochemical redox interconversion of PB and PW is not completely reversible, thus representing a deviation of the Nernstian behaviour. In the literature [Curulli *et al.* (2004), de Mattos *et al.* (2003), Pan *et al.* (2004)] PB modified platinum

Cycles	$I_p^a(\%)$	$E_p^a(mV)$	$I_p^c(\%)$	$E_p^c(mV)$	$\Delta E_p(mV)$
before exposure to -50 mV					
8	100	180	100	170	10
12	100	230	100	170	60
16	100	230	100	120	110
after exposure to -50 mV					
8	35	200	52	170	30
12	93	230	87	170	60
16	47	210	47	120	90

Table 5.2: Relative peak current (I_p^a (%)), peak potential (E_p^a (mV)) and voltage separation (ΔE_p (mV)) taken from CVs before and after exposure to cathodic potential

		8 cycles	12 cycles	16 cycles
Surface Coverage, Γ	PB	0.75	2.03	3.55
(nmol/cm^2)	PW	1.17	1.75	1.98
Ratio	PB/PW	0.6	1.2	1.8

Table 5.3: Estimation of surface coverage (Γ) of PB and PW on Pt electrodes after exposure to cathodic potential

electrodes were reported to exhibit a peak separation between 30 and 70 mV. In this study it was found that with increasing growing cycles, hence increasing thickness of the PB film, ΔE_p showed an increase (Table 5.2). This was also observed by Haghighi *et al.* (2004), in which increased peak separation was thought to be caused by high impedance.

Table 5.3 shows estimated surface coverage for PB with varied growing cycles. The estimations were calculated by integrating the area of the cathodic and anodic waves of the CVs after exposure to aging conditions. The calculations assumed a transfer of four electrons per unit cell of PB $Fe_4\,[Fe\,(CN)_6]_3 \times 12\ H_2O$ [Karyakin (2001)].

Presuming a uniform distribution of the deposited PB, the film thickness could be estimated to be 0.051 μm (8 growing cycles), 0.137 μm (12 growing cycles) and 0.241 μm (16 growing cycles) by using surface coverage values of Table 5.3 and Equation 3.7 of Chapter 3. The estimated surface coverage of PB and PW on Pt electrodes, as shown in Table 5.3, increased as expected with increasing growing cycles. The values for PB coverage reported in the literature for Pt screen printed electrodes were 2-16 nmol/cm^2 [de Mattos *et al.* (2003)] and for glassy carbon electrodes about 6 nmol/cm^2 [Karyakin *et al.* (1999)], depending on the depositing procedure. However, de Mattos *et al.* (2003) found that with a higher surface coverage the voltage separation was too high, indicating a less reversible redox reaction of PB/PW. This was in agreement with what was found in this study, in which the least effective electrochemical interconversion of PB and PW

was found with the highest surface coverage. Table 5.3 also shows the surface coverage ratio of PB to PW. The value for this ratio is most favourable for 12 growing cycles as it is closest to one.

The results with stability testing in this section showed that overall, PB electrodeposition procedure with 12 growing cycles is the most suitable for Pt electrodes. Therefore, the electrodes with 16 and 8 growing cycles are disregarded from all further experiments.

In Figure 5.10, a photographic image of PB electrochemically deposited on electrode surface is illustrated. Some of the PB film was scraped off for better visibility of the PB modified and non-modified electrode surface. The image shows the typical blue colouration of PB, verifying that the electrochemical depositing method resulted in an actual coating. Figure 5.11 illustrates a scanning electron micrograph of PB deposited on a Pt surface beneath a polymer coating. The polymer surface was carefully incised before the image was taken; a tightly packed clustering of the PB layer is clearly visible.

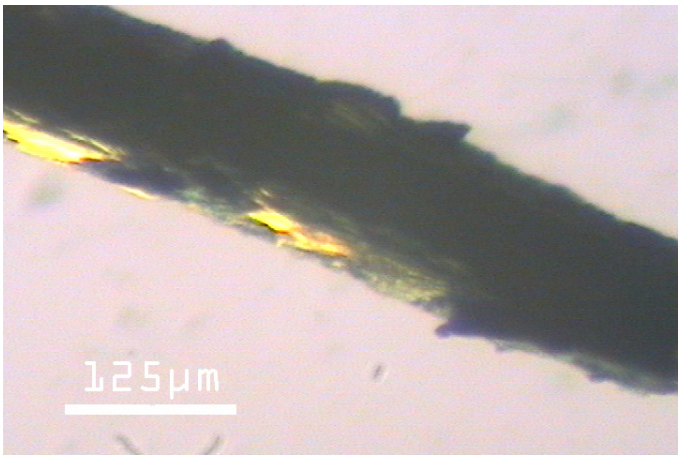

Figure 5.10: Photographic image of PB modified electrode surface

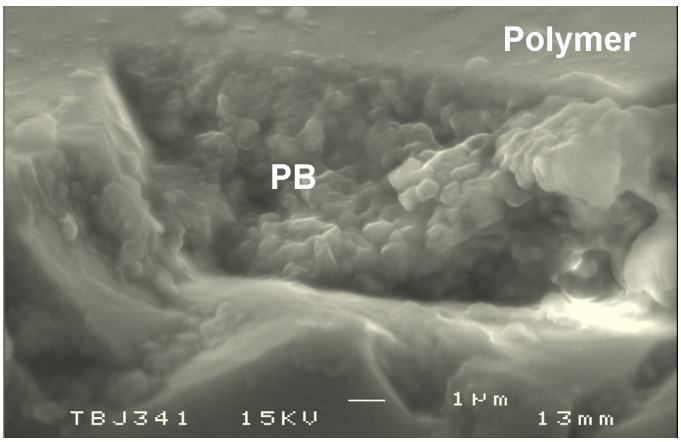

Figure 5.11: SEM of PB layer beneath polymer coating

5.3.5 Influence of the Solution pH on Stability

A stable response of PB in alkaline solutions has been reported, considering appropriate deposition methods [Karyakin *et al.* (1999)]. However, low stability of PB on platinum was found [Curulli *et al.* (2004), Garjonyte *et al.* (1999)] opposed to glassy carbon and gold for substrate [de Mattos *et al.* (2003), Ricci *et al.* (2005)]. In this section, PB modified platinum electrodes with improved depositing method were evaluated regarding their stability using buffer solutions with various pH values, 3, 7.4 and 11. The electrochemical response was related before and after exposure to aging conditions.

The CVs of PB modified electrodes at different pH values before and after exposure to cathodic potential are illustrated in Figures 5.12 to 5.14. The shape of the peaks at pH 3 (Figure 5.12) and at pH 7.4 (Figure 5.13) showed no significant changes. However, the shape of the peaks before and after stability testing at pH 11 (Figure 5.14) changed significantly, being much broader especially in the anodic range. This phenomenon can be associated with hydroxide ions being responsible for the cleavage of the PB complex due to the formation of ferric hydroxide. This was also found by other reserachers [Haghighi *et al.* (2004), Ricci *et al.* (2005), Karyakin *et al.* (1999)] and referred to as non-Faradaic degradation processes; as illustrated in Chapter 2, Equation 2.2.

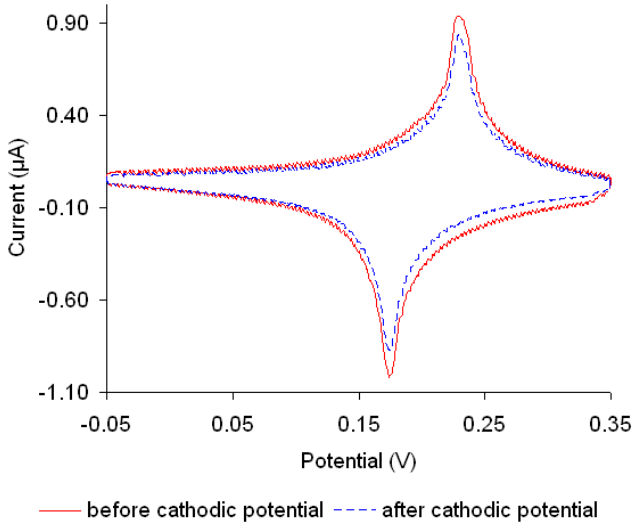

Figure 5.12: CV of PB modified Pt electrodes in phosphate buffer pH 3 before and after submission to cathodic potential (vs. Ag/AgCl; 50 mV/s; 50 cycles; electrolyte: 0.1 M HCl/KCl)

These scans indicate that the best stability of PB was obtained at pH 3 and the lowest stability was observed at pH 11, which is in agreement with data reported in the

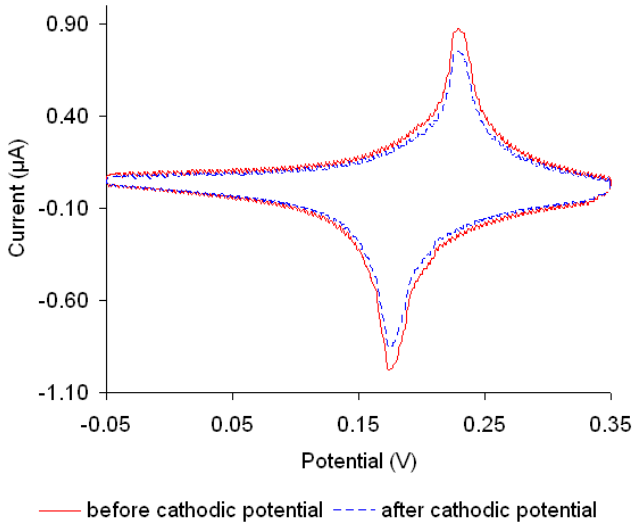

Figure 5.13: CV of PB modified Pt electrodes in phosphate buffer pH 7.4 before and after submission to cathodic potential (vs. Ag/AgCl; 50 mV/s; 50 cycles; electrolyte: 0.1 M HCl/KCl)

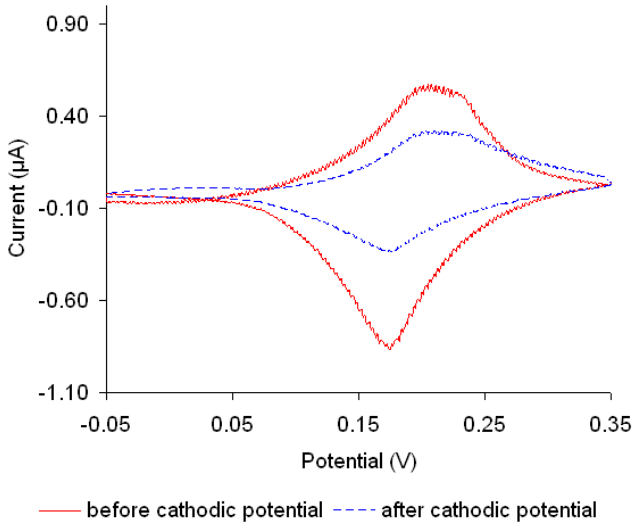

Figure 5.14: CV of PB modified Pt electrodes in phosphate buffer pH 11 before and after submission to cathodic potential (vs. Ag/AgCl; 50 mV/s; 50 cycles; electrolyte: 0.1 M HCl/KCl)

	$I_p^a(\%)$	$E_p^a(mV)$	$I_p^c(\%)$	$E_p^c(mV)$	$\Delta E_p(mV)$
before exposure to -50 mV					
after activation	100	230	100	170	60
pH 3	93	230	91	170	60
pH 7.4	87	230	87	170	60
pH 11	57	200	77	170	30
after exposure to -50 mV					
after activation	93	230	87	170	60
pH 3	83	230	78	170	60
pH 7.4	75	230	77	170	60
pH 11	32	210	30	170	40

Table 5.4: Relative peak current (I_p^a (%)), peak potential (E_p^a (mV)) and voltage separation (ΔE_p (mV)) taken from CVs at different pH values before and after exposure to cathodic potential

literature [Chaubey *et al.* (2002), Karyakin (2001), Ricci *et al.* (2005)]. However, redox peaks are formed at pH 11, showing that there was still sufficient electroactivity present.

Relative peak currents (I_p) along with peak potentials (E_p) including peak separations (ΔE_p) were determined from CVs shown in Figures 5.12 to 5.14 and are tabulated in Table 5.4. In acidic buffer, the peak current declined by 7 % in the anodic range and by 9 % in the cathodic range before exposure to cathodic potential. After exposure to the cathodic potential, the current declined a further 10 % in the anodic range and a further 13 % in cathodic range. In neutral buffer, the current declined by 13 % in both cathodic and anodic ranges before exposure to cathodic potential. After exposure to cathodic potential, the current declined a further 12 % in the anodic range and 10 % in the cathodic range. In strong alkaline buffer, the peak current overall is much smaller, declining by 43 % in the anodic range and 23 % in the cathodic range. After exposure to cathodic potential, the peak currents declined a further 25 % in the anodic range and a further 47 % in the cathodic range. Also, the peak potential in the anodic range shifted from 230 mV to 200 mV before exposure to cathodic potential and to 210 mV after cathodic potential.

After exposure of the PB modified electrodes to the accelerated degradative conditions (-50 mV), a loss of PB from the electrode surface was observed for all electrodes. This was noticed as decreased peak currents in the CVs taken after stability testing (Table 5.4). However, after the initial loss of peak current in neutral and acidic buffer solutions within the first 10 cycles, no decrease in peak currents was observed while cycling from 10 to 50 times in the range of -0.05 to +0.35 V versus Ag/AgCl at a sweep rate of 50 mV/s.

Overall, good operational stability in neutral pH was demonstrated in this work, which

was in contrast to work conducted by Curulli *et al.* (2004), in which very low stability of PB modified Pt electrodes was reported. De Mattos *et al.* (2003) also reported poor performance of PB modified platinum electrodes in comparison with PB modified gold electrodes. The greatly improved stability of PB electrodes in this study is due to the use of a more appropriate depositing method. However, the entire omission of a drying step followed by the storage of PB modified electrodes in pH 7 buffer (as Curulli *et al.* (2004)) and scarce cleaning procedures of the electrode surface (as de Mattos *et al.* (2003)) had a large impact on their poor results.

In this study, the electrode tip was subjected not only to polishing and ultrasonic rinsing, but also to electrochemical cleaning. Many low-molecular-weight substances are known to be specifically absorbed on platinum electrodes [Karyakin *et al.* (1995)]. Hence the removal of impurities on the surface of the working electrode is seen as vital prior to PB deposition and it is thought to aid in the formation of a more compact and stable PB layer formation. Also, the active surface area for PB deposition will be at its maximum. The principal improvement of PB stability reflected in obtained results may not only be due to the depositioning method as such, but also due to the use of a not previously reported additional drying stage between growing and activation procedure in addition to a final drying stage after activation of PB.

5.4 Summary

- The needle-type electrodes demonstrated electrochemical responses consistent with theory.
- Electrodes displayed microelectrode behaviour, despite their relatively large size of working electrode.
- The optimised Prussian Blue depositing method developed in this study resulted in a stable Prussian Blue film on platinum working electrodes.
- Prussian Blue showed excellent stability in acidic and neutral aqueous media.

Chapter 6

Amperometric Analyte Detection

6.1 Introduction

Chapter 4 described the successful synthesis, modification and characterisation of a range of polymers whereas Chapter 5 detailed the characterisation and PB modification of needle-type Pt electrodes. This Chapter now pulls together the work of Chapters 4 and 5 to facilitate a key project objective of performing effective polymer modification for use on delicate sensing devices. This was attempted in two ways. The first approach was to surface modify polyurethane already placed on the electrode, an activity that does not readily appear in the literature. The second approach was to bulk modify silicone rubber to achieve novel H_2O_2-permeable polymers.

Surface deposition of proteins is a particular problem with electrochemical sensors, reducing their sensitivity and possibly rendering the sensor redundant. Furthermore, analyte selectivity has to be ensured, since other electroactive species present in biological samples will give additional current responses.

In this Chapter, the analytical performance of polymer coated needle-type Pt electrodes in electrochemical sensing applications were assessed for their analyte responses to O_2 and H_2O_2, which are potential biological assay targets, using steady state amperometry.

6.2 Electrochemical Response to H_2O_2

In this section, the effect of the current responses in phosphate buffer (non-activated) and in phosphate buffer with 1 mM H_2O_2 (activated) for non-PB modified and PB modified needle-type electrodes were investigated. CVs at bare Pt (Figure 6.1(a)) and PB modified Pt electrodes (Figure 6.1(b)) are illustrated.

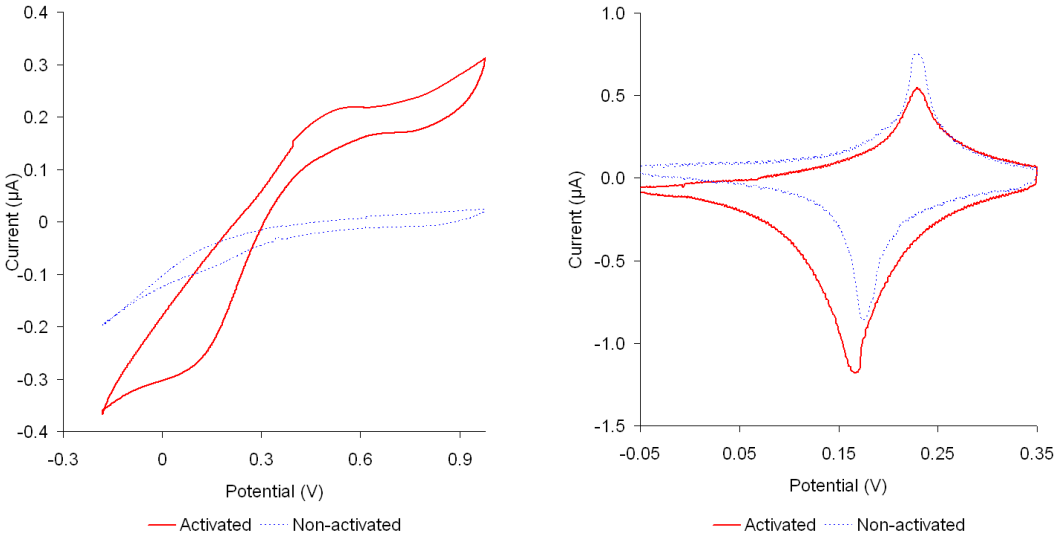

(a) (b)

Figure 6.1: CVs of (a) non-PB modified and (b) PB modified Pt electrode; both activated (with 1 mM H_2O_2) and non-activated (buffer only); (vs. Ag/AgCl; 50 mV/s; electrolyte: 0.1 M KCl, pH 7.4)

From Figure 6.1(a) it can be seen that the response current of non-PB modified electrodes in activated buffer shows a steep rise in current with increased potential and appeared to have reached a plateau starting at approximately +0.5 V up to around +0.7 V, before rising up again. The current response in non-activated buffer in comparison showed only a limited rise in current with increasing potential. Furthermore, it can also be seen that the current responses in both non-activated and activated buffer intersect at approximately +0.2 V.

The same CV profile at Pt electrodes was found by Pan *et al.* (2004), however, a plateau was reached from +0.5 V up to +1.1 V and at the potential of +0.26 V the current responses in both activated and non-activated buffer intersect, which was taken as an indication of the lowest potential H_2O_2 could be detected with their electrode system. This would mean that for non-PB modified Pt electrodes in this study, the detection potential for H_2O_2 would start at +0.2 V or higher.

The CVs in Figure 6.1(b) of PB modified electrodes showed the typical peak profile of a reversible redox interconversion of PB and PW in both, activated and non-activated buffer solutions. The cathodic peak current in activated buffer solution increased by 37 % and the anodic peak current decreased by 28 % in relation to those in the non-activated buffer. The increased current in the cathodic region is due to the promoting effect of PB on the catalytic reduction of H_2O_2. In comparison, de Mattos *et al.* (2003) found at Pt electrodes an increased cathodic peak current of only 10 % but a decreased anodic peak current of 30 %. A high anodic current decrease concomitant with a low cathodic current increase is a strong indication of PB decomposition due to Faradaic processes caused by OH^- formed during electrochemical H_2O_2 reduction (see Equations 2.2 and 2.4). A reduced electroactivity of PB is then apparent with decreased peak current output as seen with thouse obtained by de Mattos *et al.* (2003). The high increases in anodic peak current obtained in this study shows that a stable compact PB layer was obtained with improved and optimised deposition procedure.

It was further noted that in the presence of H_2O_2, the redox wave moved more towards negative potentials. However, the peak separation was with 60 mV the same in the absence or presence of H_2O_2. This is further evidence that a reversible redox reaction took place, hence that a fast electron transfer occured due out H_2O_2 reduction.

6.3 Influence of Detection Potential on Analyte Response

The choice of the applied potential at the working electrode is fundamental not only to achieve the lowest detection limit possible, but also to keep the analyte response of electrochemical interfering species low. In this section, it is determined at which potential the highest current output occured with PB modified electrodes for H_2O_2 at varied concentrations. The applied potential ranges considered were -50 mV, 0 mV, +50 mV - the current responses are tabulated in Table 6.1.

H_2O_2 (mM)	-50 mV	0 mV	+50 mV
0.05	1.19	1.60	0.98
0.2	5.04	5.95	3.25
1	17.94	20.09	12.49
10	89.39	105.39	80.30

Table 6.1: Current responses of PB modified electrodes to H_2O_2 at various analyte concentrations to three different applied potentials (vs. Ag/AgCl; electrolyte: 0.1 M KCl, pH 7.4)

The highest current output was determined with an applied zero potential, as shown in Table 6.1. This is in agreement with data reported by Garjonyte *et al.* (1999) and Curulli *et al.* (2004), both of whom also used Pt electrodes. However, the completely reduced state of Prussian Blue, Prussian White (PW), has been reported [Karyakin *et al.* (1995), (1999)] to not only reduce H_2O_2, but also oxygen which was thought to increase the background noise. In which case, it was recommended to operate at anodic electrode potential of e.g. +50 or +180 mV for H_2O_2 oxidation. Nevertheless, Karyakin *et al.* (1995), (1999) further found that PB can selectively catalyse the electroreduction of H_2O_2 even in the presence of molecular oxygen over a certain potential range.

With the Pt electrodes used in this study, parasitic electrical noise in the presence of molecular oxygen was not found to be of concern as there was no significant difference found in current output between de-oxygenated and oxygen containing analyte solutions. Therefore, the analyte detection for H_2O_2 with PB modified electrodes due out this study was conducted with 0 V without de-oxygenated solutions.

6.4 Amperometric Detection of H_2O_2

Polymers which were synthesised in Chapter 4 solely for the purpose of amperometric analyte detection were now evaluated regarding their performance in prolonged measurements. These polymers act not only as a diffusion barrier for tailoring the linear range and sensitivity towards the target analyte, but also as a protective layer to prevent electrode passivation [Wisniewski *et al.* (2000)] and to keep PB in place [Karyakin *et al.* (1999)].

H_2O_2 can diffuse to the PB layer through the polymer matrix, oxidising PW to form PB. In the negative potential range, PB is again reduced to its reduction state (PW) via electron exchange with the Pt electrode, forming another reaction loop. These reaction loops are connected as illustrated in Equation 2.3 The determination of H_2O_2 in this single sensing element is carried out amperometrically by measuring the current of the reduction of H_2O_2 catalysed by PB clusters. A densely packed ultra thin PB layer is essential to guarantee a stable electrochemical response and a rapid electron exchange. In this section, the performance of PB modified electrodes in H_2O_2 detection was monitored (Figures 6.2, 6.3, 6.4) and compared to that of non-PB modified electrodes (Figures 6.5, 6.6, 6.7). For reference purposes, electrodes without polymer coatings were also shown.

The electrochemical response of uncoated Pt electrodes to H_2O_2, for both PB modified and non-PB modified electrodes, exhibit a steeper slope than the response of any

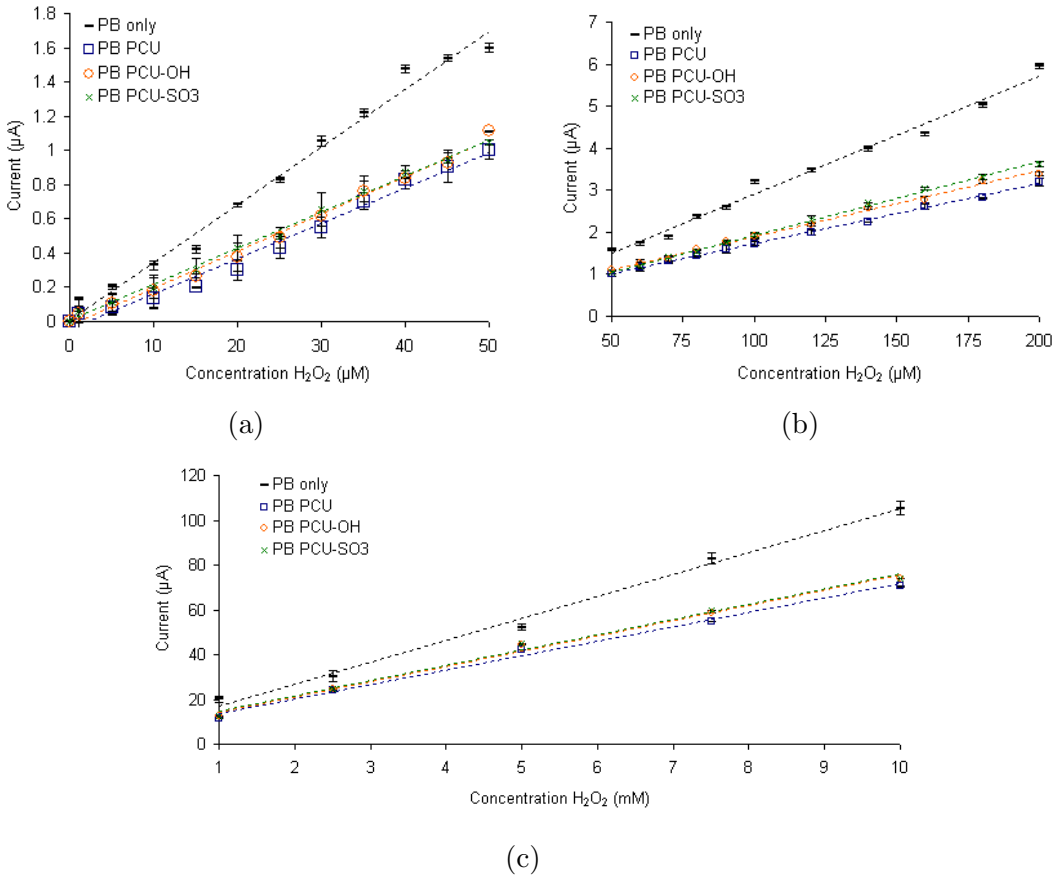

Figure 6.2: Graph to show linear ranges of PB modified electrodes, coated with PCU, PCU-OH and PCU-SO_3 towards H_2O_2 at concentration ranges of 0-50 μM, 50-200 μM and 1-10 mM respectively; (vs. Ag/AgCl; electrolyte: 0.1 M KCl; pH 7.4)

type of polymer coated electrodes. This was expected as there was no diffusion barrier present and the analyte can therefore diffuse freely to the electrode surface. However, electrodes without a diffusion barrier are prone to passivation due to adsorptive and adhesive interactions of molecules at the electrode surface. This would then suppress their electrochemical activity due to the reduced availability of reaction sites [Karyakin *et al.* (1995), Wisniewski *et al.* (2000)].

Various researchers [de Mattos *et al.* (2000), Pan *et al.* (2004)] found that polymer coated PB modified electrodes showed a lower sensitivity profile compared to those without a polymer coating. This was explained by the shielding effect these polymers provide not only for the target analyte, but also to the electrochemistry of PB. The electroactivity of PB is not only dependent on the electron transfer rate between the electrode and PB, but also on the transfer of counter cations needed which take an active part in the reversible redox interconvertion of PB and PW (Equation 2.3).

PEU coated electrodes showed an overall lower analyte response compared to PCU

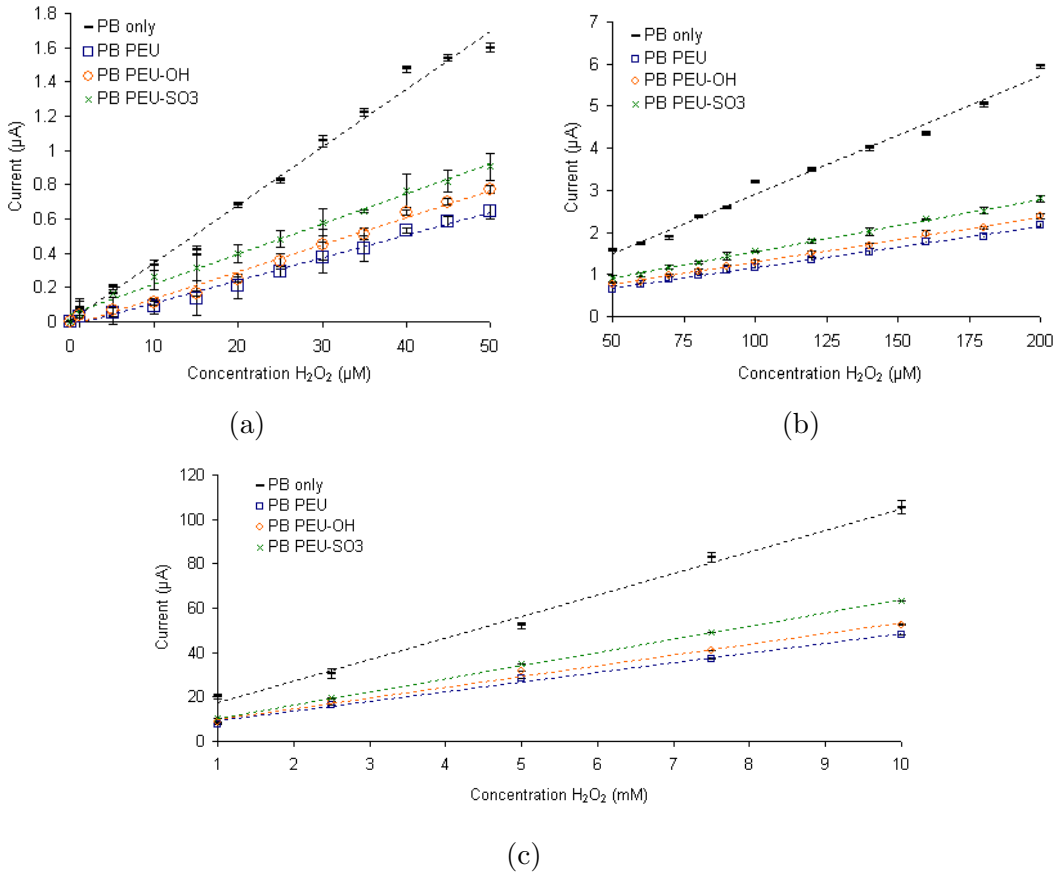

Figure 6.3: Graph to show linear ranges of PB modified electrodes, coated with PEU, PEU-OH and PEU-SO_3 towards H_2O_2 at concentration ranges of 0-50 μM, 50-200 μM and 1-10 mM respectively; (vs. Ag/AgCl; electrolyte: 0.1 M KCl; pH 7.4)

coated electrodes. It was further noted that the analyte response for PU with ether moieties in their soft segment showed an increase in the order PEU > PEU-OH > PEU-SO_3 and that with carbonate moieties was PCU > PCU-OH > PCU-SO_3. This trend was seen irrespective of whether they were PB modified or not, however, it was more apparent with PB modified electrodes. The modification of SR as outlined in Section 3.3.1 was successful regarding to H_2O_2 permeability as seen with analyte responses illustrated in Figures 6.2, 6.3, 6.4 and 6.5, 6.6, 6.7; unmodified SR showed no current response to H_2O_2. However, the current responses of electrodes coated with modified SR was the lowest of any polymer coated electrodes, specifically in the concentration range up to 200 μM. When compared over the entire 0-200 μM concentration range, the electrochemical response to H_2O_2 showed the highest current response up to 50 μM. The only one out was PB modified electrodes coated with SR in which the current response showed a moderate current increase to H_2O_2 of up to 50 μM, then between 50-200 μM the current response showed a higher slope. However, R^2 was > 0.99 for all electrode types in the

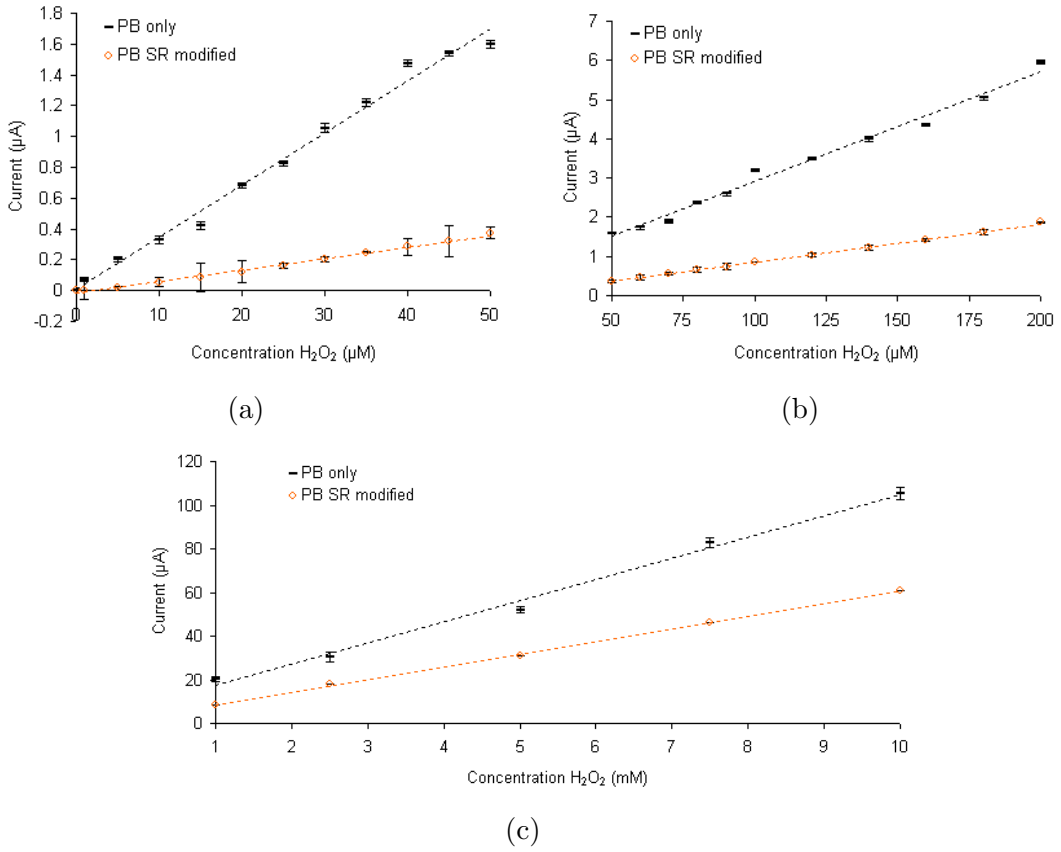

Figure 6.4: Graph to show linear ranges of PB modified electrodes, coated with SR modified towards H_2O_2 at concentration ranges of 0-50 μM, 50-200 μM and 1-10 mM respectively; (vs. Ag/AgCl; electrolyte: 0.1 M KCl; pH 7.4)

concentration range between 0 and 200 μM and that between 1-10 μM.

Furthermore, a relative decrease in current responses with H_2O_2 concentrations between 1-10 μM was observed, which was more apparent with non-PB modified Pt electrodes. A pronounced decrease of current response on bare Pt electrodes with H_2O_2 concentrations above 1 mM was also found by Zhang *et al.* (1993), which was thought to be caused by analyte saturation at the electrode surface. Various studies have been undertaken investigating a possible reaction mechanism for the electrochemical oxidation of H_2O_2 on Pt electrodes over the past decades. Hickling *et al.* (1951) found that oxidation of H_2O_2 is favoured on oxidised Pt surfaces and therefore it was assumed that platinum will be re-oxidised to platinum oxides after the oxide film was reduced by H_2O_2. The formation of an oxide film on Pt surfaces was demonstrated by Johnston *et al.* (1995), which led to the identification of the Pt binding site for H_2O_2 as being $Pt(OH)_2$ [Hall *et*

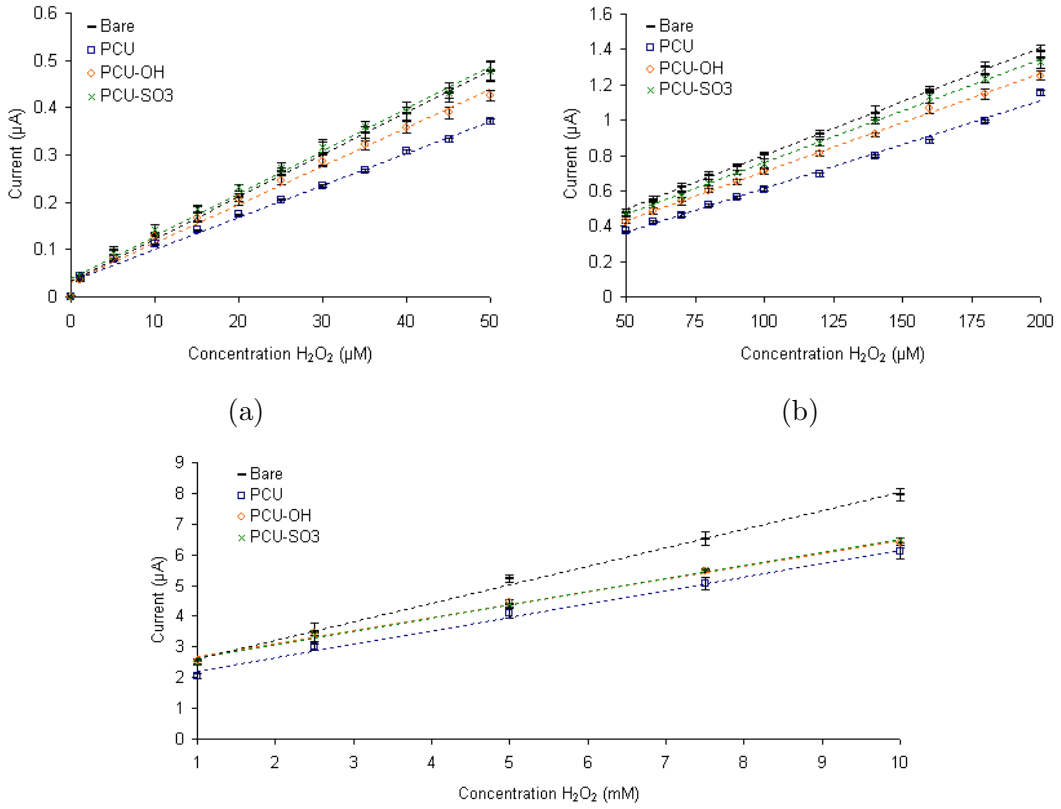

Figure 6.5: Graph to show linear ranges of non-PB modified electrodes, coated with PCU, PCU-OH and PCU-SO_3 towards H_2O_2 at concentration ranges of 0-50 μM, 50-200 μM and 1-10 mM respectively; (vs. Ag/AgCl; electrolyte: 0.1 M KCl; pH 7.4)

al. (1998a)], according to the following reaction mechanism:

$$H_2O_2 + Pt(OH) \rightleftharpoons Pt(OH)_2 \cdot H_2O_2 \rightarrow Pt + 2H_2O + O_2$$
$$Pt + 2H_2O \rightarrow Pt(OH)_2 + 2H^+ + 2e^-$$

However, during H_2O_2 oxidation on Pt electrodes two inhibiting binding modes which occur at the electrode surface were outlined. The first was a competitive binding of O_2 onto the Pt(II) binding site with the formation of a Pt oxide complex, described by

$$Pt(OH)_2 + O_2 \rightleftharpoons Pt(OH)_2 \cdot O_2$$

while the second was that of reversible protonation of the adsorbed Pt(II)/H_2O_2 complex,

$$Pt(OH)_2 \cdot H_2O_2 + H \rightleftharpoons Pt(OH)_2 \cdot H_2O_2 \cdot H^+$$

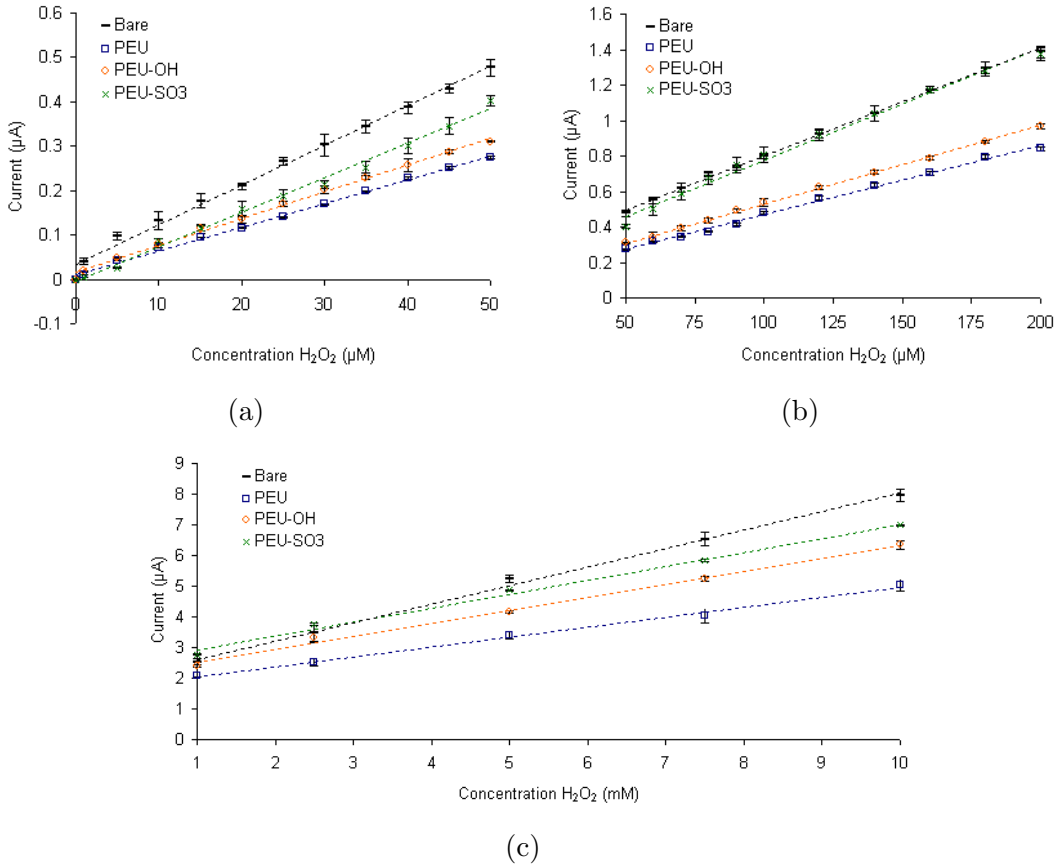

Figure 6.6: Graph to show linear ranges of non-PB modified electrodes, coated with PEU, PEU-OH and PEU-SO_3 towards H_2O_2 at concentration ranges of 0-50 μM, 50-200 μM and 1-10 mM respectively; (vs. Ag/AgCl; electrolyte: 0.1 M KCl; pH 7.4)

Hence, the availability of Pt surface sites is the determining factor on the reaction kinetics. Slow electron transfer might impose kinetic control on the overall reaction process so that the current is no longer proportional to the bulk analyte concentration. This can be seen in this study with a non-linear current response in the concentration range above 1 mM.

However, analyte diffusion across the polymer matrix is not inconsequential in amperometric analtye detection and the chemical properties of the PUs used in this study are to be considered. Yang *et al.* (1999) reported on the inherently lower chain mobility of carbonate soft segments due to their steric structure compared to the ether soft segments with their tighter packing within the polymer matrix. This may suggest that when these polymers are used in amperometric analyte detection, the target analyte would diffuse more readily across PU with carbonate moieties in their soft segments compared to ether moieties. This was confirmed with the findings in this study.

However, because PU used in this study have undergone phase inversion process, the

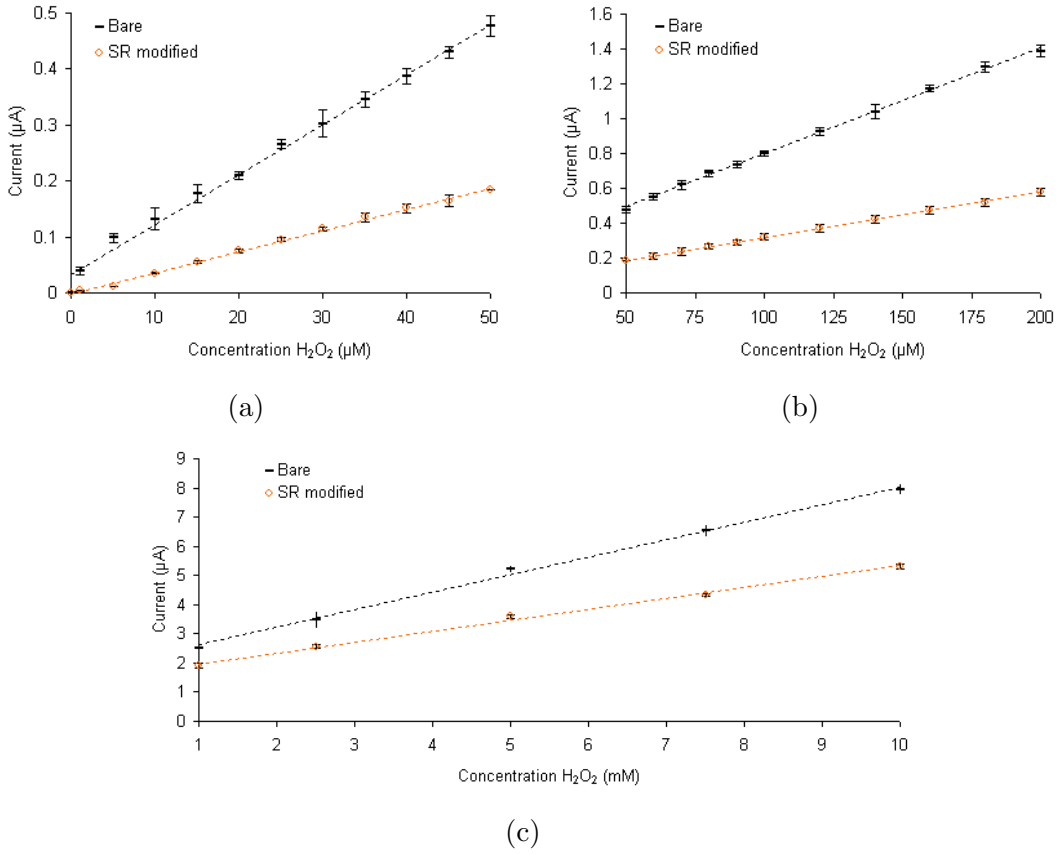

Figure 6.7: Graph to show linear ranges of non-PB modified electrodes, coated with SR modified towards H_2O_2 at concentration ranges of 0-50 μM, 50-200 μM and 1-10 mM respectively; (vs. Ag/AgCl; electrolyte: 0.1 M KCl; pH 7.4)

intermolecular bonding of the hard and soft segments in each PU requires a more detailed examination. For the hard segments, hydrogenated MDI is an aliphatic molecule and may have multiple conformations. These differing conformations may sterically hinder the process of hydrogen bonding between the H_{12}MDI segments, resulting in microdomains which are less well ordered and those with MDI hard segments are in comparison more tightly packed. This may then suggest that the target analyte is able to diffuse more readily across H_{12}MDI segments (PEU), although this was not observed in this study.

Therefore, in addition, the ability of hydrogen bonding between hard and soft segments has to be considered. In PEU, hydrogen bonding mainly occurs between the hard segments and in PCU, hydrogen bonding may occur between hard and soft segments as well as between hard segments. Considering the steric structure of the carbonate soft segment and the intermolecular connection between the the hard and soft segments in each PU, this would suggest a tighter intermolecular packing within PEU resulting in less permeability of the target analyte. Therefore, the intermolecular connection between

hard and soft segments is hypothesised to be the dominating factor for a reduced analyte diffusion across the polymer matrix with PEU seen in this study with reduced current responses compared to thouse of PCU (Figures 6.2, 6.3, 6.4 and 6.5, 6.6, 6.7).

Table 6.2 and Table 6.3 illustrate the performance calculations for PB modified and non-PB modified electrodes respectively. These tables show that the limit of detection (LOD) of PB modified electrodes is approximately one order of magnitude lower than that of electrodes without PB. Data of PB modified electrodes reported in the literature [Ricci *et al.* (2005)] for LOD ranges from 0.1 to 5 μM. One of the highest sensitivity for PB modified Pt electrodes was reported to be 1000 mA/(M cm^2) in the concentration range between 5-50 μM H_2O_2 [De Mattos *et al.* (2003)] and one of the lowest sensitivity with PB modified Pt electrodes was reported with 0.21 mA/(M cm^2) for up to 9 mM H_2O_2 [Garjonyte *et al.* (1999)]. However, the current responses in both studies were reported to be non-linear.

In comparison, sensitivities of PB modified glassy carbon electrodes were reported by various researcher to be between 188 and 1000 mA/(M cm^2) [Ricci *et al.* (2005)]. The wide range of reported results are mainly depending on the substrate used (carbon, platinum, gold), the depositing method (galvanostatic, electrochemical cycling, chemical) and the procedure of analyte measurement (flow injection, rotating, non-stirred). It is further noted that the response time (T_r) is generally lower for PB modified electrodes compared to unmodified electrodes. This was thought to be due to the oxide layer formed on Pt surfaces during H_2O_2 oxidation [Hall *et al.* (1998a) and (1998b)].

Surprisingly the reproducibility (RSD) of a batch of electrodes (n = 5) appeared to have improved with PB modified electrodes, except for PCU-OH which was 6 % higher and for PEU which remained unchanged. The RSD of the individual electrodes are in accordance to what was found in the literature [Ricci *et al.* (2003) and (2005)].

	Sensitivity (mA/(M cm^2))	T_r (sec)	LOD (μM)	RSD_5 (%)	RSD_1 (%)
PB only	148.92	31	0.3	9	3
PB PCU	90.81	12	0.3	7	2
PB PCU-OH	94.94	15	0.1	17	3
PB PCU-SO_3	92.84	11	0.1	15	3
PB PEU	57.83	16	0.2	16	3
PB PEU-OH	69.40	15	0.2	10	4
PB PEU-SO_3	76.84	16	0.1	8	2
PB SR mod.	32.88	34	0.2	13	4

Table 6.2: Performance characteristics of PB modified electrodes in amperometric H_2O_2 detection; calculated from calibration curves in the concentration range of 0-50 μM; with T_r = response time, LOD = limit of detection, RSD_5 = reproducibility using 5 individual electrodes, RSD_1 = reliability using the same electrode)

	Sensitivity (mA/(M cm^2))	T_r (sec)	LOD (μM)	RSD_5 (%)	RSD_1 (%)
Bare	39.42	50	3	18	5
PCU	29.94	15	2	11	3
PCU-OH	35.82	13	1	11	2
PCU-SO_3	39.57	12	2	17	3
PEU	23.76	22	1	16	3
PEU-OH	26.81	20	1	12	2
PEU-SO_3	34.15	21	1	14	3
SR mod.	16.62	40	2	15	3

Table 6.3: Performance characteristics of non-PB modified electrodes in amperometric H_2O_2 detection; calculated from calibration curves in the concentration range of 0-50 μM; with T_r = response time, LOD = limit of detection, RSD_5 = reproducibility using 5 individual electrodes, RSD_1 = reliability using the same electrode)

Overall, the results in this section showed that PB modified Pt electrodes produced a much higher stability and linearity during analyte detection in contrast to work conducted by other researchers using Pt as substrate. The current output was three times higher than that of non-PB modified electrodes, making PB a suitable candidate for Pt as underlying material.

6.4.1 Long- and Short Term Stability

Long- and short term stability in H_2O_2 detection is a crucial point for the transition metal hexacyanoferrate electrodes. The product in H_2O_2 reduction on PB modified electrodes is OH^-, which was found to solubilise the electrocatalyst (PW) as illustrated in Equation 2.2. Restricted lifetime of PB at pH > 7 due to OH^- has also been reported, however, the results in Chapter 5 showed that these electrodes were stable at neutral

pH. Therefore, the stability of these modified electrodes were now assessed during catalytic action of PB towards H_2O_2 reduction. Operation stability (short term) is shown in Figure 6.8 while in Figure 6.9 storage stability (long term) is illustrated.

Operational Stability of PB Modified and Non-PB Modified Electrodes

The operational stability was assessed by placing the electrodes in 0.1 mM H_2O_2 solution with zero applied potential for PB modified electrodes and +650 mV for non-PB electrodes, both versus Ag/AgCl. The current responses were recorded for 24 hours continuously and the H_2O_2 solution was renewed three times within the assay.

PB modified electrodes without a protective polymer coating (Figure 6.8) showed a stable current response for the first hour followed by a slow and constant decay in current, dropping to 97 % of the initial current within the next 7 hours. After the H_2O_2 solution was renewed, the current response appeared to decline initially slightly more. This was observed after each renewal. After the 24 hour period, the current response had declined by a total of 4 %. This can be seen in Figure 6.8(a). A reason for the observed accelerated decline in current response after H_2O_2 renewal could be the initial higher amount of hydroxyl ions produced during electrocatalytic H_2O_2 reduction. The OH^- thus formed are responsible for the cleavage of the PB complex via the Faradaic processes, which results in the formation of ferric hydroxide as detailed in equation 2.2. Since the stability testing was undertaken in a buffer solution, the excess of OH^- ions should be neutralised by hydronium ions (H_3O^+) present in the buffer, preventing a further accelerated disintegration of PB. So, leakage of PB may have caused a decline of electroactive substance on the surface, which was then no longer available for catalytic H_2O_2 reduction.

Polymer coated PB modified electrodes behaved differently. The current response recovered after each renewal of the H_2O_2 solution. Occasionally this led to a response slightly higher than the initial value. Each of the polymer coated PB modified electrodes (regardless of type of coating) behaved in a very similar manner, averaging approximately only a 3 % decline in current output after the 24 hour period. This shows that the polymer coating does prevent the negative influence of hydroxide ions on PB modified electrodes, as suggested by Haghighi *et al.* (2004). This is further in accordance with results found by Curulli *et al.* (2004) and Lukachova *et al.* (2003) in which polymer coated PB modified electrodes were shown to improve stability in contrast to uncoated PB modified electrodes.

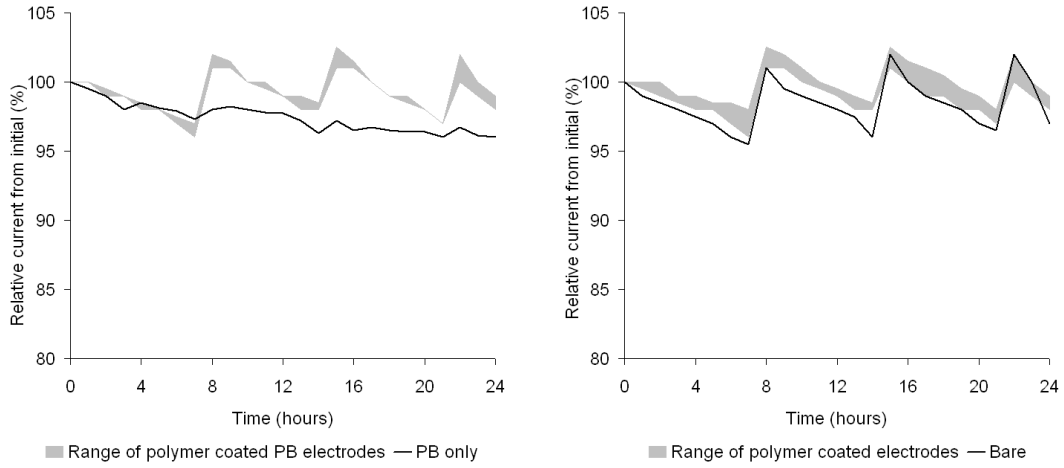

Figure 6.8: Average relative operational stability of a) PB modified electrodes and b) non-PB modified electrodes, both with and without polymer coatings towards H_2O_2 (vs. Ag/AgCl; electrolyte: 0.1 M KCl; pH 7.4)

In comparison, the operational stability of electrodes without PB modification towards H_2O_2 were measured and found to show a current stability similar to that of polymer coated PB modified electrodes - see Figure 6.8(b). This is further evidence that polymers play a significant role in the stabilisation of PB films. However, bare electrodes exhibited more varied current response overall, particularly after H_2O_2 solution was renewed.

Storage Stability of PB Modified and Non-PB Modified Electrodes

The storage stability was assessed by measuring the current responses of PB modified and non-PB modified electrodes in 0.1 mM H_2O_2 every 5 days for 6 months under the same conditions as those for operational stability.

Figure 6.9(a) shows the relative current output from initial in percentage of PB modified electrodes and polymer coated PB modified electrodes. PB modified electrodes without polymer coating (the average of three is shown by the line in Figure 6.9(a)) showed an average decrease of 13 % from the initial current value over the entire 6 months. The range of current values recorded for each of the polymer coated PB modified electrodes is indicated by the grey band in Figure 6.9(a). This range of values showed an average decrease of about 8-10 %. It was noticed that the current response did not decline monotonically; there seems to have been some recovery between measurements. In comparison, the electrodes without PB modifications (Figure 6.9(b)), coated or uncoated, showed an average decline of only 3-5 % in current. This current profile was the same as for PB

modified electrodes although the current changes were not as strongly pronounced.

Ricci *et al.* (2005) reported a 10 and 15 % decrease in current response for PB modified graphite screen printed electrodes after 24 and 48 hours of continuous measurement in 0.1 and 0.2 mM H_2O_2 solution respectively. After 100 hours of continued used, the decline in current response was reported to be about 12 %. Moreover, a recovery in the current response after renewal of the H_2O_2 solution was also seen.

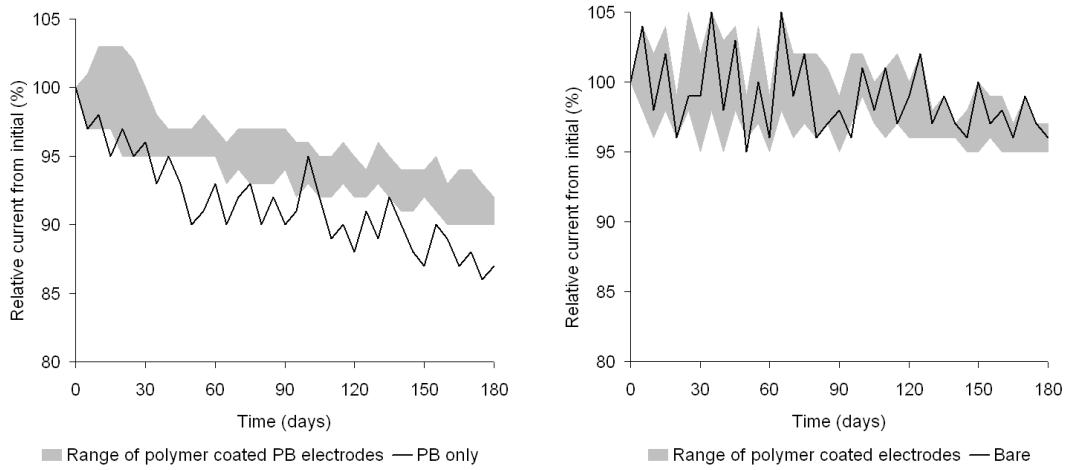

Figure 6.9: Average relative storage stability of a) PB modified electrodes and b) non-PB modified electrodes, both with and without polymer coatings towards H_2O_2; (vs. Ag/AgCl; electrolyte: 0.1 M KCl; pH 7.4)

6.4.2 Assessment of Analyte Selectivity

Amperometric sensors used at high anodic potential (> +0.6 V) in biological samples are usually subjected to interference by ascorbic acid, uric acid and acetaminophen. These reductants are oxidised at similar potentials, producing additional anodic currents hence reducing the selectivity of sensors. PB allows operation at lower potentials, which then would eliminate these parasitical current responses. Lukachova *et al.* (2003) found a minor response to uric acid and acetaminophen with PB modified glassy carbon electrodes at zero potential (versus Ag/AgCl), suggesting that through optimising the method for PB deposition it may be possible to synthesise an electrocatalyst completely selective to H_2O_2. However, ascorbic acid remained the main interferent. This section will now focus on the current responses of these interferents in relation to H_2O_2 and additionally on the current responses of interferents in the presence of H_2O_2.

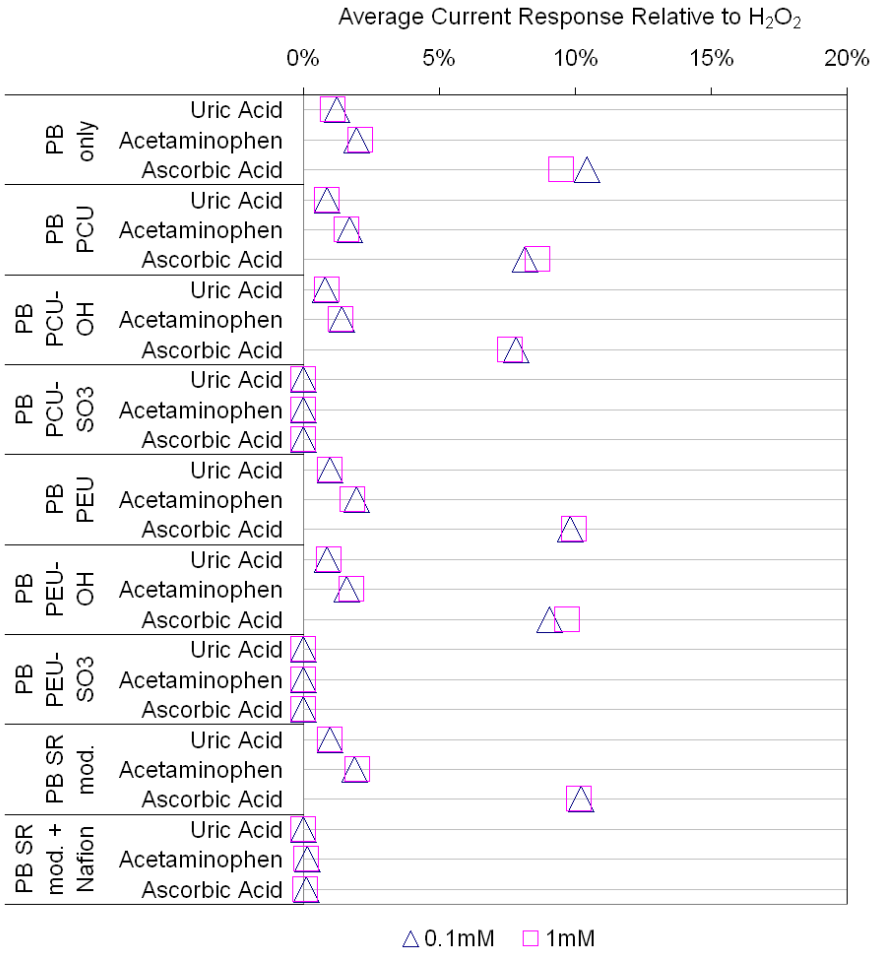

Figure 6.10: Average relative current responses of PB modified electrodes (PB only and polymer-coated) to interferents; expressed as a proportion of the current responses to H_2O_2 which is represented as 100 %. The concentrations of 0.1 mM and 1 mM were considered for both, H_2O_2 and interferents; (vs. Ag/AgCl; electrolyte: 0.1 M KCl; pH 7.4)

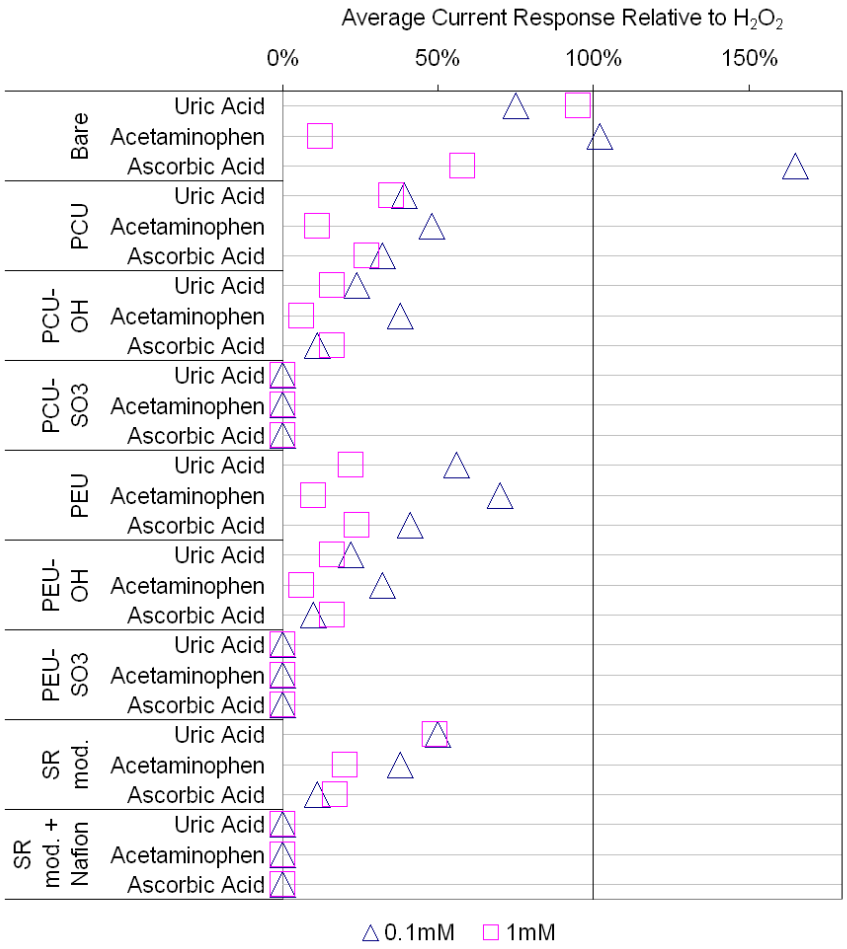

Figure 6.11: Average relative current responses of non-PB modified electrodes (bare and polymer-coated) to interferents; expressed as a proportion of the current responses to H_2O_2 which is represented as 100 %. The concentrations of 0.1 mM and 1 mM were considered for both, H_2O_2 and interferents; (vs. Ag/AgCl; electrolyte: 0.1 M KCl; pH 7.4)

Current Responses of Interferents in Relation to H_2O_2

Figure 6.10 shows the electrochemical responses of PB modified electrodes with and without polymer coatings and Figure 6.11 shows the electrochemical responses of non-PB modified electrodes with and without polymer coatings to the interferents. These responses were expressed as a percent change in current to H_2O_2, which is represented as 100 % in these graphs.

PB Modified Electrodes

PB modified electrodes without polymer coating (PB only, top section of Figure 6.10) showed current responses for all of the interferents. Whereas uric acid and acetaminophen showed minor additional current responses compared to the target analyte, ascorbic acid showed the highest current response proportional to H_2O_2 with an approximate 10 % change. PB modified electrodes coated with PCU, PCU-OH, PEU, PEU-OH and SR modified showed the same trend with ascorbic acid as the main interferent. However, those coated with sulphonated PU exhibited total repellence towards all of the interferents. For SR, when PB modified electrodes were dip-coated with Nafion prior to SR, none of the interferents gave a current response. Nafion®is a commercial perfluorinated polymer containing either sulfonic or carboxylic ionic functional groups, giving it its negative charge [Mauritz (1997)]. Hence, the interference rejection seen with SR in this study. This was also found in studies untertaken by other researchers [de Mattos *et al.* (2003), Haghighi *et al.* (2004), Karyakin *et al.* (1999)] in which a Nafion layer on PB modified electrodes was regarded as necessary. It was also noted that with all of these PB modified electrodes, a tenfold increase in concentration (1 mM) showed only minor differences in the proportion of the current responses to H_2O_2.

These results show that PB coated electrodes improved the selectivity of the electrode to H_2O_2. However, in combination with sulphonated PU and Nafion modified SR, current responses of all interferents could be successfully eliminated.

Non-PB Modified Electrodes

Bare electrodes (top section of Figure 6.11) were found to exhibit a 65 % higher current response to ascorbic acid, 2 % higher to acetaminophen and 25 % less current response to uric acid in relation to H_2O_2 with a concentration of 0.1 mM. The oxidation mechanism of uric acid is quasi-reversible and similar to that of the heterogeneous oxidation

of ascorbic acid. Ernst *et al.* (2001) found that uric acid strongly adsorbs at the Pt electrode. This phenomenon was also found by Carapuça *et al.* (1993), where it was claimed that uric acid oxidises at the electrode surface only after its adsorption. This would reduce the electron transfer kinetics at the electrode surface by hindering the formation of a product before further oxidation may occur. This may explain a generally lower electrochemical response for uric acid compared to ascorbic acid, as seen with the results in Figure 6.11. The oxidation of acetaminophen at Pt electrodes is some what less clear in the literature, while some authors have reported the reaction in neutral aqueous media to follow a two electron transfer [Nematollahi *et al.* (2009)], other literature suggested a one-electron transfer [Fang *et al.* (1997)]. In case of an one-electron transfer, the electrochemcial response would produce only half of the other electroactive interferents following a two-electron transfer, when considering a comparable concentration range. With a tenfold increase in concentration, the current responses showed a different profile: the electrochemical response for uric acid was 5 % lower, for ascorbic acid 32 % lower and for acetaminophen 88 % lower. This would suggest that in lower concentration ranges of both, H_2O_2 and interfering substances, the impact of the current responses would be mainly due to interferents and not due to the target analyte. Conversely, in higher concentration levels of both, H_2O_2 and interferents, the impact of the current response would be mainly due to H_2O_2 and not due to interferents. However, as these electrodes are designed to measure low levels of H_2O_2 (in the range of 50 μM), the dominating factor of the electrochemical signal would then be interfering substances. Thus, rendering no practical benefit of H_2O_2 detection with uncoated non-PB modified electrodes.

Pt electrodes coated with PCU showed in comparison at 0.1 mM for acetaminophen the highest proportionate current response, the lowest for ascorbic acid and a medium value for uric acid. This trend was also seen with PCU-OH, but the proportional current responses in relation to H_2O_2 were overall lower compared to PCU. PEU and PEU-OH showed also a similar trend to that of PCU and PCU-OH. However, the proportionate current response differences between hydroxylated and non-hydroxylated PEU were more pronounced than that between PCU and PCU-OH. SR showed permeability not only to H_2O_2 (Figures 6.5, 6.6, 6.7), but also to all of the interferents (Figure 6.11), with uric acid producing the highest proportion of current output and ascorbic acid the lowest. No additional current responses were recorded in combination with Nafion (as seen with PB modified electrodes coated with SR).

It was further noted that electrodes coated with hydroxylated PU showed retarded interferent detection compared to non-hydroxylated polymers. This may be attributed to their polarity due to the surface OH groups. Sulphonated PU successfully prevented the diffusion of all interferences to the electrode surface. This was thought to be due to the negative charge these sulphonate groups are holding, excluding negatively charged interferents such as ascorbic and uric acid. Acetaminophen does not hold a formal charge, but a size exclusion effect may be responsible for the selective H_2O_2 detection in view of the molecular sizes of both, H_2O_2 (34 g/mol) and acetaminophen (151 g/mol).

Current Responses of Interferents in the Presence of H_2O_2

In a biological environment, all interferents including the target analyte are present simultaneously. This could affect the electrode response in two ways: Uric acid and ascorbic acid are strong antioxidants and capable of reducing H_2O_2 directly making it no longer available for electrochemical detection, which would result in a decreased current output [Lowry *et al.* (1992)]. Furthermore, these interfering substances are known to adsorb at Pt surfaces, reducing the active surface area hence limiting the electro-kinetics. As with acetaminophen, during electrochemical oxidation, there are no adsorptive side reactions involved, hence no electrode poisoning. However, the oxidation reaction is considered to undergo either a one electron [Fang *et al.* (1997)] or a two electron transfer [Nematollahi *et al.* (2009)]. This would suggest that in case of a one electron transfer any additional current responses due to acetaminophen would only be of minor scale. Hence, the main interferents in H_2O_2 detection with both, PB modified and non-PB modified electrodes are uric acid and ascorbic acid. In this section, a mixed soluton containing all of the interferents at expected average physiological concentrations (Table 2.1) including H_2O_2 (0.01 mM) was utilised to estimate the way these species influence amperometric H_2O_2 detection.

PB Modified Electrodes

Uncoated PB modified electrodes (Figure 6.12) showed only a minor increase in current output to H_2O_2 with combined interferents compared with H_2O_2 only. This was also seen when each of the interferents were assessed individually regarding their impact on additional current responses as illustrated in Figure 6.10. However, all of the polymer coated PB modified electrodes showed a decreased current output to H_2O_2 with combined

interferents compared to that of H_2O_2 only, which was more apparent with those coated with sulphonated PU including Nafion treated SR. This could be due to the diffusion limiting properties membranes have, suppressing not only target analyte diffusion but also restricting the transfer of electroactive interference compounds to the electrode surface. This was more apparent with polymers holding a negative surface charge. However, interfering compounds, such as ascorbic acid and uric acid are known to be strong reducing agents and are thought to scavenge H_2O_2 directly [Lowry *et al.* (1992)] before it can be reduced at the electrode surface. This would then be noticable with a reduced current output when these substances are mixed together compared to H_2O_2 on its own, which was clearly seen with data obtained in this section as illustrated in Figure 6.10.

Non-PB Modified Electrodes

Non-PB modified electrodes without a polymer coating showed a much higher current output for H_2O_2 combined with interferents than H_2O_2 on its own. This was expected as both, the interferents and the target analyte are oxidised at the electrode surface and that of the interferents will then add to the H_2O_2 signals. Polymer coated Pt electrodes also showed increased current output with interferents and H_2O_2 mixed together compared to that of H_2O_2, however this was less apparent than at bare Pt electrodes. This was expected as with a polymer coating, the analtye can diffuse less readily to the electrode surface. Interestingly, Pt electrodes coated with sulphonated PU including Nafion treated SR showed a decreased current output, as seen with PB modified electrodes coated with the same type of polymers. This is a strong indication that the interferents had scavenged some H_2O_2 before reaching the electrode surface. However, electrode poisoning due to adsorption reactions with ascorbic acid and uric acid were reported in various literature. Ascorbic acid is generaly thought to be oxidised at a polarised Pt electrode via direct, quasi-reversible two electron transfer process which is followed by irreversible chemical reactions (Figure 2.17). Ernst *et al.* (2001) found that in neutral solutions, ascorbic acid reacts irreversibly dissociative to adsorbed CO at a polarised Pt surface. The adsorbed CO was thought to be oxidised to CO_2 at $Pt(OH)_2$ sites before its desorption. These findings have also been reported by Kokoh *et al.* (2002) in which acidic solutions were used. Adsorbed CO was considered to continue to grow at Pt sites during the production of dehydroascorbic acid. Therefore, it was concluded that CO comes from the dissociative adsorption of the primary alcohol of ascorbic acid. However, for this reactions to happen,

it was implied that ascorbic acid is not ionised in solution and the molecule would keep its two hydrogen. In this study, electrochemical measurements were conducted in physiological pH levels, hence the proposed electrode poisoning was thought to have a less severe impact in electrode poisoning. However, adsorbed CO would influence the electrode kinetics. Electrochemical oxidation of uric acid is similar to that of ascorbic acid. It was found that uric acid is strongly adsorbed at the surface of the Pt electrode and oxidation may occure only after adsorption process has taken place [Ernst *et al.* (2001)]. This adsorbent may reduce the electron transfer by reducing the active Pt surface.

Overall, with data obtained in this section, it was found that electroactive interfering compounds influence the electrochemcial current output in amperometric H_2O_2 detection mainly due to H_2O_2 scavenging and electrode poisoning. However, the main interfering cause at PB modified electrodes in this study was identified to be H_2O_2 scavening whereas that at non-PB modified Pt electrodes was thought to be electrode poisoning due to adsorptive interactions with interferents.

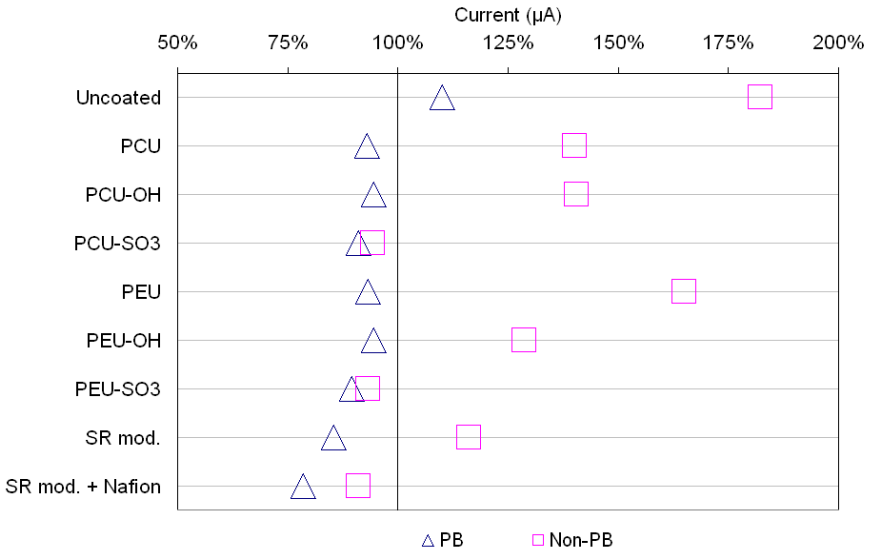

Figure 6.12: Average relative current output of PB and non-PB modified electrodes, coated and uncoated, to H_2O_2 (0.01 mM) related to H_2O_2 including interferents (0.01 mM H_2O_2, 0.4 mM uric acid + 0.1 mM ascorbic acid + 0.1 mM acetaminophen); expressed as a proportion of the current output to H_2O_2, which is represented as 100% (vs. Ag/AgCl; electrolyte: 0.1 M KCl; pH 7.4)

6.4.3 Effect of Protein Adsorption on H_2O_2 Detection

Substances such as proteins, cells and other colloidal matter are present in the biological environment, adsorbing to the sensing part of the electrode and interfering with the

electrochemical response in H_2O_2 detection. This may result in a progressive decline or even loss of analyte flux, rendering the sensor redundant. A number of different approches were taken to improve the biocompatibility of these polymers, as described in Chapter 4 and are as such:

The surface of PU was hydroxylated to create a moderate hydrophilic surface with added polarity. Hydroxylated PU was further modified by surface sulphonation for increased hydrophilicity including a negative surface charge. Moreover, these surface modifications were performed with two types of PU with different soft segment moieties of varied hydrophilicity. With these approaches, polymers with altered levels of hydrophilicity were produced. The increased biocompatibility with these strategies relied on a reduced protein adsorption and/or their denaturation at the polymer surface. Note that this would not entirely eliminate protein adsorption, but would show a high turnover in proteins on the polymer surface. The analyte flux to the electrode surface should therefore not be compromised. SR was bulk modified, which resulted in a minor decrease of hydrophobicity but allowed penetration of H_2O_2 across the polymer matrix, making this material a suitable candidate for amperometric analyte detection. The increased biocompatibility in this approach was thought to be the induced irreversible protein adsorption, creating a stable, passivating layer of proteins on the polymer surface. The more tightly the proteins are bound to the polymer surface, the lower the turnover of proteins on the surface. This additional protein layer would then have a decreased effect on analyte flux to the electrode surface.

In this section, the impact of these strategies in amperometric H_2O_2 detection will be investigated using BSA as model protein. The electrodes were exposed to 0.05 mM and 5 mM H_2O_2 buffer solution respectively including 5 % w/v BSA. The current response was monitored for twenty four hours and related to the current response before protein exposure. The results are presented in Figure 6.13.

PB modified electrodes without a polymer coating showed a gradual current decrease as a function of time during protein exposure. SR coated electrodes showed the same current profile, however, the current decrease was initially less pronounced. PCU and PEU coated electrodes showed a more rapid current decrease at the initial stage compared to their hydroxylated counterpart. However the relative current response appeared to show a reduced decrease between 1 and 24 hours of protein exposure for both, hydroxylated and non-hydroxylated PU. The electrodes coated with sulphonated PU showed the lowest

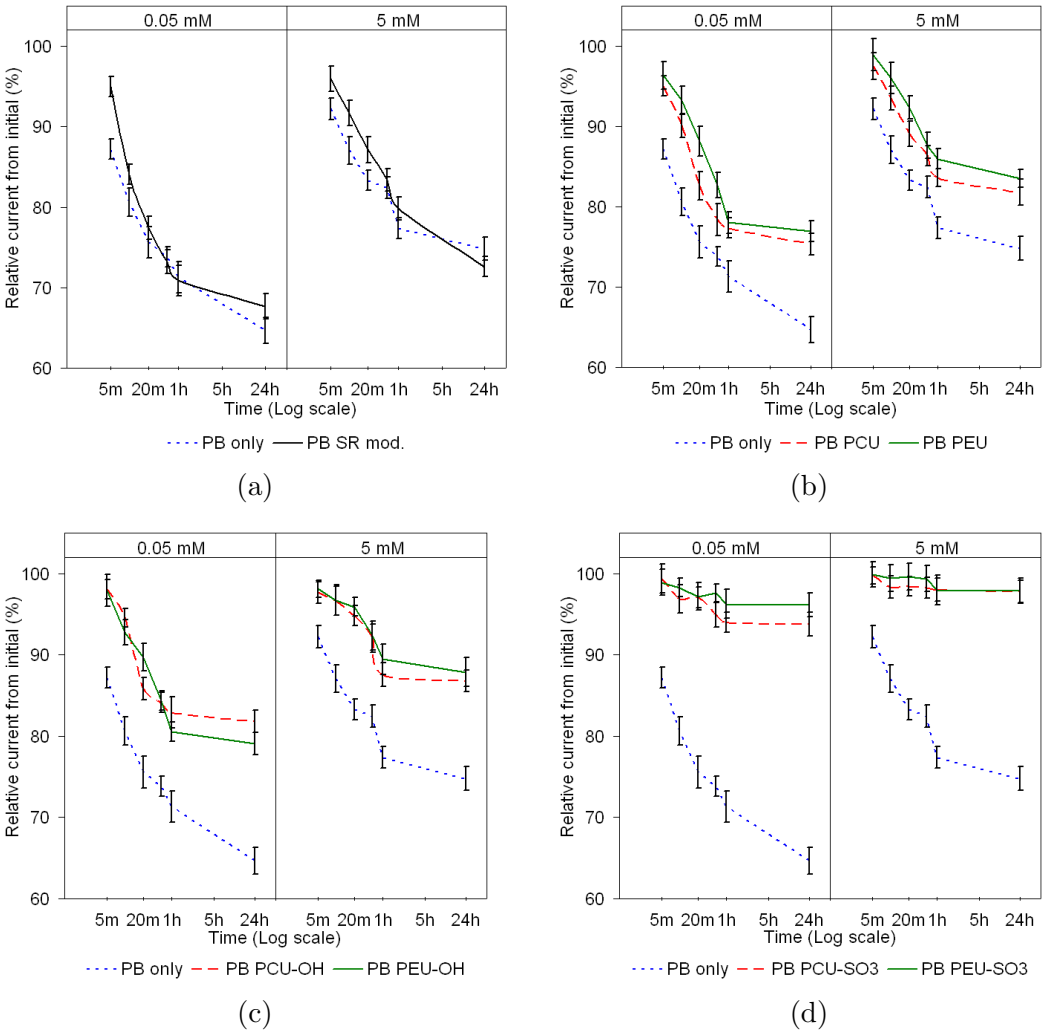

Figure 6.13: Relative current responses of PB modified electrodes (PB only and polymer-coated) towards 0.05 mM and 5 mM H_2O_2 during exposure of 5 % w/v BSA at different time intervals; expressed as percentage of initial current at time = 0; a) PB only and PB SR modified; b) PB only, PB PCU and PB PEU; c) PB only, PB PCU-OH and PB PEU-OH; d) PB only, PB PCU-SO_3 and PB PEU-SO_3; (vs. Ag/AgCl; electrolyte: 0.1 M KCl; pH 7.4)

relative current decrease from initial. Moreover, the current response after 40 minutes of protein exposure seemed to first recover, decline and then appeared to stabilise over time.

Protein adsorption is accompanied by protein desorption [Castner *et al.* (2002)]. The variations of relative current output during protein exposure found with different polymer coatings in this section (Figure 6.13) may be due to the affinity of the protein to these different polymer surfaces. The degree of hydrophilicity of the polymer has an effect on the conformation of the adsorbed protein. Depending on the conformation, the packing of the proteins will be either more or less dense. On hydrophobic surfaces, proteins were found to bind stronger and show less tendency for desorption compared to those adsorbed at hydrophilic surfaces [Elbert *et al.* (1996)]. Hence, a more dense protein layer can be expected with hydrophobic surfaces, resulting in less analyte flux to the electrode surface as seen in this section with uncoated, PB modified electrodes and those coated with SR (Figure 6.13(a)).

Amongst the PU used in this study, sulphonated PU is the most hydrophilic, followed by its hydroxylated counterpart and with unmodified PU being the least hydrophilic. The whole process of protein adsorption followed by desorption, concomitant with a rearrangement of both the protein and the surface, were found to happen fairly quickly the more hydrophilic the polymer [Castner *et al.* (2002)]. If adsorption and desorption processes occur at the same rate, hence high turnover, the active electrode surface area can be thought of being reduced only by the initial protein adsorption process. The results illustrated in Figure 6.13 (d) for sulphonated PU clearly indicate this activity occuring, as the recorded current responses show very little decrease which eventually plateaus out with prolonged protein exposure.

SR is amongst the polymers used in this study the most hydrophobic and protein adsorption will then occur due to hydrophobic forces. As detailed in Chapter 2, these hydrophobic forces alter the structure of the protein and may then change the manner and speed of further protein adsorption, hence resulting in a low turnover. Xu *et al.* (2007) reported on proteins binding more strongly to hydrophobic than hydrophilic surfaces, which was thought to be due to strong hydrophobic interactions occurring at these surfaces. This is in contrast to the repulsive salvation forces arising from strongly bound water at the hydrophilic surface.

Proteins and H_2O_2 both compete with the surface area of the electrode. However,

when proteins are adsorbed, small compounds such as H_2O_2 may still access the electrode surface in sufficient high quantities. This may be due to the turnover of the proteins occuring at the electrode surface. However, if proteins are strongly bound to the surface, this may also be due to the globular structure of albumin with dimensions of approximately 8 nm by 3.8 nm and a molecular weight of 68,480 Daltons. Green *et al.* (1997) found that considering these molecular dimensions and their potential conformation at the substrate, albumin would not entirely cover a surface. In amperometric analyte detection, this protein would not completely block the electrode surface. This can be seen in this study with more or less reduced current responses from the initial, as shown in Figure 6.13; although for albumin adsorption, all of the electrodes remain functional. This is in accordance with observations made by Pickup *et al.* (1993).

Interestingly, at higher H_2O_2 concentrations (5 mM), the proportional current output for all electrodes during protein exposure showed a less pronounced current decrease compared to that with lower H_2O_2 concentrations (0.05 mM). It was found by various researchers that when proteins are exposed to H_2O_2, they are subject to oxidation [Finch *et al.* (1993), Di Simplicio *et al.* (1991)]. It was further proposed that albumin may act as a native sacrificial antioxidant, scavenging H_2O_2 and thus preventing further damage by this toxic agent [Zhu *et al.* (1992)]. The oxidised protein will display different binding affinity due to the altered conformation. This may change the process of further protein adsorption, which was found to be a complex relationship between surface chemistry and the nature of co-adsorbed proteins [Castner *et al.* (2002)].

A denatured protein may adsorb irreversibly to a surface, showing little turnover. Additionally, scavenged H_2O_2 would no longer be available for electrochemical reduction, which would be apparent in a further current decline. The higher relative current output from initial with an increased H_2O_2 concentration as seen in this section was thought to be due to that there is still sufficient H_2O_2 available to maintain a higher current output compared to that with lower H_2O_2 concentration. Furthermore, H_2O_2 is known to be less stable in small concentrations and decomposes faster. This would make any protein fouling with a subsequently reduced active electrode surface area and a reduced current output more apparent at lower H_2O_2 concentrations.

Polymers with varied levels of hydrophilicity used in this section showed that there is a clear relatationship between hydrophilicity and relative current output in amperometric H_2O_2 detection during protein exposure. The least hydrophilic polymer, SR, showed the

highest relative current decrease and the most hydrophilic polymer, sulphonated PU, showed the lowest relative current decrease.

6.5 Amperometric Detection of O_2

For amperometric O_2 detection, the same needle-type electrodes as for H_2O_2 determination were used including the same polymer combinations. However, although Ag/AgCl for reference electrodes are frequently used in electrochemical analyte detection, stainless steel has been found to work well as the anode [Whalen *et al.* (1980)] for pseudo-reference. Since the electrode construct already contains a stainless steel needle, it was decided to utilise this available, compact system.

The initial objective was to develop a simple and low-cost calibration method for these oxygen sensors. The difficulty was to keep the oxygen concentration constant (air tight) throughout the experiment. The following considerations had to be taken into account for the design of the calibration chamber:

- Samples with varied oxygen tension had to be mixed and exchanged over the course of the experiment.
- Sample solutions had to be entirely replaced if required.
- Exchange of electrodes when required.
- The temperature had to be kept at a constant level (37°C).

These requirements had to be easily attainable, and achieved without drawing additional oxygen into the system. The fabrication of this calibration cell was modified from that of commercially available single mixing stopped-flow cells (as illustrated in Section 3.3.7). In order to test this cell for air tightness, a sample of each buffer solution was taken before and after calibration, and the pO_2 of these samples were determined using a bench-type blood gas analyser. The pO_2 values differed by only approximately ± 0.1 kPa, showing that the cell-electrode construct delivered reproducible results.

Once satisfied that the construct functioned as required, the electrodes were then submitted to pO_2 calibration. The current output for each of the electrodes over the pO_2 range 0-16 kPa is illustrated in Figure 6.14. All sensors showed good linearity with $R^2 > 0.99$. The current output was then translated into pO_2 using the measured pO_2

values from the blood gas analyser. The data was analysed and the results are listed in Table 6.4.

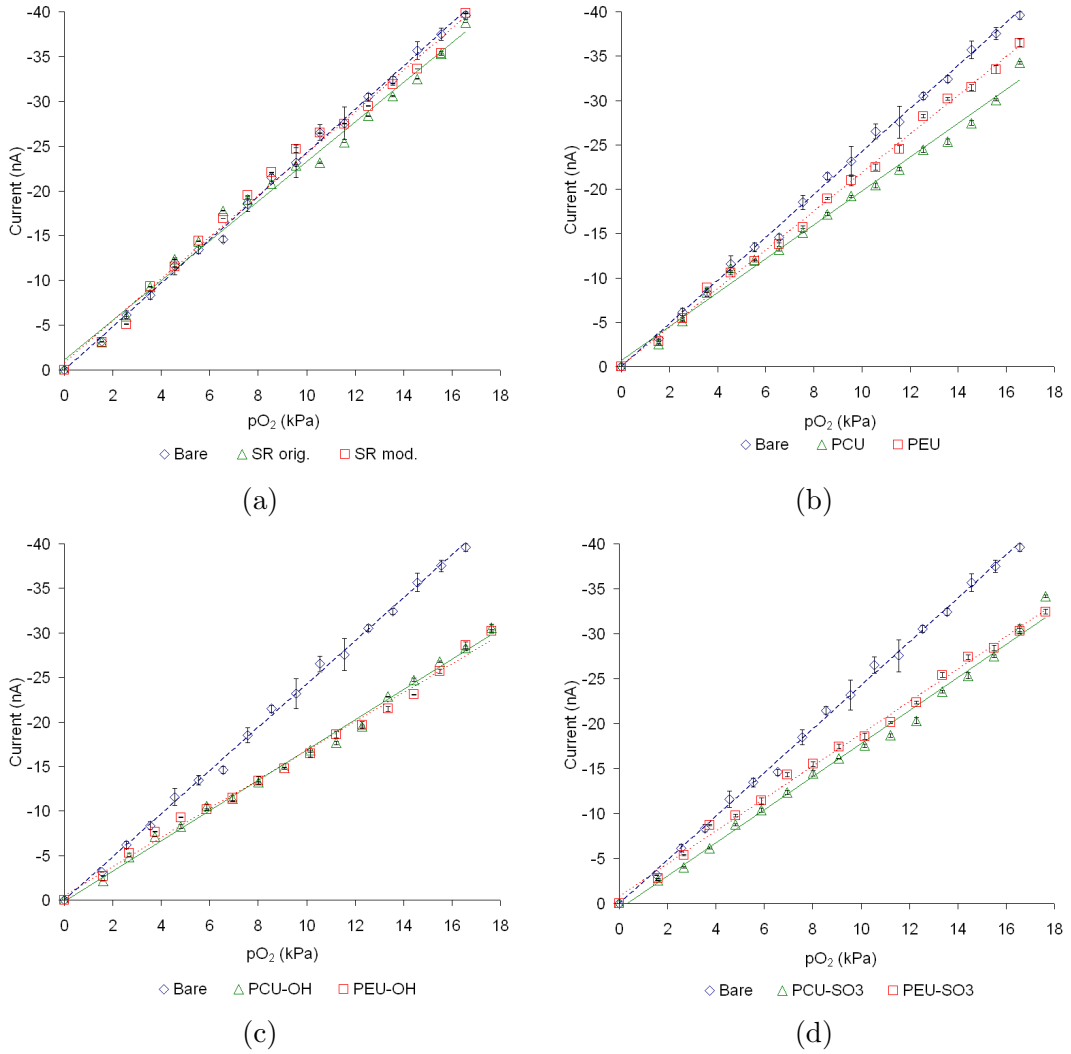

Figure 6.14: Current responses of polymer coated and bare electrodes to varying oxygen concentrations; a) Bare, SR control, SR modified; b) Bare, PCU and PEU; c) Bare, PCU-OH and PEU-OH; d) Bare, PCU-SO_3, PEU-SO_3;(vs. stainless steel pseudo-reference; electrolyte: 0.1 M KCl; pH 7.4)

Of all the electrodes, the uncoated electrodes (Figure 6.14) showed the highest current response; this was expected due to the lack of a diffusion barrier. However, the error bars indicate less repeatability compared to that of polymer coated electrodes. This could be due to additional chemical processes occuring at the working electrode surface simultaneous to the reduction process for oxygen, such as the formation of a platinum oxide surface complex which will partially inhibit further reduction processes [Drazic *et al.* (1999)]; or a slow passivation process involving the adsorption of solute borne species to the active surface [Gough *et al.* (1980)]. Furthermore, during the experiment it was

noticed that small gas bubbles formed on the uncoated electrode, which increased in size and eventually dislodged. The presence of these gas bubbles altered the current output noticeably. Hydrogen evolution at noble metal electrodes has been reported to occur at high cathodic potentials [Bard *et al.* (2001)]. However, the potential used in this study should not result in hydrogen evolution. No bubble formation was observed on any of the polymer coated electrodes.

Electrodes coated with modified SR appeared to show similar current responses to uncoated electrodes (Figure 6.14 (a)), and a much higher current response compared to those coated with PU. This again was expected, since the gas transport across a homogeneous, hydrophobic polymer is faster than across an inhomogeneous polymer with domains of amorphous, hydrophilic and semi-crystalline, hydrophobic regions, such as for PU. Also, SR is known for its good gas permeability properties and is therefore widely used in gas-sensing applications [Liu *et al.* (1995), Mizutani *et al.* (2001)].

PU coated electrodes, illustrated in Figure 6.14 (b), showed a reduced current response to that of uncoated electrodes. This was more apparent with PU containing carbonate moieties in their soft segment (PCU) than that of PU with ether moieties (PEU), suggesting that PEU appears to be more gas permeable. Kim *et al.* (2003) found that with increasing amount of impermeable regions in the block copolymer, the flow paths for gas diffusion is restricted. The PCU used in this study has a higher hard segment content in contrast to PEU (Table 4.1), which is evident with an increased relative crystallinity. However, as these polymers were phase inverted (Chapter 3, Section 3.3.1), the degree of phase separation within the material must also be considered. During phase inversion, the hard segments are reinforced to sequester away from the polymer surface (seen with relative peak height differences (FTIR) shown in Figure 4.5). Due to the relative hydrophilic nature of the hard segments compared to the soft segments, these segments then tend to cluster; the polymer network within the hard segments is then bonded more tightly, hence restricting analyte diffusion across the polymer matrix to the electrode surface. This is less apparent with PEU as due to the steric structure of the hard segments, these microdomains are less well ordered and not as tightly packed as that of PCU. Additionaly, hydrogen bonding within PEU mainly occur between the hard segments, whereas in PCU, hydrogen bonding may occur between hard and soft segments as well as between hard segments. Therefore, the intermolecular hydrogen bonding between the hard and soft segments in each PU would suggest to be more pronounced with PCU compared to

PEU, resulting in a decreased current output with PCU as seen with data illustrated in Figure 6.14 (b). However, the soft segments of PCU show steric structure and should therefore enhance analyte diffusion compared to the more tightly packed soft segments of PEU. Considering the steric structure of the hard segments, the ability to hydrogen bond between hard- and soft segments and the steric structure of the soft segments, it is hypothesised that the dominating factor for a reduced analyte diffusion is the steric structure of the hard segments.

Surface modified PU, hydroxylated and sulphonated, showed a lower current output compared to their unmodified counterpart. This is more apparent with hydroxylated PU. In general, gas permeability across a polymer depends on several factors, for example the solubility of the gas in the solution, the polymer-solvent interaction, the polymer density (free volume), the mobility of the polymer chains and the thickness and nature of the polymer including the material chemical structure. For the evaluation of current responses in comparison with electrodes coated with varied polymers in this study, the solubility of oxygen as such can be excluded as the same buffer solution was used due out this experiment. Hence, the intimate interaction of oxygen with the polymer backbone and the pendant groups including the polymer-solvent interaction are the main factors to be considered. For gases with small chemical affinity to the polymer, the transport across the polymer matrix is mainly dependant on the fractional free volume and segmental chain motions [Compañ *et al.* (2005), Williams *et al.* (1996)]. Moreover, PU used in this study was of non-porous nature and therefore, diffusion occurs through molecular gaps.

Surface modification increased the surface hydrophilicity (as seen with contact angle data shown in Table 4.8), which changed the polymer-solvent interactions resulting in a higher free volume due to hydration with increased segmental motions. This should be reflected with an enhanced oxygen diffusion. However, this was not found in this study. The reduced current output seen in Figures 6.14 (c) and (d) may have been due to that with these surface modifications, only the surface hydrophilicity changed and not that of the bulk. Hence the polymer exhibits a relatively higher hydrophobicity in the bulk compared to that of the surface. Hydrophilic polymers will absorb water when placed in aqueous media. Hydrophobic polymers will absorb water via hydrophobic attraction as well, but in much less quantities [Hoffmann (2002)]. The surface modified PU increased in thickness due to water uptake, the amount of enclosed electrolyte within the polymer matrix will be larger, which increased the diffusion path of the analyte to the electrode

surface. These may have led to a decrased analyte diffusion due to boundary layer resistance. In addition, the reduced current output could have been caused by variations in permeability within the polymer matrix induced by the surface modifications.

	Sensitivity (nA/kPa)	T_r (sec)	LOD (kPa)	RSD_5 (%)	RSD_1 (%)
Bare	2.43	6.5	1.1	17	7
PCU	1.91	9.0	0.2	12	2
PCU-OH	1.84	13.7	0.2	11	4
PCU-SO_3	1.70	12.5	0.3	13	3
PEU	2.18	9.0	0.2	15	3
PEU-OH	1.60	9.1	0.2	10	2
PEU-SO_3	1.80	9.2	0.2	12	3
SR control	2.21	6.9	0.1	8	2
SR modified	2.34	8.1	0.1	8	2

Table 6.4: Performance characteristics of polymer coated and bare electrodes in respect to pO_2; calculated from calibration curves illustrated in Figure 6.14; with T_r = response time, LOD = limit of detection, RSD_5 = reproducibility using 5 individual electrodes, RSD_1 = reliability using the same electrode)

The performance characteristics of polymer coated and bare electrodes towards O_2 were calculated from calibration curves illustrated in Figure 6.14 and are tabulated in Table 6.4. The reproducibility (RSD_1) was found to be below 5 % for all of the polymer coated electrodes. A batch of different sensors (RSD_5) showed a much lower reproducibility. This was expected as each sensors was individually made by hand. The response time (T_r) in this study for uncoated electrodes is with 6.5 seconds the lowest. All PEU coated electrodes, surface modified and unmodified, showed in comparison with an average of 9.1 $\pm$1 seconds a very similar response time. The response time for similar PEU found by Zhang *et al.* (1996) was with an average of 5.3 seconds slightly lower in comparison. However, electrodes coated with PCU showed a different T_r profile, that of PCU-OH was 52 % and that of PEU-$SO_3$was 39 % higher compared to that of unmodified PCU. Zhang *et al.* (1996) found that the response time of a sensor is largely determined by the oxygen diffusion resistance of the membranes. This would suggest that surface modification of PCU altered the analyte diffusion resistance considerably, whereas that of PEU remained virtually unchanged after surface modifications. The response times for SR coated electrodes are between 8.1 and 6.9 seconds and are in accordance to that found by Wu *et al.* (2005) of about 8.7 to 6.8 seconds albeit SR in their study was obtained from a different manufacturer, spincoated and only the 90 % response time was reported.

The LOD for all of the PU coated electrodes, surface modified and unmodified, was

with 0.2 kPa twice as high as for SR coated electrodes. Tissue oxygen tension was reported in literature to be between 0.7 and 5 kPa and that in tumors was reported to be as low as 0.3 kPa [Vaupel *et al.* (1996)] depending on the location and progress of the medical condition. Hence, the LOD found in this study was thought to be sufficiently low to accomodate these low ranges.

The sensitivities for unmodified PU showed overall a higher value compared to their surface modified counterparts. Modified SR showed the highest sensitivity of all the polymer coated electrodes. Unmodified SR showed a similar sensitivity to that of unmodified PEU. Zhang *et al.* (1996) reported a very low average sensitivity of 0.06 nA/kPa for similar PEU analogy to 1.56 nA/kPa for sensors coated with phospholipid-based copolymer membranes. However, a true comparison of results in general is not possible because of varied preparation methods and conditions, sensor designs, material and construction, different polymer composition and varying experimental conditions such as temperature, buffer solution, stirring, etc.

6.5.1 Long- and Short Term Stability

Long- and short term stability of oxygen electrodes is a crucial attribute as water soluble impurities may adhere to the working electrode surface over time, reducing the active surface area. During oxygen detection simultaneous side reactions may occur, resulting in the formation of a platinum oxide surface complex that partially inhibits further oxygen reduction processes.

Greenbaum *et al.* (1997) recommend that oxygen electrodes should be operated at the lowest potential possible without causing hydrogen evolution (which would avoid the generation of free H_2O_2 due to the intermediate HO_2^- ion). However, Hoare (1968) states that the intermediate H_2O_2, or the HO_2^- ion, is always produced when oxygen is reduced in an acidic or alkaline environment. A much simplified reaction scheme is given by:

$$O_2 + H_2O + 2e^- \rightarrow HO_2^- + OH^-$$
$$HO_2^- + H_2O + 2e^- \rightarrow 3OH^-$$

in which the net reaction would be

$$O_2 + 2H_2O + 4e^- \rightarrow 4OH^-. \tag{6.1}$$

In the presence of O_2, the catalytic decomposition of the intermediate HO_2^- ion could be as follows

$$HO_2^- \rightarrow 1/2\ O_2 + OH^- \tag{6.2}$$

in which the peroxide ion is then either reduced to OH^-, catalytically reconverted to oxygen, or it escapes out of the vicinity of the cathode into the bulk of the electrolyte [Hahn (1998)]. Gough *et al.* (1980) found that in basic media H_2O_2 is less stable, and the equivalent of four electrons per molecule of oxygen is more easily obtained at the highest potential possible, which is contrary to the recommendation of Greenbaum *et al.* (1997). It has been reported that by polarising the electrode at 10 mA/cm^2 until steady-state is reached, generated H_2O_2 would reductively remove the platinum oxide film. With this oxide-free surface, electrochemical oxygen reduction would proceed more rapidly [Gough *et al.* (1980), Ho *et al.* (2003)]. However, there have also been reports which state that clean Pt surfaces lead to even greater adsorption and oxidation, and that the chemisorption ability of OH^- depends on the surface activity and pH value of the electrolyte [Drazic *et al.* (1999)].

In this section, the operational stability (long term) and the storage stability (short term) of oxygen electrodes was assessed with regard to the influence of adsorbed species (impurities, oxide layer) which may have a detrimental effect on the performance of the electrodes. Prior to stability testing, the Pt electrode surface was electrochemically cleaned (Chapter 3, Section 3.3.5) to remove any residual impurities and oxides which may have already poisoned the electrode.

The operational stability was assessed by placing the electrodes in phosphate buffer solution with a pO_2 of 11 kPa. The current response was recorded for 24 hours continuously and the buffer solution was renewed three times within the assay. The plot of the current responses are shown in Figure 6.15(a). The storage stability was assessed under the same conditions but over a period of 6 months, in which the current response was recorded every 5 days. The current responses are illustrated in Figure 6.15(b).

The results in Figure 6.15(a) show the current response over a period of 24 hours continued use. The current for bare Pt electrodes decreased more rapidly in the first ten hours (approx. 5 %) and showed a further current decay of < 1 % within the next 14 hours. Polymer coated electrodes showed an average of < 2 % current decrease, with a steady current decay over the 24 hours. The results in Figure 6.15(b) show the

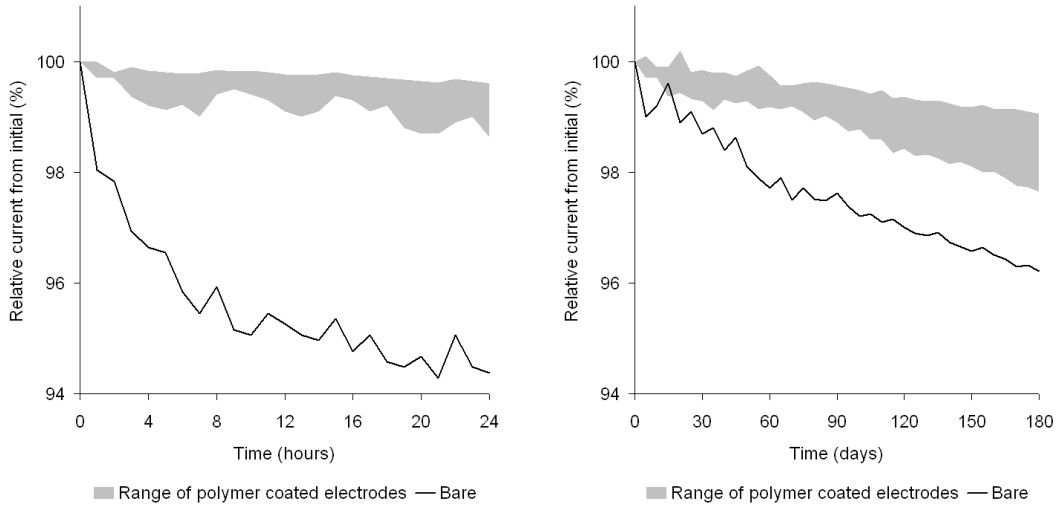

Figure 6.15: Average relative (a) operational and (b) storage stability of electrodes towards pO_2, both with and without polymer coatings; (vs. stainless steel pseudo-reference; electrolyte: 0.1 M KCl; pH 7.4)

current response over a period of 6 months in occasional use. Bare Pt electrodes showed an initial rapid current decay during the first 60 days followed by a decay rate similar to the coated electrodes, which had a constant decay rate throughout. There was no apparent steady state observed for either type of electrodes. The fluctuations of the current output could have been caused by variations in current distribution within the vicinity of the oxygen cathode. In this study, a two-electrode configuration was utilised with stainless steel as the counter and reference electrode, which is made in the form of a concentric ring located around the edge of the cathode. Gough *et al.* (1980) found that this configuration could lead to a greater current density at the edges of the cathode than at the centre. It was suggested that the non-uniform current density would be further emphasised with a membrane in place, since a uniform current flux would depend on consistent permeability of the analyte across the membrane. For PU, the phase separated nature means that analyte transport cannot be modelled as for homogenous polymers, such as SR. Diffusion of species through amorphous regions will be higher than through the glassy or semi-crystalline regions. It is recommended in literature [Gough *et al.* (1980)] that oxygen electrodes should be allowed to age under operating conditions prior to use. However, to determine the oxygen concentration directly from the resulting current with aged electrodes based on the number of electrons involved in the reduction process would become more difficult. This would be due to a slow passivation process occurring at

the electrode surface, involving the adsorption of impurities and/or the formation of an oxide layer. As has been seen with these results, a slow passivation process may have occurred in parallel with the oxygen reduction process, probably involving the adsorption of impurities and/or the formation of an adsorbed oxide layer. This may have caused the effective surface area to decrease, resulting in current decay as seen in Figure 6.15. Such a partially poisoned electrode may not be sufficiently active for rapid reduction of the peroxide intermediate, thereby decreasing the number of electrons involved in the overall process. By comparison, in short term testing (Figure 6.15(a)), there appears to still be adequate active surface area to postpone these effects, bringing the process under reaction control and showing what appears to be a steady state.

6.5.2 Effect of Protein Adsorption on pO_2 Detection

Following calibration, the electrodes were tested for current stability for twenty four hours in buffer solution mixed with BSA at a pO_2 of 11 kPa. The level of fouling was determined as a percentage difference between the current response before (control sample) and after protein exposure. The results are illustrated in Figure 6.16.

The uncoated sensor showed the highest decrease in signal over time, with the largest current drop between 5 and 10 min (Figure 6.16). The current did not stabilise, but continued to decrease during the time scale of this experiment. Cooper *et al.* (1982) found that the lower the surface energy of a material, the more stable it is. Hence the higher the surface energy of a material, the higher is the motivation for reducing the interfacial energy. A substance like metal with a high surface energy would have to adsorb a substance with a lower surface energy (protein in this case) to obtain desirable lower interfacial energy. Hence the relative higher protein adsorption and the continuous current decay seen in Figure 6.16 compared to polymer coated electrodes.

Both PCU and PEU-coated electrodes exhibited a steady decrease in current response for the first hour and only a slight decrease between 1 and 24 hours (Figure 6.16 (b)). This was in contrast to Zhang *et al.* (1996), in which a gradual current decay for his PEU coated electrodes was reported throughout a 24 hour period without any tendency for stabilisation. However, the initial current decay in this study within the first hour was smaller than that reported by Zhang *et al.* (1996). The hydroxylated PCU and PEU-coated electrodes showed much less current decay compared to the non-hydroxylated version (Figure 6.16 (c)). However, the current appeared to be stable between 10 and

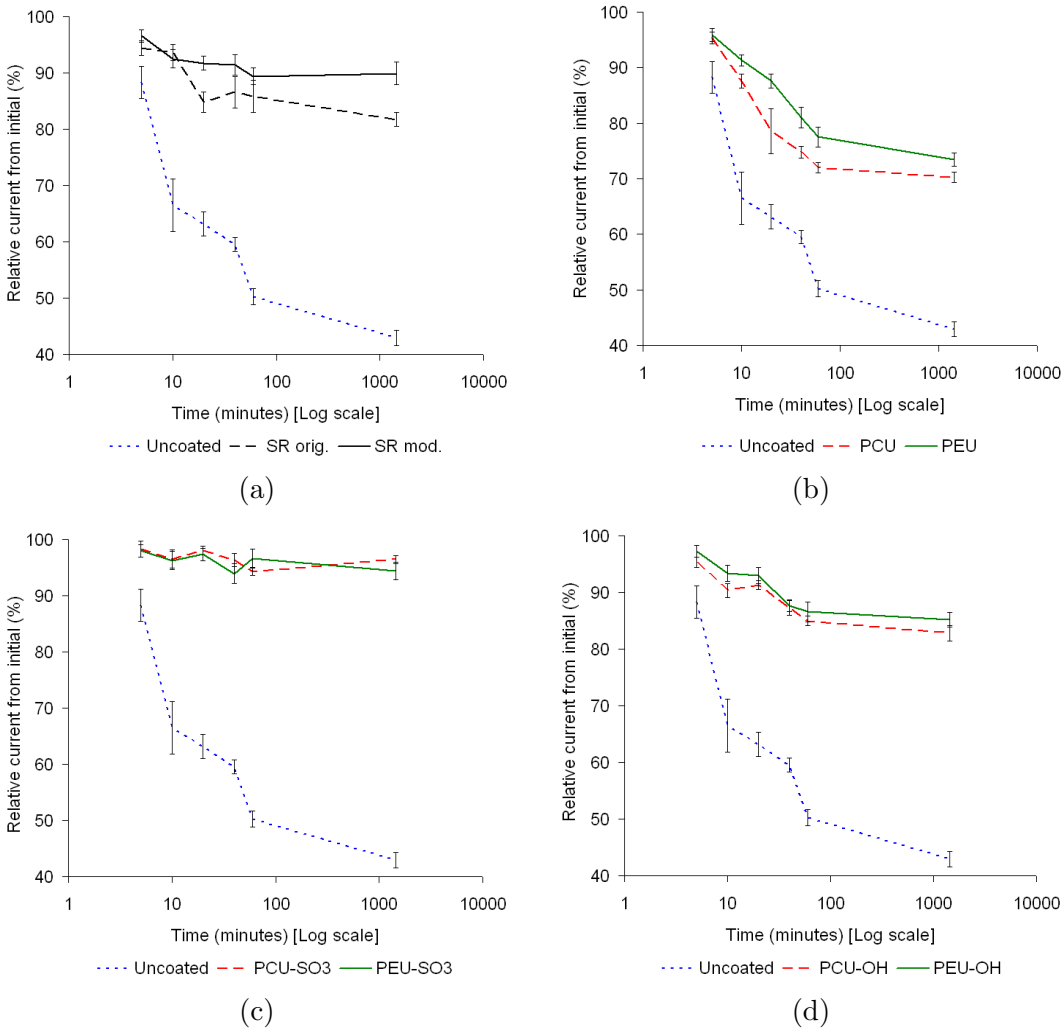

Figure 6.16: Relative current responses of polymer coated and bare electrodes towards pO_2 (11 kPa) during exposure of 5 % w/v BSA at different time intervals; expressed as percentage of initial current at time = 0; a) Bare, SR control and SR modified; b) Bare, PCU and PEU; c) Bare, PCU-OH and PEU-OH; d) Bare, PCU-SO_3 and PEU-SO_3; (vs. stainless steel pseudo-reference; electrolyte: 0.1 M KCl; pH 7.4)

20 minutes of protein exposure, followed by a sharper current decrease. Between 1 and 24 hours, the current decreased only slightly. The electrodes coated with sulphonated PCU and PEU showed in contrast initially only a slight drop in current response; after 40 minutes of protein exposure the current seemed to recover. During the remaining time up to 24 hours, both sulphonated electrodes exhibited only small decreases and increases in current output (Figure 6.16 (d))). Zhang *et al.* (1996) also found fluctuating current responses with apparent recovery of current output in protein solution with phospholipid-based copolymer coated sensors. A similar current profile with regards to the effect of protein adsorption in H_2O_2 detection is reported in Section 6.4.3. The reason was thought to be in the hydrophilic nature of the sulphonated polymer concomittant with a fast reversible ongoing adsorption and desorption of albumin. The net effect would have been that the active surface area of the electrode was thought to have remained relatively constant as seen with relative stable current responses in Figure 6.16 (d). Electrodes with SR coatings showed current responses similar to sensors with hydroxylated PU coatings when exposed to BSA for 24 hours (Figure 6.9 (a)). However, sensors with modified SR coatings exhibited a smaller decline in current than sensors with SR control coatings. This could be due to the decreased hydrophobicity of modified SR.

6.6 Summary

- Modified SR is confirmed to be permeable to H_2O_2 in contrast to conventional unmodified SR.
- The analyte response of PB modified needle-type electrodes was about three times higher than that of electrodes without PB.
- Good long- and short term stability of PB modified electrodes was achieved during catalytic action of PB towards H_2O_2 in basic buffer solution.
- Sulphonated polymers showed excellent interferent rejection.
- Simple, rapid and inexpensive procedures for surface modification of PU already placed on the electrode show linear analyte response, excellent long- and short term stability and low protein adsorption.
- A simple and low-cost calibration method for pO_2 detection was successfully developed.

Chapter 7

Conclusions And Future Work

7.1 Conclusions

This thesis has successfully demonstrated effective surface modification for PU already attached to delicate sensing devices. Furthermore, these modifications were necessary for improved functionality of the electrodes. Effective bulk modification of SR for not only O_2, but also H_2O_2 permeability, was also demonstrated. The chemical properties of these polymers are such that cell spread and growth was neither encouraged nor discouraged; this is a fact that can be taken advantage of, especially in medical applications.

Needle-type electrodes, the chosen tool for amperometric analyte detection, offer great opportunities as they require only readily available materials and are therefore cheap to produce. They show micoelectrode behaviour and require only a small sample volume, despite their relatively large size. Pt as substrate was demonstrated to show that it can be effectively modified with PB. Uniquely in this thesis, however, the modification resulted in a stable PB film. Further, the analyte response was about three times higher than that of electrodes without PB. Linear analyte response, excellent long- and short term stability and low protein adsorption was seen with all of these modified polymers. Advantages in interferent rejection, especially of that with sulphonated PU, were seen. Additionally, this thesis has investigated and demonstrated a simple, low-cost calibration method for pO_2 detection.

The research presented would serve well as a platform for further investigations as described in Future Work. Continued exploration of these modified needle-type electrodes in the medical field could be of advantage as these electrodes offer the opportunity of measuring analyte concentration locally.

7.2 Future Work

Further to work presented here, the ultimate test would be to investigate the performance of these polymer modified needle-type electrodes in true *in vivo* conditions. In a preliminary study, oxygen was measured in a heparinised human blood sample using needle-type elecrodes coated with PCU-OH.

7.2.1 Electrode Response in Heparinised Whole Blood

The electrode was conditioned in air saturated buffer solution at -650 mV versus stainless steel as pseudo-reference [Whalen *et al.* (1980)] and after a stable current reading was achieved, immersed into the unstirred and undiluted heparinised blood sample. This resulted in an initial sharp decrease followed by a gradual decay in current response. Figure 7.1 shows an illustration of the experimental outcome.

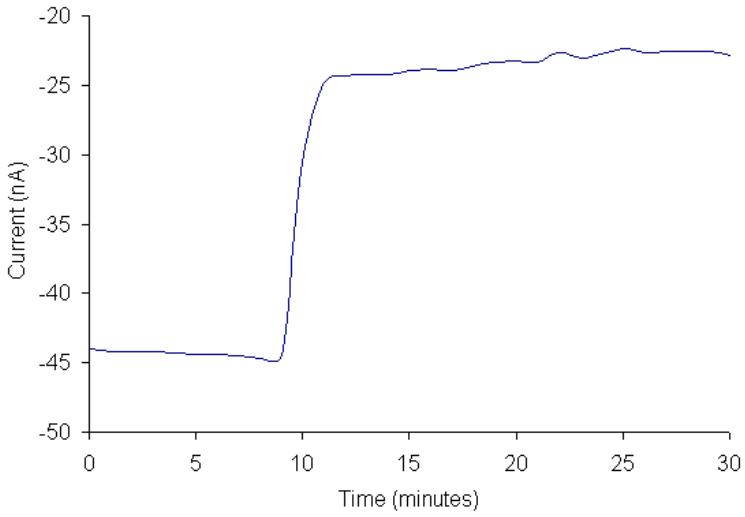

Figure 7.1: Current response towards oxygen in heparinised whole blood with PCU-OH coated needle-type electrode (vs. stainless steel as pseudo-reference)

According to literature [Ciba-Geigy (1981)], arterial blood has a pO_2 of around 100 mmHg (13 kPa) and venous blood has a pO_2 of around 40 mmHg (5 kPa). As venous blood was used in this experiment, the current response should be ~5 kPa. The measured current response to the heparinised blood of ~22 nA equated with ~4 kPa, which was in good correlation to the expected value.

The values of slightly lower pO_2 as theoretically expected were measured here and could been due to biological material, such as proteins and cells, fouling the electrode surface, thus acting as an additional diffusion barrier. Furthermore, some of the oxygen

may have already been consumed by blood cells.

However, this simple experiment has shown that the electrode can generated stable current readings in heparinised blood with only a 3 % decay at 20 minutes of blood exposure. It would be interesting to correlate observations with the full range of polymers developed in Chapter 4, to thereby assess and compare haemocompatibility.

7.2.2 Electrodes used in Cancer Research in Biological System

Cancerous cells are cells which have essentally lost the ability to die. They exhibit uncontrolled growth coupled with malignant behaviour, invasion and metastasis. Cancer is thought to be caused by the interaction between genetic susceptibility and environmental toxins. Most chemotherapeutic drugs work by impairing cell division, targeting specifically fast-dividing cells. These drugs cause not only damage to cancerous cells, but also to healthy cells. As fast growing cells show a higher metabolic rate, the oxygen uptake and perfusion in tissue is thought to be elevated at these specific areas. The basis of this experiment was to:

- Measure local pO_2 in tissue lining *in vivo*.
- Deprive healthy tissue of oxygen via a balloon-like construct (Figure 7.2).
- Examine the effect of oxygen deprivation on tissue whether it would recover and what the oxygen tension threshold would be.
- Experiment with light-activated photosensitising drug (PSD) palladium bacteriophosphorbide for altering haemoglobin oxygen concentration

If a two-electrodes system is used in which the second electrode serves as both, reference and counter electrode, the second electrode must be much larger than the working electrode to ensure proper functioning of the electrode [Gough *et al.* (1980)] as otherwise reference electrode polarisation may compromise its functioning. Therefore, the exposed area of the reference electrode to working electrode *in vivo* had to be within certain limitations. For electrodes used in this study, with a 2 cm needle immersion in medium, the ratio of pseudo-reference electrode to working electrode was estimated to be around 13800:1, and when used *in vivo* assuming 2 mm depth insertion the ratio would then be 1380:1. These are in excess of the 50:1 ratio reported by Popplewell *et al.* (2002) to furnish stable signals for a Pt working electrode - stainless steel pseudo-reference electrode combination.

Preliminary experiments were undertaken in collaboration with Dr. Ivan Hoh under supervision of Prof. Stan G. Bown and Dr. Sandy McRoberts of the National Medial Laser Centre at University College London, UK.

The study involved electrodes coated with PCU-OH to be inserted into tissue lining *in vivo* at various locations. A balloon-like construct (Figure 7.2), which is designed to be inflated and deflated for altering local circulation of oxygen and so pO_2, was also used in this study. Male Wistar rats (180-200 g) were used for all experiments. The handling of the rats including drug administration and positioning of the needle-type electrodes, balloon-like construct and fibre-optic cable was undertaken by Dr. Ivan Hoh, UCL.

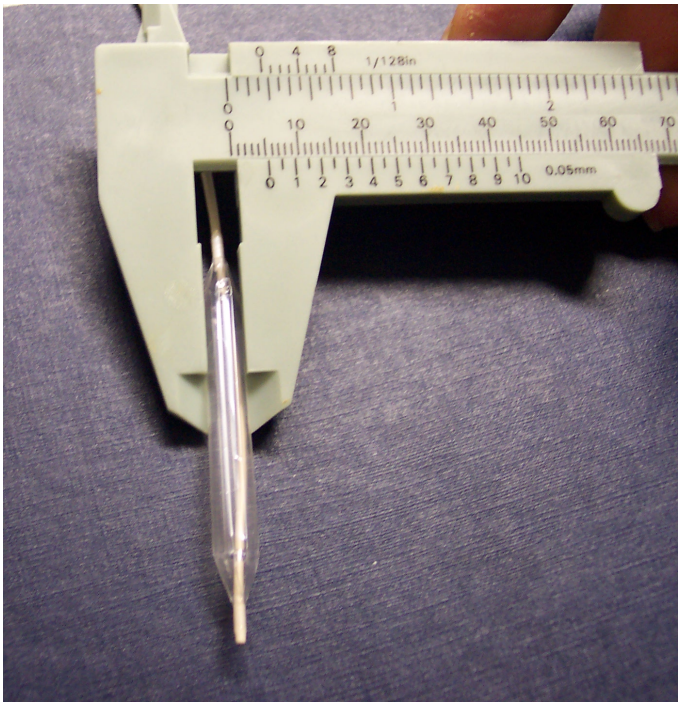

Figure 7.2: Photographic image of fully inflated balloon-like construct used in this study for induced alteration of oxygen circulation in local tissue; illustrated with measuring scale

Experiment Part 1:

In this section, it was focused on the duodenal and anal wall and the anal sphincter with and without inflation of the balloon-like construct for induced changes in pO_2 circulation. Figure 7.3 illustrates the obtained current responses.

The current responses in Figures 7.3 and 7.4 showed little fluctuation and apparent stabilisation when electrode was inserted. The induced variation of pO_2 due to inflation and deflation of the balloon-like construct when electrode was inserted in the anal wall

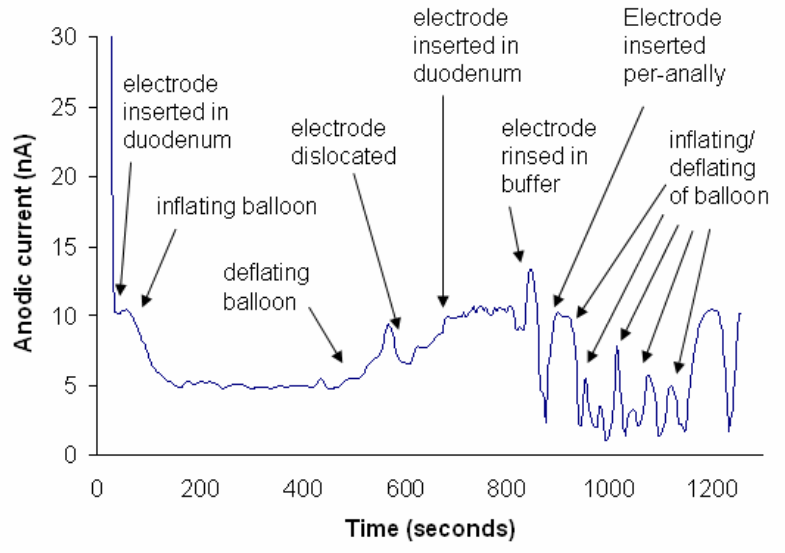

Figure 7.3: Current responses of PCU-OH coated needle-type electrodes towards oxygen in the duodenal and anal wall with and without induced alteration of local oxygen circulation utilising balloon-like construct (vs. stainless steel as pseudo-reference)

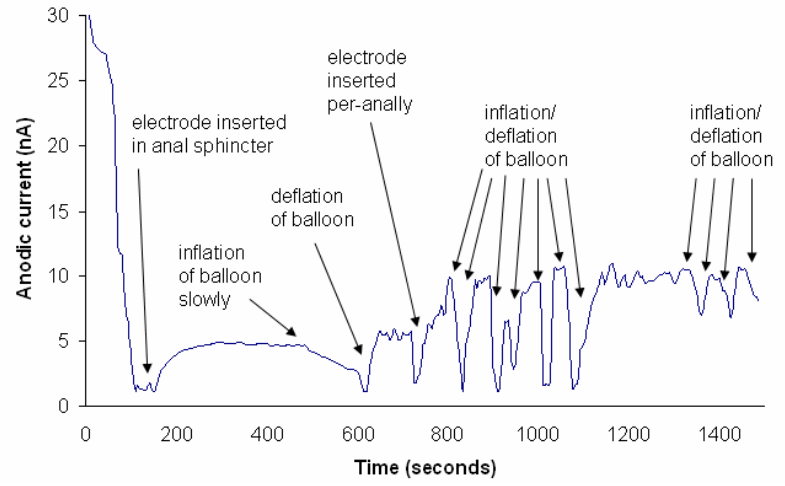

Figure 7.4: Current respnses of PCU-OH coated neeedle-type electrodes towards oxygen per anally with and without induced alteration of local oxygen circulation utilising balloon-like construct (vs. stainless steel as pseudo-reference)

showed that the electrode was functioning and responded quickly. The duodenal walls in rats are extremely thin (about 0.5 mm) even when undistended. However, the needle did not puncture the walls (confirmed by Dr. Ivan Hoh via dissection) and current responses showed stable readings. Furthermore, every change in the positioning of the needle caused an immediate current change.

Overall, the results suggested that the electrode, despite of the relatively large size, was suitable for these type of measurements. PCU-OH as coating material for the electrode showed good analytical performance. Furthermore, the area of the electrode around the polymer coating was examined unter a microscope and showed no signs of rupture.

Experiment Part 2:

This section focused on using the light-activated PSD palladium bacteriophosphorbide (WST09, Tookad) in electrochemical measurements. This drug does consume oxygen and when exposed to light the oxygen consumption increases. Local oxygenation changes in tissue induced by WST09 are monitored by measuring pO_2 [Woodhams *et al.* (2004)]. It was expected that pO_2 would decrease after drug injection during light delivery and would rise up again after illumination, which would be noticable with current changes.

The drug was administered by tail vein injection before the electrode was inserted peranally and the light was delivered with a diffusive fibre. In this section, it was focused on the anal wall with and without inflation of the balloon-like construct for induced changes in pO_2 circulation. Figure 7.5 shows the current responses due to induced oxygen variation during PSD usage.

The current response showed a subtle decrease and a further sharper decrease when the balloon was inserted. This was consistent with oxygen being reduced in the vicinity of the electrode. The current stabilised and after the balloon was removed, it increased again. During illumination, current decreased gradually over the whole illumination time. After illumination, the current continued to decrease before showing signs of plateauing out. This was possibly due to further oxygen consumption caused by residual drug. However, overall current responses were noisy and fluctuating. The area in which the needle was inserted was dissected (undertaken by Dr. Ivan Hoh) and it was confirmed that the electrode had not punctured through the intestinal wall.

Overall, the electrode appeared to follow expected trends. For further investigations, a correlation between actual and assumed pO_2 especially during PSD usage would be

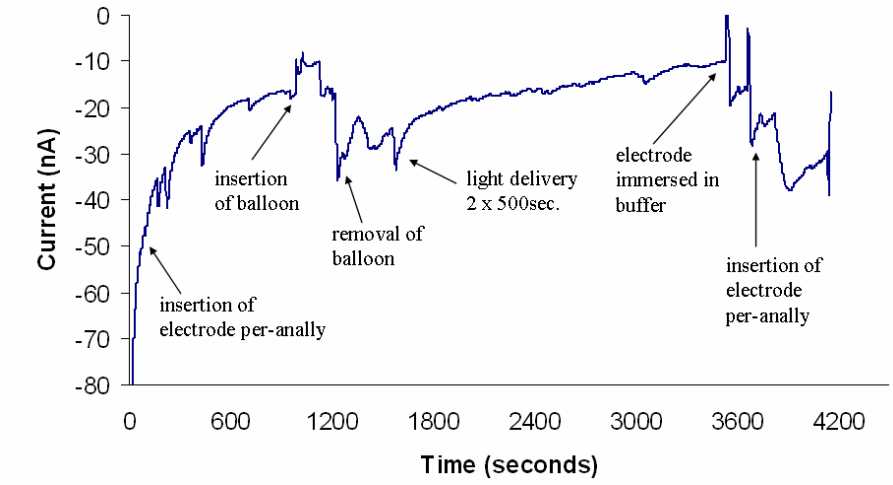

Figure 7.5: Current responses of PCU-OH coated needle-type electrodes to induced tissue pO_2 changes during experiments using balloon-like construct and light-activated PSD WST09; current recordings are shown before and after light delivery (vs. stainless steel as pseudo-reference)
Experimental settings: Light: 500 sec./200 mV; Total energy: 100 Joule; Weight of experimental rat: 195 g; Drug: 2.5 mg/ml WST09; Oxygen supply: 3 l/min. O_2 plus 3 l/min. Halothane

of interest. For this, an independent measurement would be needed, but is difficult to achieve in tissue.

References

Abe, J., & Berk, B.C. (1999). Fyn and JAK2 mediate Ras activation by reactive oxygen species. *Journal of Biological Chemistry* **274**, 21003–21010.

Absolom, D.R., Zingg, W., Van Oss, C.J. & Neumann, A.W. (1984). Protein and platelet interactions with polymer surfaces. *Biomaterials, Medical Devices, and Artificial Organs* **12**, 235–266.

Albery, W.J., Brooks, W.N., Gibson, S.P. & Hahn, C.E. (1978). An electrode for pN_2O and pO_2 analysis in blood and gas. *Journal of Applied Physiology* **45**, 637–643.

Aussedat, B., Dupire-Angel, M., Gifford, R., Klein, J.C., Wilson, G.S. & Reach, G. (2000). Interstitial glucose concentration and glycemia: implications for continuous subcutaneous glucose monitoring. *American Journal of Physiology, Endocrinology and Metabolism* **278**, E716–728.

Bae, J.Y., Chung, D.J., An, J.H. & Shin, D.H. (1999). Effect of the structure of chain extenders on the dynamic mechanical behaviour of polyurethane. *Journal of Materials Science* **34**, 2523–2527.

Bai, J., Rodriguez, A., Melendez, J. & Cederbaum, A. (1999). Overexpression of Catalase in Cytosolic or Mitochondrial Compartment Protects HepG2 Cells against Oxidative Injury. *Journal of Biological Chemistry* **274**, 26217–26224.

Bamford, C.H. & Al-Lamee, K.G. (1994). Polymer surface functionalisation and grafting by a simple and inexpensive method. *Macromolecular Rapid Communications* **15**, 379–384.

Bamford, C.H. & Al-Lamee, K.G. (1996). Studies in polymer surface modification and grafting for biomedical uses: 2. Application to arterial blood filters and oxygenators. *Polymer* **37**, 4885–4889.

Bard, A.J. & Faulkner, L.R. (2001). *Electrochemical Methods: Fundamentals and Applications*. John Wiley & Sons: New York.

Basmadjian, D., Sefton, M.V. & Baldwin, S.A. (1997). Coagulation on biomaterials in flowing blood: Some theoretical considerations. *Biomaterials* **18**, 1511–1522.

Batich, C., DePalma, D., Marotta, J. & Latorre, G. (1996). Silicone degradation reactions. *Current Topics in Microbiology and Immunology* **210**, 13–23.

Bélanger, M.C., Marois, Y., Roy, R., Mehri, Y., Wagner, E., Zhang, Z., King, M.W., Yang, M., Hahn, C. & Guidoin, R. (2000). Selection of a polyurethane membrane for the manufacture of ventricles for a totally implantable artificial heart: blood compatibility and biocompatibility studies. *Artificial Organs* **24**, 879–888.

Bellamy, K., Limbert, G., Waters, M.G. & Middleton, J. (2003). An elastomeric material for facial prostheses: synthesis, experimental and numerical testing aspects. *Biomaterials* **24**, 5061–5066.

Beriet, C. & Pletcher, D. (1993). A microelectrode study of the mechanism and kinetics of the ferro/ferricyanide couple in aqueous media: The influence of the electrolyte and its concentration. *Journal of Electroanalytical Chemistry* **361**, 93–101.

Blinks, L.R. & Skow, R.K. (1938). The time course of photosynthesis as shown by a rapid electrode method for oxygen. *Proceedings of the National Academy of Sciences of the United States of America* **24**, 420–427.

Boretos, J.W., & Pierce, W.S. (1967). Segmented polyurethane: A new elastomer for biomedical applications. *Science* **158**, 1481–1482.

Boretos, J.W. & Pierce, W.S. (1968). Segmented polyurethane: A polyether polymer. An initial evaluation for biomedical applications. *Journal of Biomedical Material Research* **2**, 121–130.

Bott, A.W. (1997). Practical Problems in Voltammetry: 4. Preparation of Working Electrodes. *Current Separations* **16**, 1–5.

Bower, D.I. & Maddams, W. F. (1992). *The vibrational spectroscopy of polymers*. *Cambridge Solid State Science Series*, Cambridge University Press: Cambridge.

Burke, J. (1984). *Solubility Parameters: Theory and Application*. The Book and Paper Group Annual, Volume Three: Conservation OnLine Document Library.

Bushman, J.A. (1975). The Measurement of oxygen concentration in respirable gas mixtures. *Oxygen Measurements in Biology and Medicine*. Eds. Payne, J.P. & Hill, D.W., Butterworths: London. 315–330.

Capek, I. (2005). Nature and properties of ionomer assemblies II. *Advances in Colloid and Interface Science***118**, 73–112.

Carapuça, H.M. & Simão, J.E.J. (1993). Square wave voltammetry at a glassy carbon electrode: The anodic oxidation of uric acid in phosphate buffer pH 6.9. *Portugaliae Electrochimica Acta* **11**, 47.

Carr, J. & Brown, J. (2000). *Introduction to Biomedical Equipment Technology, 4th Edition*. Prentice Hall: New Jersey.

Castner, D.G. & Ratner, B.D. (2002). Biomedical surface science: Foundations to frontiers. *Surface Science* **500**, 28–60.

Cavazzoni, M., Barogi, S., Baracca, A., Castelli, G. & Lenaz, G. (1999). The effect of aging and an oxidative stress on peroxide levels and the mitochondrial membrane potential in isolated rat hepatocytes. *FEBS Letters* **449**, 53–56.

Chaubey, A. & Malhotra, B.D. (2002). Mediated biosensors. *Biosensors and Bioelectronics* **17**, 441–456.

Chen, H., Zhang, Z., Chen, Y., Brook, M.A. & Sheardown, H. (2005). Protein repellant silicone surfaces by covalent immobilization of poly(ethylene oxide). *Biomaterials* **26**, 2391–2399.

Christensen, P., Hamnett, A. & Trevellick, P. (1998). In-situ infra-red studies in electrochemistry. *Journal of Electroanalytical Chemistry* **242**, 23–45.

Christenson, E.M., Anderson, J.M. & Hiltner, A. (2004a). Oxidative mechanisms of poly(carbonate urethane) and poly(ether urethane) biodegradation: *in vivo* and *in vitro* correlations. *Journal of Biomedical Materials Research* **70**, 245–255.

Christenson, E.M., Dadsetan, M., Wiggins, M., Anderson, J.M. & Hiltner, A. (2004b). Poly(carbonate urethane) and poly(ether urethane) biodegradation: *in vivo* studies. *Journal of Biomedical Materials Research* **69**, 407–416.

Chung, D. & Kim, T.G. (2007). Study on the effect of platinum catalyst for the synthesis of polydimethylsiloxane grafted with polyoxyethylene. *Journal of Industrial and Engineeing Chemistry* **13**, 571–577.

Ciba-Geigy (1981). Geigy Scientific Tables: Units of Measurement, Body Fluids, Composition of the Body, Nutrition. In *Geigy Scientific Tables, Ciba-Geigy Corporation, Medical Education Division*, Ed. Lentner, C., 296.

Clark, L.C. (1956). Monitor and control of blood and tissue oxygen tensions. *ASAIO Journal* **2**, 42–48.

Clement, M.V., Ponton, A. & Pervaiz, S. (1998). Apoptosis induced by hydrogen peroxide is mediated by decreased superoxide anion concentration and reduction of intracellular milieu. *FEBS Letters* **440**, 13–18.

Coates, J. (2000). Interpretation of Infrared Spectra, A Practical Approach. *Encyclopedia of Analytical Chemistry*, Ed. Meyers, R.A., John Wiley & Sons Ltd: Chichester. 10815–10837.

Compañ, V., Tiemblo, P. García, F. García, J.M. Gusmán, J. & Riande, E. (2005). A potentiostatic study of oxygen transport through poly (2-ethoxyethyl methacrylate-co-2,3-dihydroxypropylmethacrylate) hydrogel membranes. *Biomaterials* **26**, 3783–3791.

Cooper, S.L. & Peppas, N.A. (1982). *Biomaterials: Interfacial Phenomena and Applications. Advances in Chemistry Series 199*, American Chemical Society: Washington, D.C.

Cooper, S.L. & Tobolsky, A.V. (1966). Properties of linear elastomeric polyurethanes. *Journal of Applied Polymer Science* **10**, 1837.

Costerton, J.W., Montanaro, L. & Arciola, C.R. (2005). Biofilm in implant infections: its production and regulation. *International Journal of Artificial Organs* **28**, 1062–1068.

Cross, A.D. & Jones, R.A. (1969). *An introduction to practical infra-red spectroscopy*. Butterworths: London.

Crow, D.R. (1988). *Principles and Applications of Electrochemistry*. Chapman and Hall Ltd: London.

Curulli, A., Valentini, F., Orlanduci, S., Terranova, M.L. & Palleschi, G. (2004). Pt based enzyme electrode probes assembled with Prussian Blue and conducting polymer nanostructures. *Biosensors and Bioelectronics* **20**, 1223–1232.

Danneel, H. & Nernst, W. (1897). The electrochemical reduction of oxygen. *Zeitschrift fuer Elektrochemie* **4**, 227.

Davies, M.L., Hamilton, C.J., Murphy, S.M. & Tighe, B.J. (1992). Polymer membranes in clinical sensor applications. *Biomaterials* **13**, 971–978.

de Groot, H. & Littauer, A. (1989). Hypoxia, reactive oxygen, and cell injury. *Free Radical Biology and Medicine* **6**, 541–551.

de Mattos, I.L., Gorton, L., Laurell, T., Malinauskas, A. & Karyakin, A.A. (2000a). Development of biosensors based on hexacyanoferrates. *Talanta* **52**, 791–799.

de Mattos, I.L., Gorton, L. & Ruzgas, T. (2003). Sensor and biosensor based on Prussian Blue modified gold and platinum screen printed electrodes. *Biosensors and Bioelectronics* **18**, 193–200.

de Mattos, I.L., Gorton, L., Ruzgas, T. & Karyakin, A.A. (2000b). Sensor for hydrogen peroxide based on Prussian Blue modified electrode: improvement of the operational stability. *Analytical Sciences* **16**, 1–5.

DeFife, K.M., Shive. M.S., Hagen, K.M., Clapper, D.L. & Anderson, J.M. (1999). Effects of photochemically immobilized polymer coatings on protein adsorption, cell adhesion, and the foreign body reaction to silicone rubber. *Journal of Biomedical Materials Research* **44**, 298–307.

Dewanjee, M.K., Kapadvanjwala, M., Sanchez, A., Elson, R., Serafini, A.N., Zilleruelo, G.E. & Sfakianakis, G.N. (1992). Quantitation of comparative thrombogenicity of dog, pig, and human platelets in a hemodialyzer. *ASAIO Journal* **38**, 88–90.

Di Simplicio, P., Cheeseman, K.H. & Slater, T.F. (1991). The reactivity of the SH group of bovine serum albumin with free radicals. *Free Radical Research Communications* **14**, 253–262.

Donaldson, P.E.K. (1991). Aspects of silicone rubber as an encapsulant for neurological prostheses. Part 1: Osmosis. *Medical & Biological Engineering & Computing* **29**, 34–39.

Donaldson, P.E.K. & Aylett, B.J. (1995). Aspects of silicone rubber as encapsulant for neurological prostheses. Part 2: Adhesion to binary oxides. *Medical & Biological Engineering & Computing* **33**, 289–292.

Donaldson, P.E.K. (1997). Aspects of silicone rubber as encapsulant for neurological prostheses. Part 4: Two-part rubbers. *Medical & Biological Engineering & Computing* **35**, 283–286.

Drazic, D.M., Tripkovic, A.V., Popovic, K.D. & Lovic, J.D. (1999). Kinetic and mechanistic study of hydroxyl ion electrosorption at the Pt(111) surface in alkaline media. *Journal of Electroanalytical Chemistry* **466**, 155–164.

Duncan, J.F. & Wrigley, P.W.R. (1963). The electronic structure of the iron atoms in complex iron cyanides. *Journal of Chemical Society* **206**, 1120–1125.

El-Kalay, M.A. & Gilchrist, T. (1987). Design and fabrication of laboratory-scale membrane separation units. *Medical & Biological Engineering & Computing* **25**, 650–

654.

Elbert, D.L. & Hubbell, J.A. (1996). Surface treatments of polymers for biocompatibility. *Annual Review of Materials Science* **26**, 365–394.

Ellerbe, P., Cohen, A., Welch, M.J. & White, E.T. (1988). The stability of uric acid in ammonium hydroxide. *Clinical Chemistry* **34**, 2280–2282.

Ellis, D. Eckhoff, M. & Neff, V.D. (1981). Electrochromism in the mixed-valence hexacyanides. 1. Voltammetric and spectral studies of the oxidation and reduction of thin films of Prussian Blue. *Journal of Physical Chemistry* **85**, 1225–1231.

Emery, S.B., Hubbley, J.L. & Roy, D. (2005). Time resolved impedance spectroscopy as a probe of electrochemical kinetics: The ferro/ferricyanide redox reaction in the presence of anion adsorption on thin film gold. *Electrochimica Acta* **50**, 5659–5672.

Ernst, H. & Knoll, M. (2001). Electrochemical characterisation of uric acid and ascorbic acid at a platinum electrode. *Analytica Chimica Acta* **449**, 129–134.

Finch, J.W., Crouch, R.K., Knapp, D.R. & Schey, K.L. (1993). Mass spectrometric identification of modifications to human serum albumin treated with hydrogen peroxide. *Archives of Biochemistry and Biophysics* **305**, 595–599.

Fisher, A.C. (1993). *Electrode Dynamics*. *Oxford Chemistry Primers*, Oxford University Press: Oxford.

Fried, J.R. (2003). Conformation, Solutions and Molecular Weight. In *Polymer Science and Technology*, Ed. Fried, J.R., Prentice Hall: New Jersey. 87–151.

Frost, M.C., Reynolds, M.M. & Meyerhoff, M.E. (2005). Polymers incorporating nitric oxide releasing/generating substances for improved biocompatibility of blood-contacting medical devices. *Biomaterials* **26**, 1685–1693.

Ganguli, S. & Bhattacharya, M. (1983). Studies of different hydrated forms of Prussian Blue. *Journal of the Chemical Society, Faraday Transactions 1* **79**, 1513–1522.

Garjonyte, R. & Malinauskas, A. (1999). Operational stability of amperometric hydrogen peroxicde sensors, based on ferrous and copper hexacyanoferrates. *Sensors and Actuators B* **56**, 93–97.

Gifford, R., Kehoe, J.J., Barnes, S.L., Kornilayev, B.A., Alterman, M.A. & Wilson, G.S. (2006). Protein interactions with subcutaneously implanted biosensors. *Biomaterials* **27**, 2587–2598.

Gong, P. & Szleifer, I. (2004). Competitive adsorption of model charged proteins: the

effect of total charge and charge distribution. *Journal of Colloid and Interface Science* **278**, 81–90.

Gough, D.A. & Leypoldt, J.K. (1980). Rotated, membrane-covered oxygen electrode. *Analytical Chemistry* **52**, 1126–1130.

Goyal, R.N., Brajter-Toth, A. & Dryhurst, G. (1982). Futher insights into the electrochemical oxidation of uric acid. *Journal of Electroanalytical Chemistry* **131**, 181–202.

Green, R.J., Davies, J., Davies, M.C., Roberts, C.J. & Tendler, S.J. (1997). Surface plasmon resonance for real time in situ analysis of protein adsorption to polymer surfaces. *Biomaterials* **18**, 405–413.

Greenbaum, A., Etherington, P., Manek, S., O'Hare, D., Parker, K., Green, C., Pepper, J. & Winlove, C. (1997). Measurements of oxygenation and perfusion in skeletal muscle using multiple microelectrodes. *Journal of Muscle Research and Cell Motility* **18**, 149–159.

Guignot, C., Betz, N., Legendre, B., Le Moel, A. & Yagoubi, N. (2001). Degradation of segmented poly (etherurethane) Tecoflex induced by electron beam irradiation: Characterization and evaluation. *Nuclear Instruments and Methods in Physics Research B: Beam Interactions with Materials and Atoms* **185**, 100–107.

Gupta, T. & Adhikari, B. (2003). Thermal degradation and stability of HTPB-based polyurethane and polyurethaneureas. *Thermochimica Acta* **402**, 169–181.

Haghighi, B., Varma, S.D., Alizadeh Sh., F.M. Yigzaw, Y. & Gorton, L. (2004). Prussian Blue modified glassy carbon electrodes - study on operational stability and its application as a sucrose biosensor. *Talanta* **64**, 3–12.

Hahn, C.E.W. (1980). Techniques for measuring the partial pressures of gases in the blood. I: *in vitro* measurements. *Journal of Physics E, Scientific Instruments* **13**, 470–482.

Hahn, E. (1998). Electrochemical analysis of clinical blood-gases, gases and vapours. *Analyst* **123**, 57R–86R.

Hall, S.B. Khudaish, E.A. & Hart, A.L. (1998a). Electrochemical oxidation of hydrogen peroxide at platinum electrodes. Part 1. An adsorption-controlled mechanism. *Electrochimica Acta* **43**, 579–588.

Hall, S.B. Khudaish, E.A. & Hart, A.L. (1998b). Electrochemical oxidation of hydrogen peroxide at platinum electrodes. Part II: effect of potential. *Electrochimica Acta*

43, 2015–2024.

Halliwell, B., Clement, M.V. & Long, L.H. (2000). Hydrogen peroxide in the human body. *FEBS Letters* **486**, 10–13.

Herren, F. Fisher, P. Ludi, A. & Halg, W. (1980). Neutron diffraction study of Prussian Blue, $Fe_4[Fe(CN)_6]_3$ x H_2O. Location of water molecules and long-range magnetic order. *Inorganic Chemistry* **19**, 956–959.

Hetrick, E.M. & Schoenfisch, M.H. (2006). Reducing implant-related infections: active release strategies. *Chemical Society Reviews* **35**, 780–789.

Hickling, A. & Wilson, W.H. (1951). The anodic decomposition of hydrogen peroxide. *Journal of Electrochemical Society* **98**, 425–433.

Higgins, S.W., Gregory, C.M., Hatfield, J.V., Iacovides, H. & Vadgama, P. (1999). One-dimensional modelling of foulant reduction in a microflow, amperometric-sensor system. *Journal of Medical Engineering and Technology* **23**, 102–107.

Hill, S.S., Shaw, B.R. & Wu, A.H.B. (2003). Plasticizers, antioxidants, and other contaminants found in air delivered by PVC tubing used in respiratory therapy. *Biomedical Chromatography* **17**, 250–262.

Hirose, S., Shimizu, A. & Nose, T. (1979). Preparation and structures of the poly(vinyl chloride) porous membranes. *Journal of Applied Polymer Science* **23**, 3193–3204.

Ho, K.C., Hung, W.T. & Yang, J.C. (2003). On the electrooxidation and amperometric detection of NO gas at the Pt/Nafion electrode. *Sensors* **3**, 290–303.

Hoare, J.P. (1968). *The Electrochemistry of Oxygen*. Wiley: New York.

Hoffmann, A.S. (2002). Hydrogels for biomedical applications. *Advanced Drug Delivery Reviews* **43**, 3–12.

Howell, J.O. (1987). Voltammetric Microelectrodes.Current Separations **8**, 2–14.

Hron, P. (2003). Hydrophilisation of silicone rubber for medical applications. *Polymer International* **52**, 1531–1539.

Hu, S.W. Ren, X.Q. Bachman, M. Sims, C.E. Li, G.P. & Albritton, N. (2002). Surface modification of poly(dimethylsiloxane) microfluidic devices by ultraviolet polymer grafting. *Analytical Chemistry* **74**, 4117–4123.

Huang, S.L. & Lai, J.Y. (1997). Structure-tensile properties of polyurethanes. *European Polymer Journal* **33**, 1563–1567.

Huang, S.L., Ou, C.F. & Lai, J. Y. (1999). Polyurethane membrane preparation via dry/wet phase inversion method for protein adsorption. *Journal of Applied Poly-*

mer Science **74**, 1334–1340.

Huang, W. & McCreery, R. (1992). Electron transfer kinetics of $Fe(CN)_6^{3-/4-}$ on laser-activated and CN-modified Pt electrodes. *Journal of Electroanalytical Chemistry* **326**, 1–12.

Hunt, J.A., Flanagan, B.F., McLaughlin, P.J., Strickland, I. & Williams, D.F. (1996). Effect of biomaterial surface charge on the inflammatory response: evaluation of cellular infiltration and TNF alpha production. *Journal of Biomedical Materials Research* **31**, 139–144.

Imisides, M.D., John, R. & Wallace, G.G. (1996). Microsensors based on conducting polymers. *Chemtech* **26**, 19–25.

Ishihara, K., Nomura, H., Mihara, T., Kurita, K., Iwasaki, Y. & Nakabayashi, N. (1998). Why do phospholipid polymers reduce protein adsorption? *Journal of Biomedical Materials Research* **39**, 323–330.

Itaya, K. Ataka, T. & Toshima, S. (1982). Spectroelectrochemistry and electrochemical preparation method of Prussian Blue modified electrodes. *Journal of American Chemical Society* **104**, 4767–4772.

Itaya, K. Shoji, N. & Uchida, I. (1984). Catalysis of the reduction of molecular oxygen to water at Prussian Blue modified electrodes. *Journal of American Chemical Society* **106**, 2423–2429.

Itaya, K. Uchida, I. & Neff, V.D. (1986). Electrochemistry of polynuclear transition metal cyanides: Prussian Blue and its analogues. *Accounts of Chemical Research* **19**, 162–168.

Jenke, D. (2006). Extractable substances from plastic materials used in solution contact applications: an updated review. *PDA Journal of Pharmaceutic Scientific Technology* **60**, 191–207.

Jenkins, C.S., Packham, M.A., Guccione, M.A. & Mustard, J.F. (1973). Modification of platelet adherence to protein-coated surfaces. *The Journal of Laboratory and Clinical Medicine* **81**, 280–290.

Jeon, S.I., Lee, J.H., Andrade, J.D. & De Gennes, P.G. (1991). Protein - surface interactions in the presence of polyethylene oxide I: Simplified theory. *Journal of Colloid and Interface Science* **142**, 149–158.

Jiang, Y., Rongbing, B., Ling, T., Jian, S. & Sicong, L. (2004). Blood compatibility of polyurethane surface grafted copolymerization with sulfobetaine monomer.

Colloids and Surfaces B: Biointerfaces **36**, 27–33.

Johnson, K. & Sawyer, D. (1974). The electrochemical reduction of nitrous oxide in alkaline solution. *Journal of Electroanalytical Chemistry* **49**, 95–103.

Johnston, D.A. Cardosi, M.F. & Vaughan, D.H. (1995). The elecctrochemistry of hydrogen peroxide on evaporated gold/palladium composite electrodes. Manufacture and electrochemical characterization. *Electroanalysis* **7**, 520–526.

Karyakin, A.A. (2001). Prussian Blue and its analogues: Electrochemistry and analytical applications. *Electroanalysis* **13**, 813–819.

Karyakin, A.A., Gitelmacher, O.V. & Karyakina, E.E. (1994). A high-sensitive glucose amperometric biosensor based on Prussian Blue modified electrodes. *Analytical Letters* **27**, 2861–2869.

Karyakin, A.A., Gitelmacher, O.V. & Karyakina, E.E. (1995). Prussian Blue-based first-generation biosensor. A sensitive amperometric electrode for glucose. *Analytical Chemistry* **67**, 2419–2423.

Karyakin, A., Karyakina, E. & Gorton, L. (2000). Amperometric biosensor for glutamate using prussian blue-based "artificial peroxidase" as a transducer for hydrogen peroxide. *Analytical Chemistry* **72**, 1720–1723.

Karyakin, A., Karyakina, E. & Gorton, L. (1999). On the mechanism of H_2O_2 reduction at Prussian Blue modified electrodes. *Electrochemistry Communications* **1**, 78–82.

Karyakin, A.A., Puganova, E.A., Budashov, I A., Kurochkin, I.N., Karyakina, E.E., Levchenko, V.A., Matveyenko, V.N. & Varfolomeyev, S.D. (2004). Prussian Blue based nanoelectrode arrays for H_2O_2 detection. *Analytical Chemistry* **76**, 474–478.

Keggin, J.F. & Miles, F.D. (1936). Structures and formulae of the Prussian Blues and related compounds. *Nature* **3466**, 577–578.

Kellawi, H. Rosseinsky, D.R. (1982). Electrochemical bichromic behaviour of ferric ferrocyanide (Prussian Blue) in thin film redox processes. *Journal of Electroanalytical Chemistry* **131**, 373–376.

Kennan, J.J., Peters, Y.A., Swarthout, D.E., Owen, M.J., Namkanisorn, A. & Chaudhury, M.K. (1997). Effect of saline exposure on the surface and bulk properties of medical grade silicone elastomers. *Journal of Biomedical Materials Research, Part A* **36**, 487–497.

Keogh, J.R., Wolf, M.F., Overend, M.E., Tang, L. & Eaton, J. W. (1996). Biocompatibility of sulphonated polyurethane surfaces. *Biomaterials* **17**, 1987–1994.

Kim, Y.H., Han, D.K., Park, K.D. & Kim, S.H. (2003). Enhanced blood compatibility of polymers grafted by sulfonated PEO via a negative cilia concept. *Biomaterials* **24**, 2213–2223.

Kiremitçi, M., Pulat, M., Senvar, C., Serbetçi, A.I. & Piskin, E. (1990). Structural and cellular characterization of solvent-casted polyurethane membranes. *Clinical Materials* **6**, 227–237.

Koberstein, J.T. & Russell, T. (1986). Simultaneous SAXS-DSC study of multiple endothermic behavior in polyether-based polyurethane block copolymers. *Macromolecules* **19**, 714–720.

Kocha, T., Yamaguchi, M., Ohtaki, H., Fukuda, T. & Aoyagi, T. (1997). Hydrogen peroxide-mediated degradation of protein: different oxidation modes of copper- and iron-dependent hydroxyl radicals on the degradation of albumin. *Biochimica et Biophysica Acta* **1337**, 319–326.

Kokoh, K.B. Hahn, F. Métayer, A. & Lamy, C. (2002). FTIR spectroelectrochemical investigation of the electrocatalytic oxidation of ascorbic acid at platinum electrodes in acid medium. *Electrochimica Acta* **47**, 3965–3969.

Konopka, S.J. & McDuffie, B. (1970). Diffusion coefficients of ferri- and ferrocyanide ions in aqueous media, using twin-electrode thin-layer electrochemistry. *Analytical Chemistry* **42**, 1741–1746.

Korematsu, A., Takemoto, Y., Nakaya, T. & Inoue, H. (2002). Synthesis, characterization and platelet adhesion of segmented polyurethanes grafted phospholipid analogous vinyl monomer on surface. *Biomaterials* **23**, 263–271.

Krauskopf, L.G. & Godwin, A. (2005). Plasticizers. In *PVC Handbook*, Eds. Wilkes, C.E., Summers, J.W. & Daniels, C.A., Carl Hanser Verlag: Munich. 179–200.

Kruczek, B. & Matsuura, T. (2003). Effect of solvent on properties of solution-cast dense SPPO films. *Journal of Applied Polymer Science* **88**, 1100–1110.

Kunimatsu, K., Shigematsu, Y., Uosaki, K. & Kita, H. (1989). Study of the $Fe(CN)_6^{3-}$ / $Fe(CN)_6^{4-}$ redox system on Pt by EMIRS : Part I. Infrared spectra of the intermediates in the charge transfer. *Journal of Electroanalytical Chemistry* **262**, 195–209.

Labarre, D.J. (1990). Heparin-like polymer surfaces: control of coagulation and comple-

ment activation by insoluble functionalized polymers. *The International Journal of Artificial Organs* **13**, 651–657.

Lacy, F., Gough, D. & Schmid-Schoenbein, G. (1998a). Role of Xanthine Oxidase in Hydrogen Peroxide Production. *Free Radical Biological Medicine* **25**, 720–727.

Lacy, F., O'Connor, D. & Schmid-Schoenbein, G. (1998b). Plasma hydrogen peroxide production in hypertensives and normotensive subjects at genetic risk of hypertension. *Journal of Hypertension* **16**, 291–303.

Lamba, N.M.K., Woodhouse, K.A. & Cooper, S.L. (1998). *Polyurethanes in Biomedical Applications*. CRC Press: New York.

Lee, I., Bender, E. & Kadenbach,B. (2002). Control of mitochondrial membrane potential and ROS formation by reversible phosphorylation of cytochrome c oxidase. *Molecular Cell Biochemistry* **234–235**, 63–70.

Lee, Y., Combe, C., Kumar, M., Wang, Y., Riley, R. & Clark, M.M. (2000). Characterization and fouling of SPEES/PES-PS UF membranes. *11th Annual Meeting of the North American Membrane Society*, Boulder, Colorado

Lelah, M.D., Grasel, T.G., Pierce, J.A. & Cooper, S.L. (1986). Ex vivo interactions and surface property relationships of polyetherurethanes. *Journal of Biomedical Materials Research* **20**, 433–468.

Lelah, M.D., Pierce, J.A., Lambrecht, L.K. & Cooper, S.L. (1985). Polyether-urethane ionomers: Surface property-ex vivo blood compatibility relationships. *Journal of Colloid and Interface Science* **104**, 422–439.

Lewis, A.L. (2000). Phosphorylcholine-based polymers and their use in the prevention of biofouling. *Colloids and Surfaces B: Biointerfaces* **18**, 261–275.

Li, Y.J., Nakaya, T., Zhang, Z. & Kodama, M. (1997). Blood compatible phospholipid-containing polyurethanes: synthesis characterization and blood compatibility evaluation. *Journal of Biomaterials Application* **12**, 167–191.

Li, Y.J., Yokawa, T., Matthews, K.H., Chen, T.M., Wang, Y.F., Kodama, M. & Nakaya, T. (1996). Synthesis and blood compatibility evaluation of segmented polyurethanes based on cholesterol and phosphatidylcholine analogous moieties. *Biomaterials* **17**, 2179–2189.

Lin, D.T., Young, T.H. & Fang, Y. (2001). Studies on the effect of surface properties on the biocompatibility of polyurethane membranes. *Biomaterials* **22**, 1521–1529.

Lindner, E., Cosofret, V.V., Ufer, S., Buck, R.P., Kao, W.J., Neuman, M.R. & Ander-

son, J.M. (1994). Ion-selective membranes with low plasticizer content: electroanalytical characterization and biocompatibility studies. *Journal of Biomedical Materials Research* **28**, 591–601.

Liston, E.M. Martinu, L. & Wertheimer, M.R. (1994). Plasma surface modification of polymers for improved adhesion: a critical review. *Plasma Surface Modifications of Polymers: Relevance to Adhesion* In *VSP*, NL-Utrecht Ed. M. Strobel, C. Lyons and K. L. Mittal, 3–39.

Liu, S. (1997). Generating, partitioning, targeting and functioning of superoxide in mitochondria. *Bioscience Reports* **17**, 259–272.

Liu, S.J., Shen, H.X. & Feng, J.X. (1995). Effects of gas flow-rates on a Clark-type oxygen gas sensor. *Analytica Chimica Acta* **313**, 89–92.

Loetters, J.C., Olthuis, W., Veltink, P.H. & Bergveld, P. (1997). The mechanical properties of the rubber elastic polymer polydimethylsiloxane for sensor applications. *Journal of Micromechanics and Microengineering* **7**, 145–147.

Loff, S., Subotic, U., Reinicke, F., Wischmann, H. & Brade, J. (2004). Extraction of Di-ethylhexyl-phthalate from Perfusion Lines of Various Material, Length and Brand by Lipid Emulsions. *Journal of Pediatric Gastroenterology and Nutrition* **39**, 341–345.

Lowry, J.P. & O'Neil, R.D. (1992). Homogeneous mechanism of ascorbic acid interference in hydrogen peroxide detection at enzyme-modified electrodes. *Analytical Chemistry* **64**, 453–456.

Ludi, A. & Gudel, H.U. (1973). Structural chemistry of polynuclear transition metal cyanides. In *Structure and Bonding*, Springer Verlag: Berlin. **14**, 1–22.

Lukachova, L.V., Kotel'nikova, E.A., D'Ottavi, D., Shkerin, E.A., Karyakina, E.E., Moscone, D., Palleschi, G., Curuli, A. & Karyakin, A.A. (2003). Nonconducting Polymers on Prussian Blue Modified Electrodes: Improvement of Selectivity and Stability of the Advanced H_2O_2 Transducer. *IEEE Sensors Journal* **3**, 326–332.

Lyman, D.J., Knutson, K., McNeil, B. & Shibatani, K. (1975). The effects of chemical structure and surface properties of synthetic polymers on the coagulation of blood. IV: The relation between polymer morphology and protein adsorption. *ASAIO Journal* **21**, 49–54.

Lyman, D.J., Kwan-Gett, G.C., Zwart, H.H., Bland, A., Eastwood, N., Kawai, J.

& Kolff, W.J. (1971). The development and implantation of a polyurethane hemispherical artificial heart. *ASAIO Journal* **17**, 456–463.

Martz, H., Paynter, R. & Forest, J.C. (1987). Microporous hydrophilic polyurethane vascular grafts as substitutes in abdominal aorta of dogs. *Biomaterials* **8**, 3–11.

Mathur, A.B., Collier, T.O., Kao, W.J., Wiggins, M., Schubert, M.A., Hiltner, A. & Anderson, J.M. (1997). In vivo biocompatibility and biostability of modified polyurethanes. *Journal of Biomedical Materials Research* **36**, 246–257.

Mauritz, K. (1997). Nafion - Perfluorosulfonate Ionomer. *The Mauritz Research Group* , .

McCarthy, S.J., Meijs, G.F., Mitchell, N., Gunatillake, P.A., Heath, G., Brandwood, A. & Schindhelm, K. (1997). In-vivo degradation of polyurethanes: transmission-FTIR microscopic characterization of polyurethanes sectioned by cryomicrotomy. *Biomaterials* **18**, 1387–1409.

McClelland, J.F., Jones, R.W. & Bajic, S.J. (2002). *Handbook of Vibrational Spectroscopy – Volume 2*. Eds. Chalmers, J.M. & Griffiths, P.R., John Wiley & Sons, Ltd: Chichester.

McNaught, A. & IUPAC (1997). *Compendium of Chemical Terminology - IUPAC Recommendations, 2nd Edition*. Eds. McNaught, A. & Wilkinson, A., Blackwell Science: Oxford.

Miller, J.A., Lin, S.B., Hwang, K.K.S., Wu, K.S., Gibson, P.E. & Cooper, S.L. (1985). Properties of Polyether-Polyurethane Block Copolymers: Effects of Hard Segment Length Distribution. *Macromolecules* **18**, 32–44.

Miller, J.C. & Miller, J.N. (1988). *Statistics for Analytical Chemistry*. *Ellis Horwood Series in Analytical Chemistry*, Ellis Horwood Ltd: Aberdeen.

Mirzadeh, H., Shokrolahi, F. & Daliri, M. (2003). Effect of silicon rubber crosslink density on fibroblast cell behavior in vitro. *Journal of Biomedical Materials Research, Part A* **67**, 727–732.

Mizutani, F., Yabuki, S., Sawaguchi, T., Hirata, Y., Sato, Y. & Iijima, S. (2001). Use of a siloxane polymer for the preparation of amperometric electrodes: O_2 and NO electrodes and enzyme electrodes. *Sensors and Actuators B* **76**, 489–493.

Mohr, J.M. & Paul, D.R. (1991). Effect of casting solvent on the permeability of poly(4-methyl-1-pentene). *Polymer* **32**, 1236–1243.

Moore, S. (1968). Amino acid analysis: aqueous dimethyl sulfoxide as solvent for the

ninhydrin reaction. *Journal of Biological Chemistry* **243**, 6281–6283.

Moore, S. & Stein, W.H. (1954). A modified ninhydrin reagent for the photometric determination of amino acids and related compounds. *Journal of Biological Chemistry* **211**, 907–913.

Mortimer, R.J. & Rosseinsky, D.R. (1984). Iron hexacyanoferrate films: spectroelectrochemical distinction and electrodeposition sequence of "soluble" (K^+-containing) and "insoluble" (K^+-free) Prussian Blue, and composition changes in polyelectrochromic switching. *Journal of the Chemical Society, Dalton Transactions* **9**, 2059–2062.

Morimoto, N., Watanabe, A., Iwasaki, Y., Akiyoshi, K. & Ishihara, K. (2004). Nanoscale surface modification of a segmented polyurethane with a phospholipid polymer. *Biomaterials* **25**, 5353–5361.

Morton, M. (1987). Rubber Technology. In *Kluwer Academic Publishers*, NL-AH Dortrecht Ed. M. Morton, 652.

Moscone, D., D'Ottavi, D., Compagnone, D., Palleschi, G. & Amine, A. (2001). Construction and analytical characterization of Prussian Blue based carbon paste electrodes and their assembly as oxidase enzyme sensors. *Analytical Chemistry* **73**, 2529–2535.

Mothe, C.G. & de Araújo, C.D. (2000). Properties of polyurethane elastomers and composites by thermal analysis. *Thermochimica Acta* **357-358**, 321–325.

Mowery, K.A., Schoenfisch, M.H., Saavedra, J.E., Keefer, L.K. & Meyerhoff, M.E. (2000). Preparation and characterization of hydrophobic polymeric films that are thromboresistant via nitric oxide release. *Biomaterials* **21**, 9–21.

Nagaoka, S. & Kawakami, H. (1995). Inhibition of bacterial adhesion and biofilm formation by a heparinized hydrophilic polymer. *ASAIO Journal* **41**, M365–368.

Nair, P.D., Mohanty, M., Rathinam, K., Jayabalan, M. & Krishnamurthy, V.N. (1992). Studies on the effect of degree of hydrophilicity on tissue response of polyurethane interpenetrating polymer networks. *Biomaterials* **13**, 537–542.

Narasaiah, D. (1994). An enzyme electrode for hydrogen peroxide detection based on peroxidase immobilized on a glassy carbon electrode. *Biosensors & Bioelectronics* **9**, 415–422.

Nation, J.L. (1983). A new method using hexamethyldisilazane for preparation of soft insect tissues for scanning electron microscopy. *Stain Technology* **58**, 347–351.

National Toxicology Program (1997). NTP toxicology and carcinogenesis studies of butyl benzyl phthalate (CAS No. 85-68-7) in F344/N rats. *National Toxicology Program technical report series* **458**, 1–195.

Neff, V.D. (1978). Electrochemical oxidation and reduction of thin films of Prussian Blue. *Journal of Electrochemical Society* **125**, 886–887.

Nematollahi, D. Shayani-Jam, H. Alimoradi, M. & Niroomand, S. (2009). Electrochemical oxidation of acetaminophen in aqueous solutions: Kinetic evaluation of hydrolysis, hydroxylation and dimerization processes. *Electrochimica Acta* **54**, 7407–7415.

Nohl, H., Gille, L. & Staniek, K. (2005). Intracellular generation of reactive oxygen species by mitochondria. *Biochemical Pharmacology* **69**, 719–723.

Oezdemir, T. & Usanmaz, A. (2007). Degradation of poly(carbonate urethane) by gamma irradiation. *Radiation Physics and Chemistry* **76**, 1069–1074.

Oh, B.K. & Meyerhoff, M.E. (2003). Spontaneous catalytic generation of nitric oxide from S-nitrosothiols at the surface of polymer films doped with lipophilic copperII complex. *Journal of the American Chemical Society* **125**, 9552–9553.

Okano, T., Nishiyama, S., Shinohara, I., Akaike, T., Sakurai, Y., Kataoka, K. & Tsuruta, T. (1981). Effect of hydrophilic and hydrophobic microdomains on mode of interaction between block polymer and blood platelets. *Journal of Biomedical Materials Research* **15**, 393–402.

Okkema, A.Z., Grasel, T.G., Zdrahala, R.J., Solomon, D.D. & Cooper, S.L. (1989). Bulk, surface and blood-contacting properties of polyetherurethanes modified with polyethylene oxide. *Journal of Biomaterials Science Polymer Edition* **1**, 43–62.

Okuno, H., Renzo, K. & Uragami, T. (1993). Influence of casting solution additive, degree of polymerization, and polymer concentration on poly(vinyl chloride) membrane properties and performance. *Journal of Membrane Science* **83**, 199–209.

Olander, B. Wirsen, A. & Albertsson, A.C. (2004). Oxygen microwave plasma treatment of silicone elastomer: kinetic behavior and surface composition. *Journal of Applied Polymer Science* **91**, 4098–4104.

Packham, M.A., Evans, G., Glynn, M.F. & Mustard, J.F. (1969). The effect of plasma proteins on the interaction of platelets with glass surfaces. *The Journal of Laboratory and Clinical Medicine* **73**, 686–697.

Pan, D., Chen.J., Nie, L., Tao, W. & Yao, S. (2004). Amperometric glucoes biosensor based on immobilization of glucose oxidase in electropolymerized o-aminophenol film at PB-modified platinum electrode. *Electrochimica Acta* **49**, 795–801.

Papra, A. Bernard, A. Juncker, D. Larsen, N. B. Michel, B. & Delamarche, E. (2001). Microfluidic networks made of poly(dimethylsiloxane), Si, and Au coated with polyethylene glycol for patterning proteins into surfaces. *Langmuir* **17**, 4090–4095.

Park, H.D., Lee, W.K., Ooya, T., Park, K.D., Kim, Y. H. & Yui, N. (2003). In vitro biocompatibility assessment of sulfonated polyrotaxane-immobilized polyurethane surfaces. *Journal of Biomedical Materials Research, Part A* **66**, 596–604.

Peteu, S.F., Emerson, D. & Worden, R.M. (1996). A Clark-type oxidase enzyme-based amperometric microbiosensor for sensing glucose, galactose, or choline. *Biosensors & Bioelectronics* **11**, 1059–1071.

Petrovic, S. (2000). Cyclic Voltammetry of Hexachloroiridate(IV): An alternative to the electrochemical study of the ferricyanide ion. *The Chemical Educator* **5**, 231–235.

Petrovic, Z.S., Zavargo, Z., Flyn, J. H. & Macknight, W.J. (1994). Thermal degradation of segmented polyurethanes. *Journal of Applied Polymer Science* **51**, 1087–1095.

Pharr, C.M. & Griffiths, P.R. (1997). Infrared Spectroelectrochemical analysis of adsorbed hexacyanoferrate species formed during potential cycling in the ferrocyanide/ferricyanide redox couple. *Analytical Chemistry* **69**, 4673–4679.

Picha, G.J. & Gibbons, D.F. (1978). Effect of polyurethane morphology on blood coagulation. *Journal of Bioengineering* **2**, 301–311.

Pickup, J.C., Claremont, D.J. & Shaw, G.W. (1993). Responses and calibration of amperometric glucose sensors implanted in the subcutaneous tissue of man. *Acta Diabetollogica* **30**, 143–148.

Pielichowski, K. Pielichowski, J. Altenburg, H. & Balloff, H. (1996). Thermal degradation of polyurethanes based on MDI: Characteristic relationships between the decomposition parameters. *Thermochimica Acta* **284**, 419–428.

Pinchuk, L. (1994). A review of the biostability and carcinogenicity of polyurethanes in medicine and the new generation of biostable polyurethanes. *Journal of Biomaterials Science Polymer Edition* **6**, 225–267.

Rahman, M., Brazel, C.S. (2006). Ionic liquids: New generation stable plasticizers for

poly(vinyl chloride). *Polymer Degradation and Stability* **91**, 3371–3382.

Rankl, M., Laib, S. & Seeger, S. (2003). Surface tension properties of surface-coatings for application in biodiagnostics determined by contact angle measurements. *Colloids and Surfaces B: Biointerfaces* **30**, 177–186.

Reddy, S.M. & Vadgama, P. (1997). Surfactant-modified poly(vinyl chloride) membranes as biocompatible interfaces for amperometric enzyme electrodes. *Analytica Chimica Acta* **350**, 77–89.

Ricci, F., Amine, A., Palleschi, G. & Moscone, D. (2003a). Prussian Blue based screen printed biosensors with improved characteristics of long-term lifetime and pH stability. *Biosensors and Bioelectronics* **18**, 165–174.

Ricci, F. & Palleschi, G. (2005). Sensor and biosensor preparation, optimisation and applications of Prussian Blue modified electrodes. *Biosensors and Bioelectronics* **21**, 389–407.

Ricci, F., Palleschi, G., Yigzaw, Y., Gorton, L., Ruzgas, T. & Karyakin, A.A. (2003b). Investigation of the effect of different glassy carbon materials on the performance of Prussian Blue based sensors for hydrogen peroxide. *Electroanalysis* **15**, 175–182.

Rolfe, P. (1990). In vivo chemical sensors for intensive-care monitoring. *Medical & Biological Engineering & Computing* **28**, B34–47.

Royall, J. & Ischiropoulos, H. (1993). Evaluation of 2',7'-dichlorofluorescein and dihydrorhodamine 123 as fluorescent probes for intracellular H_2O_2 in cultured endothelial cells. *Archives of Biochemistry and Biophysics* **302**, 348–355.

Sa Da Costa, V., Merrill, E.W. & Salzman, E.W. (1983). Polyurethanes as biomaterials. Assessment of blood compatibility. *Polymer Science and Technology* **23**, 231–245.

Salvemini, D., Radziszewski, W., Korbut, R. & Vane, J. (1990). The use of oxyhaemoglobin to explore the events underlying inhibition of platelet aggregation induced by NO or NO-donors. *British Journal of Pharmacology* **101**, 991–995.

Salzman, E.W., Merrill, E.W., Binder, A., Wolf, C.F., Ashford, T.P. & Austen, W.G. (1969). Protein-platelet interaction on heparinized surfaces. *Journal of Biomedical Materials Research* **3**, 69–81.

Sanchez-Adsuar, M.S. (2000). Influence of the composition on the crystallinity and adhesion properties of thermoplastic polyurethane elastomers. *International Journal*

of Adhesion and Adhesives **20**, 291–298.

Schubert, M.A., Wiggins, M.J., Anderson, J.M. & Hiltner, A. (1997a). Comparison of two antioxidants for poly(etherurethane urea) in an accelerated in vitro biodegradation system. *Journal of Biomedical Materials Research* **34**, 493–505.

Schubert, M.A., Wiggins, M.J., Anderson, J.M. & Hiltner, A. (1997b). Role of oxygen in biodegradation of poly(etherurethane urea) elastomers. *Journal of Biomedical Materials Research* **34**, 519–530.

Schubert, M.A., Wiggins, M.J., Schaefer, M.P., Hiltner, A. & Anderson, J.M. (1995). Oxidative biodegradation mechanisms of biaxially strained poly(etherurethane urea) elastomers. *Journal of Biomedical Materials Research* **29**, 337–347.

Schuettler, M. & Stieglitz, T. (2002). The combination of polyimide microtechnology and medical grade silicone allows realisation of high channel FES mini-implants. Supplementary Proceedings of the 1st FESnet Conference: Glasgow, Scotland.

Shibuya, Y., Semba, U., Okabe, H., Kambara, T. & Yamamoto, T. (1994). Primary structure of bovine Hageman factor (blood coagulation factor XII): comparison with human and guinea pig molecules. *Biochimica et Biophysica Acta* **1206**, 63–70.

Singleton, D.L. & Swinehart, J.H. (1967). A kinetic study of the hexaaquoiron(III)-hexacyanoferrate(III) complex. *Inorganic Chemistry* **6**, 1536–1539.

Skarja, G.A. & Brash, J.L. (1997). Physicochemical properties and platelet interactions of segmented polyurethanes containing sulfonate groups in the hard segment. *Journal of Biomedical Materials Research* **34**, 439–455.

Smith, R. & Pitrola, R. (2002). Influence of Casting Substrate on the Surface Free Energy of Various Polyesters. *Journal of Applied Polymer Science* **83**, 997–1008.

Sperling, C., Maitz, M.F., Talkenberger, S., Gouzy, M.F., Groth, T. & Werner, C. (2007). In vitro blood reactivity to hydroxylated and non-hydroxylated polymer surfaces. *Biomaterials* **28**, 3617–3625.

Sperling, C., Schweiss, R.B., Streller, U. & Werner, C. (2005). In vitro hemocompatibility of self-assembled monolayers displaying various functional groups. *Biomaterials* **26**, 6547–6557.

Stefan, R.I., van Staden, J.F. & Aboul-Enein, H.Y. (2001). *Electrochemical Sensors in Bioanalysis*. CRC Press: New York.

Stokes, K.B., Urbanski, P. & Upton, J. (1990). The *in vivo* auto-oxidation of polyether

polyurethane by metal ions. *Journal of Biomaterials Science Polymer Edition* **1**, 207–230.

Suda, Y., Marques, D., Kermode, J.C., Kusumoto, S. & Sobel, M. (1993). Structural characterization of heparin's binding domain for human platelets. *Thrombosis Research* **69**, 501–508.

Sun, S., Yue, Y., Huang, X. & Meng, D. (2003). Protein adsorption on blood-contact membranes. *Journal of Membrane Science* **222**, 3–18.

Szycher, M. (1999). Elastomers. *Szycher's Handbook of Polyurethanes* In *CRC Press*, Ed. M. Szycher, 696.

Szymula, M. & Narkiewicz-Michalek, J. (2003). Atmospheric and electrochemical oxidation of ascorbic acid in anionic, nonionic and cationic surfactant systems. *Colloid and Polymer Science* **281**, 1142–1148.

Takahara, A., Okkema, A.Z., Cooper, S.L. & Coury, A.J. (1991). Effect of surface hydrophilicity on ex vivo blood compatibility of segmented polyurethanes. *Biomaterials* **12**, 324–334.

Tanzi, M.C., Mantovani, D., Petrini, P., Guidoin, R. & Laroche, G. (1997). Chemical stability of polyether urethanes versus polycarbonate urethanes. *Journal of Biomedical Materials Research* **36**, 550–559.

Test, S. & Weiss, S. (1986). Assay of the extracellular hydrogen peroxide pool generated by phagocytes. *Methods in Enzymology* **132**, 401–406.

Thévenot, D.R., Toth, K., Durst, R.A. & Wilson, G.S. (2001). Electrochemical biosensors: Recommended definitions and classification. *Biosensors & Bioelectronics* **16**, 121–131.

Tickner, J.A., Schettler, T., Guidotti, T., McCally, M. & Rossi, M. (2001). Health risks posed by use of Di-2-ethylhexyl phthalate (DEHP) in PVC medical devices: a critical review. *American Journal of Industry and Medicine* **39**, 100–111.

Timpe, D.C. (2007). Silicone Rubber flame resistance. Presented at the Hose Manufacturers Conference: Cleveland, Ohio.

Vadgama, P. (2002). Development of open microflow for stable drift-free monitoring of tissue glucose by glucose biosensor. *JDRF Final Report [File No. 1-1999-133]*.

Vaidya, R. & Wilkins, E. (1994). Use of charged membranes to control interference by body chemicals in a glucose biosensor. *Medical Engineering and Physics* **16**, 416–421.

Varma, S. & Devamanoharan, P. (1991). Hydrogen peroxide in human blood. *Free Radical Research Communications* **14**, 125–131.

Vaupel, P., Thews, O. & Hoeckel, M. (1996). Tumor Oxygenation: Characterization and Clinical Implications. In *rhErythropoietin in Cancer Supportive Treatment*, Ed. Smyth, J. F., Dekker: New York. 205–239.

Velankar, S. & Cooper, S.L. (1998). Microphase separation and rheological properties of polyurethane melts. Effect of block length. *Macromolecules* **31**, 9181–9192.

Völcker, N., Klee, D., Hocker, H. & Langefeld, S. (2001). Functionalization of silicone rubber for the covalent immobilization of fibronectin. *Journal of Materials Science: Matererials in Medicine* **12**, 111–119.

Vrentas, J.S., Duda, J.L. & Ling, H.C. (1988). Antiplasticization and volumetric behavior in glassy polymers. *Macromolecules* **21**, 1470–1475.

Wang, W., Winlove, C. & Michel, C. (2003). Oxygen partial pressure in outer layers of skin of human finger nail folds. *Journal of Physiology* **549**, 855–863.

Wang, X., Martindale, J., Liu, Y. & Holbrook, N. (1998). The cellular response to oxidative stress: influences of mitogen-activated protein kinase signalling pathways on cell survival. *Biochemical Journal* **333**, 291–300.

Ward, R., Anderson, J., McVenes, R. & Stokes, K. (2007). In vivo biostability of polyether polyurethanes with fluoropolymer and polyethylene oxide surface modifying endgroups; resistance to metal ion oxidation. *Journal of Biomedical Matererials Research, Part A* **80**, 34–44.

Whalen, W.J. & Spande, J.I. (1980). A hypodermic needle pO_2 electrode. *Journal of Applied Physiology* **48**, 186–187.

Williams, R.L. Wilson, D.J. & Rhodes, N.P. (2004). Stability of plasma-treated silicone rubber and its influence on the interfacial aspects of blood compatibility. *Biomaterials* **25**, 4659–4673.

Williams, S., Pardue, H.L. Uhegbu, C.E. Smith, A.M. & Studley, J. (1996). Measurement/data-processing method to improve the ruggedness of membrane-based sensors: Application to amperometric oxygen sensor. *Talanta* **43**, 1379–1385.

Williams-Wynn, D. (2006). Addition Cures: Hydrosilation. *Nusil Presentation*, Polymer Systems Technology Ltd: High Wycombe.

Winlove, C.P. & O'Hare, D. (1993). Electrochemical methods in physiology. *Current*

Topics in Electrochemistry **2**, 345–360.

Wisniewski, N. & Reichert, M. (2000). Methods for reducing biosensor membrane biofouling. *Colloids and Surfaces B: Biointerfaces* **18**, 197–219.

Wisniewski, N., Klitzman, B., Miller, B. & Reichert, W. (2001). Decreased analyte transport through implanted membranes: Differentiation of biofouling from tissue effects. *Journal of Biomedical Materials Research* **57**, 513–521.

Woodhams, J.H., Kunz, L., Bown, S.G. & MacRobert, A.J. (2004). Correlation of real-time haemoglobin oxygen saturation monitoring during photodynamic therapy with microvascular effects and tissue necrosis in normal rat liver. *British Journal of Cancer* **91**, 788–794.

Wu, C.C., Yasukawa, T., Shiku, H. & Matsue, T. (2005). Fabrication of miniature Clark oxygen sensor integrated with microstructure. *Sensors and Actuators B* **110**, 342–349.

Wu, Y.K., Lodoen, G.A., Anderson, J.M., Baer, E. & Hiltner, A. (1994). Creep of a poly(etherurethane urea) in an oxidative environment. *Journal of Biomedical Materials Research* **28**, 515–522.

Xie, H.Q. & Guo, J.S. (1997). Adhesives made from interpenetrating polymer networks for bonding rusted iron without pretreatment. *International Journal of Adhesion and Adhesives* **17**, 223–227.

Xinhua, D. (2006). Preparation of uric acid standard stock solution. *Clinical Chemistry* **52**, 2117–2118.

Xu, L.C. & Siedlecki, C.A. (2007). Effects of surface wettability and contact time on protein adhesion to biomaterial surfaces. *Biomaterials* **28**, 3273–3283.

Yamauchi, A. Togami, K. Chaudry, A.M. & El Sayed, A.M. (2005). Characterization of charged film of fluorocarbon polymer (Nafion) and blended fluorocarbon polymer (Nafion)/Collodion composite membranes by electrochemical methods in the presence of redox substances. V. *Journal of Membrane Science* **249**, 119–126.

Yang, M., Zhang, Z., Hahn, C., Laroche, G., King, M.W. & Guidoin, R. (1999). Totally implantable artificial hearts and left ventricular assist devices: selecting impermeable polycarbonate urethane to manufacture ventricles. *Journal of Biomedical Materials Research* **48**, 13–23.

Yoo, H.J. & Kim, H.D. (2005). Characteristics of crosslinked blends of Pellethane and multiblock polyurethanes containing phospholipid. *Biomaterials* **26**, 2877–2886.

Yoo, H.J. & Kim, H.D. (2004). Properties of crosslinked blends of Pellethane and multiblock polyurethane containing PEO for biomaterials. *Journal of Applied Polymer Science* **91**, 2348–2357.

Young, T.H., Lin, D.T. & Chen, L.Y. (2000). Human monocyte adhesion and activation on crystalline polymers with different morphology and wettability in vitro. *Journal of Biomedical Materials Research* **50**, 490–498.

Yuan, J., Zhang, J., Zhu, J., Shen, J., Lin, S.C., Zhu, W. & Fang, J.L. (2003). Reduced platelet adhesion on the surface of polyurethane bearing structure of sulfobetaine. *Journal of Biomaterials Applications* **18**, 123–135.

Zhang, J., Yuan, J., Yuan, Y., Zang, X., Shen, J. & Lin, S. (2003). Platelet adhesive resistance of segmented polyurethane film surface-grafted with vinyl benzyl sulfo monomer of ammonium zwitterions. *Biomaterials* **24**, 4223–4231.

Zhang, S., Benmakroha, Y. & Rolfe, P. (1996a). Development of a haemocompatible pO_2 sensor with phospholipid-based copolymer membrane. *Biosensors and Bioelectronics* **11**, 1019–1029.

Zhang, Y. & Wilson, G.S. (1993). Electrochemical oxidation of H_2O_2 on Pt and Pt + Ir electrodes in physiological buffer and its applicability to H_2O_2-based biosensors. *Journal of Electroanalytical Chemistry* **345**, 253–271.

Zhang, Y.Z., Bjursten, L.M., Freij-Larsson, C., Kober, M. & Wesslen, B. (1996b). Tissue response to commercial silicone and polyurethane elastomers after different sterilization procedures. *Biomaterials* **17**, 2265–2272.

Zhu, L. & Crouch, R.K. (1992). Albumin in the cornea is oxidized by hydrogen peroxide. *Cornea* **11**, 567–572.

Zoski, C.G. (2002). Ultramicroelectrodes: Design, fabrication, and characterization. *Electroanalysis* **14**, 1041–1051.

Windsor Treaty Project

Development of Membrane-Modified Electrodes for Electrochemical Biosensors

This project was undertaken as a joint research program in collaboration with University of Coimbra, Portugal and Queen Mary, University of London, UK. The purpose of this project was to develop membrane modifications for thin carbon-film electrodes. Enzymes, e.g. glucose oxidase, immobilised on the surface of electrodes, have been widely used as recognition elements for decades. A key feature of successful immobilisation is to retain the enzyme's native structure as far as possible and to sustain its activity. There are numerous methods to immobilise enzymes on electrode surfaces, however encapsulation in silica sol-gel is relatively little studied and has been reported to lead to sensitive electrode responses whilst retaining substrate selectivity characteristics [Kuenzelmann *et al.* (1997), Salimi *et al.* (2004)]. Polymeric films were, however, utilized as outer membranes to achieve additional features: increased sensor stability, reduced enzyme leaching, reduced fouling and protection of the inner transducer surface from passivation [Wisniewski *et al.* (2000)]. In this study, glucose oxidase was encapsulated in trioxysilane-based sol-gels and applied to poly(neutral red) (PNR) modified carbon film electrodes [Pauliukaite *et al.* (2005)].

Preparaton of Thin Carbon-Film Electrodes

Commercially available carbon film resistors (2 Ω nominal resistance) were made into electrodes according to a protocol established by Brett *et al.* (2001). These resistors were enclosed in tight-fitting metal caps, which were joined to thin conducting wires at each end. One cap including wire were removed from the resistor and the other wire was covered in plastic tubing and affixed with epoxy resin onto the cap/cylinder in a way

that the exposed electrode area was about 0.20 cm^2 - see Figure 6 for illustration. Prior to use, these electrodes were carefully cleaned with acetone and then cycled between -1 and +1.0 V versus a saturated calomel electrode (SCE) in 0.1 M KNO_3 solution with a sweep rate of 50 mV/s until stable voltammograms were obtained.

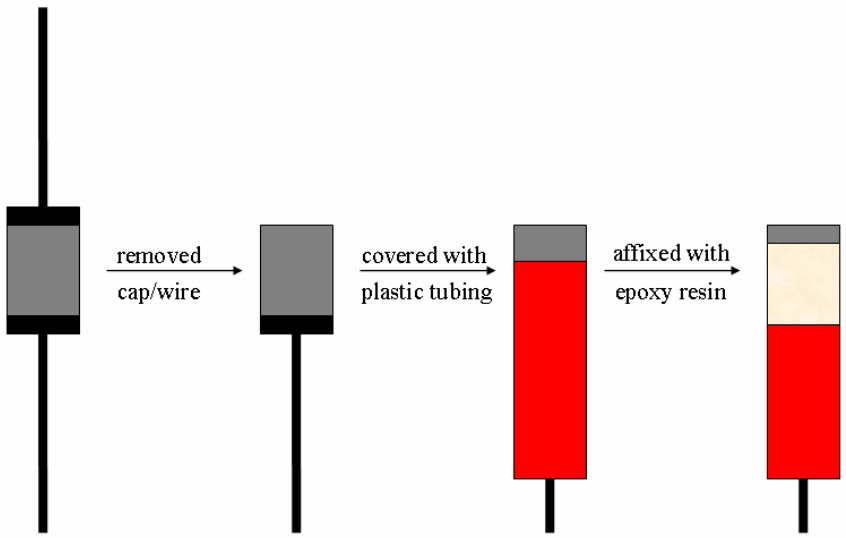

Figure 6: Photographic image of thin carbon-film electrodes

PNR was electrochemically polymerised on the carbon film electrodes according to a pre-established protocol [Benito *et al.* (2002)]. The electrodes were immersed into phosphate buffer (pH 5.5) with a monomer concentration of 1 mM and a supporting electrolyte of 0.3 M KNO_3 and cycled 10 times with a switching potential of -1 to +1 V and a sweep rate of 50 mV/s to obtain redox active film. These electrodes were then left for one day to dry at room temperature prior to use. A cyclic voltammogram in phosphate buffer (pH 7, 0.1 M) with a scan rate of -1 to +1 V and a sweep rate of 50 mV/s, was taken before further coatings were applied (Figure 7).

Sol-gel solution was prepared by mixing 130 μl 3-glycidoxypropyl-trimethoxysilane (GOPMOS), 70 μl methyltrimethoxysilane (MTMOS), 600 μl deionised water and 2 μl of $\sim$ 6 M HCl. This solution was intensively stirred for a few minutes before being sonicated for 15 minutes. This mixture was then exposed to $\sim$ 70°C until the volume decreased to $\sim$ 60 % to ensure that the alcohol, which was formed during sol-gel precursor hydrolysis, had evaporated. The mixture was left at room temperature to cool down and then neutralised to pH 7 with 0.1 M NaOH. A 10 % (w/v) glucose oxidase (GOx) stock solution in phosphate buffer (pH 7, 0.1 M) was prepared and 12.5 μl of this solution was added in 50 μl of the sol-gel mixture. This solution was then carefully mixed and left

for 2 hours to equilibrate. PNR modified carbon film electrodes were then immersed into the sol-gel-enzyme mixture for 5 minutes, and then left for sol-gel formation at +4°C for 3 days. The electrodes were stored at +4°C in phosphate buffer when not in use.

Cyclic voltammograms were taken of PNR mediated carbon electrodes with and without GOx loaded silica sol-gel coating (Figure 7). The redox-peaks for polymer coated PNR modified electrodes show less pronounced redox waves compared to those without polymer coating. This reduced peak height is due to the fact that the additional layer creates a diffusional barrier and will therefore suppress PNR peak current.

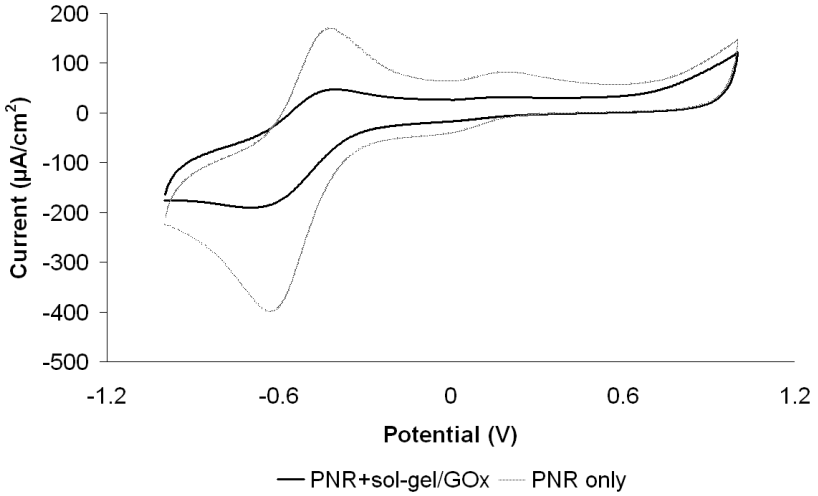

Figure 7: CV of PNR modified carbon film electrode with and without sol-gel/GOx polymer coating (vs. SCE; 50 mV/s; electrolyte: 0.1 M NaCl; pH 7

Electrode performance in electrochemical analyte detection towards glucose

The current response of PNR modified carbon film electrodes coated with sol-gel/GOx towards glucose as target analyte was assessed amperometricaly and is illustrated in Figure 8. The current increased with increasing amount of target analyte, however, a non-linear analyte response was observed for glucose concentrations higher than 1 mM. This could be due to that sol-gel is shrinking over time when stored under dry conditions, which will lead to cracks on the surface thus causing the enzyme to leach out of the polymer matrix. However, Yao *et al.* (1998) found a decreased current response due to enzyme leaching for electrodes stored in phosphate buffer. Analogous to enzyme leaching, Prof. Brett's group found that carboxyl acid may have formed on the electrode surface, interfering with PNR causing a decreased current response.

Therefore, an additional permselective polymer coating was proposed to be applied as

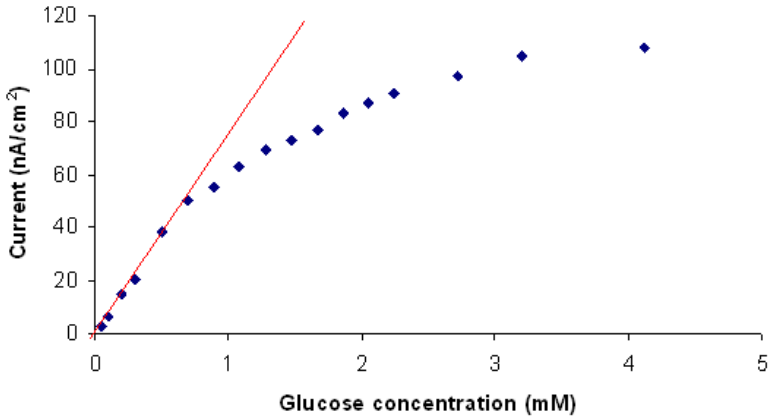

Figure 8: Current response of PNR modified carbon film electrodes coated with sol-gel/GOx towards glucose (applied potential: -250 mV vs. SCE; electrolyte: 0.1 M KCl; pH 7)

outer membrane to reduce enzyme leaching and to protect the sensor surface from passivation, hence to increase sensor stability. Table 1 shows the range of polymers including permutations tested as candidate material to use as outer membrane over enzyme loaded silica sol-gel coating. PNR modified carbon film electrodes coated with sol-gel/GOx are referred to as a "mediated biosensor" throughout this study.

Preparaton of mediated biosensors with outer membranes

The membrane solutions were prepared by mixing the components as summarised in Table 1 for five minutes at room temperature. Mediated biosensors were coated by dipping the electrode tip into the membrane solution for a few seconds. These coated electrodes were then left to dry at room temperature overnight.

Mediated biosensor coated with silica sol-gel (TEOS/MTEOS, ratio 1:1)

A sol-gel is a porous glass, made through hydrolysis and subsequent condensation of metal alkoxides such as tetraethyl orthosilicate (TEOS) and methyltriethoxy silane (MTEOS) used in this study. One method for the modification of the surface properties of a sol-gel is to mix two or more precursors. Here, two precursors were mixed in a 1:1 (v/v) ratio, providing a surface with a mixture of ethyl and methyl groups. Another potential method to change the properties of the sol-gel would be the immobilisation of dye molecules. Tropaeolin, which is a pH sensitive dye, was immobilized in the porous structure of

Silica sol-gel (TEOS/MTEOS, ratio 1:1) • unmodified • doped with dye (0.3% Tropaeolin)
Poly (vinyl chloride), 4% v/w in THF • unmodified • with incorporated surfactant (5% v/v Aliquat®336) • with incorporated lipid (1.6% IPM)
Carboxylated poly (vinyl chloride), 4.8% w/v in THF • unmodified • with incorporated surfactant (5% v/v Aliquat®336) • with incorporated lipid (1.6% v/v IPM)
Polyurethane (Trixene^{TM}), 50% v/v in THF • unmodified • with incorporated surfactant (5% v/v Aliquat®336) • with incorporated lipid (1.6% v/v IPM)

Table 1: List of polymeric materials including plasticiser used for preparation of outer membrane

this sol-gel, it was thought to form covalent bonds within the sol-gel matrix, decreasing pore sizes, hence keeping the enzyme in place. After the electrodes were dipped into silica sol-gel membrane solutions for a few seconds, the formation of an uneven layer and possibly crystals was observed. Also, the remaining sol-gel solution was coloured slightly purple, which indicates dissolution of PNR possibly due to ethanol. Figure 9 shows cyclic voltammograms of TEOS/MTEOS coated mediated biosensors with and without dye. No defined redox peaks were visible. The misshapen PNR peaks may have been been caused by the dissolution of PNR upon coating.

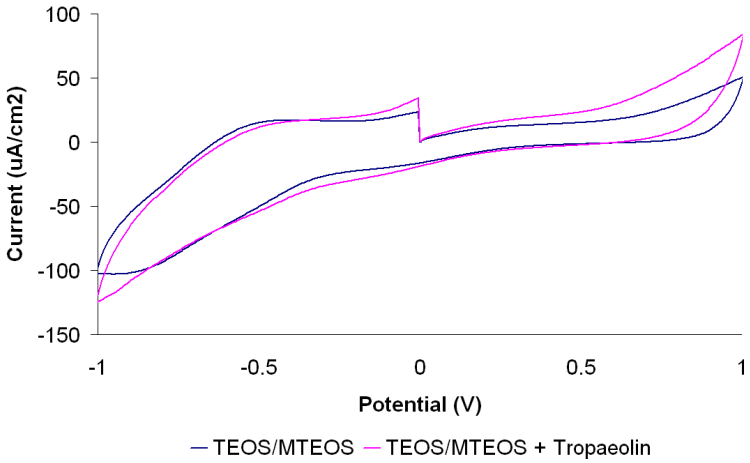

Figure 9: CV of mediated biosensor coated with TEOS/MTEOS with/without dye (vs. SCE; electrolyte: 0.1 M KCl; pH 7)

Mediated biosensor coated with PVC

Poly (vinyl chloride) is an amorphous polymer comprised of repeated units of its monomer vinyl chloride. It is used for containers and tubes for blood and blood-product cellection, storage and infusion, examination gloves, dental retainers, respiratory-support equipment, catheters, tubing and components for external organ assist devices such as haemodialysis and extracorporeal oxygenators, coating material for medical devices, etc. Plasticisers are essential additives used in PVC-based materials and may constitute up to 40 % of the finished material. The most commonly used plasticers are phthalates including di-ethylhexyl phthalate (DEHP) and diisononyl phthalate (DINP). Unplasticised PVC membranes are water impermeable, rigid and inflexible, the inclusion of such "additives" can lead to drastic changes in their properties.

In this study, Aliquat®336 and isopropyl myristate (IPM) have been chosen as additives for these PVC membranes. Aliquat®336 is a cationic surfactant and will give the membrane hydrophilic properties assisting in an enhanced diffusion of glucose across the membrane, thus increasing the electrochemical current output. IPM is a lipid and will give the membrane hydrophobic properties. It is thought that this hydrophobic layer will keep the hydrophilic enzyme in place. After the electrodes were dipped into PVC membrane solutions (Table 1) for a few seconds, an uneven layer and possibly crystals were formed with membrane combinations of unplasticised PVC and PVC with incorporated IPM. PVC membranes modified with Aliquat did not show a visible change on the surface.

Figure 10 shows cyclic voltammograms of PVC membranes including plasticised combinations. Mediated biosensors coated with plasticised or unplasticised PVC membranes did not show defined redox peaks. This is due to that each layer of membranes is restricting the diffusion of the analyte, suppressing the electrical response. However, the membrane combination PVC + Aliquat does show a slightly bigger wave compared to PVC and PVC + IPM. Also, the sol-gel/GOx layer could have been partly dissolved during the dip coating process, as the apparent crystal formation would suggest.

Mediated biosensor coated with carboxylated PVC

Carboxylated PVC (PVC-COOH) was found to exhibit improved biocompatibility compared to non-carboxylated PVC (Cosofret *et al.* (1994)). Therefore, this material was chosen as candidate material for outer membrane with/without plasticiser. The elec-

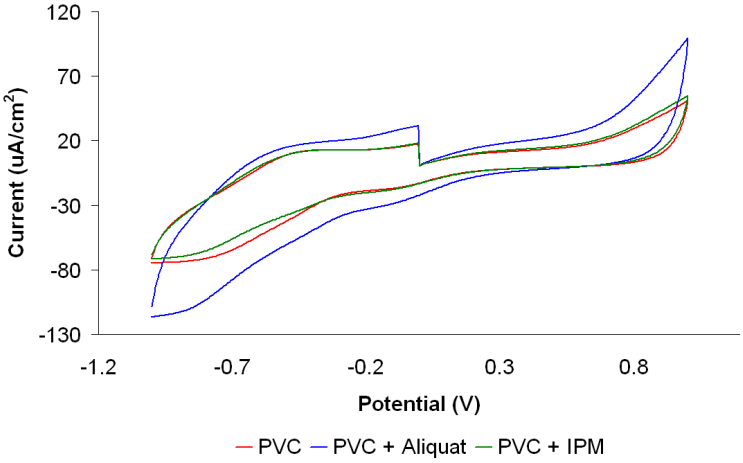

Figure 10: CV of mediated biosensor coated with PVC with/without additives (vs. SCE; electrolyte: 0.1 M KCl; pH 7)

trodes were dipped into PVC-COOH membrane solution (Table 1) for a few seconds. An uneven layer and possibly crystals were formed for a short period of time with membrane combinations containing both plasticisers. Unplasticised PVC-COOH did not show any visible changes on the surface. Figure 11 shows cyclic voltammograms for mediated biosensor coated with PVC-COOH with/without additives. Carbon film electrodes coated with PVC-COOH with or without plasticiser did not show redox peaks. An explanation for this phenomenon would be that during dip coating process, the sol-gel/GOx layer was partly dissolved exposing the enzyme.

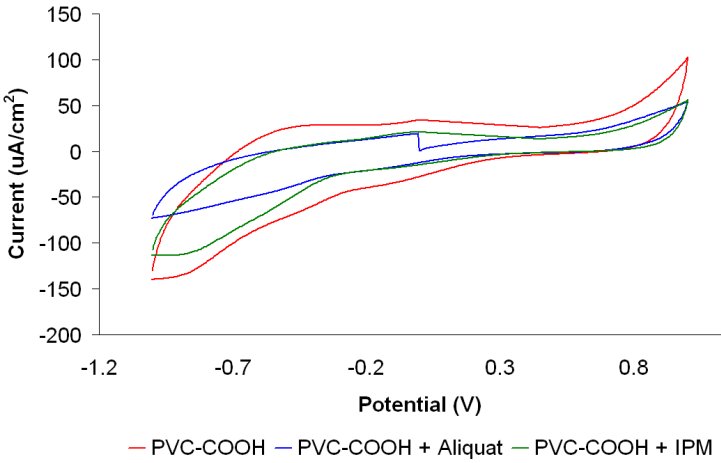

Figure 11: CV of mediated biosensor coated with PVC-COOH with/without additives (vs. SCE; electrolyte: 0.1 M KCl; pH 7)

Mediated biosensor coated with polyurethane

Polyurethanes along with PVC are one of the most widely used materials for medical devices. They show extensive structural diversity, due to the large number of possible variations in chemical structures including modifications possible. In the medical field, polyurethanes are widely used as blood-contacting biomaterials, such as catheters, artificial heart valves, blood bags etc. due to their good haemocompatibility and mechanical properties. Nevertheless, their compatibility with blood is still not adequate for more demanding biomedical applications. Bulk modification is one effective way to improve biocompatibility. Trixene^{TM}SC7602, a commercial isocyanate terminated prepolymer was used with and without plasticiser in this set of experiments. Polyurethane membrane solution was applied as the outer membrane on a mediated biosensor via dip coating for a few seconds. Upon coating, there were no visible changes observed on any of the electrodes. Figure 12 shows cyclic voltammograms for a mediated biosensor coated with polyurethane with and without additives. Polyurethane with or without plasticiser did not show any redox peaks.

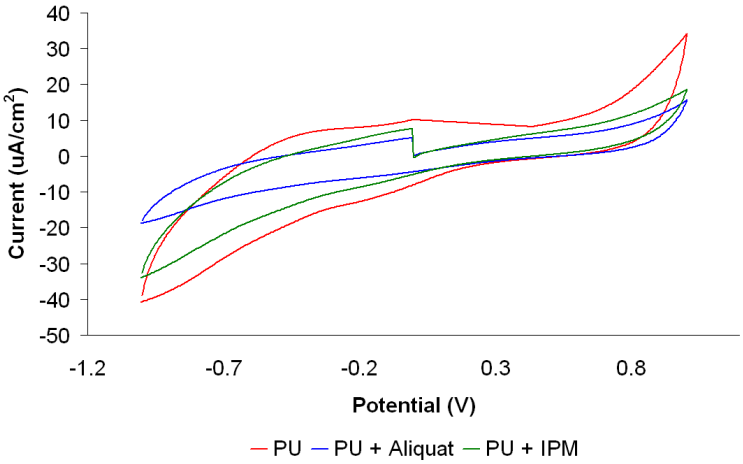

Figure 12: CV of mediated biosensor coated with PU with/without additives (vs. SCE; electrolyte: 0.1 M KCl; pH 7)

Electrochemical response to glucose as target analyte:

The response to glucose was measured amperometricaly with a fixed potential of -250 mV. The electrodes were immersed in 10 ml of phosphate buffer solution (0.1 M) and conditioned until a stable background current was achieved. Then, additions of 5, 10, 20 and 50 μl of 0.1 M glucose solutions were made and the current response was moni-

tored electronically (Figure 13). The highest current response was achieved with PVC-COOH, whereas the incorporation of any plasticiser showed a lower current response. Non-carboxylated PVC (plasticised or non-plasticised) showed a lower current response to its carboxylated counterpart, but the analyte response showed an improved linearity. TEOS/MTEOS with incorporated dye showed higher current response compared to its undoped version. Polyurethane, modified and unmodified, showed the lowest analyte response. From calibration data illustrated in Figure 13, the linearity and sensitivity was determined and is illustrated in Table 2 including the correlation coefficients.

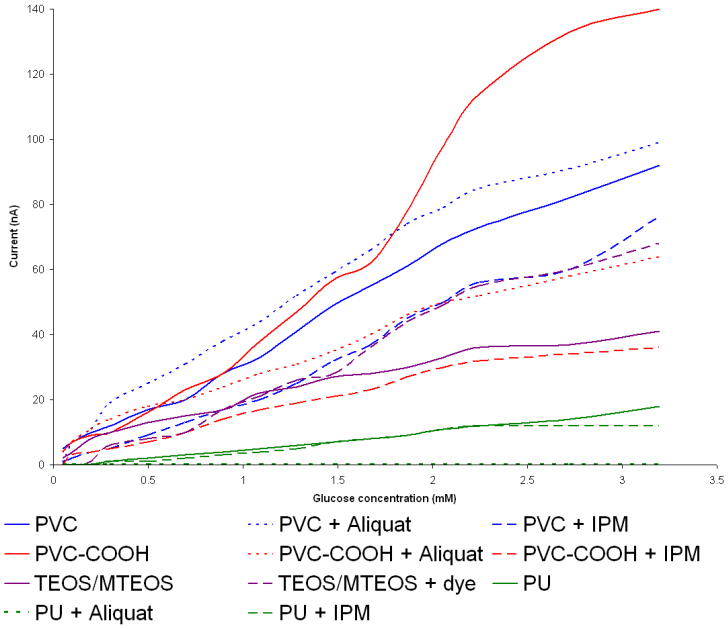

Figure 13: Current response of mediated biosensors coated with a selection of outer membranes towards glucose (applied potential: -250 mV vs. SCE; electrolyte: 0.1 M KCl; pH 7)

Overall Conclusions

Silica sol-gel membrane with dye as outer membrane did show the highest linearity with a moderate sensitivity. This membrane combination did cause PNR to leach out, possibly due to ethanol present in the membrane solution. If ethanol would be evaporated before applying sol-gel on electrode, this coating might be a promising candidate. Polyurethane did show a high linearity with a very low current output. Plasticised Polyurethane with IPM showed even less current response. For polyurethane with incorporated Aliquat, the analyte appeared to not have reached the sensing part of the electrode. Mediated biosensors without an outer membrane showed the highest sensitivity but the lowest

Membrane	Linear range (mM)	Sensitivity (nA/mM)	Correlation Coefficient (R)
PVC	0.05-2.70	30.48	0.997
PVC + Aliquat	0.05-2.20	36.90	0.997
PVC + IPM	0.05-2.20	24.57	0.992
PVC-COOH	0.05-1.70	36.03	0.993
PVC-COOH + Aliquat	0.05-2.70	20.21	0.995
PVC-COOH + IPM	0.05-2.20	14.02	0.998
Polyurethane	0.05-3.20	5.62	0.997
Polyurethane + Aliquat	0	0	0
Polyurethane + IPM	0.05-2.20	6.42	0.996
TEOS/MTEOS	0.05-2.20	14.39	0.991
TEOS/MTEOS + dye	0.05-3.20	23.40	0.993
Mediated biosensor (no outer membrane)	0.05-0.60	74.74	0.998

Table 2: Performance characteristics of mediated biosensors with and without outer membrane in electrochemical analtye detection towards glucose

linearity. This could be due to a loss of activity and could have resulted from a loss of the enzyme, a loss of mediator or possibly both. The dye doped sol-gel was thought to form covalent bonds within the silica sol-gel network, hence restricting the diffusion of the analyte across the membrane. If the analyte diffusion is restricted, the analyte response was expected to show increased linearity combined with a decreased sensitivity. This was the case in this experiment, as the non-doped silica sol-gel showed a lower linearity with a higher sensitivity. PVC with incorporated Aliquat showed the highest relative linearity and sensitivity compared to PVC + IPM and unplasticised PVC.

Overall unplasticised carboxylated PVC showed the highest linearity and sensitivity, plasticised carboxylated PVC showed appart from PU the lowest linearity and sensitivity. Polyurethane and polyurethane with incorporated IPM showed high to moderate linearity, but the sensitivity is the lowest detected for all of the samples. Polyurethane with incorporated surfactant did not show any current response at all.

These findings show that for PU, the initial membrane solution was too concentrated giving rise to a homogenous, impermeable barrier. The higher the concentration of the casting polymer, the lower is the diffusion of analyte across the membrane (as seen with polyurethane). However, these outer protective membranes did generate improvements to analyte response. As membranes may act as a variable diffusion barrier, the rate of diffusion of the analyte and linear response can be tailored to needs by optimising their composition, density and thickness. However, this data clearly shows that the outer membrane leads to a much more linear responses compared to mediated biosensors

without an outer protective coating. More experiments will be carried out with lower concentrations of membrane casting solutions with the event of publications.

References

Benito, D., Gabrielli, C., Garca-Jareo, J., Keddamb, M., Perrot, H. & Vicente, F. (2002). An electrochemical impedance and ac-electrogravimetry study of PNR films in aqueous salt media. *Electrochemistry Communications* **4**, 613.

Brett, C., Angnes, L., & Liess, H.-D. (2001). Carbon Film Resistors as Electrodes: Voltammetric Properties and Application in Electroanalysis. *Electroanalysis* **13**, 765–769.

Cosofret, V. V., Erdosy, M., Buck, R. P., Kao, W. J., Anderson, J. M., Lindner, E. & Neuman, M. R. (1994). Electroanalytical and biocompatibility studies on carboxylated poly(vinyl chloride) membranes for microfabricated array sensors. *Analyst* **119**, 2283–2292.

Farahani, M., Wallace, W., Antonucci, J. & Guttman, C. (2006). Analysis by mass spectgrometry of the hydroysis/condensation reaction of a trialkoxysilane in various dental monomer solutions. *Journal of Applied Polymer Science* **99**, 1842–1847.

Kuenzelmann, U. & Boettcher, H. (1997). Biosensor properties of glucose oxidase immobilized within SiO_2 gels. *Sensors and Actuators B* **38-39**, 222–228.

Pauliukaite, P. & Brett, A. M. O. (2005). Characterization of novel glucose oxysilane sol-gel electrochemcial biosensors with copper hexacyanoferrate mediator. *Electrochimica Acta* in press.

Salimi, A., Compton, R. G. & Hallaj, R. (2004). Glucose biosensor prepared by glucose oxidase encapsulated sol-gel and carbon-nanotube-modified basal plane pyrolytic graphite electrode. *Anals of Biochemistry* **333**, 49–56.

Wisniewski, N. & Reichert, M. (2000). Methods for reducing biosensor membrane biofouling. *Colloids and Surfaces B: Biointerfaces* **18**, 197–219.

Yao, T. & Takashima, K. (1998). Amperometric biosensor with a composite membrane of sol-gel derived enzyme film and electrochemically generated poly(1,2-diaminobenzene) film. *Biosens Bioelectron* **13**, 67–73.

Presentations

Poster Presentations

- "Plasticised Poly(vinyl chloride) membranes for controlled drug release using Rhodamine B as drug model", Queen Mary University of London, 2005

Oral Presentations

- "Biosensors - minimal invasive needle electrodes", Student Symposium, QMUL 2004
- "Biosensors - needle electrodes", UCL, 2004
- "Electrodes for *in vitro* and *in vivo* monitoring of pO_2", UCL, 2004
- "Developing and Characterising Polymeric films for H_2O_2 and pO_2 sensing with needle electrodes", Student Symposium, QMUL, 2005
- "Membrane-Modified Carbon-Film Electrodes for Biosensors", 4th Postgraduate Research Topics in Electroanalysis Meeting, Birkbeck College, 2005
- "Polymeric material - bulk and surface modification", Work package leaders meeting: Healthy Aims Project, QMUL, 2006
- "Improved stable sol-gel encapsulated enzyme biosensors with protective polymer membranes" [Prof. Chris Brett], Congress Singapore, 2006
- "New protective polymer membrane coating strategies for sol-gel enzyme biosensors" [Prof. Chris Brett], 57th Annual Meeting of the International Society of Electrochemistry, Edinburgh, 2006
- "Complex electronic implants and polymer packaging needs", [Prof. Pankaj Vadgama], World Congress, South Korea, 2006

Plasticised Poly(vinyl chloride) membranes for controlled drug release using Rhodamine B as drug model

M.Schoenleber[a], Loo-Teck Ng[b] , M. Grahn[c], P. Vadgama[a]

[a]IRC in Biomedical Materials, Queen Mary, University of London, Mile End Road, E1 4NS, London, UK
[b]School of Science, Food & Horticulture, University of Western Sydney, Australia
[c]Centre for Academic Surgery, Institute of Cell and Molecular Science, Barts and The London Queen Mary's School of Medicine and Dentistry, University of London

Introduction

Over the past decade, polymers have been utilised as drug delivery systems. In these systems, low molecular weight compounds were used as carriers for bioactive agents, such as peptides and proteins, whose effectiveness as drugs is very much dependant on their distribution in the body.

The surface properties of these particles, e.g. hydrophilicity, determine their efficiency as drug carriers. It is reported that cells may readily take up particles with a hydrophobic surface, whereas particles with a more hydrophilic surface may avoid this uptake to a greater extend, thus achieving a better chance to efficiently deliver the therapeutic agent.

PVC is used in this study as matrix for drug delivery as it is a cheap and readily available material. It is easy to process and with the inclusion of plasticisers, the surface properties can be changed as desired.

Materials and methods

PVC membrane solution were prepared as follow. First, a given amount of PVC was dissolved in THF, then different percentages of various plasticisers were added into the mixture (see table). This mixture was stirred for a few minutes. 6 ml of this solution were transferred into a glass petri dish (10mm diameter) and left covered under a fume hood to dry for about 2 days.

Diffusion Chamber Apparatus

- Consisting of two half-cells
- Each cell has an equal volume of 170 ml
- The donor cell is filled with 0.03mM Rhodamine B solution
- The receiver cell is filled with a blank solution
- diffusion across the membrane is measured with a spectro-photometer
- Rhodamine B is a cationic dye and contains ionisable groups
- UV-Vis spectrum: 545 +/- 2 nm

Experimental results

Composition	PVC	Aliquat	IPM
	3	1	0
R	3	0.8	0.2
a	3	0.4	0.6
t	3	0.2	0.8
I	3	0	1
o	3	3.6	0
	3	0	3.6
	3	3.6	3.6

Table of composition

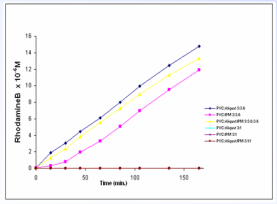

Effect of plasticiser concentration on rhodamine B diffusion

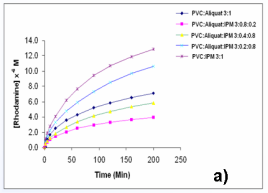

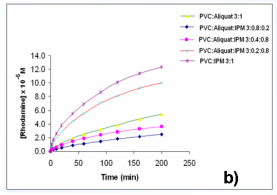

Effect of plasticiser concentration on rhodamine B release
a) in demin. Water b) in saline PBS

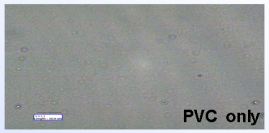

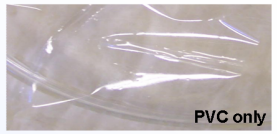

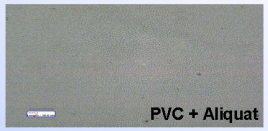

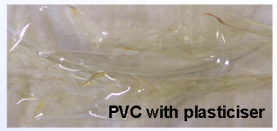

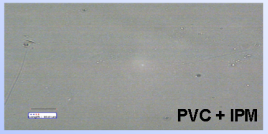

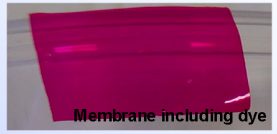

Conclusions

Unplasticised PVC does not allow any diffusion or release of the dye due to its hydrophilic nature. However, the use of plasticiser allows rhodamine B transport thanks to separatation of chain-chain packing in PVC films.

For a given plasticiser, at low concentrations, there is no diffusion of dye across the plasticised membrane, whereas at higher concentrations, the dye diffused readily across the membrane. This could be due to an increase in pore size and pore density. Moreover, this effect may be enhanced by the fact that both rhodamine B and aliquat are hydrophilic molecules, while IPM is hydrophobic and will repel the dye.

The dye release from IPM loaded membranes is higher than from aliquat loaded membranes, possibly due to the fact that IPM might be forcing the dye out of the membranes, while aliquat has the opposite effect on rhodamine B, allowing the dye to remain inside the membranes for longer residency times.

Release study was carried out in both demineralised water and saline PBS buffer. The trends for dye release in both media are similar, but the release rates in saline PBS are lower for all of the samples. This phenomenon could be due to the effect of ionic strength.

Future Work

Future work remains to be done regarding the diffusion properties of the membranes using various concentrations of plasticisers. It will also be relevant to determine the pore size and pore density of the studied membranes by Atomic Force Microscopy and Scanning Electron Microscopy.

References

M.A. Desai, M. Mutlu and P. Vadgama, A study of macromolecular diffusion through native porcine mucus, *Experientia*, 48, 22-26 (1992)

G. Caponetti, et al., Microparticles of novel branched copolymers of lactic acid and amino acids: preparation and characterization, *J. Pharm. Sci.*, 88, 136-141 (1999)

Acknowledgements

The author would like to thank the IRC for financial support and the staff for their valuable contributions.

Improved stable sol-gel encapsulated enzyme biosensors with protective polymer membranes

Rasa Pauliukaite[a], Madalina Barsan[a], Christopher M.A. Brett[a]*,
Monika Schoenleber[b], Pankaj Vadgama[b]

[a] *Departamento de Química, Universidade de Coimbra, 3004-535 Coimbra, Portugal*

[b] *IRC in Biomedical Materials, Queen Mary University of London, Mile End Road, London E1 4NS, UK*

∗brett@ci.uc.pt

Significant efforts have been devoted to developing long lifetime and sensitive biosensors by stabilising and immobilising enzymes on different electrode substrates. Different polymer materials are usually used for immobilisation or as a protective membrane against interference or enzyme leaching. An attractive enzyme entrapment method is the sol-gel technique. Enzymes and the other active biomaterials encapsulated within sol-gels appeared to retain their activity and selectivity, particularly when silica alkoxides were used as sol-gel precursors. However, sol-gel electrodes in some cases gave unsatisfactory lifetimes [1], inappropriate for disposable biosensors.

Characterisation and optimisation of silica based sol-gel encapsulation of glucose oxidase, aldehyde dehydrogenase, and NADH oxidase based biosensors at poly(neutral red) (PNR) modified carbon film electrodes will be presented. Sol-gels were prepared using an optimised mixture of oxysilane precursors, particularly 3-glycidoxypropyl-trimethoxysilane (GOPMOS), and methyltrimethyloxysilane (MTMOS), without alcohol addition. The sol-gel protocol was improved by thermal removal of the alcohol, formed during oxysilane hydrolysis in acidic medium.

Enzyme was entrapped by mixing a solution of it with a neutralised sol-gel mixture and placing on a carbon film electrode, electrochemically modified with PNR. An outer protective polymer membrane was applied over the encapsulated enzyme layer in order to prevent enzyme leaching and loss of sensitivity from macromolecule adsorption [2]. Polyurethane and carboxylated polyvinyl chloride were used for membrane preparation and optimisation.

The results of glucose and acetaldehyde assay in relation to sensitivity, stability and response time in standard solutions obtained at sol-gel-enzyme-polymer membrane biosensors will be discussed.

References

1. R. Pauliukaite, C.M.A. Brett. Electrochim. Acta 50 (2005) 4973.
2. S. Ahmed, C. Dack, J. Farace, G. Rigby, P. Vadgama. Anal. Chim. Acta 537 (2005) 153.

S2•O-16 57th Annual Meeting of the International Society of Electrochemistry

New protective polymer membrane coating strategies for sol-gel enzyme biosensors

Christopher M.A. Brett[a]*, Rasa Pauliukaite[a], Madalina Barsan[a],
Ana Maria Chiorcea – Paquim[a], Ana Maria Oliveira Brett[a],
Monika Schoenleber[b], Pankaj Vadgama[b]

[a] *Departamento de Química, Universidade de Coimbra, 3004-535 Coimbra, Portugal*

[b] *IRC in Biomedical Materials, Queen Mary University of London, Mile End Road, London E1 4NS, UK*

∗brett@ci.uc.pt

Significant efforts have been devoted to developing long lifetime and sensitive biosensors by stabilising and immobilising enzymes on different electrode substrates. Different polymer materials are usually used for immobilisation or as a protective membrane against interference or enzyme leaching. An attractive enzyme entrapment method is the sol-gel technique and these films have been characterised by atomic force microscopy (AFM). Enzymes and the other active biomaterials encapsulated within sol-gels appeared to retain their activity and selectivity, particularly when silica alkoxides were used as sol-gel precursors. However, sol-gel electrodes in some cases gave unsatisfactory lifetimes [1], inappropriate for disposable biosensors.

Characterisation and optimisation of silica based sol-gel encapsulation of glucose oxidase, aldehydedehydrogenase, and NADH oxidase based biosensors at poly(neutral red) (PNR) modified carbon film electrodes will be presented. Sol-gels were prepared using an optimised mixture of oxysilane precursors, particularly 3-glycidoxypropyl-trimethoxysilane (GOPMOS), and methyltrimethyloxysilane (MTMOS). The sol-gel protocol was improved by thermal removal of the alcohol, formed during oxysilane hydrolysis in acidic medium.

Enzyme was entrapped by mixing a solution of it with a neutralised sol-gel mixture and placing on a carbon film electrode, electrochemically modified with PNR. An outer protective polymer membrane was applied over the encapsulated enzyme layer in order to prevent enzyme leaching and loss of sensitivity from macromolecule adsorption [2]. Polyurethane and carboxylated polyvinyl chloride were used for membrane preparation and optimisation.
The results of glucose and acetaldehyde assay in relation to sensitivity, stability and response time in standard solutions and in natural samples will be discussed.

References

1. R. Pauliukaite, C.M.A. Brett. Electrochim. Acta 50 (2005) 4973.

2. S. Ahmed, C. Dack, J. Farace, G. Rigby, P. Vadgama. Anal. Chim. Acta 537 (2005) 153.

Publications

Wang, W. & Vadgama, P. (2004). O_2 microsensors for minimally invasive tissue monitoring. *Journal of the Royal Society Interface* **1**, *(1)*, 109–117. Acknowledgement to Ms. Monika Schoenleber for her help with this manuscript.

Gargiuli, F.J., Gill, A, Lillie, G, Schoenleber, M, Pearson, J, Kyriakou, G & Vadgama, P (2005). Stable use of biosensors at the sample interface. In *Surfaces and Interfaces for Biomaterials*, Woodhead Publishing Ltd.: Cambridge. 103–149.

Wang, W. & Vadgama, P. (2005). Microelectrodes and Biocompatible Sensors for Skin pO_2 Measurements. In *Pressure Ulcer Research: Current and Future Perspecives*, Eds. Dan L. Bader, Carlijn V.C. Bouten, Denis Colin and Cees W.J. Oomens, Springer: Berlin Heidelberg. Acknowledgement to Ms Monika Schoenleber for her help in preparing Figs. 19.1 to 19.3.

Schoenleber, M., Vaghela, J., Ismail, F., Grahn, M., Popa, C., Rehman, I. & Vadgama, P. (2006). Complex electronic implants and polymer packaging needs. *Book Chapter IFMBE Proceedings, World Congress on Medical Physics and Biomedical Engineering 2006, Vol 14, Parts 1-6 Book Series IFMBE Proceedings Vol 14 Pages 703-706, Part 1-6 and Part 7; 978-3-540-36839-7 (Print) 978-3-540-36841-0 (Online)* **14**, *7*, 703–706.

Pauliukaite, R., Schoenleber, M., Vadgama, P., & Brett, C. (2008). Development of electrochemical biosensors based on sol-gel enzyme encapsulation and protective polymer membranes. *Analytical and Bioanalytical Chemistry* **390**, *(4)*, 1121–1131.

Vadgama, P & Schoenleber, M (2008). *In vivo* Applications: Glucose Monitoring, Fuel Cells. In *Handbook of Bioelectrochemistry*, John Wiley and Sons Ltd: London. 443–463.

Ismail, F., Schoenleber, M., Mansour, R., Bastani, B., Fielden, P. & Goddarda, N. J. (2009). Strength of Interactions between Immobilized Dye Molecules and Sol-Gel matrices. In preparation.

Complex electronic implants and polymer packaging needs

Monika Schoenleber[1], Jaina Vaghela[1], Fanya Ismail[1], Mike Grahn[1], Catalin Popa[2], Ihtesham Rehman[1], Pankaj Vadgama[1]

[1] IRC in Biomedical Materials, Queen Mary, University of London, UK
[2] Department of Materials Science and Technology, Technical University of Cluj-Napoca, Romania

Abstract— **Implantable and direct contact electronic devices for underpinning complex tissue functions as well as physiological monitoring have the opportunity to revolutionize health care in an ageing population. A major EU-consortium of 25 partners has been developing electronic devices for functional electrical stimulation, glaucoma and CNS pressure monitoring and as cochlear, retinal and urethral implants. A key need, however, is the packaging of such complex devices to enhance tissue biocompatibility, and to protect conducting elements from *in vivo* corrosion during extended use. Accordingly, we have investigated candidate polymeric barriers as hydration resistant and solute impermeable in interphases to mitigate the major problems of chronic implantation. Materials include silicone rubber, PVC, polyurethane, sulphonated polyetherether sulphone polyether-sulphone (SPEES-PES) and polycarbonate as underlayer and diamond like carbon (DLC), sol-gel modified oxides and ParyleneC for top layers. A key strategy is polymer modification through incorporation variously of surfactant (Aliquat336) and synthetic lipid (isopropyl myristate) to manipulate permeability to water and to low molecular weight solutes. Surface biocompatibility was assessed on the basis of protein film deposition in vitro and by cell viability studies in tissue culture. Polypyrrole deposited on gold coatings was used as a substrate for cell testing. None of the materials tested showed short-term toxicity, though there were substantial differences in hydration. Results with polypyrrole suggest that both electrical conductivity and tissue interfacing to be viable if used as coatings over active electrode components.**

Keywords— **microelectrodes, polymer packing, silicone, diamond like carbon, PVC**

I. Introduction

Microelectronic devices promote *in vivo* "intelligent" interfacing systems capable of sensing and activating functions for a range of medical applications. Deployment is usually for major tissue failure and for an aging population the ongoing needs are increasing. A major European consortium funded by the EU 6th Framework Program is undertaking development of a family of such devices under the project Healthy Aims (Ambient Intelligent Microsystems for Health). Microsystems are being developed here variously for cochlear and retinal implants, functional electrical stimulation, CNS and ocular pressure monitoring and for urethral devices [1]. Whilst a range of technologies is being progressed in parallel, including high-density power systems, interconnects and communication relays, a key requirement is selective sealing of the vulnerable electronic components using packaging materials. Of these silicone rubber has been the most frequently investigated [2]. However, packaging effectiveness is far from perfect, not least with regard to uptake of water. Also, though silicone rubber does have good biocompatibility, this could be improved upon. There is a lack of relevant literature on the fundamental process governing biocompatibility [3], and ultimately semi-empirical approaches are required to progress suitable materials and to test these out in increasingly realistic bioenvironments from biological fluids to cell populations and then *in vivo*. We report here our strategy for the Healthy Aims Program utilizing to date the two former methods. The number of materials developed remains limited, and include multilayer coatings on flexible films, e.g. spin-on polyimides and DLC [4].

Whatever the elegance of the synthetic polymer chemistry, a natural conservatism in clinical application has arisen because of concerns about residual synthetic side products with bioeffects and the transient influence of any surface chemical modification in the face of a chronic tissue response at the implant locus. We have modified bulk polymer properties through physical entrapment of lipid or surfactant, and thereby achieved non-covalent modification of surface properties, applied solvent casting to produce test barrier structures of polycarbonate, PVC and SPEES-PES, and explored use of sol-gels and DLC.

II. EXPERIMENTAL

A. Materials

Several polymers were produced as underlayers in hydration resistant barrier layers. Polymer films were obtained through a chemical route starting with the raw material as solid state - PVC, sulphonated polyether ethersulphone polyethersulphone (SPEES-PES) - or in solution – silicone rubber, polyurethane (Trixene™ SG7602). Silicone rubber (MED-4211) was the kind gift of Cochlear Technology Centre (661 Drie Eikenstraat, Edegem, Belgium), provided

through NuSil, USA. Subsequently, polymers were dissolved in an appropriate solvent: THF for polyurethane and PVC, DMSO for SPEES-PES; silicone rubber was suspended in 2-Propanol until homogeneous. Plasticisers (1.6% v/v IPM or 5% v/v Aliquat336) were added into PVC, PU and SPEES-PES solutions. After stirring until homogeneous, 2 ml of the polymer solution obtained was cast on to 96mm diameter Petri dishes. The films were allowed to dry at room temperature for two days then removed for further characterization.

The hydration resistant top barrier layers studied were made of diamond-like carbon, sol-gel modified silica or ParyleneC.

Diamond-like carbon coatings were obtained through plasma assisted chemical vapor deposition (PACVD) using acetylene as a precursor gas (5 minutes at 300V); DLC provided good pore free conformal coatings. Because it lacks crystallinity, as a C-H alloy, it is better suited for biointerfacing compared to high crystallinity materials.

Modified silica sol was obtained starting with ethanol/HCl (pH1), dissolved tropaeoline and a mixture of methyltriethoxy silane (MTEOS) and phenyltriethoxy silane (PhTEOS). Tropaeoline was used in order to fill the pores that form in a sol-gel silica layer during drying. Continuous layers were obtained on glass slides by spin-coating at 500rpm followed by complete drying at 75°C for 15 days.

Parylene C was coated onto the substrate by vapor generation at 690°C, 0.5torr. Deposition of Parylene C was performed at room temperature. Parlyene C is a linear poly-para-xylylene with a single aromatic chlorine substitution and has low moisture permeability.

B. Characterisation Methods

The layers obtained were examined by optical microscopy (MoticBA400) in order to check for specific features. The interaction between polymers and water was monitored by FTIR (Nicolet-800FTIR). Electrochemical surface characteristics were assessed by the means of electrical impedance (Gamry instruments PC4/300). Polypyrrole was deposited on gold sputtered surfaces to provide electrodes for impedance analysis. Polypyrrole layers were obtained by electrochemical deposition, starting from a pyrrole monomer solution.

Cytotoxicity was tested using Alamar Blue assay on 3T3 fibroblasts grown directly on the synthesized materials. Tested samples were cut into 5mm squares, disinfected in ethanol for one day and then inserted into 24-wells plates with two negative and one positive control for each test run. Cells were seeded over samples (10,000 cells per well) and incubated for up to 96 hours. Experimental time points were 24, 48, 72 and 96 hours. At each time point, one ml of a 10% v/v solution of Alamar Blue was added to each well. The plates were then incubated for another 4 hours and then the fluorescence was measured using a plate reader at 570nm and 600nm.

C. Results and Discussion

Silicone rubber is medically acceptable, and was modified with IPM to confer greater hydrophobic properties to the surface and to increase water resistance. FTIR measurements of 24h water soaked membranes were compared with ambient air dried membranes and absorption peaks recorded between 3500-4000nm (Fig. 1).

Absorbance shows very low levels of water in both cases, and IPM certainly had not induced water uptake; possible improvement would require more extended testing but greater hydrophobicity has advantages for tissue interactions.

PVC, whilst not a viable implant polymer, provided a model support structure for IPM/surfactant additives. Aliquat had been selected for its known cationic properties (as a methyltrialkyl chloride) and, therefore, the contrast with lipid loaded films. Permeability to water was increased compared with IPM; if used within a chemically usable polymer, Aliquat could possibly protect active electrode surfaces whilst allowing water and electrolyte mediated conductivity. It has recently been shown by us to confer solute permeability to PVC used in metabolite sensors [5].

Polyurethane is the end product of isocyanate, macroglycol and a chain extender. A commercial isocyanate terminated prepolymer when solvent cast gave highly adherent films with both IPM and Aliquat and whilst not tested for hydration, could well give strong conformal barrier for

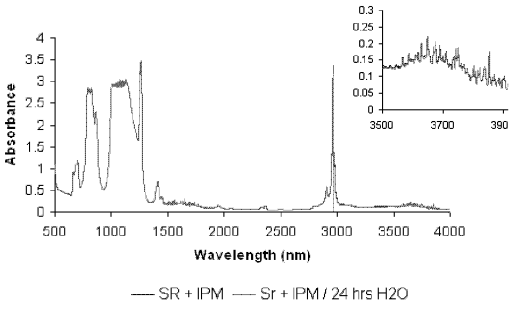

Fig. 1 FTIR, modified silicone film (dry/24h in water)

complex 3-D microelectrode structures.

SPEES-PES, potentially permeable, low molecular weight cut-off ion selective coatings [6] are of possible use over active microelectrode surfaces. The degree of sulphonation allows modulation of ion permeability through variation of surface fixed charge. IPM incorporation was not possible, but Aliquat inclusion led to a complex vacuole structured interface. The membrane is thus best used without additives, with a synthesis-based shift from the current sulphonation of 8% of the aromatic rings in order to vary properties.

DLC led to ultrathin <1μm coherent, adherent films on a dense, relatively inflexible substrate such as glass and polycarbonate. It had highly solute resistant properties and showed promise as a hydration barrier, depending upon the C-H ratio used for the source gas for deposition. However, coating of flexible polymers led different degrees of surface cracking (Fig. 2). So, it is less suitable as an outer versus inner barrier layer.

By contrast, ParyleneC gave uniform adherent films over PVC containing IPM and Aliquat and over silicone, though it did not adhere to PVC and for all polymer surfaces, a long-term problem of delamination remains.

Sol-gels are porous glasses made here, by the hydrolysis and condensation of metal alkoxides such as phenyltriethoxy silane (PhTEOS) and methyltriethoxy silane (MTEOS). A mixture of these gave surfaces with mixed phenyl and methyl groups and the addition of an aromatic (pH sensitive) dye Tropaeolin conferred strong adhesive function and resistance to abrasion. The sol-gels took up water, which was removed only very slowly after extended dehydration at 75°C (Fig. 3). As such the films could be used over active

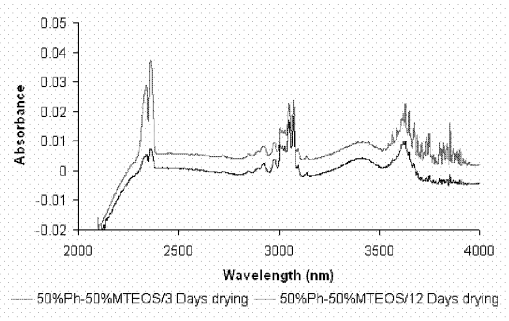

Fig. 3 Silica sol-gel dried at 75°C / hydrated upper curve for 2 days

but not passive electrode surfaces, provided toxicity was not evident.

Cytotoxicity testing using Alamar Blue dye as cell metabolic activity indicator with 3T3 fibroblasts was undertaken with the membrane constructs. Fibroblast attachment and spreading (Fig. 4) was observed for all membrane surfaces. However, uniquely, cell attachment was inhibited on PVC loaded with Aliquat (Fig. 5). The comparative metabolic rate reduction of 3T3 cells on the membranes is shown in Fig. 6. This confirms that none of the membranes were toxic to the cells, including IPM, but that Aliquat (possibly through minor degrees of leaching) was distinctly toxic – to a level seen for the positive control. Moreover, Paralene C over such membranes had no effect on cytotoxicity and certainly did not reduce the effect of Aliquat – the likelihood here was edge leaching of Aliquat, a problem that might be avoided through intact deposited outer coating layers.

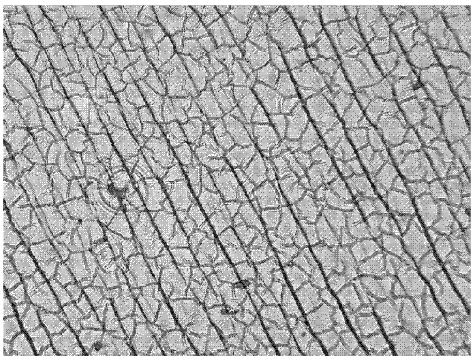

Fig. 2 DLC coating onto PVC (IPM) film (200x)

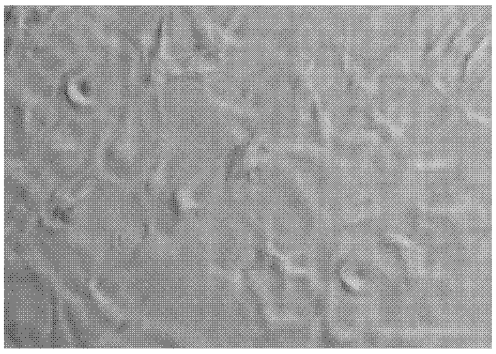

Fig. 4 Fibroblasts attached onto polymeric film

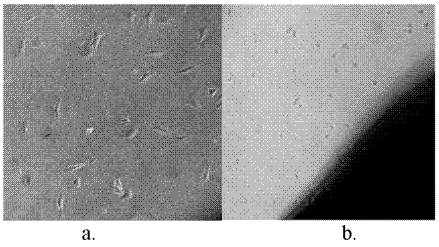

Fig. 5 Fibroblasts on (a) control substrate only versus (b) PVC film loaded with Aliquat (24 h incubation)

When polypyrrole was deposited over electrode surfaces, provided the appropriate counterion, notably a growth factor or connective tissue polymer, was incorporated, good cell growth was evident and electrode impedance was not impaired compared with the bare electrode surface.

III. Conclusions

A range of candidate test materials were established as possible encapsulants for passive micromolecluar device surfaces. These have variable H_2O permeability, and could be adapted alternatively for the active and passive components of microelectronic devices. Silicone modification appears especially promising as it is a tried and tested material, and lipid inclusion, generally, is worth investigating. Whilst considerable past success has been achieved with Parylene C, DLC might be able, either alone or as a laminate, to improve on the former material, particularly for low dimension geometries where there may be advantages in using plasma assisted chemical vapour deposition. The disadvantage of continuing with any new material, no matter how promising, however is that chronic implantation may not be possible with short-term cytotoxicity testing inadequate to the task of long-term biocompatibility prediction.

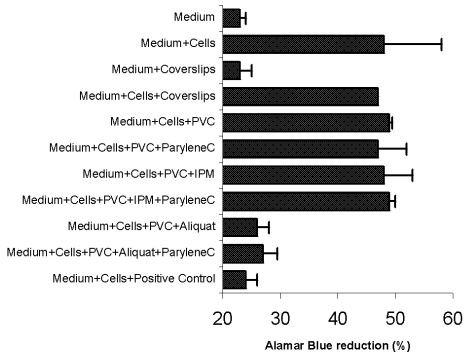

Fig. 6 Cytotoxicity assessment, fibroblasts, 96 hours

Acknowledgment

We acknowledge generous support from the EU (IST-2002-1-001837).

References

1. HealthyAims www.healthyaims.org.
2. Donaldson P (1991) Aspects of silicone rubber as an encapsulant for neurological prostheses. Part1. Osmosis. Medical & Biological Engineering & Computing 29:34-39
3. Thull R (2002) Physicochemical principles of tissue material interactions. Biomol Eng 19:43-50
4. Eckhardt H, Cuomo J, Guarnieri J, Sakhrani V, Nagle H, Ufer S, Premitec I, Raleigh N (2002) Insulating barrier coatings for flexible ribbon cables and microelectrodes suitable for implantable devices. Advancing Microelectronics Magazine 29:Medical Packaging
5. Reddy S, Vadgama P (1997) Surfactant-modified PVC membranes as biocompatible interfaces for amperometric enzyme electrodes. Analytical Chimca Acta 350:77-89
6. Hajatdoost S, Sammon C, Yarwood J (2002) FTIR–ATR studies of diffusion and perturbation of water in polyelectrolyte thin films. Part 4. Diffusion, perturbation and swelling processes for ionic solutions in SPEES/PES membranes. Polymer 43:1821-1827

Address of the corresponding author:
Author: Professor Pankaj Vadgama
Institute: Queen Mary, University of London
Street: Mile End Road
City: London
Country: UK
Email: p.vadgama@qmul.ac.uk

Anal Bioanal Chem (2008) 390:1121–1131
DOI 10.1007/s00216-007-1756-3

ORIGINAL PAPER

Development of electrochemical biosensors based on sol-gel enzyme encapsulation and protective polymer membranes

Rasa Pauliukaite · Monika Schoenleber · Pankaj Vadgama · Christopher M. A. Brett

Received: 2 August 2007 / Revised: 26 October 2007 / Accepted: 14 November 2007 / Published online: 16 December 2007

Abstract Protective polymer coatings have been used to enhance the retention of enzymes in sol-gel films as immobilisation phases in electrochemical biosensors. Carbon film electrodes were electrochemically modified with poly(neutral red) (PNR). These electrodes were coated with oxysilane sol-gels incorporating glucose oxidase and an outer coating of carboxylated PVC (CPVC) or polyurethane (PU), with and without Aliquat-336 or isopropyl myristate (IPM) plasticizer, was applied. The biosensors were characterised electrochemically using cyclic voltammetry and amperometry, electrochemical impedance spectroscopy and scanning electron microscopy. Impedance spectra showed that the electrode surface is most active when the sol-gel–GOx layer is not covered with a membrane. However, membranes without plasticizer extend the lifetime of the biosensor to more than 2 months when PU is used as an outer membrane. The linear range of the biosensors was found to be 0.05–0.50 mM of glucose and the biosensor with PU outer membrane exhibited higher sensitivity (ca.117 nA mM^{-1}) in the region of linear response than that with CPVC. The biosensors were applied to glucose measurement in natural samples of commercial orange juice.

R. Pauliukaite · C. M. A. Brett (✉)
Departamento de Química, Universidade de Coimbra,
3004-535 Coimbra, Portugal
e-mail: brett@ci.uc.pt

M. Schoenleber · P. Vadgama
IRC in Biomedical Materials, Queen Mary University of London,
Mile End Road,
London E1 4NS, UK

Keywords Carbon film electrode · Poly(neutral red) · Biosensor · Amperometry · Cyclic voltammetry · Electrochemical impedance spectroscopy · Glucose determination · Polymer membrane

Introduction

The sol-gel technique is often used for the encapsulation of bioactive substances, particularly enzymes, in the development of biosensors [1–5]. Organic–inorganic silanes polymerised by the sol-gel method are attractive materials since they combine, in a single phase, both the properties of the rigid three-dimensional porous silica network and the particular chemical reactivity of the organic components [4]. Some parameters, such as pH, gelation time, transparency and hydrophobicity can be adapted to encapsulate labile protein molecules such as enzymes [1–3, 5]. Usually the sol-gel is formed from the oxysilane in a two-step reaction: hydrolysis, and condensation, which is responsible for building the SiO_2 matrix within which enzyme molecules can be encapsulated [3].

Sol-gel enzyme encapsulation has been applied to different electrochemical [3, 6–15] and optical [16, 17] biosensors in the last few years. However, instability problems in some electrochemical biosensors have been reported [8, 13–15], which could be due to a small amount of enzyme leaching or to its inactivation. In order to solve this problem polymer membranes, particularly polyurethane (PU), were applied as an outer protecting layer [15].

Polymer membranes have been widely used for protein retention for over two decades [18–20]. Different non-sol-gel membranes have been used for this purpose, including poly(vinyl chloride) (PVC), different polyacry-

lates and polyurethane [19–23]. For example, membrane constructs can be created with incorporated protein/enzyme molecules by cross-linking using amine functional groups [19, 24], or a discrete protective layer can be formed over an enzyme layer [25]. The polymers should be chosen according to the conditions under which the sensor would operate, e.g. buffered samples, natural biological samples, in vivo, in vitro, etc. Modified PVC with carboxyl groups, carboxylated PVC (CPVC), has been applied to biosensor preparation by the covalent bonding of alcohol oxidase [26] or urease [27, 28].

Different electrode materials have been employed for biosensor preparation; however, carbon-based electrodes are most widely used for this purpose. Carbon film electrodes, obtained by coating a ceramic substrate with a thin deposit of pyrolytic carbon [29–31], have been successfully utilised. They have been used for developing glucose biosensors without mediators [32] but, in order to improve selectivity, biosensors have been modified with redox mediators, particularly copper [13] or cobalt [33] hexacyanoferrates, methyl viologen [34] and poly(neutral red) [35].

In previous studies [13, 14], it was reported that sol-gel enzyme electrodes can lead to unsatisfactorily short lifetimes, partly due to enzyme leaching. Therefore, in this work several polymer membranes, particularly polyurethane and carboxylated poly(vinyl chloride), were applied over the sol-gel-enzyme layer to prevent enzyme leaching. The results of glucose assay in relation to sensitivity, stability and response time in standard solutions obtained at sol-gel–enzyme–polymer membrane biosensors are presented.

Experimental

Chemicals and solutions

3-Glycidoxypropyltrimethoxysilane (GOPMOS), methyltrimethoxysilane (MTMOS) and neutral red (N^8,N^8,3-trimethylphenazine-2,8-diamine), and Aliquat-336 were obtained from Aldrich (Germany) (structures of these compounds are presented in Table 1). Glucose oxidase (GOx) from *Asperigillus niger* (EC 1.1.3.4) and anhydrous α-D(+)-glucose crystals were from Sigma (Germany). Carboxylated poly (vinyl chloride) and isopropyl myristate (IPM; see structure in Table 1) were purchased from Fluka (Switzerland), and polyurethane prepolymer was a kind gift from Baxenden (UK). Tetrahydrofuran (THF) was obtained from Riedel-de Haën (Germany). All products were analytical grade and were used without any further purification.

Electrolyte solution, 0.1 M phosphate buffer saline (PBS), pH 7.0, was prepared from sodium dihydrogenphosphate and disodium hydrogenphosphate (Riedel-de Haën, Germany), to which 0.05 M NaCl was added. Millipore Milli-Q nanopure water (resistivity >18 MΩ cm) was used for the preparation of all solutions. Experiments were performed at room temperature, 25±1 °C.

Biosensor preparation

Electrodes were made from carbon film resistors of ca. 2-Ω nominal resistance, as described elsewhere [29–31]. The exposed electrode geometric area was ca. 0.20 cm^2. The electrodes were electrochemically pretreated prior to electropolymerisation with neutral red by cycling between −1.0 and +1.0 V vs. saturated calomel electrode (SCE) in deoxygenated 0.1 M KNO_3 solution for not less than ten cycles, until stable cyclic voltammograms were obtained.

Poly(neutral red) (PNR) was polymerised on carbon film electrodes by electropolymerisation from a 1 mM solution of its monomer (neutral red, structure in Table 1) in aqueous 0.05 M phosphate buffer, pH 5.5, and 0.1 M KNO_3 solution, by cycling the applied potential from −1.0 to 1.0 V vs. SCE 15 times at a potential sweep rate of 50 mV s^{-1}. The electrode was then rinsed with deionised water to remove free monomer, after which it was left to dry for 1 day in air at room temperature.

Sol-gel solution was prepared by mixing the two oxysilanes with water in optimised ratios [13, 14]: GOPMOS/MTMOS/H_2O 130:70:600 μL, respectively. A 2-μL aliquot of 6 M HCl solution was added to the mixture obtained to accelerate hydrolysis of the oxysilanes. The mixture obtained was intensively stirred for a few minutes and then sonicated for 15 min. The solution was then heated in a hot air stream (ca. 70 °C) to evaporate the alcohol formed during hydrolysis of the oxysilanes [36] until the mixture lost 40% of its volume. It was then left for 1 h at room temperature to cool down and neutralized to pH 7.0 with 0.1 M NaOH solution. A 50-μL aliquot of this solution was carefully mixed with 15 μL of GOx (10%) solution in 0.1 M PBS solution pH 7.0 and left for 1 h to equilibrate. The PNR-coated carbon film electrode was then immersed in sol-gel–enzyme solution for 5 min, removed and left to form a xerogel at 4 °C for 2 days.

Membrane solutions were prepared by dissolving either CPVC or PU in THF by sonication of the polymer–solvent mixture until transparent solutions were obtained. The optimised composition for polymer preparation was 3.5% (w/v) CPVC or 20% PU (v/v). Some plasticizers, 5% (v/v) Aliquat-336 or 1.6% (v/v) IPM, were added to the solutions to improve membrane properties. The mixtures were sonicated once again to obtain homogeneous solutions. Six different membrane solutions were used: (1) 3.5% CPVC, (2) 3.5% CPVC + 5% Aliquat-336, (3) 3.5% CPVC + 1.6% IPM, (4) 20% PU, (5) 20% PU + 5% Aliquat-336 and (6) 20% PU +

Anal Bioanal Chem (2008) 390:1121–1131 1123

Table 1 Structures of organic compounds used for biosensor preparation

Compound	Structure
N8,N8,3-trimethylphenazine-2,8-diamine (Neutral red monomer)	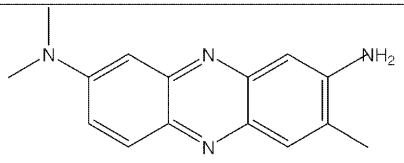
3-Glycidoxypropyltrimethoxysilane (GOPMOS)	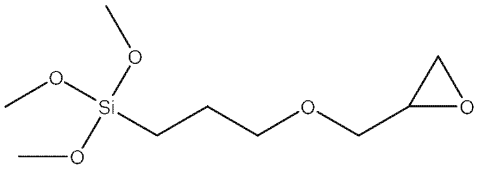
Methyltrimethoxysilane (MTMOS)	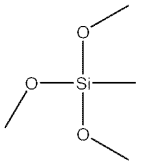
Carboxylated polyvinyl chloride	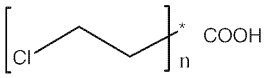
Polyurethane	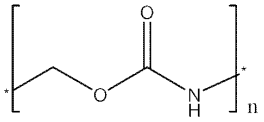
Aliquat-336	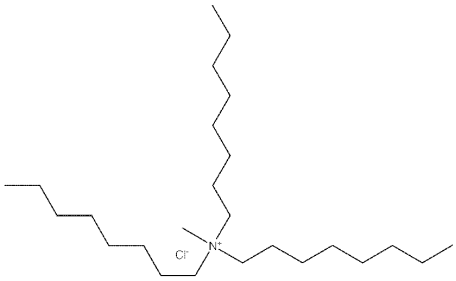
Isopropyl myristate (IPM)	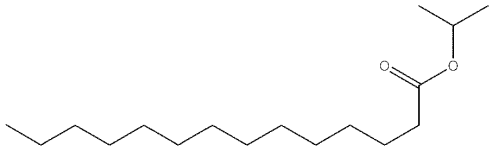

1.6% IPM. The electrodes with the formed sol-gel layer (after 2 days) were immersed in one of the membrane solutions for a few seconds and left in air for 30 min for solvent evaporation to leave a thin outer membrane layer.

Prepared biosensor assemblies were stored at 4 °C in PBS solution when not in use.

Methods and instruments

Cyclic voltammetry (CV) and amperometric measurements were performed in a three-electrode electrochemical cell containing a sol-gel encapsulated enzyme carbon film working electrode, a platinum foil as counter electrode and a saturated calomel electrode (SCE) as reference. Measurements were performed using a computer-controlled μ-Autolab Type II potentiostat/galvanostat with GPES 4.9 software (Eco Chemie, Netherlands).

Electrochemical impedance spectroscopy (EIS) measurements were carried out in the same electrochemical cell as described above with a PC-controlled Solartron 1250 frequency response analyser coupled to a Solartron 1286 electrochemical interface using ZPlot 2.4 software (Solartron Analytical, UK). The frequency was scanned from 65 kHz to 0.1 Hz with ten points per frequency decade, with a sinusoidal voltage perturbation amplitude of 10 mV, auto-integration time 60 s, with short accuracy mode, at 90% significance level. Fitting to electrical equivalent circuits was performed with ZView 2.4 software (Scribner Associates, USA).

Scanning electron microscopy investigations were performed using a JEOL JSM 6300 scanning electron microscope after the specimens had been plated with gold under vacuum.

Independent analysis of glucose concentrations in commercial samples was done using a spectrophotometric enzyme assay kits (Cat 0 139 106, Boehringer, Mannheim) and analysis at 340 nm using a SPECORD S100 (Analytik Jena GmbH, Jena, Germany) UV-VIS spectrophotometer running Aspect Plus Version 1.5 software.

Results and discussion

Electrochemical and surface characterisation of sol-gel/membrane biosensors

In order to follow changes in the electrochemical behaviour of the sol-gel/membrane-based biosensor during its preparation, cyclic voltammograms (CVs) and impedance spectra were recorded after each step of electrode preparation in 0.1 M PBS solution, pH 7.0. The results obtained are presented and described in this section.

The sol-gel was prepared from a GOPMOS and MTMOS mixture, volume ratio 2:1 in water and with the addition of HCl as catalyst (see Experimental). The composition of the outer polymer coating was also optimised via the response to glucose in PBS solution. Table 2 presents results from optimisation of the polymer concentration for the preparation of CPVC and PU membrane coatings without plasticizer. The best concentrations were found to be 3.5 and 20% (w/v) for CPVC and PU, respectively, in THF. These concentrations were used for further biosensor characterisation and application. Membranes made from more concentrated polymer solutions did not allow analyte to pass through to the sol-gel layer sufficiently easily for reaction with the enzyme so amperometric response was attenuated. For too low concentrations of polymer solution the results suggest that uniform membranes were probably not formed, see Table 2. However, there is a report of the use of a PU membrane applied over the sol-gel layer for glucose microsensors made using a lower polymer concentration, and the sensor response was sufficient; however, here PU was blended with a hydrophilically modified PU in the weight ratio 7:3 [15].

Cyclic voltammetry

CVs were registered in PBS solution in the potential range from −1.0 to +1.0 V vs. SCE. Neutral red polymerisation has been described in detail in previous work [14, 35] and in the Experimental. The PNR film was left to stabilise for 1 day, and before sol-gel deposition, CVs were registered in 0.1 M PBS pH 7.0 (see Fig. 1 dotted line). The electrochemical behaviour of PNR strongly depends on pH and well-defined polymer peaks are obtained at pH 4–6 [37, 38]. However, the polymer peaks are broader and the peak current is lower at neutral pH, as is seen in Fig. 1. The

Table 2 Optimisation of CPVC and PU concentration for membrane preparation according to PNR/sol-gel–GOx/membrane electrode amperometric response to 200 μM of glucose in 0.1 M PBS, pH 7.0 at −0.25 V vs. SCE

Polymer concentration in THF (%)	Response to glucose (nA)
CPVC	
4.8	10
3.5	15
3.0	13
2.5	9
PU	
50	5
40	10
30	25
20	37
10	20

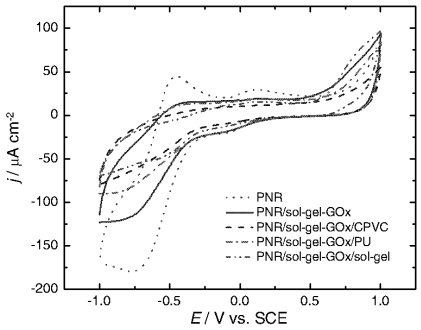

Fig. 1 Cyclic voltammograms at carbon film electrodes modified by PNR (····), PNR/sol-gel and PNR/sol-gel–GOx (——), PNR/sol-gel–GOx/CPVC (- - -), PNR/sol-gel–GOx/PU (-·-·), PNR/sol-gel–GOx/sol-gel (-···). Supporting electrolyte 0.1 M PBS, pH 7.0. Potential scan rate 50 mV s^{-1}

monomer oxidation peak, usually present at potentials between +0.8 and +0.9 V vs. SCE, is shifted to a significantly more positive potential and is out of the potential range studied.

Cyclic voltammograms were recorded on PNR-modified electrodes, after deposition of the sol-gel layer with encapsulated enzyme and with and without outer coatings (Fig. 1). As expected, the sol-gel acts as a diffusion membrane for counterions and the Faradaic current corresponding to PNR decreases significantly (Fig. 1, solid line). Addition of enzyme hardly changes the electrochemical behaviour of the biosensor, since the enzyme is electrochemically inactive and any co-factor concentration is too small to make changes to the CV of poly(neutral red). All the other CVs with any type of membrane presented in Fig. 1 are with entrapped enzyme. It is interesting that with a superimposed sol-gel layer an oxidation wave again appears at approximately +0.8 V vs. SCE, where there is usually irreversible oxidation of neutral red monomer. This wave is seen with or without enzyme and so does not appear to be caused by the biosensing component itself. The mediated system here is quite distinct from those where the sol-gel-immobilised oxidase generates an indirect response via H_2O_2 [39].

After application of an outer protecting membrane of CPVC or PU (Fig. 1, dashed and dash-dot-dash lines, respectively), the PNR peak current again decreases and it is difficult to distinguish the peaks; the oxidation wave at +0.8 V also disappears. These CVs were recorded using overlying membranes from solutions of 3.5% CPVC in THF (w:v) and 20% PU in THF (v:v), optimised with respect to the response signal to glucose (see above).

As an alternative, a second sol-gel layer (without enzyme) was also deposited as an outer membrane coating on top of the first layer with enzyme. In this case, the CV recorded in PBS is rather similar to one with CPVC (Fig. 1, dash-dot-dot-dash curve). However, PNR redox peaks are still lower than at the biosensor with CPVC and there is a quite well defined oxidation wave at +0.8 V, which suggests that this oxidation wave comes from some electrochemical changes in the sol-gel itself.

Usually plasticizers are used to improve the physical properties of a polymer material [18–20]; Aliquat-336 and isopropyl myristate (see structure in Table 1) were used as plasticizers in this work to manipulate permeability. The influence of the plasticizers on the voltammetric behaviour of the biosensors is shown in Fig. 2. In the case of CPVC, plasticizers have a greater influence on the electrochemical behaviour of the biosensor, especially IPM (Fig. 2a, dash-dot-dash line). This probably occurs due to the lower CPVC concentration compared with PU. Addition of 5% Aliquat to the CPVC membrane composition led to higher reduction peak currents in the potential region between −0.6 and −1.0 V, i.e. in the region of PNR reduction, as well as in the monomer oxidation region, from +0.7 to +1.0 V, (Fig. 2a, dashed line) compared with CPVC without any plasticizer. These effects are even more marked when IPM is used as plasticizer; however, oxidation of PNR is also significantly suppressed. This suggests enhanced glucose transport through plasticized membranes, which

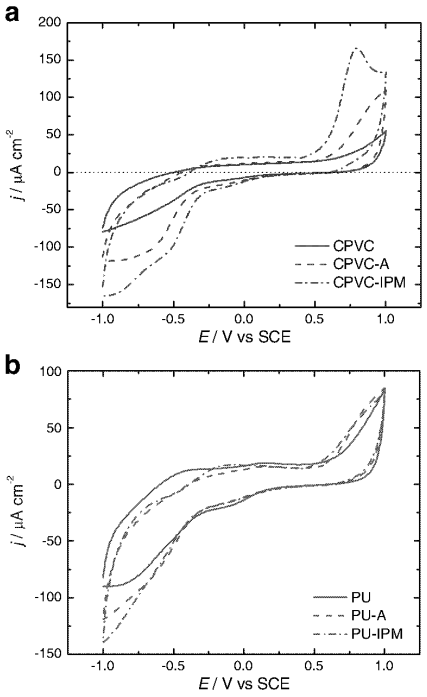

Fig. 2 Cyclic voltammograms at **a** PNR/sol-gel–GOx/CPVC and **b** PNR/sol-gel–GOx/PU without plasticizer, and with Aliquat (A) or IPM as plasticizer. All other conditions as in Fig. 1

was certainly expected with the hydrophilic surfactant, thought not with the non-polar IPM. The effect of IPM-enhanced transport could have been the result of structural (depth, porosity) changes to the formed membrane. Similar behaviour was observed at the biosensor with a PU outer membrane except that in this case, due to the higher polymer concentration, there was not such a large difference between PU with and without plasticizer (Fig. 2b).

Electrochemical impedance spectroscopy

Impedance spectra were recorded after each biosensor preparation step in the same way as in cyclic voltammetry, i.e. after electropolymerisation of neutral red; sol-gel deposition with and without enzyme; and outer membrane deposition. The sol-gel layer without enzyme was deposited to study any influence from the presence of enzyme on the electrode interfacial characteristics. Impedance spectra are presented in Fig. 3 which shows both complex plane and Bode plots. Spectra were recorded at three different potentials: at 0.0 V, where slow protonation of ionogenic groups occurs; at −0.25 V, the chosen operating potential; and at −0.5 V, where the redox process of PNR takes place.

Impedance spectra in the complex plane plots at 0.0 V remain similar in form after each step in biosensor preparation—only the magnitude of the impedance varies.

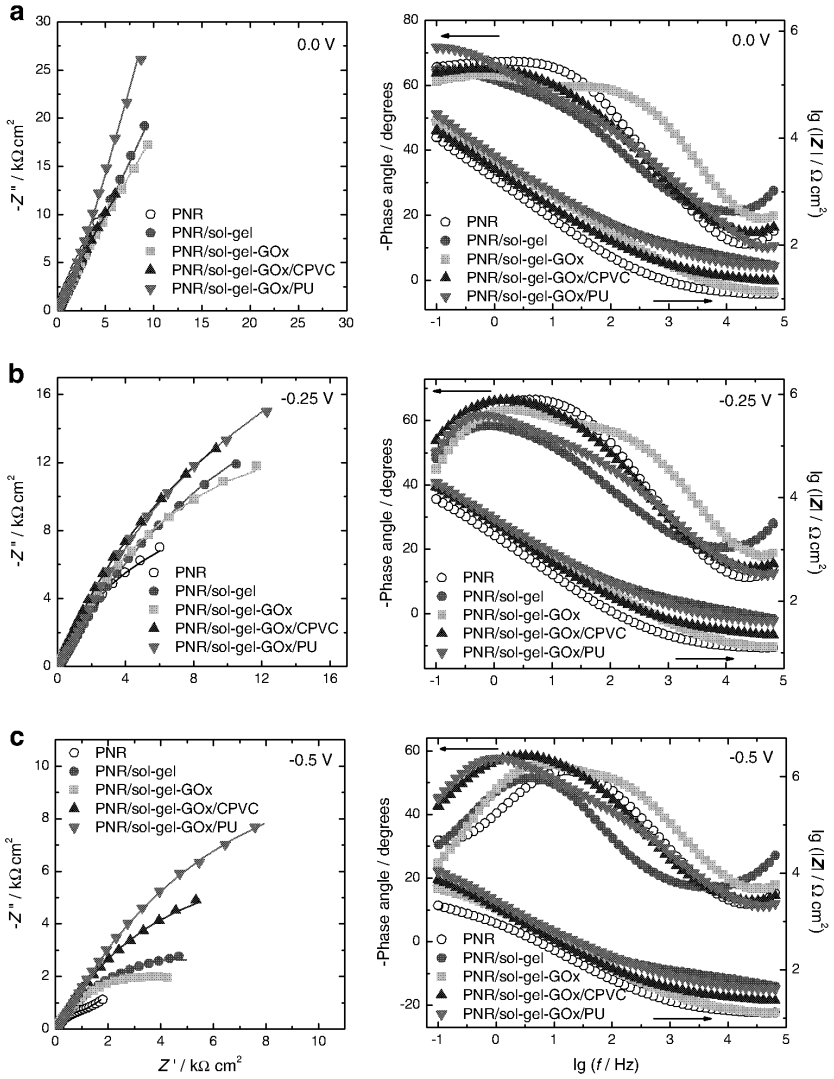

Fig. 3 Complex plane (*left*) and Bode plots (*right*) at PNR-modified carbon film electrodes (*open circles*), with sol-gel layer without enzyme (*red circles*), with GOx immobilised without any protecting membrane (*turquoise squares*) and with CPVC (*blue triangles*) or PU (*green triangles*). Spectra were recorded at **a** 0.0 V, **b** −0.25 V and **c** −0.50 V vs. SCE

The linear nature of the spectra indicates charge separation over the whole frequency region. At −0.25 V, impedance values are lower and spectra curve in the low frequency region due to the oxidation of PNR. At −0.5 V, closer to the formal potential of the PNR redox couple, impedance values again decrease and the shapes of the spectra depend to a greater extent on the exact biosensor assembly in contrast to the other potentials. Uncoated PNR films show a more complex behaviour at this potential compared with coated ones, since, as is seen from Fig. 1, there are significantly higher PNR redox peaks than at sol-gel-coated PNR mediator films under these conditions. Differences in the shape of the spectra are seen between PNR/sol-gel and PNR/sol-gel–GOx electrodes which suggests that the enzyme changes the sol-gel morphology and structure as was found using AFM in sol-gel morphology studies [40].

Usually sol-gel and polyurethane films are investigated by EIS in the context of corrosion protection, so that spectra are recorded at the open circuit potential [41, 42]. The spectra from the complex plane and Bode plots at sol-gel-coated metals are rather similar those in this study at −0.25 V vs. SCE in Fig. 3 and depend significantly on the identity of the substrate material (metal or alloy) [41]. Spectra of polyurethane films on stainless steel at +0.1 V vs. SCE are different from those at the biosensor investigated here: there was mass transport control over the whole frequency range [42]. These facts demonstrate that the film structure can depend strongly on the electrode substrate and modifying layers.

In order to describe the processes occurring at the surface of PNR, an equivalent circuit model was used for fitting all spectra, consisting of the cell resistance, R_Ω, in series with a parallel combination of a charge-transfer resistance, R_{ct} and a constant phase element, CPE, modelled as a non-ideal capacitance, according to [43]

$$\mathrm{CPE} = 1/(Ci\omega)^{\alpha} \quad (1)$$

where C is capacitance in μF cm^{-2} s$^{\alpha-1}$, ω is the frequency in radians, and α represents surface non-uniformity, being equal to unity if the surface is smooth and uniform. This model was combined in series with a resistance, R_f, and another CPE to represent the electrical properties of all the extra film components, when PNR was covered with sol-gel or sol-gel–enzyme layer and with the outer membrane layer. Table 3 gives the parameters deduced from the first R-CPE couple representing the interfacial processes and corresponding to the fitting of the high frequency part of the spectra. Values of R_Ω vary from 11 to 15 Ω cm^2, except at PNR/sol-gel–GOx/PU, where R_Ω was ca. 32 Ω cm^2. The charge-transfer resistance decreases with increasingly negative potential due to electrochemical reactions of the PNR [34–36]. An exception is PNR/sol-gel–GOx, demonstrating evidence of an additional reaction which is going on at this electrode as is also easy to identify from the Bode plot (Fig. 3). The α values vary from 0.7 to 1.0 and depend on the electrode composition: α is closest to 1.0 at the PNR/sol-gel–GOx electrode which indicates that the surface is almost homogeneous and uniform.

Scanning electron microscopy

Figure 4 presents the SEM images at carbon film electrodes coated in various ways. All electrodes were coated with PNR film and sol-gel layer and some of them had GOx entrapped into the sol-gel layer and an outer polymer membrane without any plasticizer. The sol-gel layer seems

Table 3 Analysis of the electrochemical impedance data at carbon film electrodes

E vs. SCE (V)	C film electrode coating	R_{ct} (kΩ cm^2)	C (μF cm^{-2} s$^{\alpha-1}$)	α
0.0	PNR	193±8	73.6±4.4	0.81±0.01
	+sol-gel	437±13	67.7±3.6	0.73±0.01
	+sol-gel–GOx	7±1	533.7±7.9	1.00±0.01
	+CPVC	153±7	99.9±5.3	0.76±0.01
	+PU	524±15	54.3±3.8	0.84±0.01
−0.25	PNR	56±3	57.9±5.1	0.83±0.01
	+sol-gel	49±3	78.8±7.2	0.75±0.01
	+sol-gel–GOx	10±1	137.6±6.0	0.94±0.01
	+CPVC	51±2	77.7±6.0	0.79±0.01
	+PU	33±2	89.0±3.3	0.88±0.01
−0.50	PNR	1±0	114.9±7.1	1.00±0.01
	+sol-gel	9±1	133.6±6.7	0.75±0.01
	+sol-gel–GOx	5±0	157.8±7.0	0.77±0.01
	+CPVC	17±1	141.4±1.0	0.71±0.01
	+PU	15±1	135.9±8.1	0.84±0.01

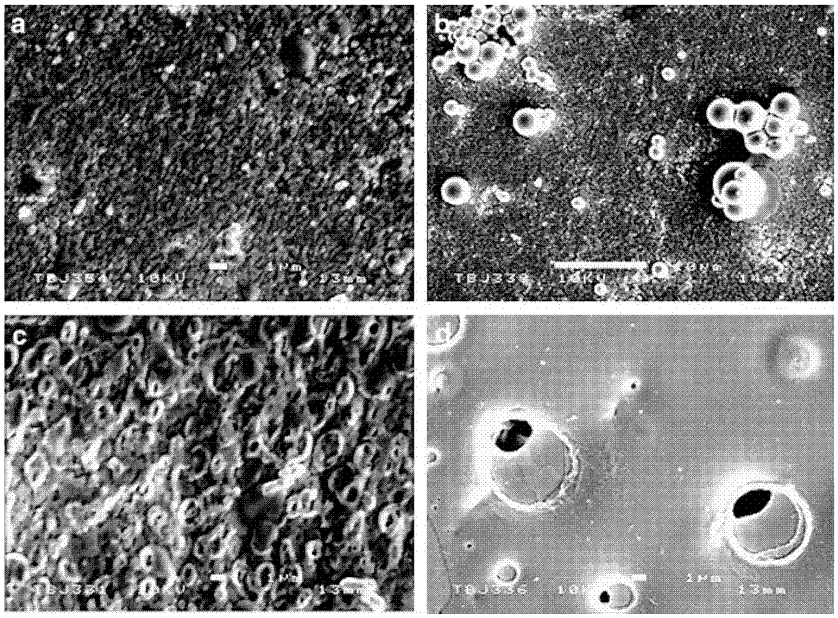

Fig. 4 SEM images of PNR film polymerised on carbon film electrodes covered with **a** sol-gel, **b** sol-gel-entrapped GOx, **c** sol-gel-entrapped GOx with outer membrane of CPVC, and **d** sol-gel-entrapped GOx with outer membrane of PU

to be rather flat and homogeneous (Fig. 4a) as would be expected from a glass-like xerogel layer. Interestingly, after GOx entrapment the sol-gel layer is no longer homogeneous and some clusters are visible at the surface (Fig. 4b). These clusters are possibly due to enzyme aggregates. Similar changes in the sol-gel layer after enzyme entrapment have been found using AFM [40].

After application of the outer polymer membrane the surface topography is different and depends on the nature of the polymer. When CPVC was used as a protective membrane the electrode surface was rather homogeneous but not perfectly flat, showing onion-ring-shaped structure (Fig. 4c). The other polymer, PU, formed a much more uniform and flat surface, although a few islands of discrete defects are seen, as highlighted in Fig. 4d. These results agree with those obtained using electrochemical methods and can explain the response and stability of the biosensors prepared with these polymer membranes (see below).

Response to the analyte

The biosensors with the outer diffusion membranes were calibrated in standard glucose solutions in 0.1 M PBS, pH 7.0. Calibration data were analysed and the main analytical parameters calculated. The biosensors were also checked for interference from some sugars, organic acids and phenol. Additionally, their lifetime and storage stability over a period of 70 days was examined. The electrodes were stored at +4 °C in PBS solution when not in use.

Calibration of the biosensors

Calibration curves were recorded at biosensors without an outer membrane, and at biosensors with CPVC and PU outer diffusion membranes with and without plasticizers (Aliquat-336 and IPM). Application of the diffusion membrane decreased the current response to glucose but it still remained acceptable for glucose measurement, as shown in Fig. 5, except in cases when Aliquat was used as plasticizer where a marked loss in response was observed during the assay; this is a possible result of enzyme loss induced by the hydrophilic surfactant. When PU was used

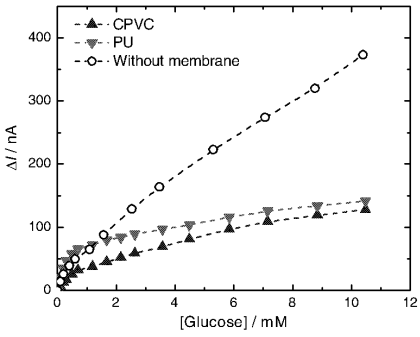

Fig. 5 Glucose calibration curves at PNR/sol-gel–GOx (*open circles*), PNR/sol-gel–GOx/CPVC (*blue triangles*) and PNR/sol-gel–GOx/PU (*green triangles*) in 0.1 M PBS solution, pH 7.0. Operating potential −0.25 V vs. SCE

Anal Bioanal Chem (2008) 390:1121–1131 1129

Table 4 Parameters calculated from calibration curves at carbon film electrodes modified with PNR as a mediator and sol-gel-encapsulated glucose oxidase with or without outer diffusion membrane (n=3)

Biosensor composition	Linear range (mM)	Sensitivity (nA mM^{-1})	Limit of detection (μM)	K_M (mM)	Correlation coefficient (R^2)
PNR/sol-gel–GOx	0.05–0.60	74.7±2.8	21.1	1.4	0.992
PNR/sol-gel–GOx/CPVC	0.05–0.50	65.7±5.3	58.2	1.6	0.997
PNR/sol-gel–GOx/CPVC-IPM	0.05–0.50	52.0±2.9	68.0	1.6	0.991
PNR/sol-gel–GOx/PU	0.05–0.50	116.9±14.9	15.8	1.7	0.997
PNR/sol-gel–GOx/PU-IPM	0.05–0.50	57.0±5.8	62.6	1.6	0.990

All conditions as in Fig. 5

as a diffusion membrane the sensitivity in the region of the linear range appeared marginally higher than that at uncovered sol-gel. The biosensor without outer membrane had a much higher response at higher glucose concentration, which is probably related to the PNR mediation mechanism as well as some saturation of analyte diffusion through the membranes.

When IPM was used as membrane plasticizer, the response to glucose was slightly lower than that without any plasticizer (not shown) and Aliquat suppressed the signal too much (not shown), so it was not used for further investigations. Data calculated from the calibration curves are given in Table 4. The lowest limit of detection (LOD) was obtained at biosensors with the PU outer membrane but without any plasticizer. This is possibly the result of a thinner barrier layer in the absence of plasticiser. The apparent Michaelis–Menten constant obtained using Lineweaver–Burk linearisation was very similar in almost all cases, Table 4. Nevertheless, the highest sensitivity, as mentioned above, was found to be at the PNR/sol-gel–GOx/PU biosensor. Thus, according to the data obtained, the best composition for the biosensor is a carbon film electrode modified with PNR and with enzyme immobilised in a sol-gel layer and using a 20% (w/v) PU outer membrane.

The stability of the biosensors coated with outer membranes with and without IPM plasticizer was also studied. The biosensor was used once per day every day for the first 30 days and after this every second day. The results presented in Fig. 6 show that the most stable biosensor was the one with the PU outer membrane without any IPM. Note that the second measurement on the first day was used as reference as there was a significant response drift from the first measurement to the second, possibly due to leaching of free enzyme residues and some hydration effect of the sol-gel protein membrane [44]. The response did not drop further with PU even after 70 days. However, the biosensor with PU and plasticizer was stable for only 30 days and then the signal started to decrease progressively reaching 50% after 70 days. When CPVC was used as the outer membrane, stability was significantly lower and at the biosensor without plasticizer the signals started to decrease after 40 days. IPM makes the sensor even less stable than sol-gel without any outer membrane. It is possible that the plasticizers here changed the membrane morphology, e.g. by altering pore geometry [45], in addition to the effect on the dielectric properties of the polymer phase; this would affect enzyme retention ability. Alternatively it could be an ageing effect of the membrane itself. The lifetime of the biosensor without any outer membrane was 40 days [40].

The storage stability of the biosensors was at least 5 months when the sensors were kept at +4 °C in PBS and at least 1 month under dry conditions at the same temperature for biosensors with outer membranes without plasticizer and 2 months with plasticizers. The membranes began to crack after they had been stored under dry conditions for a longer period of time.

Investigation of interferences

Interference from some organic acids and some other organic compounds, such as fructose and phenol, was in-

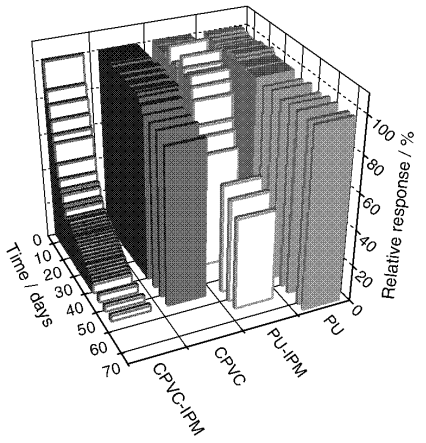

Fig. 6 Response to 0.3 mM glucose over time relative to initial value at PNR/sol-gel–GOx electrodes covered by PU, PU-IPM, CPVC and CPVC-IPM outer membranes. All other conditions as in Fig. 5

Table 5 Interference of some compounds on response to 0.2 mM of glucose at PNR/sol-gel–GOx/CPVC and PNR/sol-gel–GOx/PU biosensors

Biosensor	Compound	Glucose/interfering compound ratio	Response signal (%)
PNR/sol-gel–GOx/CPVC	Fructose	1:5	100.0
	Phenol	1:5	112.5
	Acetaldehyde	1:1	108.3
		1:5	133.3
	Acetic acid	1:5	100.0
	Ascorbic acid	1:5	97.9
	Citric acid	1:1	100
		1:5	75.6
	Tartaric acid	1:1	92.8
		1:5	75.6
PNR/sol-gel–GOx/PU	Fructose	1:5	100.0
	Phenol	1:1	111.1
		1:5	129.6
	Acetaldehyde	1:1	85.7
		1:5	71.4
	Acetic acid	1:5	100.0
	Ascorbic acid	1:5	91.7
	Citric acid	1:5	100.0
	Tartaric acid	1:1	100.0
		1:5	77.8

All conditions as in Fig. 5

vestigated at biosensors with both CPVC and PU outer membranes, without any plasticizer. Most organic acids only interfered at much higher concentrations than glucose (Table 5). Fructose hardly interferes, but quite a significant interference was found from phenol, which increased the glucose signal. The interferences are lower when a PU membrane is used, except from acetaldehyde. This is possibly related to the higher concentration of PU compared with CPVC so that a more homogeneous PU membrane is formed (see Scanning electron microscopy) which better prevents penetration of an interfering compound. The interferents react with PNR, which easily reacts electrochemically with compounds having carboxylic or alcohol groups [14, 37, 38, 46]. On the other hand, after application of the outer membranes the interferences decreased significantly compared with other biosensors based on PNR mediators [38], which confirms that these membranes, especially PU, hinder access of interferent to the mediator layer. The much reduced interference also confirms the relatively defect-free PU membranes produced.

Application to natural samples

The biosensors were applied to glucose determination in a commercially available orange drink, which consists of 10% (v/v) natural orange juice and either sugar syrup or a glucose/fructose mixture, or both. Biosensors with both outer membranes (CPVC or PU) were employed for glucose determination in the orange drink by the standard addition method. The sample was diluted 100 times to be within the biosensor linear range. Concentrations of 0.229±0.011 M (41.2±2.0 g L^{-1}) and 0.204±0.026 M (36.8±4.7 g L^{-1}) of glucose were found at biosensors with CPVC and PU outer membranes, respectively. The PNR/sol-gel–GOx/PU biosensor showed a lower value and a higher uncertainty than the PNR/sol-gel–GOx/CPVC one. However, these values are in a good agreement with the value obtained by the spectrophotometric reference method using an enzymatic test kit according to the procedure described elsewhere [47]: 0.214±0.005 M (38.6±0.8 g L^{-1}).

Conclusions

The performance of sol-gel-based biosensors was improved by application of an outer protecting polymer membrane, particularly carboxylated PVC and polyurethane. Three types of membrane composition were investigated: polymer without any plasticizer and with two different plasticizers, Aliquat-336 and IPM. These biosensors were first characterised electrochemically, using CV and EIS. Sol-gel and protecting membrane layers decreased the PNR re-oxidation current since they act as diffusion membranes. The membranes decrease interferences significantly, and extend the lifetime of the biosensor to more than 2.5 months, especially in the case when PU without any plasticizer is used as outer membrane. The membrane-coated biosensor with PU outer membrane also exhibited higher sensitivity and a lower limit of detection. This biosensor construction, i.e. with sol-gel enzyme layer covered by a polyurethane membrane, is recommended for future studies and applications.

Acknowledgements The financial support of the Treaty of Windsor Anglo-Portuguese Joint Research Programme 2005-6, of ICEMS-Coimbra (Research Unit 103) Portugal, and of the Biotechnology and Biological Sciences Research Council, UK, is gratefully acknowledged. R. Pauliukaite thanks Fundação para a Ciência e Tecnologia (FCT) for a postdoctoral grant (SFRH/BPD/14518/2003).

References

1. Gill I, Ballesteros A (1998) J Am Chem Soc 120:8587
2. Gill I (2001) Chem Mater 13:3404
3. Pierre AC (2004) Biocatal Biotransform 22:145
4. Walcarius A, Mandler D, Cox JA, Collinson M, Lev O (2005) J Mater Chem 15:3663
5. Tripathi VS, Kandimalla VB, Ju H (2006) Sens Actuat B 114:1071

6. Anitha S, Mohan SV, Reddy SJ (2004) Biosens Bioelectron 20:848
7. Lei CX, Hu SQ, Gao N, Shen GL, Yu RQ (2004) Bioelectrochem 65:33
8. Roman G, Pappas ACh, Kovala-Demertzi D, Prodromidis MI (2004) Anal Chim Acta 523:201
9. Salimi A, Compton RG, Hallaj R (2004) Anal Biochem 333:49
10. Teh HF, Yang X, Gong H, Tan SN (2004) Electroanalysis 16:769
11. Xu JZ, Zhang Y, Li GX, Zhu JJ (2004) Mater Sci Eng C 24:833
12. Tu YF, Di JW, Chen XJ (2005) J Sol-Gel Sci Technol 33:187
13. Pauliukaite R, Brett CMA (2005) Electrochim Acta 50:4973
14. Pauliukaite R, Brett CMA, Chiorcea-Paquim AM, Oliveira Brett AM (2006) Electrochim Acta 52:1
15. Oh BK, Robbins ME, Nablo BJ, Schoenfisch MH (2005) Biosens Bioelectron 21:749
16. Pastor I, Esquembre R, Micol V, Mallavia R, Reyes Mateo C (2004) Anal Biochem 334:335
17. Wu HJ, Choi MMF (2004) Anal Chim Acta 514:219
18. Wang J (1999) Anal Chem 71:328R
19. Gill I, Ballesteros A (2000) Trends in Biotechnol 18:469
20. Wisniewski N, Reichert M (2000) Coll Surf 18:197
21. Reddy SM, Vadgama P (2002) Anal Chim Acta 461:57
22. Maines A, Ashworth D, Vadgama P (1996) Anal Chim Acta 333:223
23. Puig-Lleixa C, Jiménez C, Bartroli J (2001) Sens Actuat B 72:56
24. Vastarella W, Nicastri R (2005) Talanta 66:627
25. Choi SH, Lee SD, Shin JH, Ha J, Nam H, Cha GS (2002) Anal Chim Acta 461:251
26. Lau RCW, Choi MHF, Lu J (1999) Talanta 48:321
27. Koncki R, Kopczewska E, Glab S (1994) Anal Lett 27:475
28. Karakuş E, Pekyardımcı Ş, Kılıç E (2005) Art Cell Blood Subst Biotechnol 33:329
29. Brett CMA, Angnes L, Liess H-D (2001) Electroanalysis 13:765
30. Filipe OMS, Brett CMA (2003) Talanta 61:643
31. Filipe OMS, Brett CMA (2004) Electroanalysis 16:994
32. Florescu M, Brett CMA (2005) Talanta 65:306
33. Florescu M, Brett CMA (2004) Anal Lett 37:871
34. Ghica ME, Brett CMA (2005) Anal Chim Acta 532:145
35. Pauliukaite R, Ghica ME, Barsan M, Brett CMA (2007) J Solid State Electrochem 11:899
36. Ferrer ML, del Monte F, Levy D (2002) Chem Mater 14:3619
37. Karyakin AA, Bobrova OA, Karyakina EE (1995) J Electroanal Chem 399:179
38. Ghica ME, Brett CMA (2006) Electroanalysis 18:748
39. de Jesus DS, Couto CMCM, Araujo AN, Montenegro MCBSM (2003) J Pharm Biomed Anal 33:983
40. Chiorcea Paquim AM, Pauliukaite R, Brett CMA, Oliveira Brett AM In preparation
41. Buenfeld NR, Zhang JZ (2000) J Mater Sci 35:39
42. Khobaib M, Reynolds LB, Donley MS (2001) Surf Coat Technol 140:16
43. Orazem ME, Shukla P, Membrino MA (2002) Electrochim Acta 47:2027
44. Chen JY, Cox W, Tehan E, Bright FV, Cerne J, Markelz AG (2004) Can be downloaded online at http://arxiv.org/ftp/cond-mat/papers/0307/0307558.pdf
45. Tan K, Obendorf SK (2006) J Memb Sci 274:150
46. Broncova G, Shishkanova TV, Matejka P, Volf R, Kral V (2004) Anal Chim Acta 511:197
47. Bergmeyer HU, Bernt E, Schmidt F, Stork H (1974) Methoden der enzymatischen Analyse, 3rd edn, Vol 2. Verlag Chemie, Weinheim

Surfaces and interfaces for biomaterials, Edited by Pankaj Vadgama
CRS Press, Woodhead Publishing Ltd., Cambridge England

5
Stable use of biosensors at the sample interface

JF GARGIULI, University of London, UK, A GILL and
G LILLIE, University of Manchester, UK, M SCHOENLEBER,
University of London, UK, J PEARSON, University of Manchester, UK,
G KYRIAKOU and P VADGAMA, University of London, UK

5.1 Introduction

Biosensors provide a high degree of elegance in regard to their simple juxtaposition of a bioreagent and a transducer function. To work properly, there must be a direct alignment of a functionally responsive biolayer and a transducer element, which is able to directly extract the binding information resulting from the encounter with the analyte. There is a difficult associated with such a simple, structurally inflexible combination, due to the fact that optimisation is limited as compared with say the use of a liquid phase bioreagent with its attendant optimised solution parameters of pH, pI, concentration and regent additives.

However, the net result is a solid-state monolithic structure with the potential to perform analyses and to operate potentially in optically opaque samples. In biomedicine, the latter capability holds considerable advantages. Indeed, most if not all biofluids contain colloidal materials that are liable to render the sample optically opaque or, at the very least, to induce a certain amount of light scattering. Furthermore, the majority of clinical sample assays rely on absorbance techniques. Therefore, it is necessary to have access to biosensors that would perform reliably even in opaque samples.

Nonetheless, there are still a few drawbacks associated with the use of biosensors in vivo. Although the established biosensor systems operate on the "macro" scale and have seen varying degrees of clinical exploitation, a key rapid alteration of the biosensor interface through the surface activity of the colloidal elements of any unmodified biological sample. This problem is also intricately linked to that of biocompatibility of the exposed surface of the biosensor in direct contact with either living tissue or the physiological fluids present in the body.

Handbook of Bioelectrochemistry, John Wiley and Sons Ltd. (2008)

In vivo Applications: Glucose Monitoring, Fuel Cells

P Vadgama and M Schoenleber, University of London, UK

Introduction

Glucose is a key target of intermediary metabolism for which innumerable bioelectrochemicial sensors have been designed. This effort is primarily driven by the central clinical importance of glucose in diabetes monitoring. The need here goes beyond the added assurance of knowing the state of glucose at any particular moment or even in avoiding the extremes of glucose variations, hypo- and hyperglycaemia, leading to extreme and life- threatening states. It is, in fact, fundamentally linked to the observation that the long term "killer" complications of diabetes vascular, neurological, renal and ocular can be considerably reduced by improving glucose control [1]. Given the unpredictability of glucose changes in any diabetic from day to day and even hour to hour, it has proved difficult to interpolate precise levels from standard intermittent glucose measurement regimens, even if linked to complex computational models or self-learning neural nets. This problem of uncertainty, therefore, has not been overcome using handheld glucose sensors, notwithstanding their convenience, accessibility and high impact on diabetes generally.

There is a clear need for real-time monitoring of glucose in order to achieve ideally tailored insulin treatment regimens, preferably using a closed-loop control insulin delivery system such as the implanted insulin pump [2]. However, open-loop control based on real-time data is also likely to go a substantial way to achieving glucose profiles approaching the physiological. Of all the approaches proposed for glucose monitoring (e.g. near-infrared spectroscopy, tissue refractive index change, direct electrochemistry and optical sensing), only bioelectrochemical sensors have come close to the reliability and selectivity acceptable for clinical purposes.

In vivo monitoring poses a major challenge to the technology of bioelectrochemical sensors. The in vivo environment does not allow for sample preparation or manipulation, and, of course, sample variables such as viscosity, flow and colloid/cell content are beyond conventional strategies of buffer dilution or cell separation. Therefore, the sensor needs to be a truly sample matrix independent system. In structural terms, it must also be a miniaturised construct, eliciting the absolute minimum tissue or blood reaction [3]. Importantly, whatever the analytical capability and elegance of the associated chemistry, it must also be sufficiently self-contained as to not be a source of toxic, carcinogenic, immunologic, teratogenic or pyrogenic leachables. Moreover, the constituent materials in direct tissue or blood contact must be of proven medical acceptability or to have undergone the full range of trial and evaluation appropriate to any new biomaterial. The associated effort is actually far more demanding than establishing the inherent bioelectrochemical measurement principle. In this respect, the in vivo bioelectrochemical sensor has more of the attributes of a functional implant than of a chemical sensor.

This Chapter will cover, respectively, the design, in vivo adaptation and interfacing challenges of bioelectrochemical glucose sensors. Basic chemistries are covered elsewhere, so the emphasis will be on the additional fabrication and design concepts that have emerged over the past 20 years of research in this specialist field. The treatment of more limited work on enzyme-driven bioelectrochemical fuel cells will be on similar lines. The background to all this, however, will be provided through the description of the concept of biocompatibility as a generic biomaterial.